School of Chemistry
University of Hyderabad

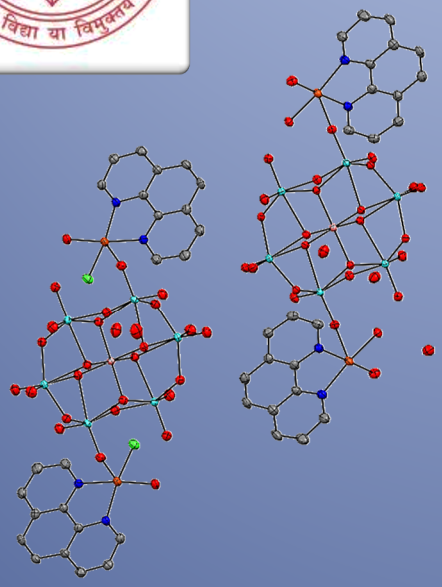

Designing Polyoxometalate Based Hybrid Compounds as Electrocatalysts for Water Splitting

A Thesis submitted for the degree of

Doctor of Philosophy

by

Chandani Singh

School of Chemistry, University of Hyderabad, Hyderabad-500 046, India

Designing Polyoxometalate Based Hybrid Compounds as Electrocatalysts for Water Splitting

हैदराबाद विश्वविद्यालय
University of Hyderabad

प्रतिष्ठित संस्थान
INSTITUTION OF EMINENCE
राष्ट्रीय अपेक्षाएँ, वैश्विक मानक
National Needs, Global Standards

A Thesis Submitted for the degree of

DOCTOR OF PHILOSOPHY

By

CHANDANI SINGH

School of Chemistry, University of Hyderabad-500 046, India.

December 2020

न चोरहार्यं, न च राजहार्यं,
न भ्रातृभाज्यं न च भारकारी,
व्यये कृते वर्धते एव नित्यं विद्याधनं सर्वधन प्रधानम् ।

Dedicated to
My Parents

CONTENTS

Page No.

Declaration i

Certificate ii

Acknowledgments iii

Synopsis vi

Chapter 1. General Overview of Polyoxometalate and Related Hybrid Compounds for Electrocatalytic OER and HER: Introduction and Motivation of the Thesis Work

1.1. Introduction 3

1.2. Polyoxometalates: structural aspect and its role in electrochemical water splitting 7

1.2.1. Polyoxometalate: History and structural description 7

1.2.2. POM based hybrid compounds: structure and its application 11

1.2.2.1. POMs and its related hybrid structures as an electrocatalyst for Oxygen Evolution Reaction (OER) 15

1.2.2.2. POM and its related hybrid structures as an electrocatalyst for Hydrogen Evolution Reaction (HER) 18

1.3 Motivation of the work 21

Chapter 2. Polyoxometalate Supported Bis(bpy)mono(aqua)Ni(II) Coordination Complex: An Efficient Electrocatalyst for Water Oxidation

2.1. Introduction 34

2.2. Experimental Section 37

2.2.1. Material and methods 37

2.2.1.1. General materials and methods 37

2.2.1.2. Crystal data collection 37

2.2.1.3. Electrochemical studies 37

2.2.2. Synthesis 38

2.2.2.1. Synthesis of $K_6[CoW_{12}O_{40}].6H_2O$ (POM) 39

2.2.2.2. Synthesis of compound **1** 39

2.3. Results and Discussion 40

2.3.1. Physical Characterization 40

2.3.1.1. Single-crystal XRD analysis 40

2.3.1.2. Bond Valence Sum (BVS) analysis of compound **1** 42

2.3.1.3. PXRD analysis of compound **1** 43

2.3.1.4. FTIR of POM and compound **1** 43

2.3.1.5. TGA of compound **1** and POM 44

2.3.1.6. UV-Visible spectral analysis of compound **1** and POM 45

2.3.1.7. Field Emission Scanning Electron Microscopy (FESEM) and Energy-dispersive X-ray (EDX) Analysis 46

2.3.1.8. X-ray photoelectron spectroscopy 48

2.3.1.9. Elemental analysis of compound **1** from ICP-OES and CHN analysis 48

2.3.2. Electrochemical measurements and water oxidation studies of compound **1** 50

2.3.2.1. WO properties of compound 1 50

2.3.2.2. Electrochemical stability analysis of **1** 51

2.3.2.3. ICP OES report of electrolyte solution after 1000 cycles CV scans 53

2.3.2.4. Controlled experiments 54

2.3.2.5. Kinetics and Mechanism involved in catalyzing water oxidation by compound **1** 62

2.3.2.6. Tafel plot 64

2.3.2.7. Faradic efficiency 65

2.3.2.8. Turnover Frequency (TOF) Calculation 67

2.4. Conclusion

2.5. References

Chapter 3. Designing POM Supported Metal Complex as an Efficient Electrocatalyst for HER

3.1. Introduction 79

3.2. Experimental Section 81

3.2.1. Material and methods 81

3.2.1.1. General materials and methods 81

3.2.1.2. Crystal data collection 81

3.2.1.3. Electrochemical studies 82

3.2.2. Synthesis 82

3.2.2.1. Synthesis of compound **1** 82

3.3. Results and Discussion 83

3.3.1. Physical Characterization 83

3.3.1.1. Single-crystal XRD analysis 83

3.3.1.2. PXRD analysis of POM and compound **1** 86

3.3.1.3. UV-vis. DRS, FTIR and Raman spectral analysis of compound **1** 87

3.3.1.4. TGA of compound **1** 89

3.3.1.5. Field Emission Scanning Electron Microscopy (FESEM) and Energy-dispersive X-ray (EDX) Analysis 90

3.3.2. Electrochemical measurements and HER studies of compound **1** 90

3.3.2.1. Electrocatalytic HER catalyzed by compound **1** 91

3.3.2.2. Analysis of Electrochemical stability for **1** 93

3.3.2.3. Controlled Experiments to understand the HER catalysis by compound **1** 97

3.3.2.4. Hydrogen detection by Gas Chromatography (GC) 98

3.3.2.5. Mechanistic and Kinetic analysis 100

3.3.2.5.1 Tafel Plot 100

3.3.2.5.2 pH dependent studies 100

3.3.2.5.3 Catalyst loading 101

3.3.2.5.4 Scan rate variation 102

3.3.2.6. Quantitative hydrogen evolution and Faradic efficiency calculation 102

3.3.2.7. Turnover Frequency (TOF) calculation 104

3.4. Conclusion 105

3.5. References 105

Chapter 4. Anderson Polyoxometalate Supported {Cu(H_2O)(phen)} Complex as an Electrocatalyst for Hydrogen Evolution Reaction in Neutral Medium

4.1. Introduction 112

4.2. Experimental Section 113

4.2.1. Material and methods 113

4.2.1.1. General materials and methods 113

4.2.1.2. Electrochemical studies 114

4.2.2. Synthesis 114

4.2.2.1. Synthesis of compound **1** 114

4.2.2.2. Synthesis of compound **1** 115

4.3. Results and Discussion 115

4.3.1. Physical Characterization 115

4.3.1.1. description of crystal structures 115

4.3.1.2. PXRD analysis 117

4.3.1.3. FTIR and UV-vis. DRS spectral analysis 118

4.3.2. Electrochemical studies 119

4.3.2.1. General features of CVs of both the compounds 119

4.3.2.2. HER using compound **1** as electrocatalyst 120

4.3.2.3. HER using compound **2** as electrocatalyst 120

4.3.2.4. Electrochemical stability of both compounds 121

4.3.2.5. Recognizing active site: POM or POM attached Cu-complex 122

4.3.2.6. Mechanistic and kinetic analysis 124

4.3.2.7. Quantitative hydrogen evolution and Faradic efficiency calculation 126

4.3.2.8. Hydrogen detection by gas chromatogram (GC) 128

4.3.2.8. Turnover Frequency (TOF) Calculation 128

4.4. Conclusion 130

4.5 References 130

Chapter 5. Cu(II)-bipyridine Complex and Anderson POM hybrid as a Pre-catalyst for Electrochemical Hydrogen Evolution Reaction

5.1. Introduction 138

5.2. Experimental Section 140

5.2.1. Material and methods 140

5.2.1.1. General materials and methods 140

5.2.1.2. Electrochemical studies 140

5.2.2.Synthesis 141

5.2.2.1. Synthesis of compound **1** 141

5.3. Results and Discussion 141

5.3.1. Physical Characterization 141

5.3.1.1. Structural description of compound **1** 141

5.3.1.2. PXRD analysis 143

5.3.1.3. FTIR and Diffused reflectance UV-vis. spectral analysis 143

5.3.2. Electrochemical studies 144

5.3.2.1. Electrochemical property of compound **1** 144

5.3.2.2. Insights of the plausible structural changes 146

5.3.2.3. Stability of **1´** (active catalyst) 146

5.3.2.4. Controlled experiment 146

5.3.2.5. Mechanistic and Kinetic study 149

5.3.2.6. Quantitative hydrogen evolution and Faradic efficiency calculation 150

5.3.2.7. Turnover Frequency (TOF) Calculation 151

5.4. Conclusion 152

5.5. References 153

Concluding Remarks and Future Scope 156

Appendix 161

List of Publications 184

Posters and Presentations 185

DECLARATION

I, **Chandani Singh,** hereby declare that the matter embodied in the thesis "***Designing Polyoxometalate Based Hybrid Compounds as Electrocatalysts for Water Splitting***" is the result of my investigation carried out in School of Chemistry, University of Hyderabad, Hyderabad, India, under the supervision of **Prof. Samar K. Das**.

In keeping with the general practice of reporting scientific observations, due acknowledgements have been made wherever the work described is based on other investigators' findings. Any omission, which might have occurred by oversight or error, is regretted. This research work is free from plagiarism. I hereby agree that my thesis can be deposited in Shodhganga/INFLIBNET. A report on plagiarism statistics from the University Library is enclosed.

30/12/2020

Chandani Singh

(15CHPH09)

S. K. Das

Professor Samar K. Das

(Supervisor) 30/12/2020

Prof. Samar K. Das
School of Chemistry
University of Hyderabad
Hyderabad-500 046., INDIA.

हैदराबाद विश्वविद्यालय
University of Hyderabad

प्रतिष्ठित संस्थान
INSTITUTION OF EMINENCE
राष्ट्रीय अपेक्षाएँ, वैश्विक मानक
National Needs, Global Standards

CERTIFICATE

This is to certify that the thesis entitled "***Designing Polyoxometalate Based Hybrid Compounds as Electrocatalysts for Water Splitting***" submitted by **Ms. Chandani Singh** bearing registration number **15CHPH09** in partial fulfillment of the requirements for award of Doctor of Philosophy in the School of Chemistry is a bonafide work carried out by her under my supervision and guidance.

This thesis is under acceptable percentage limits of plagiarism and has not been submitted previously in part or in full to this or any other University or Institution for award of any degree or diploma.

Parts of this thesis have been published in the following publications:

1. **Chandani Singh**, Subhabrata Mukhopadhyaya and Samar K. Das, *Inorg. Chem.* **2018**, *57*, 6479–6490 (Chapter 2).
2. **Chandani Singh** and Samar K. Das, *Polyhedron*, **2019**, *172*, 80–86 (Chapter 4).

She has also participated and presented oral/poster presentations in the following conferences:

1. Poster presentation at **20th CRSI-NSC**, CSIR-NCL-and IISER-Pune, India.
2. Poster presentation at **i2CAM-Energy School**, JNCASR, Bangalore, India.
3. Poster presentation at **MTIC-XVII** (IISER Pune and NCL, Pune, India) and **MTIC XVIII** (IIT-Guwahati, India).
4. Poster presentation at **CHEMFEST-2016, 2018 and 2020**, SoC, UoH, Hyderabad, India.
5. Oral presentation at **CHEMFEST-2020**, SoC, UoH, Hyderabad, India.
6. Oral presentation at **CPCE-2020**, virtual conference organized by NIT Jamshedpur, India.

The student has passed the following courses towards fulfilment of coursework requirement for Ph.D.

	Course	Title	Credits	Pass/Fail
1.	CY-801	Research Proposal	3	Pass
2.	CY-806	Instrumental Methods B	3	Pass
3.	CY-802	Chemistry Pedagogy	3	Pass
4.	CY-571	Organometallic Chemistry	2	Pass
5.	CY-575	Computational Chemistry	2	Pass

S. K. Das

Prof. Samar K. Das
(Supervisor)

30/12/2020

Prof. Samar K. Das
School of Chemistry
University of Hyderabad
Hyderabad-500 046., INDIA.

Dean
School of Chemistry

Dean
SCHOOL OF CHEMISTRY
University of Hyderabad
Hyderabad-500 046

Acknowledgments

I take great pleasure in taking this opportunity to acknowledge all those who had their role in the fulfillment of my 'doctoral of philosophy.'

I convey my profound gratitude and sincere thanks to my thesis supervisor Dr. Samar K. Das, for his invaluable guidance, constant encouragement, and the liberty he gave me in carrying my research work. His positive approach in every aspect was admirable and inspiring. He has always been approachable, helpful, completely supportive, and cooperative. I thank Prof. Anunay Samanta, Dean, School of Chemistry, and all the former Deans of the School of Chemistry for providing the facilities needed for my research work. I extend my heartfelt thanks to my Doctoral Committee members, Prof. K. Muralidharan and Prof. R. Nagarajan, and all the School of Chemistry faculty members for their co-operation on various occasions.

I would like to acknowledge my present labmates, Tanmaya, Joycy, Olivia, Hema, Athira, Debu, Sateesh M., Dr. N. Rajendar, Dr.Vinod, Dr. Pinki, for making maintaining wonderful work environment. I feel fortunate that I got to learn from former labmates and postdoctoral fellows; Dr. Paulami, Dr. Krishna, Dr. Ramakrishna, Dr. Suresh, Dr. Subhabrata, Dr. Joyashish, Dr. Suranjana, Dr. K. Prathap, Dr. Y. Sridevi, Dr. Girijesh, Dr. Veera Reddy, Dr. M. Pradeep, Dr. K. Sathish Mrs. Olivia Neogi and Mrs. Ramathulasamma.

I also thank all the non-teaching staff/instrument operators, especially Dr. Durgaprasad, Mr. Sunil, Mr. Venkat Ramanna, Mr. Mahesh Rathod, Mr. Shyam, of the School of Chemistry for their assistance on various occasions. I thank DST funded National Single Crystal X-ray Diffraction Facility, UGC/ UPE for providing the basic requirements and UGC-BSR for the financial support.

A special token of thanks to the M.Sc project students Mr. Atanu Haldar, Mr. Subhankar Chowdhury, and NRC project student Mr. P. Santosh Kumar, for their contribution to some of the projects.

I would like to thank Joyashish da, Surajana di, Subha da for teaching and helping me with the electrochemistry and clearing all my doubts no

matter how silly they sound. I would like to thank Suresh Anna, Sattesh K. Anna, and Sateesh M. for their help in the crystallographic analysis.

I would like to acknowledge seniors on whom I could rely under any situation, Sneha di, Situ, Subha da, for being there during all the ups and downs of this Ph.D. life. A special thanks to situ for understanding and helping me cope through the lowest period during this Ph.D. journey. I am grateful to Divya di and all electrochemical workstation users, which has a significant contribution to my thesis work for the instrument's smooth functioning. A special mention of Prof. T. P. Radhakrishnan sir and his lab for MiliQ water supply. I would like to acknowledge my batchmates Sameeta, Sipra, Mou, Tasneem, Ankit, Saddam, Apurba, and all the juniors from school of chemistry, HCU, for all the help they have provided required for the study.

I would like to acknowledge my parents for supporting me throughout my academic journey. My siblings (Rekha, Rajni, and Bipin) for being there throughout my Ph.D. journey. And the newest member of our Family, Ruhi, brought all the happiness along with her.

I would like to acknowledge my B.Sc. college faculty for encouraging me to pursue research. A special mention of Dr. Vithal Kawade and Dr. V. K. Khanna for their encouragement and guidance to seek this path.

I have been fortunate enough to be around people to share all my small and big achievements. I would like to acknowledge my friends Manjeet, Disha, Mehapara, Simmi, Rinu, Pranoti, Jyoti, and all those I might have lost contact over time.

Towards the end of my Ph.D. period, the pandemic COVID-19 changed the work equilibrium with an unexpected twist. During the crucial time when I was close to submission, with lab work yet to finish, I have been fortunate enough to have an understanding supervisor, Prof. Samar K. das, who helped me in arranging the permission letter to work in the lab.

Even though this pandemic changed everything and disturbed our life's equation, but when I look at the positive side, it allowed me to stay with old friends, reconnect with people, and helped me manage the stressful period. I have been fortunate to get Pallavi and Kathir, one of the best

flatmates who came as a savior when I needed a place to stay during this corona-crisis. The acknowledgment is incomplete without mentioning the jhatpat recipe by Pallavi and Kathir special sambar & biryani, which let me continue my stay during the corona crisis period.

I am very thankful to Rajendar anna, and his flatmates (Varsha and Naresh) for the tasty lunch during my thesis writing period. And last but not least, those distant but close to my soul, accompanying me from time to time when I am facing the odd, make me laugh, share my grief, and cherish my joy, will always be remembered by me.

My sincere apologies if I have missed anyone, but I wish to extend my heartful gratitude to everyone who has been involved in my life and helped me in one way or another.

Chandani Singh

University of Hyderabad

December 2020

SYNOPSIS

Of the Thesis Entitled

Designing Polyoxometalate Based Hybrid Compounds as Electrocatalysts for Water Splitting

To be submitted to the

University of Hyderabad

For the degree of

DOCTOR OF PHILOSOPHY

By

CHANDANI SINGH

(15CHPH09)

School of Chemistry, University of Hyderabad-500 046, India.

December 2020

The doctoral thesis entitled "**Designing Polyoxometalate Based Hybrid Compounds as Electrocatalysts for Water Splitting"** consists of five chapters: four working chapters and one chapter on the general introduction focused on the literature available and motivation of the work. These chapters are as follows: (**1**) General Overview of Polyoxometalate and Related Hybrid Compounds for Electrocatalytic OER and HER: Introduction and Motivation of the Thesis Work, (**2**) Polyoxometalate Supported Bis(bpy)mono(aqua)Ni(II) Coordination Complex: An Efficient Electrocatalyst for Water Oxidation, (**3**) Designing POM Supported Metal Complex as an Efficient Electrocatalyst for HER, (**4**) Anderson Polyoxometalate Supported {Cu(H_2O)(phen)} Complex as an Electrocatalyst for Hydrogen Evolution Reaction in Neutral Medium (**5**) Cu(II)-bipyridine Complex and Anderson POM hybrid as a Pre-catalyst for Electrochemical Hydrogen Evolution Reaction.

Besides the first chapter, all the chapters are divided into the following parts: (a) Overview (contains a brief overview of the work), (b) Introduction (literature survey relevant to the study), (c) Experimental section (includes materials and methods employed for the study), (c) Results and discussion (discussing the physical characterization of the compounds utilized for the study followed by an extensive discussion on the electrochemical activity with all the relevant experiments to support the result), (d) Conclusion and (e) References. All the compounds utilized in this work, are characterized by single crystal X-Ray diffraction (wherever required), powdered X-Ray diffraction (PXRD) pattern analysis for bulk purity of the compounds utilized, FT-IR spectral analysis, UV-vis. diffused reflectance spectroscopy (DRS), FESEM images and EDS analysis, thermogravimetric analysis (TGA), dynamic light scattering (DLS) analysis, whereas gas chromatography (GC) was used to detect hydrogen obtained from the HER catalysis (**Chapters 3-5**). Apart from this, less frequently availed techniques includes; ICP-OES and XPS. All the electrochemical studies were done in the aqueous medium in both homogeneous and heterogeneous manner.

Chapter 1

General Overview of Polyoxometalate and Related Hybrid Compounds for Electrocatalytic OER and HER: Introduction and Motivation of the Thesis Work

In this chapter, we have started the discussion by addressing the alarming situation of the energy crisis the world is facing today. All the factors contributing to this energy crisis and the consequences have been discussed in detail. This lays the foundation in motivating the development of catalysts for water splitting since hydrogen generated from water splitting could be used in fuel cells to generate energy or be directly utilized for energy storage purposes. Following this, a brief discussion on polyoxometalate (POM) mentioning the timeline of POM chemistry based on structural diversity. We have also discussed POM's functionalization by synthesizing POM-based hybrids by supporting transition metal complex on POM, followed by the importance of their diverse structures. Recent literature reports of POM-based hybrids with their applications are listed and discussed in a tabular manner. This is followed by a dedicated discussion on POM based hybrids for both oxygen evolution reaction (OER) and hydrogen evolution reaction (HER). Limited availability of POM based hybrids, consisting of POM supported transition metal complexes (PSTMCs) which can electrocatalyze OER and HER, motivated us for this thesis work.

Chapter 2

Polyoxometalate Supported Bis(bpy)mono(aqua)Ni(II) Coordination Complex: An Efficient Electrocatalyst for Water Oxidation

Polyoxometalate (POM) supported transition metal complexes are one of the popular hybrid compounds derived from the POM, which have the properties of both the POM unit and the supported transition metal complexes complemented by value-added property due to the synergistic effect. This makes polyoxometalate supported transition metal complexes (PMSTCs) a better candidate than its constituent units. With this in mind, we have synthesized a polyoxometalate (POM) supported nickel(II) coordination complex $[Ni^{II}(2,2'\text{-bpy})_3]_3[\{Ni^{II}(2,2'\text{-bpy})_2(H_2O)\}\{HCo^{II}W^{VI}_{12}O_{40}\}]_2\cdot 3H_2O$ (**1**). Since the compound **1** has been characterized with a

$\{Ni^{II}(2,2'\text{-bpy})_2(H_2O)\}^{2+}$ fragment coordinated to the surface of the Keggin anion ($[H(Co^{II}W_{12}O_{40}]^{5-}$) *via* terminal oxo group of tungsten and the $[Ni^{II}(2,2'\text{-bpy})_3]^{2+}$ coordination complex cation sitting as the lattice component in the concerned crystals, the electronic spectroscopy of compound **1** has been described by comparing its electronic spectral features with those of $[Ni^{II}(2,2'\text{-bpy})_2(H_2O)Cl]Cl$, $[Ni^{II}(2,2'\text{-bpy})_3]Cl_2$ and $K_6[Co^{II}W_{12}O_{40}]\cdot 6H_2O$. Most importantly, compound **1** can function as a heterogeneous and robust electrochemical water oxidation catalyst (WOC). To gain insights into the water oxidation protocol and interpret the active catalyst's nature, diverse electrochemical experiments have been conducted. During the electrochemical process, the WOC mode of action is accounted through confirming no formation/participation of metal oxide during different controlled experiments. It is found that the title compound acts as a true catalyst that has Ni(II) coordinated to the POM surface, serving as the active catalytic center. It is also found to follow a proton-coupled electron transfer (PCET) pathway (2 electrons and 1 proton) for WO catalysis with a high turnover frequency of 18.49 $(mol\ O_2)(mol\ Ni^{II})^{-1}\ s^{-1}$.

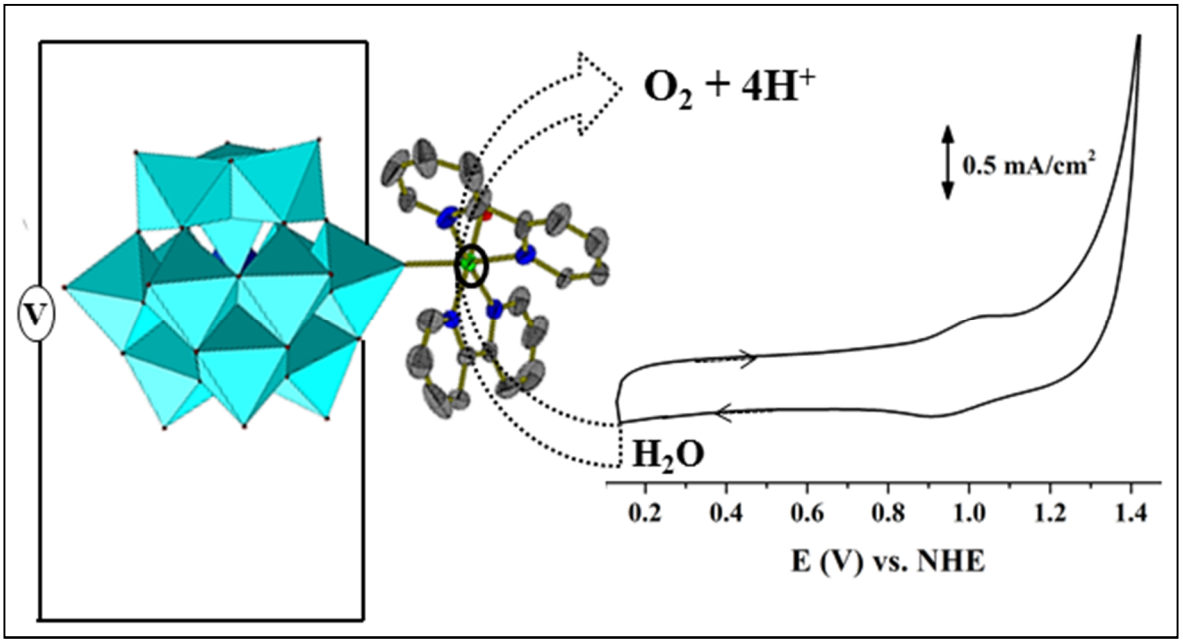

Figure 1. Graphical representation of Ni-complex supported on Keggin POM as an electrocatalyst for water oxidation.

Chapter 3

Designing POM Supported Metal Complex as an Efficient Electrocatalyst for HER

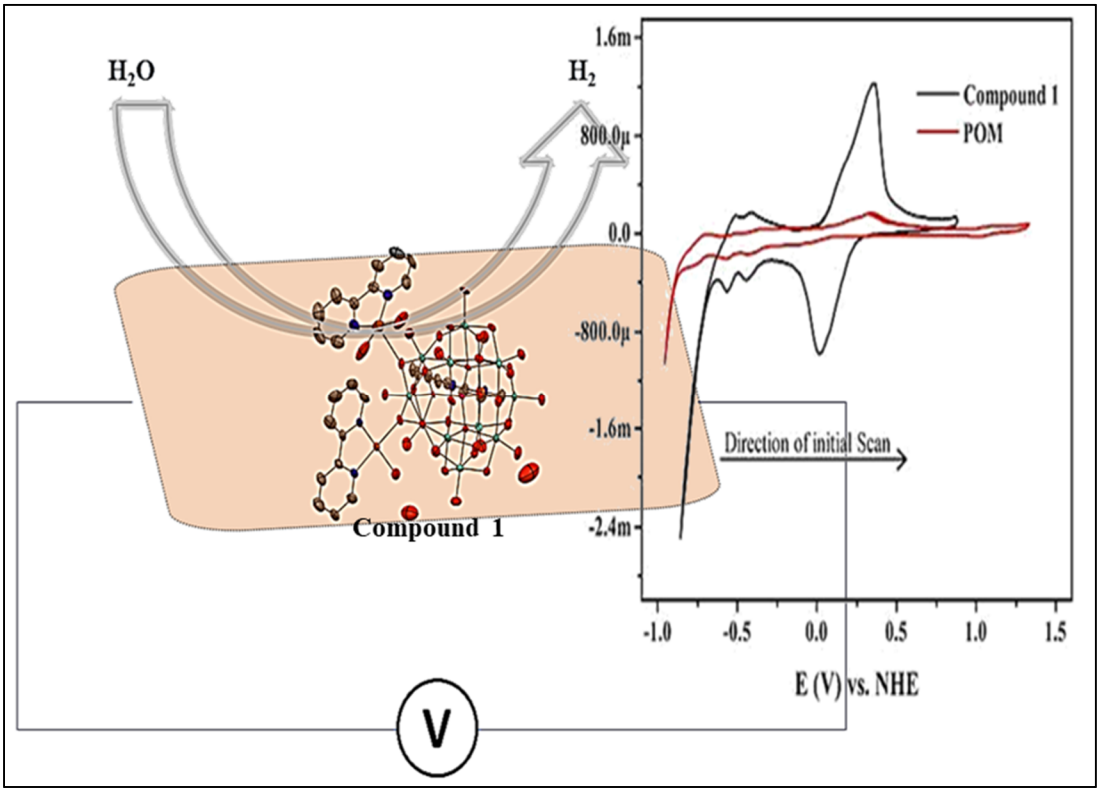

Figure 2. Illustration of the electrochemical HER activity exhibited by the POM hybrid consisting of Cu-complex on Keggin POM.

Hydrogen is the solution to all the problems associated with the energy crisis. Generating hydrogen from water splitting is one of the greener approaches, but it requires an efficient catalyst, which is economical for the bulk production of hydrogen. In this work, we have demonstrated a POM supported Cu-complex utilization for the electrochemical HER activity. This is among the few reports available with POM supported transition metal complexes (PSTMCs) for electrochemical HER. Polyoxometalate (POM) supported transition metal complexes are one of the popular hybrid compounds derived from the POM unit, with properties associated with both the POM and the supported transition metal complexes with additional value-added properties due to the synergistic effect making PSTMCs a better candidate then its

constituent units. In this chapter, we have demonstrated the successful synthesis of a Cu-complex coordinated to a Keggin POM ($[Co^{II}W_{12}O_{40}]^{6-}$), forming a 2D-network with the molecular formula of $[\{Cu^{II}(2,2´\text{-bpy})(H_2O)_2\}][\{Co^{II}W^{VI}_{12}O_{40}\}\{(Cu^{II}(2,2´\text{-bpy})(H_2O)\}\{(Cu^{II}(2,2´\text{-bpy})\}]\bullet 2H_2O$ (**1**). From the electrochemical studies, we found compound **1** can function as an efficient electrochemical catalyst for hydrogen evolution reaction (HER) in a near-neutral medium (pH 4.8) under buffered conditions (acetate buffer). The detailed study has been conducted through varied electrochemical experiments to gain insights into the electrocatalysis exhibited by **1**. Compound **1** follows a PCET pathway with one proton and one electron involvement for electrocatalyzing HER. The overpotential required to achieve the current density of 1 mA/cm^2 was 520 mV with the Faradic efficiency of 81.02%.

Chapter 4

Anderson Polyoxometalate Supported {Cu(H_2O)(phen)} Complex as an Electrocatalyst for Hydrogen Evolution Reaction in Neutral Medium

This chapter has employed two structurally analogous Anderson polyoxometalate (POM) supported copper complexes for the electrochemical studies to check the activity towards hydrogen evolution reaction (HER). These POM supported transition metal complexes, mentioned as compound **1** and **2** have the molecular formulas, $[Cr(OH)_6Mo_6O_{18}\{Cu(phen)(H_2O)_2\}_2][Cr(OH)_6Mo_6O_{18}\{Cu(phen)(H_2O)Cl\}_2].5H_2O$ (**1**) and $[Al(OH)_6Mo_6O_{18}\{Cu(phen)(H_2O)_2\}_2][Al(OH)_6Mo_6O_{18}\{Cu(phen)(H_2O)Cl\}_2].5H_2O$ (**2**) respectively. Both these compounds exhibited electrochemical activity for catalyzing hydrogen evolution reaction (HER) from water (phosphate buffer, pH 7) with relatively low overpotentials of 300 mV (compound **1**) and 644 mV (compound **2**) at the current density of 1 mA/cm^2 respectively. Compounds **1** and **2** show remarkable Faradic efficiencies of 95.7% and 89.4%, respectively. In terms of overpotential and Faradic efficiency, compound **1** turns out to be a superior electrocatalyst for HER from water over compound **2**. In this chapter, we have evidently proved that the active site of this electrochemical HER is the water coordinated Cu(II) center, supported onto POM cluster anion; the polyoxometalate, onto which this aqua-Cu (phen)-complexes are supported, plays an essential role in making the overall system heterogeneous, for

designing a better electrocatalyst for direct reduction of neutral water. The compounds' analogous structure allowed us to understand the role of heteroatom of the Anderson POM in the activity of PSTMCs for catalyzing HER.

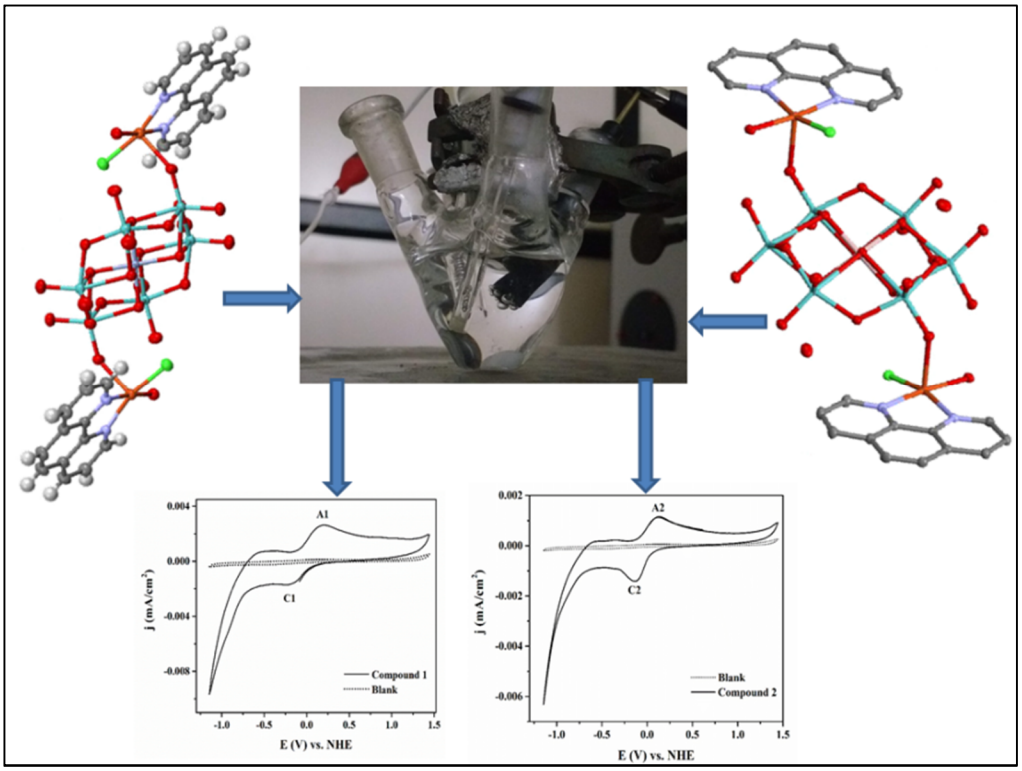

Figure 3. Schematic representation of HER activity displayed by the two analogous Anderson POM hybrids.

Chapter 5

Cu(II)-bipyridine Complex and Anderson POM hybrid as a Pre-catalyst for Electrochemical Hydrogen Evolution Reaction

In this chapter, we utilized a chain-like structured Cu-complex supported Anderson POM, $[Cu^{II}(2,2'\text{-bpy})(H_2O)_2Cl][Cu^{II}(2,2'\text{-bpy})(H_2O)_2Al(OH)_6Mo_6O_{18}]\cdot 4H_2O$ (**1**), which undergoes structural rearrangement (labeled as compound **1´)** under the electrochemical condition on the application of high cathodic potential resulting in the formation of the active catalyst for the electrochemical HER activity. In this chapter, we have discussed POM's role in the active catalyst's stability, which is otherwise difficult to achieve. Even though compound **1** is a pre-

catalyst to the active catalyst towards electrochemical HER, POM plays a substantial role in achieving the catalysis's withstanding result. Compound **1´** achieves the current density of 1mA/cm^2 with overpotential of 348 mV, which is relatively low compared to such POM-based hybrids discussed in other chapters of this thesis work.

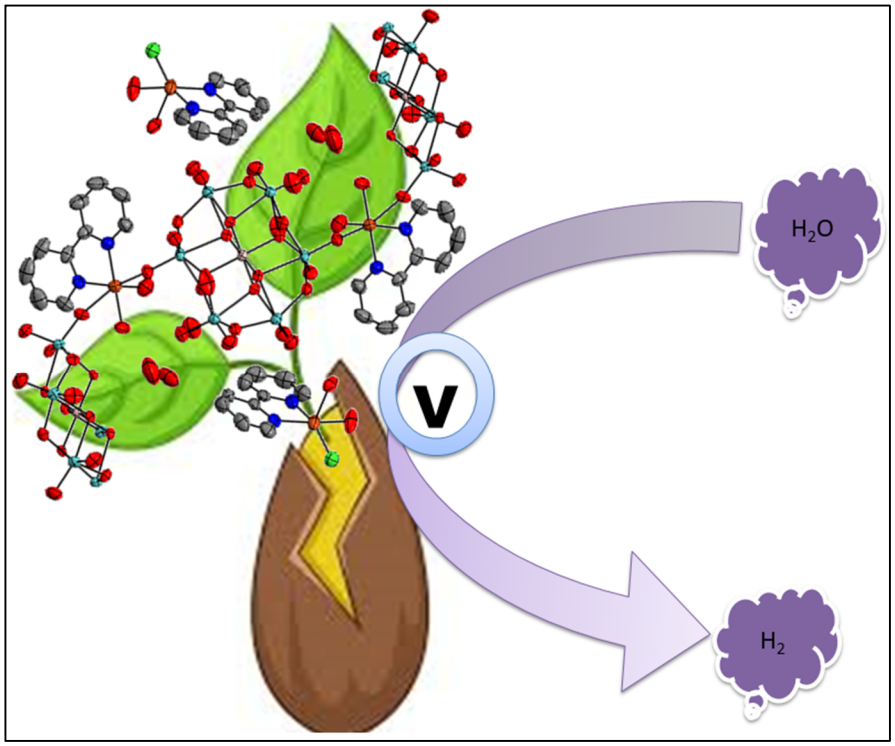

Figure 4. Pictorial depiction of Anderson POM supported Cu-complex as an electrocatalyst for water reduction.

Summary and Future Scope

The summary and future scopes of the work done so far in this thesis are discussed at the end of all the working chapters. Understanding the chemistry involved in the electrocatalysis of OER or HER by POM based hybrids is dictated by varied factors, such as type of POM employed, transition metal present in the hybrid, the nature of ligand utilized, mode of coordination of TM-complex to the POM unit, *etc*., In this thesis, we could only work on a few of them. From chapters **2** and **3**, we concluded the nature of the transition metal complex's importance coordinated to the same Keggin POM. This work could be further studied by changing the ligand used; instead of 2,2´-bipyridine, one can employ a different type of ligands such as 1,2-bis(4-

pyridyl)ethane (bpa); 1,3-bis(1H-imidazol-l-yl)methyl)-benzene (m-bimb); 1,3-bis(4-pyridyl)-propane (bpp); 4,4′-di(1H-imidazol-1-yl)-1,1′-biphenyl (bibm). Chapters **3** to **4** could be correlated in one way or another as all of them are Cu-complexes coordinated to the POM unit. Here we have discussed the importance of different types of POM with similar TM-complex coordinated to it. In the future, we can work with Ni-based complex coordinated to similar Anderson POM as employed in chapters **4** and **5** and compare the observations to that of chapter **2**.

****

***************************END**************************

Chapter 1

General Overview of Polyoxometalate and Related Hybrid Compounds for Electrocatalytic OER and HER: Introduction and Motivation of the Thesis Work

OVERVIEW

Polyoxometalate chemistry is one of the oldest known chemistry in the scientific world, which has completed 85 years in 2020. With POM chemistry reaching towards centenary, there are still a lot of properties to be understood, researched, and well documented for future references. POM has broader spectra of application starting from biomedical application in tumor sensor to material synthesis in sustainable energy (as in photochemical/electrochemical OER/as an electrode in fuel cell/proton-conducting membrane). The versatility of POM, owing to its structural arrangement, complete inorganic skeleton, low lying MOs, and electron-rich structure (rich redox chemistry), make it interesting to explore under the varied conditions and for a different purposes. One such aspect would be transition metals (TM) complexes supported to the POM units, which add to both POM and TM-complexes' functionality. Such a structural arrangement leads to parental properties' inheritance and introduces new property arising from the change in the molecule's electronic level. Electrochemical water oxidation or water reduction is one field that is not well explored using theses hybrids. The lack of sufficient literature, interesting structure with the ease of structural tuning, motivated us to work in this direction. We started working with different POM supported TM-complexes in above said direction, which gave us overwhelming results.

In this chapter, we have discussed a brief history of POM and its application, followed by the main discussion on POM based hybrid compounds, which includes mainly different catalytic properties towards water reduction and water oxidation by electrochemical method. Weighing the work done so far in this field, which is available in the literature and what is lacking in this regard which is followed by the motivation of our work and the overall result we obtained in this direction.

1.1. Introduction

Globalization and modernization have led to advancement; the human race has never thought of before. All the positives that came with these advances cannot undo the harm it did and will do in the future to earth if a proper step is not taken before it is too late. The expansion of technology comes with energy expenses, and this energy is drawn mostly from fossil fuels due to their high energy density values. The exploitation of fossil fuels to this extent has increased the CO_2 emission in the atmosphere. From the ongoing trends of global emission, it is forecasted by the Global Carbon Project that emissions due to CO_2 might increase roughly by 2.7%, making it 37.1 giga-tons by the end of the year 3000.[1] The leading cause of the deteriorating air quality is fossil fuel consumption in power plants, industrial work, or transport systems.[2,3]

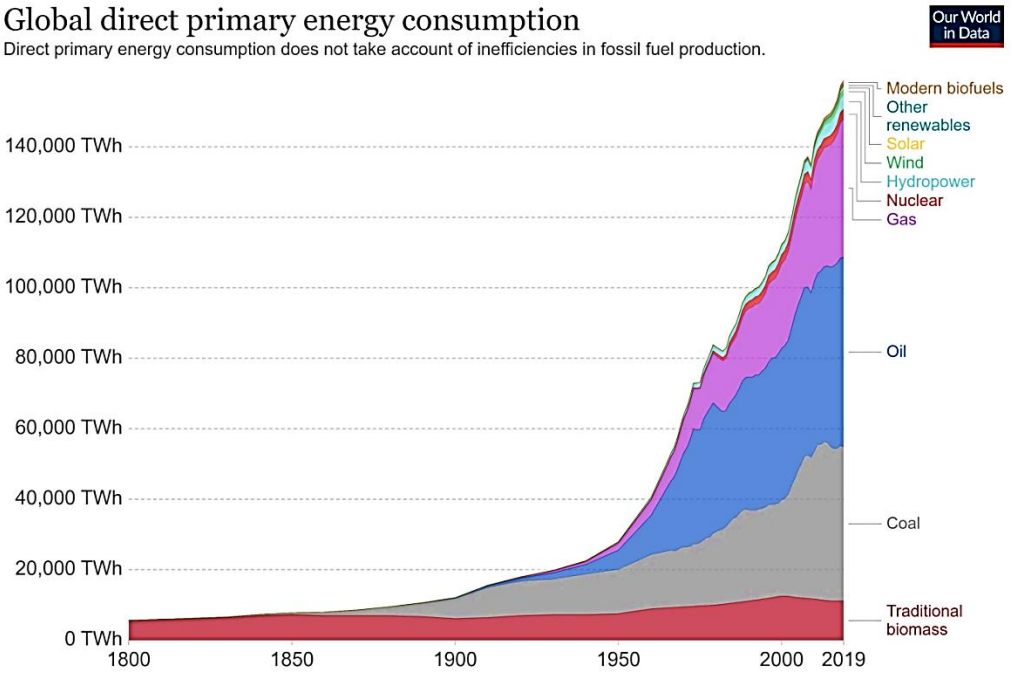

Figure 1.1. Global primary energy consumption of the world.[2]

The dependency on fossil fuels for everyday usage to advanced industrial applications has worsened the CO_2 emission. Though science has opened many doors for new opportunities, fossil fuel dependency to attain our daily energy needs is yet to be solved. The inefficiency in handling energy-related problems has thrown us to this situation where our fossil fuel sources are at the threat of extinction, and the air quality is at its worst form and is getting worsened with

every passing day. The survey conducted by the International Energy Agency (IEA) in its report of the year 2019 confirms this data (**Figures 1.1. and 1.2.**). In its statement of 2019, IEA showed that the primary source of energy used globally is a fossil fuel, thereby posing a constant threat to the environmental conditions.[3] The ever increasing demand for energy due to modernization has forced the exploitation of fossil fuel faster than that ventured. This surge in the global energy economy has negative repercussions on the environment, making it high time to switch our approach to greener and sustainable ways to uphold the alarming situation of both energy crisis and environmental conditions. This brings down us to two significant concerns/objectives:

1. development of greener and efficient way for energy production and
2. storage of the energy.

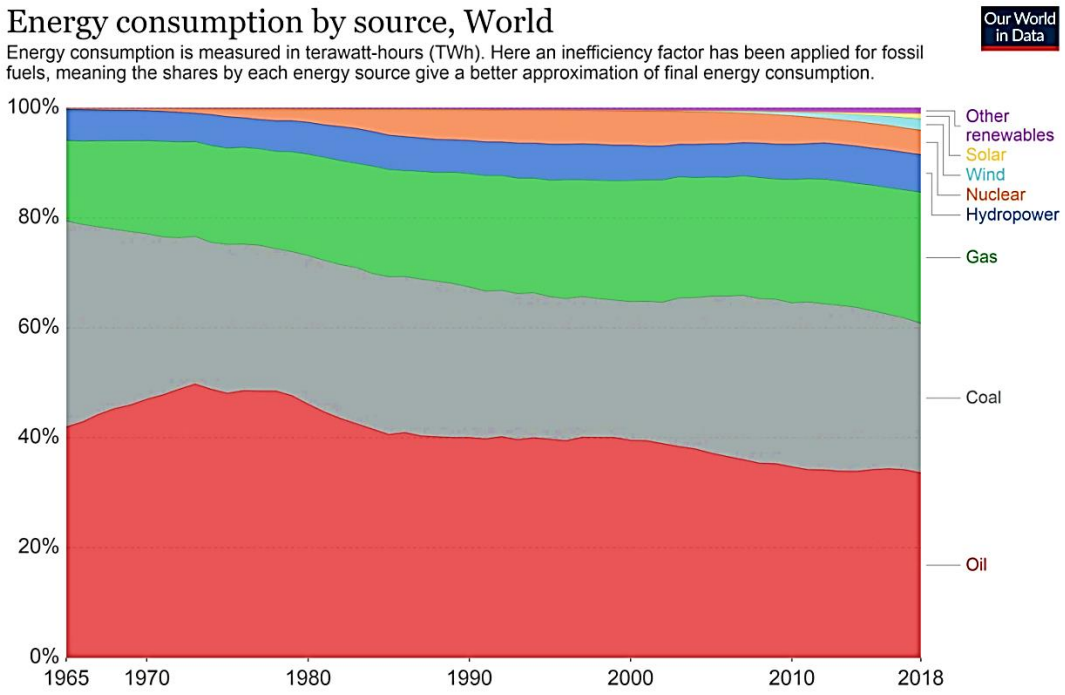

Figure 1.2. Global energy consumption based on different sources.[2]

Fuel cells of various types steal the limelight for the generation of greener and sustainable energy sources, thereby answering the first concern. This fundamental research is broken down into different areas where people are currently working; few are electrode development, electrolyte search/ development of better PEM membrane, *etc*.[4-10] But this part of research alone cannot solve the problems we face today, emphasizing the importance of the second point mentioned

earlier about energy storage. Energy generated by various means needs to be stored appropriately to create less wastage, thereby solving the energy crisis and environmental issues.

Hydrogen is the smallest molecule that can solve this energy crisis due to its low mass density and high energy density (0.0899 Kg/Nm^3) values making it best suited for energy storage.[11] Hydrogen can be obtained by various methodologies, out of which steam refining of natural gas is the popular choice. Steam refining of natural gas is a cheap method, but it comes at the cost of an increase in CO_2 emission to the environment (**Figure 1.3.**). Thus, it is high time to shift to a greener, sustainable, and cheaper form for practical purposes. Therefore, water splitting is one such appropriate way to produce the purest form of hydrogen with no carbon-based waste. Water being the simplest compound, it has only two components on its degradation, *i.e.*, hydrogen and oxygen.

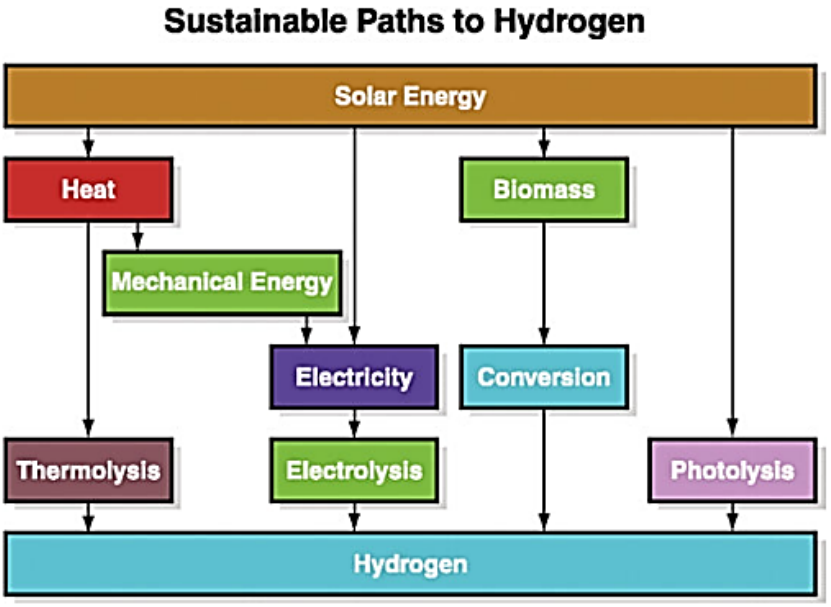

Figure 1.3. Pathways for hydrogen generation using solar energy.[12]

Water splitting is the process of decomposition or splitting of a water molecule into its constituent molecules, *i.e.*, hydrogen and oxygen molecules. The overall water splitting process could be achieved by administering a suitable energy source to cleave the 'H–O' bond from the water molecule. Some of these sources are worth mentioning as the following: photochemical (applying the electromagnetic radiation; mostly solar energy), electrical energy (electrochemical process), thermal energy (thermochemical process), or *via* the chemical method. A water-

splitting reaction could be written in the form of its two half-reactions, *i.e.*, oxygen evolution reaction (OER) and hydrogen evolution reaction (HER). Thus the overall water splitting (WS) could be represented as:

$2\ H_2O \rightleftharpoons H_2 + 2\ O_2$ (WS) $E^0 = 1.23$ V *vs.* NHE **1**

$2\ H_2O \rightleftharpoons O_2 + 4\ H^+ + 4\ e^-$ E= 1.23 V *vs.* NHE (OER) **2**

$4\ H^+ + 4e^- \rightleftharpoons 2\ H_2$ E= 0.0 V *vs.* NHE (HER) **3**

From the above reactions, it is easy to elucidate that OER is the bottleneck process for water splitting (WS) due to its thermodynamic uphill process and slow kinetic process. Apart from OER, WS's other half-reaction, known as HER, also has its demerit. For water reduction (WR) or HER process, the thermodynamic potential is 0 V. *vs.* NHE. Still, Pt and other noble metals are the only known catalyst to date to catalyze HER with negligible overpotential in alkaline medium.[13] These noble metals are expensive, increasing the overall cost of catalyzing the HER process. Hence, they need to be replaced by more abundant materials on earth and catalyze HER effectively for a practical purpose. Thus, both the components of WS, namely OER and HER, need the development of catalysts for the reasons above. Indulging into earth-abundant materials, such as transition metal for designing the catalyst can reduce the catalyst cost, making it better for the practical purpose of bulk electrolysis. Consequently, we have worked in this direction by incorporating transition metal complexes onto the polyoxometalate (POM) unit to catalyze OER and HER. This chapter will discuss OER and HER catalysts based on POM-based materials after a brief introduction on POM.

1.2. Polyoxometalates: structural aspect and its role in electrochemical water splitting

1.2.1. Polyoxometalate: History and structural description

From the revelation of the first polyoxometalate structure (POM) structure by Keggin in 1933 to date, POM chemistry has developed many folds both in terms of structural diversity and application.[14-18] POM chemistry could be traced back to the year 1778, thereby completing more than two centuries in the year 2020. A brief outline providing the timeline mapping of POM

chemistry is provided in **Figure 1.4.**[19-24] The scientific community knew POM's existence before the availability of the first structural data of POM.[20,21] Polyoxometalate (POM) belongs to a particular class of metal oxides that self-assemble under different reaction conditions to acquire interesting structures. POMs generally consist of transition metals which are connected by oxo-bridge. In most cases, if provided the right reaction conditions (temperature, pH, and concentration), oxoanions (MO_4^{2-}) of this transition metal (M=W/Mo/V/Nb/Ta in their highest oxidation state) undergoes protonation to undergo polycondensation. The reaction conditions play a very critical role in the assembly of a POM compound.

Figure 1.4. Timeline showing POM development along with the scientists involved in its discovery/development.

Based on structural diversity, POMs are broadly classified into two main categories, namely isopolyanion and heteropolyanion. Isopolyanion has only one type of metal transition metal present in it. Hence the term "iso" is used for isopolyanion, whereas in heteropolyanion, a

hetero-atom is present apart from the main transition metal oxides (also referred to as addenda atom). The general formula for isopolyanion is $[M_mO_y]^{p-}$ and heteropolyanion follows the general formula of $[X_xM_mO_y]^{q-}$. In heteropolyanion, the following relation is observed, *i.e.*, $x \leq m$ and M is called addenda atom, which mostly belongs to group V and VI of the periodic table.

Lindqvist type of POM belongs to the class of isopolyanion, which was discovered in the year 1950. The following are well known and quite popular subclass of POM known under heteropolyanion: Keggin POM, Anderson-Evans POM, Dawson-Well POM, and Strandberg POM (**Figure 1.5.**). Lacunary POMs are also one class of heteropolyanion, which are generally derived from the Keggin type of POMs. These are formed by partial hydrolysis of the Keggin structure, creating vacancy or 'lacunae,' hence the name. Based on the vacancy created, these are classified under mono-, bi- and tri- lacunary POMs. The vacant sites are often used to substitute the transition metal-aqua group (mostly 3d and 4d series metal ions).[25]

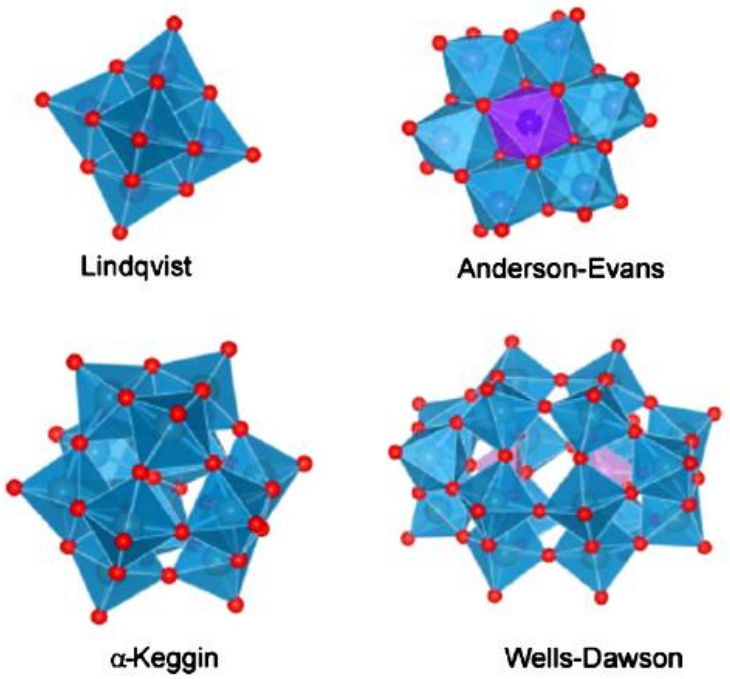

Figure 1.5. Structure of different polyoxometalates.[18d]

In this thesis work, we have dealt mainly with Keggin and Anderson's POM type only; hence, we have provided a detailed discussion of only these POMs.

[A] Keggin Polyoxometalate: Keggin POM was named after J. F. Keggin after he successfully deduced its structure from the PXRD pattern in the year 1933, thereby laying a foundation stone for POM chemistry. Thus, phosphotungstic acid became the first fully characterized POM structure.[23a] Keggin POM has the general formula of $[XM_{12}O_{40}]^{n-}$ where X is heteroatom (such as Si(IV)/P(III)/Co(II)/Fe(II)) and M is addenda atom (*e.g.* M= W^{6+}/ Mo^{6+}). The central atom forms tetrahedron, which corresponds to 'XO_4'. This 'XO_4' unit shares the vertices with the four 'M_3O_{13}' (triad). The oxygen in the 'XO_4' unit is shared by the MO_6 octahedral which forms the triad. In the Keggin POM, major bonds between addenda and oxygen atoms are as follows: (a) twelve M-O-M (bridged), (b) twelve corner bridging M-O-M which are connected to the MO_6 units sharing the oxygen from the central 'XO_4' unit and (c) twelve M=O bonds (terminal bonds) (**Figure 1.6.**).

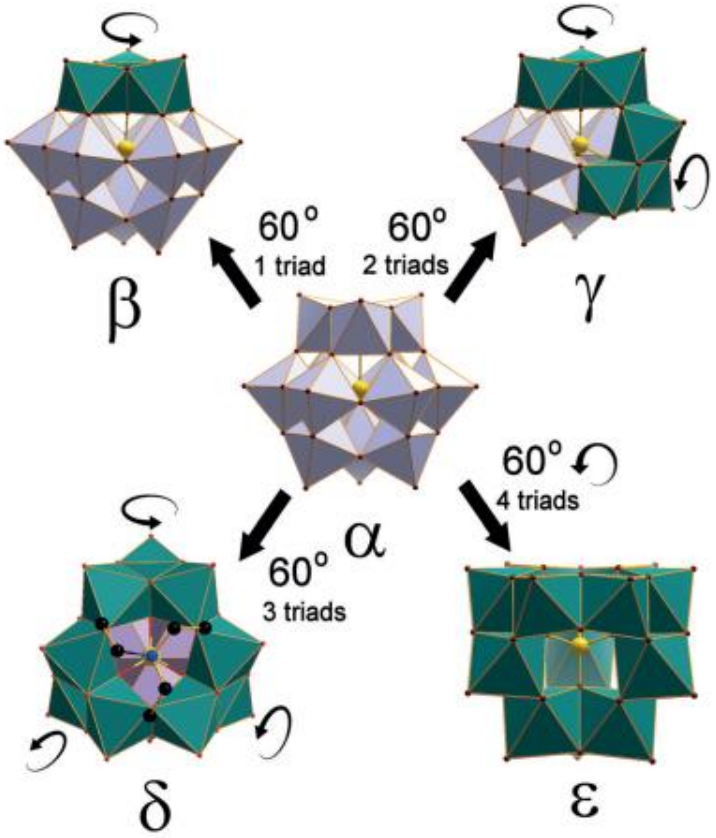

Figure 1.6. Keggin POM and its isomeric structures.[26a]

Keggin POM has different isomers as a result of rotation around the basic $\{M_3O_{13}\}$ unit. Each 60° rotation of one or more of the $\{M_3O_{13}\}$ gives rise to a different isomer. Theoretically, as

reported by Baker and Figgis, there are five possible isomers of Keggin POM, namely α, β, γ, δ, ε (**Figure 1.6.**) α-Keggin POM is the most stable and common type of POM among all the isomers.[26]

[B] Anderson-Evans POM: J. S. Anderson suggested Anderson POM or Anderson-Evans POM structure in the year 1937, which was confirmed later in 1974 by Evans.[23b] Anderson-Evans POM has the general formula of $[H_y(XO_6)(OH)_6M_6O_{18}]^{n-}$, where X is the heteroatom (in this case, it is generally $Al^{3+}/Cr^{3+}/Fe^{3+}/Te^{6+,}$ *etc.*) and M is addenda atom (transition metal ion in its higher oxidation state such as W^{6+}/Mo^{6+}). Heteroatom in Anderson POM acquires octahedral geometry (XO_6) and is surrounded by six MO_6 units arranging themselves in a ring-like structure, giving a planar arrangement with D_{3d} symmetry (**Figure 1.7.**).

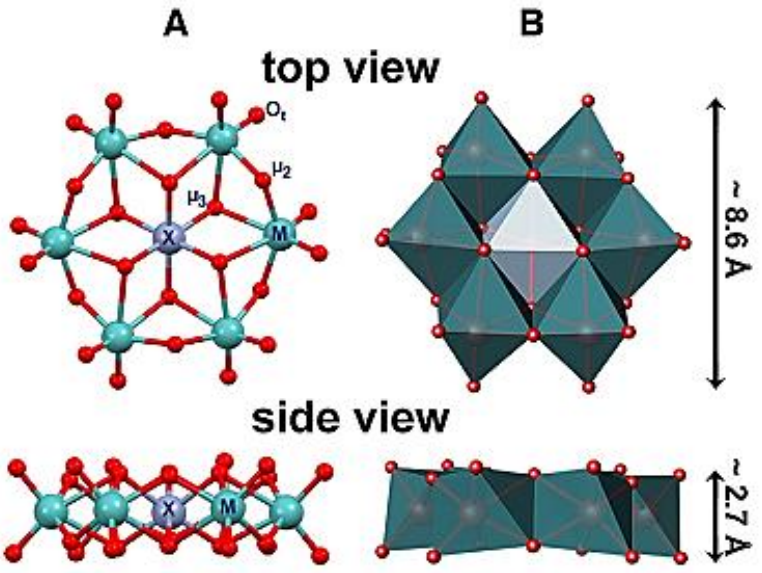

Figure 1.7. Anderson-Evans POM structural description where A represents ball and stick model and B is polyhedral representation from the Top and side view.[14b]

Oxygen uses three different modes of coordination in this structure: bridged oxygens, μ_3-O, and μ_2-O, and *via* terminal oxygen (O_t). Based on the protonation of the structure, Anderson-Evans POM is categorized under two types, namely, protonated Anderson-Evans POM, B-type, and non-protonated Anderson-Evans POM, A-type with the general formula of $[X^{n+}M_6O_{24}]^{(12-n)-}$ and $[X^{n+}(OH)_6M_6O_{18}]^{(6-n)-}$ respectively. A-Type POM has central heteroatom in high oxidation state,

such as Te(VI)/I(VII). In contrast, B-type has central heteroatom in relative lower oxidation states such as Cr(III)/Fe(III), *etc.*[14b]

1.2.2. POM based hybrid compounds: structure and its application

POM-based hybrid compounds are also referred to as an inorganic-organic hybrid of POM unit with either organic ligands or transition metal complexes. This is one of the ways to functionalize polyoxometalates. These hybrids could be both covalently or non-covalently attached to the POM unit. Based on the organic unit's mode of linkage with POM, these hybrids are classified under two categories: type-I and type-II.[27] Type-I hybrids have a non-covalent linkage of organic part/metal complex with the POM unit. These are mostly electrostatic interactions/H-bond/weak interactions. On the contrary, type-II combinations have direct coordination covalent linkage between POM and organic/metal complex counterpart.[27c]

In this thesis work, we have worked with type-II POM hybrids where the metal complex unit is directly linked to the POM unit through a direct covalent bond *via* either terminal or bridged oxygen atom parent POM unit. These hybrids are also addressed as POM supported metal complex. Literature is filled with such systems.[27,28] Even with such rich literature, POM chemistry grows exponentially with still a lot to explore. With its rich electronic structure, POM can be used in various applications for renewable and green energy sources, catalysis, and green chemistry.[29-45]

The polyoxometalate-based hybrid compounds can be efficiently designed and tuned by either altering the organic ligand structure or introducing a different POM anion altogether. The ease of fine-tuning these compounds' structures makes it an excellent choice to design a catalyst and understand the chemistry behind it. Transition metal-based compounds, typically containing Co, Ni, Fe, Cu, are among the few which are highly explored. **Table 1.1.** enlists a few examples of POM supported transition metal complexes (PSTMCs) with Keggin and Anderson type POM anion as POM unit. If we look closely, most PSTMCs are explored for their electrocatalytic behavior in the oxidation of ascorbic acid (AA), reduction of nitrate, and H_2O_2 reduction.[29-49] Apart from these, PSTMCs have also been shown to work well in photocatalysis, medicinal chemistry, molecular magnetism, proton conduction, materials chemistry, *etc.*[28] Features of PSTMCs that make it so versatile are POM and metal complex conjugation, causing the electron

transfer facile. Designing PSTMCs is also among the ones that allow the highly soluble (in water) POM molecule to become insoluble by making it heterogeneous. As per the literature, Keggin type POM makes a higher percentage among other types of POM anion known in the literature for PSTMCs (**Figure 1.8.**).

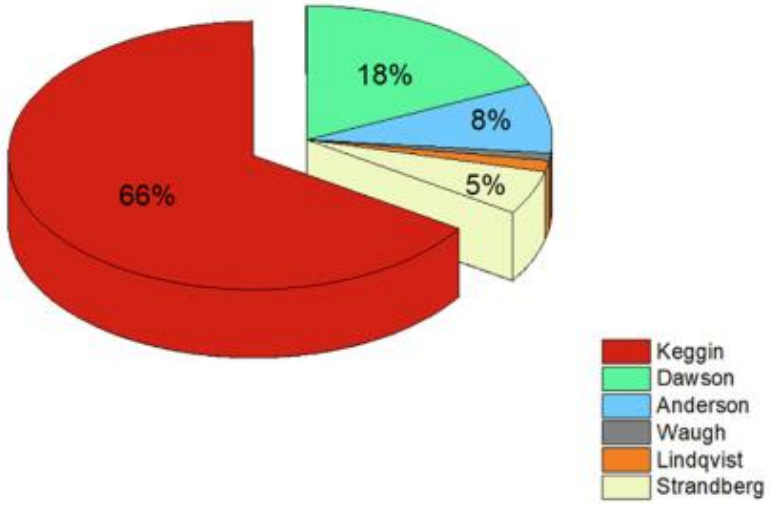

Figure 1.8. The available literature on PSTMCs involving different POM unit.[16b]

Table 1.1. PMSTMCs: Structural formula and its application

S.No.	Compound	Application	Ref
1.	$H\{Co_2(Hpyttz\text{-}I)_2(H_2O)_6[CrMo_6(OH)_6O_{18}]\}.8H_2O$	Electrocatalyst for reduction of H_2O_2 and BrO_3^- ions	29
2	$[Ag_6(btp)(pyttz)_6\cdot(HSiMo_{12}O_{40})_2]\cdot 4H_2O$	Esterification (as a catalyst)	30
3.	$[\{Cu^I(pyr)_2\}_6(As_2Mo_6O_{26})]\cdot H_2O$	Electrocatalyst for AA oxidation and NO_2^- reduction	31
4.	$\{Ag_8O(Htrz)_4(4,4'\text{-}bpy)_2\}\{AgPMo_{12}O_{40}\}$	Electrocatalyst for reduction of H_2O_2 and BrO_3^- ions.	32
5	$[Ag_4(pz)_6(SiW_{12}O_{40})\cdot H_2O]$	Photocatalytic dye degradation of RhB	33
6.	$[Ni(Htib)_4][PW_{12}O_{40}]_2$ and $[Nitib]_2(H_2O)_4](GeW_{12}O_{40})\cdot 2H_2O$	Electrocatalyst for AA oxidation and NO_2^- reduction	34
		Photocatalytic dye	35

7.	{Zn(Htib)(tib)$PMo_{12}O_{40}$}	degradation of RhB	
8.	$K_{10}H_2[Ni_5(OH)_6(OH_2)_3(Si_2W_{18}O_{66})]\cdot 34H_2O$	Photochemical WO	36
9.	$Na_{24}[Ni_{12}(OH)_9(CO_3)_3(PO_4)(SiW_9O_{34})_3]\cdot 56H_2O$ $Na_{25}[Ni_{13}(H_2O)_3(OH)_9(PO_4)_4(SiW_9O_{34})_3]\cdot 50H_2O$ $Na_{50}[Ni_{25}(H_2O)_2OH)_{18}(CO_3)_2(PO_4)_6(SiW_9O_{34})_6]\cdot 85H_2O$	photochemical WO	37
10.	$[Cu_2(btc)_{4/3}(H_2O)_2]_6[H_nXM_{12}O_{40}]\cdot(C_4H_{12}N)_2$ (X=Si, Ge, P, As; M=W, Mo)	Ester hydrolysis	38
11.	$[Cd(en)_2]_2[(en)_2Cd_2Si_8V_{12}O_{40}(OH)_8(H_2O)_{0.5}]\cdot 5H_2O$	Styrene oxidation	39
12.	$(HTEA)_2\{[Na(TEA)_2]H[SiW_{12}O_{40}]\}\bullet 5H_2O$, $(HTEA)_2\{[Na(TEA)_2][PW_{12}O_{40}]\}\bullet 5H_2O$ and $(HTEA)_2\{[Na(TEA)_2]H[GeW_{12}O_{40}]\}\bullet 4H_2O$ (TEA = triethanolamine)	Photocatalytic HER	40
13.	$\{[Co^{II}(2,2'\text{-bpy})]_2[PMo^{V}_4Mo^{VI}_8O_{40}]\}^{3-}$ (**Figure 1.9.**)	Photocatalytic OER	41
14.	$Na_{10}[Co_4(H_2O)_2(VW_9O_{34})_2]\cdot 35H_2O$	Photocatalytic OER	42
15.	$[\{Ru_4O_4(OH)_2(H_2O)_4\}(\gamma\text{-}SiW_{10}O_{36})_2]^{10-}$	Photocatalytic OER	43
16.	$[Co_4(H_2O)_2(PW_9O_{34})_2]^{10-}$	Photocatalytic OER	44
17.	$Na_{10}[Mn_4(H_2O)_2(VW_9O_{34})_2]$	Photocatalytic OER	45
18.	$\alpha\text{-}K_6Na[\{Ru_3O_3(H_2O)Cl_2\}(SiW_9O_{34})]\cdot 17H_2O$	Photocatalytic OER	46

19.	$[\{Co(H_2O)_3\}_2\{CoBi_2W_{19}O_{66}(OH)_4\}]^{10-}$	Photocatalytic OER	47
20.	$[H_5O_2][imi]_4\,[BW_{12}O_{40}]\cdot nH_2O$	Nitrite reduction and photocatalytic methylene blue degradation.	48
21.	$[Cd(C_2H_8N_2)_2]_2\{[Cd(C_2H_8N_2)]_2[Ge_8V_{12}O_{40}(OH)_8](H_2O)\}\cdot 7H_2O$	Nitrite reduction	49

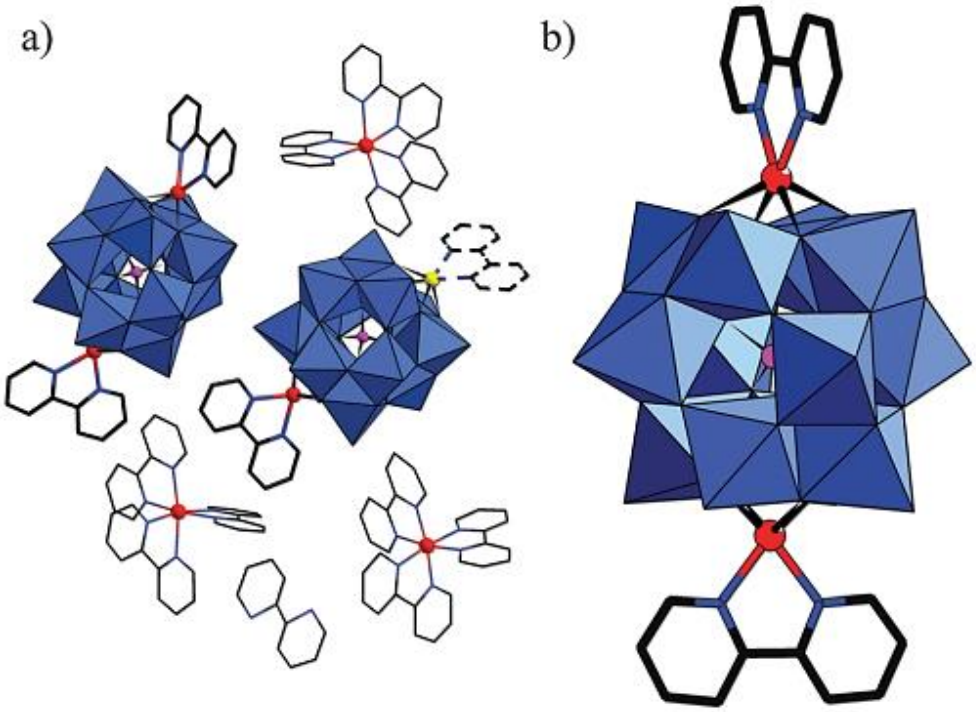

Figure 1.9. (a) Co complex supported on POM unit. (b) Bicapped Keggin structure with Co(2,2´-bpy) unit coordinated to POM unit.[41]

1.2.2.1. POMs and its related hybrid structures as an electrocatalyst for Oxygen Evolution Reaction (OER)

Polyoxometalate, owing to its rich redox chemistry and the scope to introduce more redox-active metals, makes it suitable for designing new catalysts for various electrocatalytic processes. The initial success observed with sandwiched POM and transition metal substituted POM towards photocatalytic OER encouraged to explore the similar compounds for electrocatalytic OER.

Shan and his co-workers in the year 2010, synthesized PSTMC, $[Hpy]_2\{[Co(4,4'\text{-}bpy)_2(H_2O)_2][SiCoW_{11}O_{39}]\}$ which in the presence of $[Ru(2,2'\text{-}bpy)_3]^{3+}$, catalyzed OER under acidic condition (pH=4.5). This work showed the synergistic effect between Ru-salt and POM hybrid compounds, resulting in OER activity.[50]

In 2018, Yong Ding and his co-worker reported a homogeneous Cu(II)-substituted POM, $[(\alpha\text{-}SbW_9O_{33})_2Cu_3(H_2O)_3]^{12-}$, which acts as an electrocatalyst for WO under neutral pH.[51] This was shown to have stability for over 100 cycles and from 2.5 h of CPE measurements without the formation of any CuO_x, confirming the true nature of catalyst to be the POM itself.

Initially, POM based sandwiched compounds were synthesized and explored for both electro/photocatalytic water oxidation. These sandwiched compounds generally have M_nO_n or $M_n(OH_2)_n$ core, where M is transition metal (M=Co/Ni/Mn/Ru), sandwiched between either two Keggin POM units or Wells-Dawson type of POM. These are the most common and highly explored POM units known as WOC.

Shanon and Co-workers in 2004 showed the sandwiched POM, $[Ru_2Zn_2(H_2O)_2(ZnW_9O_{34})_2]^{14-}$, as an efficient electrocatalyst for OER under mild basic condition (phosphate buffer, pH 8). Ru-based sandwiched compounds exhibited great result in both electrochemical and photochemical OER.[52]

In this regard, G.R. Patzke and her co-workers & Hill and his co-workers have contributed significantly.[46,47] In the year 2012, an interesting sandwiched compound, $[Co_4(H_2O)_2(PW_9O_{34})_2]^{10-}$, showing electrocatalytic water oxidation remained under conflict on the nature of the catalyst for OER, a true catalyst or mere precatalyst for the formation of CoO_x. C. L. Hill and his co-workers finally solved this conflict in the year 2013, confirming $[Co_4(H_2O)_2(PW_9O_{34})_2]^{10-}$ as molecular catalyst barring all the allegation of formation of CoO_x in the course of WOC.[42-45] This is a rarest case of POM based WOC was successfully experimentally proven to be stable under the catalytic WO conditions.

Following this work, a nona-cobalt-based POM compound with the molecular formula of $\{Co_9(H_2O)_6(OH)_3(HPO_4)_2(PW_9O_{34})_3\}^{16-}$ (=$\{Co_9\}$). $\{Co_9\}$ exhibited electrocatalytic OER activity, but when studied closely to understand the nature of the true catalyst, it was found that there was leaching of Co^{2+} ions forming CoO_x layers on the working electrode. Thus, $\{Co_9\}$ was

found to be precatalyst for the formation of CoO_x under the electrochemical condition for catalyzing WO.[53]

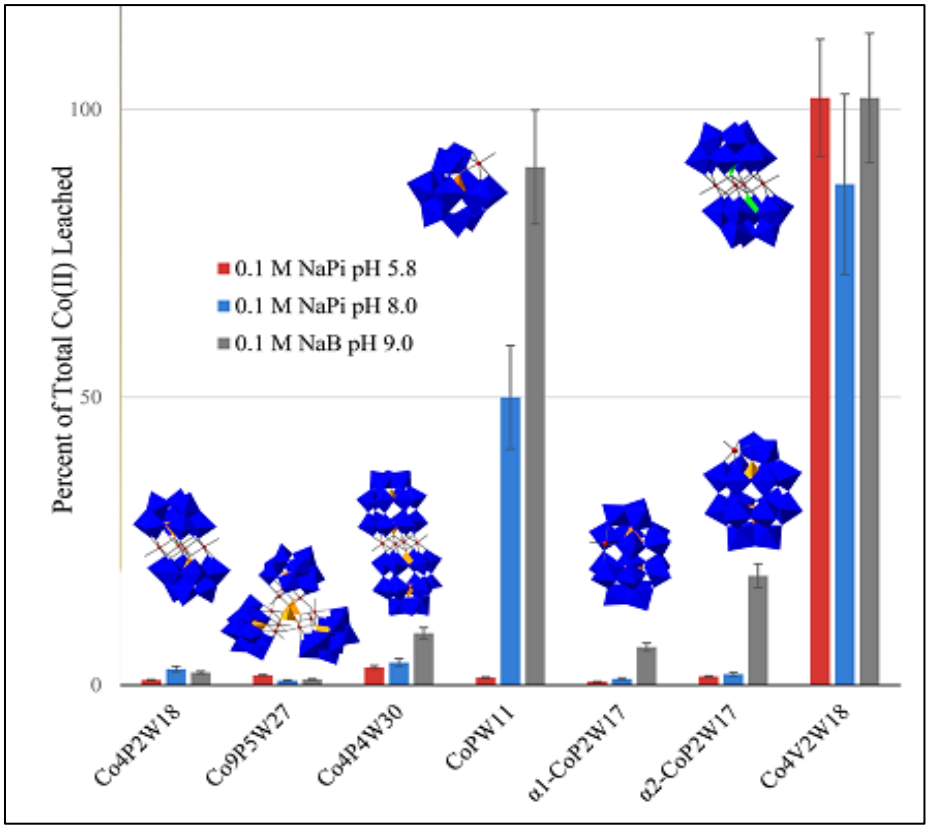

Figure 1.10. Comparison of Percent of total cobalt from different Co-POM (500 μM), present in solution under different pH conditions after 3 h of aging [0.1 M NaPi with pH= 5.8 (red) and pH = 8.0 (blue), as well as in 0.1 M NaB pH = 9.0 (gray)].[54a]

Even though, some of the TM substituted POM and POM-based sandwiched compounds showed promising results towards catalyzing WO electrochemically, there were constant questions on the catalyst's true nature.[54] Most of the polyoxometalates, as we know them, are stable under acidic conditions. The range of pH of its stability varies from one kind of POM molecule to the other. Alkaline medium or higher pH and high oxidizing potential under which these POMs or POM based molecules showed OER activity might result in structural disintegration of POM and POM based compounds, thereby raising questions on the stability of POM under electrocatalytic OER conditions (**Figure 1.10.**).[54c,54d] There is massive conflict in terms of the stability of POMs for WOC. POMs, generally Keggin type or those derived from Keggin structure, are stable in an acidic medium. As pH starts to move up on the scale, the $\{WO_3\}$ unit starts to leave and finally disintegrating the whole POM molecule into its corresponding metal oxides. Under

electrochemical conditions, the stability of POMs becomes an issue that raises the question of the true nature of the catalyst and the role of POM in it.

The issues of catalyst stability under OER conditions persisted for the catalysts designed from transition-metal complexes. Some of them were known to act as a pre-catalyst for OER. One of the approaches to solve the stability issue is to use the guest-host chemistry by trapping the metal complex/POM into MOF's cavity. In 2016, our group showed that the Co^{II}-aqua mononuclear complex trapped inside the MOF cavity showing exceptional results as an OER catalyst with high stability and low overpotential of 390 mV in alkaline pH (pH-13).[55]

Inspired by our group's result and determined to solve the issue of the stability under electrochemical WO condition, we thought of merging POM and metal complex both by synthesizing TMSPOM and utilizing the TM for WO. These hybrids are known to be much more stable than its parent constituent. By designing such a catalyst, we would be able to incorporate all the POM properties, which should help us develop a better catalyst.

POM supported TM complexes are not well exploited in this regard. The first report we found was in the year 2016 by Wang group showing electrocatalyst WO by three different PSTMC with similar transition metal complexes and different POM unit.[56] They reported four different TMSPOM (1-4), formulated as $[Ni(2,2\text{-bpy})_3]_5[PW_{11}NiO_{39}(H_2O)]_2 1.08H_2O$ (**1**), $[Ni(2,2\text{-bpy})_3]_{1.5}[Ni(2,2\text{-bpy})_2(H_2O)BW_{12}O_{40}]$ (**2**), $\{[Ni(2,2\text{-bpy})_3]_{1.5}[Ni(2,2\text{-bpy})_2(H_2O)GeW_{12}O_{40}]\}^-$ (**3**), and $\{[Ni(2,2\text{-bpy})_3]_{1.5}[Ni(2,2\text{-bpy})_2(H_2O)PW_{12}O_{40}]\}_2$ (**4**). Out of these four compounds, compounds **1**, **2**, and **4** were studied for electrochemical WO under basic conditions (pH=8) (**Figure 1.11.**). These compounds showed an overpotential of 591, 632, and 616 mV for 1/2/4-CPE, respectively. This report lacks information about the kinetics and plausible mechanism. This work only gave the possibility of such a compound to act as an electrocatalyst but lacks any in-depth information for the same. TMSPOMs have rich literature but are not explored in the field of electrochemical WO. These compounds are highly tunable, adds the overall compound's stability, and the synergistic effect adds to the value-added property to the overall stability.

The lack of literature and the previous reports by our group showing the importance of mono-aqua ligand in designing the WOC motivated us to pursue this path in quest of developing more WOCs.

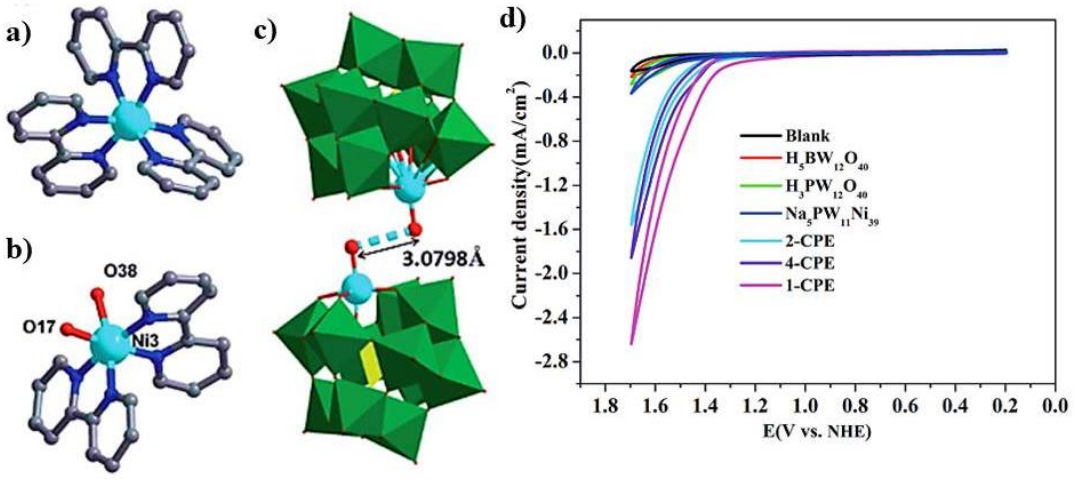

Figure 1.11. (a) & **(b)** represents $[Ni^{II}(2,2\text{-bpy})_3]^{2+}$ and $[Ni^{II}(2,2\text{-bpy})_2OH_2O]^{2+}$ units respectively. **(c)** Core shell structure consisting of $[PW_{11}NiO_{39}(H_2O)]_2$ unit. Color code: P (yellow), W (green), B (pink), Ni (light blue), C (gray), O(red), N (blue). **(d)** Cyclic Voltammograms of a blank GC electrode, different POMs and their hybrid (1/2/4-CPE) in 0.2 M sodium borate buffer (pH-8).[56]

1.2.2.2. POM and its related hybrid structures as an electrocatalyst for Hydrogen Evolution Reaction (HER)

POM owing to its particular archetype, as stated in the above section, also contributes substantially to catalyzing HER at different pH ranges. POMs, as such, have befitted as an apt candidate for catalyzing both photocatalytic and electrocatalytic HER. Following are different types of POM based compounds employed for electrocatalytic HER activity: 1.POM-based hybrid structures, 2.POM supported metal complexes, or TM substituted POM compounds, 3. POMOF or POM based composite using different supporting materials and 4.POM derived metal oxides/sulphides/nitrides.[57-60]

Over the last few decades, POM has attracted significant attention in sustainable energy research. Till now, POM-based electrocatalysts have been under constant surveillance for electrochemical water oxidation/reduction owing to its stability issue, as explained in the previous section. Scientists figured out different approaches to utilize POM properties for the OER/HER catalysis by creating different hybrids and composites. Low HOMO-LUMO gap enables fast electron transfer, plus the oxygen atoms coordinated to the addenda atoms are relatively basic, which helps in the catalysis. There is a synergistic effect between POM and the group, directly coordinated to it or the composite prepared using POM molecule as parent base.

In the year 2007, Louis Nadjo and his co-workers used different polyoxometalates for activating glassy carbon electrode for the HER activity.[61] POM was either adsorbed directly on the electrode surface or entrapped in the polyvinylpyridine films of the electrode. Polyoxometalates taken for this study were $[H_7P_8W_{48}O_{184}]^{33-}$, $[Co_6(H_2O)_{30}\{Co_9Cl_2(OH)_3(H_2O)_9(\beta\text{-}Si\text{-}W_8O_{31})_3\}]^{5-}$ and $[\{Co_3(B\text{-}\beta\text{-}SiW_9O_{33}(OH))(B\text{-}\beta\text{-}Si\text{-}W_8O_{29}OH)_2\}_2]^{22-}$. In this work, they have shown the importance of the microenvironment around the electrode for HER activity. Electrodes modified with POM exhibited excellent results for HER due to the electron and proton-rich nature of POMs. Following this work, the scientific community started designing various methodologies to incorporate POM for developing the catalyst for HER.

POM based metal-organic frameworks (POMOFs) gained popularity for exhibiting various exciting properties.[62] In 2011, Nohra *et al.* synthesized three new novel POMOFs using ε-Keggin as a building block.[62a] These POMOFs showed exceptionally high TOF with low overpotential. The presence of POM, high porosity of POMOF, and the use of conjugated ligand for the connection with POM unit are all decisive factors for the exceptional results seen for HER catalysis.

The last few years have seen advancement in POM usage for developing composite materials for electrocatalytic HER. One such approach used different electroactive materials onto POM material to facilitate the overall composite's stability for the HER activity. M.-R. Gao & S.-H. Yu and their co-workers recently implemented this methodology by linking the POM molecule to the cobalt diselenide nanobelt's surface.[63] This showed exceptional results in terms of stability of $CoSe_2$ with the overpotential of 187 mV to obtain a current density of 10 mA/cm^2.

Utilizing POM or POM based hybrid compounds as the precursor for developing electroactive materials has recently shown quite a few reports. H. Ma and H. Pang and their co-workers utilized a POM-based hybrid compound to prepare the bimetallic sulfides containing Ni_3S_2–MoS_2 and CoS_2–MoS_2 having mesoporous structure.[64] POM facilitates the easy formation of these bimetallic sulfides, which presented an overpotential of 224 (Ni_3S_2–MoS_2@Carbon Cloth (CC)) and 222 mV (CoS_2–MoS_2@CC) for a current density of 10 mA/cm^2.

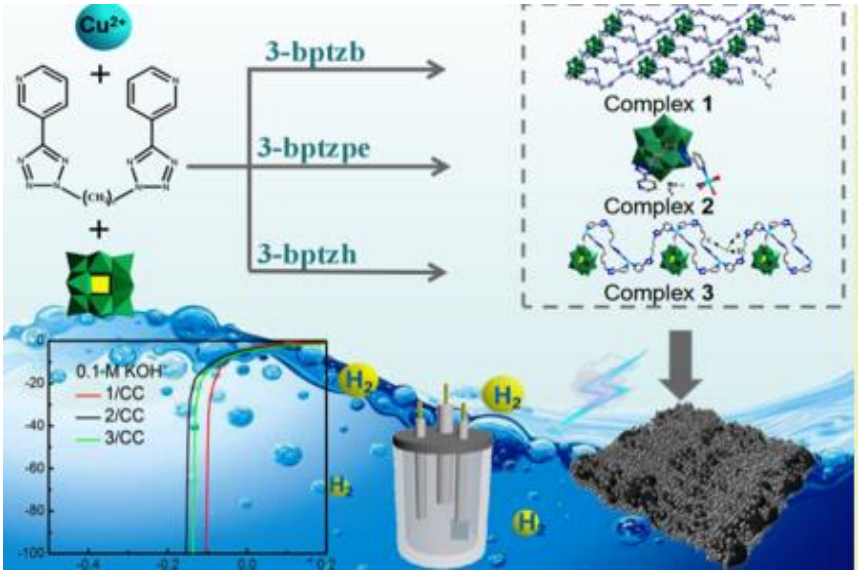

Figure 1.12. Cu-metal complexes coordinated to Keggin POM with high electrocatalytic HER activity.[65a]

With all these advancements and reports of POM based compounds for electrocatalytic HER, there are still very few reports of usage of PSTMCs for electrocatalytic HER. Li and his co-workers synthesized a PSTMC using Lindqvist POM *via* hydrothermal reaction.[65b] The compound synthesized has the formula of $[Cu_2(bimb)_2(ox)(W_6O_{19})]\cdot 4H_2O$, where bmib=1,3bis(1-imidazolyl)benzene and ox=oxalic acid. This compound forms a layered structure having complementary charges. This special intercalation is suspected to be responsible for the ease of diffusing the H^+ ions through the pores. Thus, this compound showed high electrocatalytic HER activity with an overpotential of 146 mV at a current density of 10 mA/cm^2.

Recently, Wang and his co-workers designed a series of Cu-complexes on Keggin POM using the hydrothermal method.[65a] These compounds showed the HER activity in acidic and alkaline medium. These compounds were formulated as: $\{Cu_2(3\text{-bptzp})_3(H_2O)_4[SiW_{12}O_{40}]\}\cdot H_2O$ (**1**), $\{Cu_2(3\text{-bptzpe})_2(H_2O)_8[SiW_{12}O_{40}]\}\cdot 4H_2O$ (**2**), and $\{Cu_2(3\text{-bptzh})_3(H_2O)_6[SiW_{12}O_{40}]\}$ (**3**) (**Figure 1.12.**). Compound (**1**) showed the lowest overpotential of 59.4 mV for electrocatalytic HER in 0.1 M KOH with a current density of 10mA/ cm^2. This is the lowest value of overpotential reported to date by any POM based electrocatalyst for HER activity.

These reports in the literature for POM based electrocatalysts emphasize the importance of structure in designing a better electrocatalyst for HER. With the nudge to understand the POM

unit's role for HER activity, we have developed different PSTMC using Keggin and Anderson-Evans POM (discussed in **Chapters 3-5**) and explained their function.

1.3. Motivation of the work

Water splitting (WS) could be the answer to the biggest question of sustainable energy. The importance of developing a catalyst for WS, working in this direction, and exploring a new molecule is a step towards a sustainable lifestyle. WS with its constituent reactions *viz.* OER and HER both have their pitfall and needs to be addressed.

Motivated from our group's previous reports for OER catalyst where mono-nuclear aqua Co-complex trapped into MOF's cavity showed exceptional results, we designed various reactions to develop PSTMCs having aqua ligand coordinated to it. Our primary focus in these projects was to look into POM's importance in different PSTMC for OER and HER. The scarcity of literature on PSTMC for electrocatalytic OER and HER is one of the primary reasons to pursue the work in this direction. PSTMCs have excellent properties, with the ease of tunability for such compounds being an added benefit when looking closely into the reaction mechanism for OER/HER.

In this thesis work, we have synthesized a few new POM supported metal complexes (PSTMCs), and a few of them are those reported earlier by our group, to study the role of POM in the overall catalysis process. We started our work from Ni-2,2´-bpy-complex supported on Keggin POM as a water oxidation catalyst (**Chapter 2**). Following a similar synthetic protocol in the next chapter, we have studied the effect of change in transition metal complex on its electrochemical activity (**Chapter 3**). This led to two new POM-supported complexes, which have Cu-2,2´-bpy complex coordinating to it. This mere replacement of transition metal leads to a change in the property as these compounds show water reduction rather than oxidation. This study intrigued us to look into POM's role in OER/HER activity, which led to the next project discussed in **Chapters 4** and **5** where Anderson-type of POM substituted transition metal complex was studied towards electrocatalytic HER activity.

Thus, to sum up, this thesis work, we have designed the projects to understand the role of both transition metal and POM in a PSTMC for electrocatalytic OER and HER.

1.4. References

1. Statistical Review of World Energy, **2020** 69th edition.
2. Energy Transitions: Global and National Perspectives. & BP Statistical Review of World Energy, **2019**.
3. US EIA, International Energy Outlook 2019 (IEO2019) Key Takeaways. *Int. Energy Outlook* **2019**, IEO2019.
4. Qazi, A.; Hussain, F.; Rahim, N. A.; Hardaker, G.; Alghazzawi, D.; Shaban, K.; Haruna, K. Towards Sustainable Energy : A Systematic Review of Renewable Energy Sources , Technologies , and Public Opinions. *IEEE Access*. **2019**, *7*, 63837-63851.
5. Kumar, S. S.; Himabindu, V.; Materials Science for Energy Technologies Hydrogen production by PEM Water Electrolysis – A review. *Mater Sci. Energy Technol*. **2019**, *2*, 442-454.
6. Carmo, M.; Fritz, D. L.; Mergel, J.; Stolten, D. A Comprehensive Review on PEM Water Electrolysis. *Int J. Hydrogen Energy*. **2013**, *38*, 4901-4934.
7. (a) Song, Z.; Zhou, H. Towards Sustainable and Versatile Energy Storage Devices: An Overview of Organic Electrode Materials. *Energy Environ Sci.* **2013**, *6*, 2280-2301. (b) Kan, W. H.; Samson, A. J.; Thangadurai, V. Trends in Electrode Development for Next Generation Solid Oxide Fuel Cells. *J Mater Chem A.* **2016**, *4*, 17913-17932. (c) Yabuuchi, N.; Komaba, S. Recent Research Progress on Iron- and Manganese-based Positive Electrode Materials for Rechargeable Sodium Batteries. *Sci. Technol. Adv. Mater.* **2014**,*15*, 43501-43530. (d) Geng, J.; Bonnet, J. P.; Renault, S.; Dolhem, F.; Poizot, P. Evaluation of Polyketones with N-cyclic Structure as Electrode Material for Electrochemical Energy Storage: Case of Tetraketopiperazine Unit. *Energy Environ Sci.* **2010**, *3*, 1929-1933. (e) Oltean, V. A.; Renault, S.; Volvo, M.; Brandell, D. Sustainable Material for Sustainable Energy Storage: Organic Na Electrodes. *Materials*, **2016**, *9*, 142-169.
8. (a) Zheng, J. Lochala, J. A.; Kwok, A.; Deng, Z. D.; Xiao, J. Research Progress Towards Understanding the Unique Interfaces between Concentrated Electrolytes and Electrodes for Energy Storage Applications. *Adv Sci.* **2017**, *4*, 1-19. (b) Meng, Q.; Cai, K.; Chen, Y.; Chen, L.; Research Progress on Conducting Polymer Based Supercapacitor Electrode Materials. *Nano Energy.* **2017**, *36*, 268-285. (c) Dyatkin, B.; Presser, V.; Heon, M.; Lukatskaya, M. R.; Beidaghi, M.; Gogotsi, Y. Development of a Green Supercapacitor Composed Entirely of Environmentally Friendly Materials. *ChemSusChem*. **2013**, *6*, 2269-2280. (d) Navale, S. T.; Mali, V. V.; Pawar, S. A.; Mane, R. S.; Naushad, M.; Stadlerd, F. J.; Patil, V. B. Electrochemical Supercapacitor Development Based on Electrodeposited Nickel Oxide Film. *RSC Adv.* **2015**, *5*, 51961-51965.

(e) Chang, S. K.; Zainal, Z.; Tan, K. B.; Yusof, N. A.; Yusoff, W. M. D. W.; Prabaharan, S. R. S. Recent Development in Spinel Cobaltites for Supercapacitor Application. *Ceram Int.* **2015**, *41*, 1-14. (f) Karandikar, P. B.; Talange, D. B.; Mhaskar, U. P.; Bansal, R. Development, Modeling and Characterization of Aqueous Metal Oxide Based Supercapacitor. *Energy***. 2012**, *40*, 131-138.

9. (a) Chen, H.; Armand, M.; Demailly, G.; Dolhem, F.; Poizot, P.; Tarascon, J. M. From Biomass to a Renewable $Li_XC_6O_6$ Organic Electrode for Sustainable Li-ion Batteries. *ChemSusChem.* **2008**, *1*, 348-355. (b) Ma, T.; Yang, H.; Lu, L. Development of Hybrid Battery-Supercapacitor Energy Storage for Remote Area Renewable Energy Systems. *Appl Energy.* **2015**, *153*, 56-62. (c) Akram, U.; Khalid, M.; Shafiq, S. An Innovative Hybrid Wind-Solar and Battery-Supercapacitor Microgrid System—Development and Optimization. *IEEE Access.* **2017**, *5*, 25897-25912.
10. Abioye, A. M.; Nasir, F. Recent Development in the Production of Activated Carbon Electrodes from Agricultural Waste Biomass for Supercapacitors : A Review. *Renew Sustain Energy Rev*. **2015**, *52*, 1282-1293.
11. Møller, K. T.; Jensen, T. R.; Akiba, E.; Li, H.-W. Hydrogen - A sustainable energy carrier, Progress in Natural Science: Materials International, **2017**, *27*, 34-40.
12. Turner, J.A. (1999). A Realizable Renewable Energy Future. *Science*, **1999**, *285*, 687-689.
13. (a) Markovic, N. M.; Sarraf, S. T.; Gasteigert, H. A.; Ross Jr., P. N. Hydrogen Electrochemistry on Platinum Low-Index Single-Crystal Surfaces in Alkaline Solution *J. Chem. SOC., Faraday Trans.*, **1996**, *92*, 3719-3725. (b) Kim, J.; Kim, H.; Lee, W.-J.; Baik, B.-R. H.; Oh, H.-S.; Paek, S.-M.; Lim, H.-K.; Choi, C. H.; Choi, S. Theoretical and Experimental Understanding of Hydrogen Evolution Reaction Kinetics in Alkaline Electrolytes with Pt-Based Core−ShelL Nanocrystals. *J. Am. Chem. Soc.* **2019**, *141*, 18256−18263.
14. (a) Yamase, T. Photo- and Electrochromism of Polyoxometalates and Related Materials. *Chem Rev*. **1998**, *98*, 307-325. (b) Blazevic, A.; Rompel, A. The Anderson-Evans Polyoxometalate: From Inorganic Building Blocks *via* Hybrid Organic-Inorganic Structures to Tomorrows "Bio-POM." *Coord. Chem. Rev*. **2016**, *307*, 42-64. (c) Pope, M. T.; Sadakane, M.; Kortz, U. Celebrating Polyoxometalate Chemistry. *Eur J Inorg Chem*. **2019**, *3*, 340-342. (d) Miras, H. N.; Yan, J.; Long, D. L.; Cronin, L. Engineering Polyoxometalates with Emergent Properties. *Chem Soc Rev*. **2012**, *41*, 7403-7430.
15. (a) Long, D. L.; Tsunashima, R.; Cronin, L. Polyoxometalates: Building Blocks for Functional Nanoscale Systems. *Angew Chemie - Int Ed*. **2010**, *49*, 1736-1758. (b) Long, D. L.; Burkholder, E.; Cronin, L. Polyoxometalate Clusters, Nanostructures and Materials: From Self Assembly to Designer Materials and Devices. *Chem Soc Rev*. **2007**, *36*, 105-121. (c) Katsoulis, D. E. A Survey of Applications of Polyoxometalates. *Chem Rev*. **1998**, *98*, 359-387. (d) Izzet, G.;

Volatron, F.; Proust, A. Tailor–made Covalent Organic-Inorganic Polyoxometalate Hybrids: Versatile Platforms for the Elaboration of Functional Molecular Architectures. *Chem Rec*. **2017**,*17*, 250-266.

16. (a) Casan-Pastor, N.; Gomez-Romero, P. Polyoxometalates: from Inorganic Chemistry to Materials Science. *ChemInform*. 2005;36(16). (b) Li D, Ma P, Niu J, Wang J. Recent advances in transition-metal-containing Keggin-type polyoxometalate-based coordination polymers. *Coord Chem Rev*. 2019;392:49-80. (c) Proust, A.; Matt, B.; Villanneau, R.; Guillemot, G.; Gouzerh, P.; Izzet, G. Functionalization and Post-Functionalization: A Step Towards Polyoxometalate-Based Materials. *Chem Soc Rev*. **2012**, *41*, 7605-7622.
17. (a) Cui FY, Ma XY, Li C, et al. Two New Organic-Inorganic Hybrid Compounds Based on Metal-Pyrazine Coordination Polymers and Keggin Polyoxometalates: Effect of Metal Ions on the Structure. *J. Solid State Chem.* **2010**, *183*, 2925-2931. (b) Bu, Y.; Liu, R.; Zhen, M.; Li, F.; Sun, Z.; Xu, L. A Hybrid Compound Containing Polyoxoanions and Organic Dye Cations with Visible-Light Photocatalytic H_2 Evolution Activity. *Inorg Chem. Commun*. **2015**, *62*, 34-36. (c) Li, M. X.; Zhang, Y.; Zhu, Z. M.; Su, F.; Zhang, L. C.; Sang, X. J. Synthesis, Characterization and Electrocatalytic Properties of two New Open Wells-Dawson-type Tungstosilicates. *J. Coord. Chem.* **2020**, 0, 1-13. (d) Walsh, J. J.; Bond, A. M.; Forster, R. J.; Keyes, T, E. Hybrid Polyoxometalate Materials for Photo(electro-) *Chemical Applications. Coord. Chem. Rev.* **2016**, *306*, 217-234.
18. (a) Hajizadeh, F.; Zonoz, F. M.; Duval, S.; Maleki, B.; Amiri, A.; Synthesis and Investigation of two New Crystalline Organic Inorganic Nano-Hybrids Based on Wells-Dawson Vanadotungstates and 1H-1, 2, 4-triazole as Electro- and Photocatalysts. *J. Mol. Struct.* **2021**;*1224*, 129003-129013. (b) Niu, J.-Q.; Zhao, Q.; Xin, X.; Zhang, Y.-Q.; Hu, N.; Ma, Y.-Y.; Han, Z.-G. Krebs-type Polyoxometalate-based Crystalline Materials: Synthesis, Characterization and Catalytic Performance. *J. Coord. Chem.* **2020**, *73*, 2391-2401. (c) Ye, J. J.; Wu, C. De. Immobilization of Polyoxometalates in Crystalline Solids for Highly Efficient Heterogeneous Catalysis. *Dalton Trans.* **2016**, *45*, 10101-10112. (d) Lefebvre, F. Chapter 11 - Polyoxometalates Encapsulated in Inorganic Materials: Applications in Catalysis. Editor(s): Suib, S. L. New and Future Developments in Catalysis, *Elsevier*, **2013**, 265-288.
19. (a) Scheele, C. W.; in Niederwalluf/Wiesbaden (reprint: original **1793**), ed. M. Sändig, **1971** (b) Gouzerh, P.; Che, M. From Scheele and Berzelius to Murller. Polyoxometalates (POMs) Revisited and the "Missing Llink" Between the Bottom up and top Down Approaches *Actual. Chim.* **2006**, *298*, 9–22.
20. (a) Berzelius, J. J. *Poggend. Ann. Phys. Chem.*, **1826**, *6*, 369. (b) Svanberg, L.; Struve, H. *Justus*

Liebigs Ann. Chem., **1848**, *68*, 209–218. (c) Marignac, J.-C. G. d. *Ann. Chim. Phys*., **1864**, *4*, 1.

21. (a) Struve, H. J. *Prakt. Chem*., **1854**, *61*, 449 (b) Werner, A. *Z. Anorg. Chem*., **1893**, 267. (c) Miolati, A.; Pizzighelli, R. *J. Prakt. Chem.*, **1908**, *77*, 417–456. (d) Rosenheim, A.; Jaenicke, J. *J. Prakt. Chem.*, **1917**, *100*, 304. (e) Pauling, L. The Principles Determining the Structure of Complex Ionic Crystals. *J. Am. Chem. Soc.*, **1929**, *51*, 1010–1026.
22. (a) Lindqvist, I. *Arkiv Kemi*, **1950**, *2*, 349–355. (b) Friedrich, W.; Knipping, P.; Laue, M.; *Sitzungsber. K. Bayer. Akad. Wiss. Math. Phys. Kl.*, **1912**, 303–322. (c) Laue, M. *Phys. Z.*, **1913**, *14*, 1075–1079. (d) Bragg, W. H. X-rays and Crystals. *Nature*, **1912**, *90*, 219. (d) Fuchs, J.; Knopnadel, I. Crystal Structure of Disodium Tetramethylammonium Octamolybdate Dihydrate ($Na_2[N(CH_3)_4]_2Mo_8O_{26}.2H_2O$) and the relation between molybdenum-oxygen distance and bond order in polymolybdates *Z. Kristallogr. Kristallgeom. Kristallphys. Kristallchem.*, **1982**, *158*, 165.
23. (a) Keggin, J. F. Structure of the Crystals of 12-Phosphotungstic Acid. *Nature*, **1933**, 132, 351. (b) Anderson, J. S. Constitution of the Poly-acids. *Nature*, **1937**, *140*, 850. (c) Evans, H. T. The Crystal Structures of Ammonium and Potassium Molybdotellurates J. *Am. Chem. Soc.*, **1948**, *70*, 1291–1292. (d) Evans, H. T. Refined molecular structure of the heptamolybdate and hexamolybdotellurate ions. *J. Am. Chem. Soc.*, **1968**, *90*, 3275–3276. (e) Evans, H. T. The Molecular Structure of the Hexamolybdotellurate ion in the Crystal Complex with Telluric acid $(NH_4)_6[TeMo_6O_{24}].Te(OH)_6.7H_2O$ *Acta Crystallogr., Sect. B: Struct. Crystallogr. Cryst. Chem.*, **1974**, *30*, 2095–2112.
24. (a) Fuchs, J.; Hartl, H. Anion Structure of Tetrabutylammonium Octamolybdate $[N(C_4H_9)_4]_4Mo_8O_{26}]$. *Angew. Chem., Int. Ed. Engl.*, **1976**, *15*, 375–376. (b) Gouzerh, P.; Proust, A. Main-Group Element, Organic, and Organometallic Derivatives of Polyoxometalates. *Chem. Rev.*, **1998**, *98*, 77–111. (c) Song, Y.-F.; Long, D.-L.; Cronin, L. *Angew. Chem., Int. Ed.*, **2007**, *46*, 3900–3904. (e) Song, Y.-F.; Long, D.-L.; Kelly, S. E.; Cronin, L. Sorting the Assemblies of Unsymmetrically Covalently Functionalized Mn-Anderson Polyoxometalate Clusters with Mass Spectrometry. *Inorg. Chem.*, **2008**, *47*, 9137–9139. (f) Hasenknopf, B.; Delmont, R.; Herson, P.; Gouzerh, P. Anderson-Type Heteropolymolybdates Containing Tris(alkoxo) Ligands: Synthesis and Structural Characterization. *Eur. J. Inorg. Chem*., **2002**, 1081–1087.
25. (a) Marignac, C.; Ann. Chim. Phys. 1864, 3, 5. (b) Matsumoto, K.; Sasaki, Y.; The Crystal Structure of α-$K_8SiW_{11}O_{39}\cdot 13H_2O$. *Bull. Chem. Soc. Jpn.* **1976**, *49*, 156–158. (c) Patel, A.; Narkhede, N.; Singh, S.; Pathan, S. Keggin-type Lacunary and Transition Metal Substituted Polyoxometalates as Heterogeneous Catalysts: A Recent Progress. *Catal. Rev.*, **2016**, *58*, 337-370.

26. (a) Sartzi, H.; Miras, H. N.; Vil-Nadal, L.; Long, D.-L.; Cronin, L. Trapping the δ Isomer of the Polyoxometalate-Based Keggin Cluster with a Tripodal Ligand. *Angew. Chem. Int. Ed.* **2015**, *54*, 15488 –15492. (b) Baker, L. C. W.; Figgis, J. S. A New Fundamental Type of Inorganic Complex: Hybrid between Heteropoly and Conventional Coordination Complexes. Possibilities for Geometrical Isomerisms in 11-, 12-, 17-, and 18-Heteropoly Derivatives. *J. Am. Chem. Soc.*, **1970**, *92*, 3794–3797.
27. (a) Taleghani, S.; Mirzaei, M.; Eshtiagh-Hosseini, H.; Frontera, A. Tuning the Topology of Hybrid Inorganic-Organic Materials Based on the Study of Flexible Ligands and Negative Charge of Polyoxometalates: A Crystal Engineering Perspective. *Coord. Chem. Rev.* **2016**, *309*, 84-106. (b) Qi, W.; Wu, L.; Polyoxometalate/Polymer Hybrid Materials: Fabrication and Properties. *Polym Int.* **2009**, *58*, 1217-1225. (c) Dolbecq, A.; Dumas, E.; Mayer, C. R.; Mialane, P. Hybrid Organic-Inorganic Polyoxometalate Compounds: From Structural Diversity to Applications. *Chem Rev*. **2010**, *110*, 6009-6048. (d) Mirzaei, M.; Eshtiagh-Hosseini, H.; Alipour, M.; Frontera, A. Recent developments in the crystal engineering of diverse coordination modes (0-12) for Keggin-type Polyoxometalates in Hybrid Inorganic-Organic Architectures. *Coord. Chem. Rev.* **2014**, *275*, 1-18. (e) Santoni, M. P.; Hanan, G. S.; Hasenknopf, B. Covalent Multi-Component Systems of Polyoxometalates and Metal Complexes: Toward Multi-Functional Organic-Inorganic Hybrids in Molecular and Material Sciences. *Coord. Chem. Rev.* **2014**, *281*, 64-85.
28. (a) Iturrospe, A.; Felices L. S.; Reinoso, S.; Artetxe, B.; Lezama, L.; Gutiérrez-Zorrilla, J. M. Reversible Dehydration in Polyoxometalate-Based Hybrid Compounds: A Study of Single-Crystal to Single-Crystal Transformations in Keggin-Type Germanotungstates Decorated with Copper(II) Complexes of Tetradentate N-donor Ligands. *Cryst. Growth Des.* **2014**, *14*,2318-2328. (b) Ding, Y.; Chen, H.; Chen, W.; Wang, E.; Meng, J. Synthesis, Structures and Electrochemical Properties of Four Organic-Inorganic Hybrid Polyoxometalates Constructed from Polyoxotungstate Clusters and Transition Metal Complexes. *Transit. Met. Chem.* **2009**, *34*, 281-288. (c) Kumar, N. T.; Bhoi, U.; Naulakha, P.; Das, S. K. A Polyoxometalate Supported Copper Dimeric Complex: Synthesis, Structure and Electrocatalysis. *Inorganica Chim. Acta.* **2020**, *506*, 119554. (d) Jamshidi, A.; Zonoz, F. M.; Wei, Y.; Maleki, B. An Organic-Inorganic Nano-Hybrid Material Containing a Mixed-Addenda Keggin-type Polyoxometalate, Piperazine: Synthesis, Characterization, its Electrochemical Investigation. *Inorganica Chim. Acta.* **2018**, *477*, 233-241.
29. Wang, X.; Bai, X.; Lin, H.; Sun, J.; Wang, X.; Liu, G. A Series of New Polyoxometalate-Based Metal-Organic Complexes with Different Rigid Pyridyl-bis(triazole) Ligands: Assembly,

Structures and Electrochemical Rroperties. *RSC Adv.* **2018**, *8*, 22676-22686.

30. Zhu, P.-P.; Sheng, N.; Liu, G.-D.; Sha, J.-Q.; Yang, X.-Y. Two Keggin Polyoxometalate-Based Hybrid Compounds with Different Helix: Syntheses, Structure and Catalytic Activities. *Polyhedron* **2017**, *131*, 52–58.
31. Zhang, M.; Lv, J.; Yu, K.; Wang, K.; Meng, F.; Zhou, B. An Unusual 2, 12-connected 3-D Open Framework Based on $\{As_2Mo_6O_{26}\}$-type Polyoxometallate and Copper-Pyrazole Complex. *Inorg. Chem. Commun.* **2018**,*97*, 74-78.
32. Wang, C.-J.; Wang, T.-T.; Lan, Q.; Yao, S.; Wu, H.-L.; Zhou, Y.-Y.; Zhang, Z.-M.; Wang, E.-B. Polyoxometalate-Based Supramolecular Architecture Constructed from a Purely Inorganic 1D Chain and a Metal–Organic Layer with Efficient Catalytic Activity *RSC Adv.*, 2016, 6, 15513-15517.
33. Zhou, W.-L.; Liang,J.; Zhao, L.; Wang, X.-L.; Shao, K.-Z.; Su, Z.-M. Hydrothermal Synthesis, Crystal Structure and Properties of a 3D Inorganic–Organic Hybrid Based on Keggin-Type Polyanion and Silver-Pyrazine Circles. *Inorg. Chem. Commun.* **2014**, *147*, 48-51.
34. Zhang, Z.; Sun, X.; Ma, H.; Pang, H.; Li, S.; Zhao, C. Two Hybrid Compounds Constructed From Ni-tris(imidazolyl) Complexes and Keggin Clusters: Syntheses, Structures and Electrochemical Properties. *Journal of Molecular Structure*. **2016**, *1116*, 174-179.
35. Zhang, Z.; Ma, H.; Pang, H.; Zhang, C.; Chai, D.; Hou, Y. A Zn-tib Porous Framework Sandwiched with Keggin Synthesis, Structure, Photocatalytic and Luminescent Properties. *J. solid state chem.*, **2018**, *258*, 170-175.
36. Zhu, G.; Glass, E. N.; Zhao, C.; Lv, H.; Vickers, J. W.; Geletii, Y. V.;. Musaev, D. G.; Song, J.; Hill, C. L. A Nickel Containing Polyoxometalate Water Oxidation Catalyst. *Dalton Trans*., **2012**, *41*, 13043-13049.
37. Han, X.-B.; Li, Y.-G.; Zhang, Z.-M.; Tan, H.-Q.; Lu, Y.; Wang, E.-B. Polyoxometalate-Based Nickel Clusters as Visible Light-Driven Water Oxidation Catalysts. *J. Am. Chem. Soc.* **2015**, *137*, 5486–5493.
38. Sun, C. Y.; Liu, S. X.; Liang, D. D.; Shao, K. Z.; Ren, Y. H.; Su. Z. M. Highly Stable Crystalline Catalysts Based on a Microporous Metal−Organic Framework and Polyoxometalates. *J. Am. Chem. Soc.* **2009**, *131*, 1883 – 1888.
39. Zhou, T.; Zhang, J.; Ma, Y. Y.; Gao, X.; Xue, Q.; Gao, Y.; Han, Z,-G. A Bicadmium-Substituted Polyoxometalate Network Based on a Vanadosilicate Cluster for the Selective Oxidation of Styrene to Benzaldehyde. Inorg. Chem. 2020, 59, 5803–5807.
40. Nie, Y.; Chen, W.; Liu, Z.; Wang, E. Synthesis and Photocatalytic Hydrogen Evolution Activity of Three Keggin-type Polyoxometalates With Different Central Atoms. *Inorg. Chem. Commun.*

2015, *61*, 184-186.

41. Zhang, C.; Lin, X.; Zhang, Z.; Long, L. S.; Wang, C.; Lin, W. A Hybrid Polyoxometalate-Organic Molecular Catalyst for Visible Light Driven Water Oxidation. *Chem. Commun.* **2014**, *50*, 11591-11594.
42. Lv, H.; Song, J.; Geletii, Y. V.; Vickers, J. W.; Sumliner, J. M.; Musaev, D. G.; Kögerler, P,; Zhuk, P. F.; Bacsa, J.; Zhu, G.; Hill, C. L. An Exceptionally Fast Homogeneous Carbon-Free Cobalt-Based Water Oxidation Catalyst. *J. Am. Chem. Soc.* **2014**, 1*36*, 9268-9271.
43. Geletii, Y. V.; Botar, B.; Kögerler, P.; Hillesheim, D. A.;. Musaev, D. G.; Hill, C. L. An All-Inorganic, Stable, and Highly Active Tetraruthenium Homogeneous Catalyst for Water Oxidation. *Angew. Chem., Int. Ed.*, **2008**, *120* , 3960-3963.
44. Yin, Q.; Tan, J. M.; Besson, C.; Geletii, Y. V.; Musaev, D. G.; Kuznetsov, A. E.; Luo, Z.; Hardcastle, K. I.; Hill, C. L. A Fast Soluble Carbon-Free Molecular Water Oxidation Catalyst Based on Abundant Metals. *Science* **2010**, *328*,342–345.
45. Lv, H.; Song, J.; Zhu, H.; Geletii, Y. V.; Bacsa, J.; Zhao, C.; Lian, T.; Musaev, D. G.; Hill, C. L. Visible-Light-Driven Hydrogen Evolution From Water Using a Noble-Metal-Free Polyoxometalate Catalyst. *J. Catal.* **2013**, *307*, 48–54.
46. Car, P. E.; Guttentag, M.; Baldridge, K. K.; Alberto, R.; Patzke, G. R. Synthesis and Characterization of Open and Sandwich-Type Polyoxometalates Reveals Visible-Light-Driven Water Oxidation via POM-Photosensitizer Complexes. *Green Chem.* **2012**, *14*, 1680–1688.
47. Evangelisti, F.; Car, P. E.; Blacque, O.; Patzke, G. R. Photocatalytic Water Oxidation with Cobalt-Containing Tungstobismutates: Tuning the Metal Core. *Catal. Sci. Technol.* **2013**, *3*, 3117-3129.
48. Ali, J.; Zonoz, F. M.; Wei, Y. A New Organic-Inorganic Nano Hybrid Based on Borotungstic Anion and Imidazole Ring as a two-Functional Green Catalyst. *Solid State Science*, *100*, **2020**, 106093.
49. Cao, J.-P.; Cui, C.-H.; Luo, X.-M.; Li, N.-F.; Xu, Y.; Xu, Y. Polyoxovanadatogermanates-Based Photoelectric Bifunctional Materials: The Ratio of $V_{12}Ge_8$ and $V_{24}Ge_{16}$ Controlled by Solvent. *Inorganic chimica acta*, *483*, **2018**, 544-549.
50. Wang, H.; You, W.; Meng, B.; Sun, X.; Chen, H.; Shan, W. A New 2D Layered Co(II) Complex Based on Monosubstituted Keggin Anions and its Electrocatalytic O_2 Evolution. *J. Clust. Sci.* **2010**, *21*, 857–865.
51. Yu, L.; Lin, J.; Zheng, M.; Chen, M.; Ding, Y. Homogeneous Electrocatalytic Water Oxidation at Neutral pH by a Robust Trinuclear Copper(II)-Substituted Polyoxometalate. *Chem. Commun*. **2018**, *54*, 354-357.

52. Howells, A. R.; Sankarraj, A.; Shannon, C. A Diruthenium-Substituted Polyoxometalate as an Electrocatalyst for Oxygen Generation. *J. Am. Chem. Soc.* **2004**, *126*, 12258-12259.

53. Soriano-López, J.; Goberna-Ferrón, S.; Carbó, J. J.; Poblet, J. M.; Galán-Mascarós, J. R. Chapter Six, $[Co_9(H_2O)_6(OH)_3(HPO_4)_2(PW_9O_{34})_3]^{16-}$: A Highly Efficient Catalyst for Water Oxidation, Editor(s): Eldik, R. V.; Cronin, L. Advances in Inorganic Chemistry, Academic Press. **2017**, *69*, 155-179.

54. (a) Folkman, S. J.; Soriano-Lopez, J.; Galán-Mascarós, J. R.; Finke, R. G. Electrochemically Driven Water-Oxidation Catalysis Beginning with Six Exemplary Cobalt Polyoxometalates: Is It Molecular, Homogeneous Catalysis or Electrode-Bound, Heterogeneous CoO_x Catalysis? *J. Am. Chem. Soc.* **2018**, *140*, 12040−12055. (b) Stracke, J. J.; Finke, R. G. Distinguishing Homogeneous from Heterogeneous Water Oxidation Catalysis when Beginning with Polyoxometalates. *ACS Catal.* **2014**, *4*, 909−933. (c) Folkman, S. J.; Finke, R. G. Electrochemical Water Oxidation Catalysis Beginning with Co(II) Polyoxometalates: The Case of the Precatalyst $[Co_4V_2W_{18}O_{68}]^{10-}$. *ACS Catal.* **2017**, *7*, 7−16. (d) Stracke, J. J.; Finke, R. G. Water Oxidation Catalysis Beginning with $[Co_4(H_2O)_2(PW_9O_{34})_2]^{10-}$ When Driven by the Chemical Oxidant Ruthenium(III)tris(2,2′-bipyridine): Stoichiometry, Kinetic, and Mechanistic Studies en Route to Identifying the True Catalyst. *ACS Catal.* **2014**, *4*, 79−89.

55. (a) Manna, P.; Debgupta, J.; Bose, S.; Das, S. K. A Mononuclear CoII Coordination Complex Locked in a Confined Space and Acting as an Electrochemical Water-Oxidation Catalyst: A "Ship-in-a-Bottle" Approach. *Angew. Chem., Int. Ed.* **2016**, *55*, 2425-2430. (b) Mukhopadhyay, S.; Debgupta, J.; Singh, C.; Kar, A.; Das, S. K. A Keggin Polyoxometalate shows Water Oxidation Activity in Neutral pH: POM@ZIF-8 an Efficient and Robust Electrocatalyst. *Angew. Chem., Int. Ed.* **2018**, *57*, 1918-1923.

56. Wang, C.-J.; Yao, S.; Chen, Y.-Z.; Zhang, Z.-M.; Wang, E.-B. Assembly of Polyoxometalates and Ni-2,2´-bpy Cationic Units into the Molecular Core–Shell Structures as Bifunctional Electrocatalysts. *RSC Adv.* **2016**, *6*, 99010–99015.

57. (a) Zhang, L. N.; Li, S. H.; Tan, H. Q.; Khan, S. U.; Ma, Y.-Y.; Zang, H.-Y.; Wang Y.-H.; Li, Y.-G. MoP/Mo_2C@C: A New Combination of Electrocatalysts for Highly Efficient Hydrogen Evolution over the Entire pH Range. *ACS Appl Mater Interfaces.* **2017**, *9*, 16270-16279. (b) Zhang, L.; Li, S.; Gómez-García C. J.; Ma, H.; Zhang, C.; Pang, H.; Li, B. Two Novel Polyoxometalate-Encapsulated Metal-Organic Nanotube Frameworks as Stable and Highly Efficient Electrocatalysts for Hydrogen Evolution Reaction. *ACS Appl Mater Interfaces*. **2018**, *10*, 31498-31504. (c) Jia W, Zhang, J.; Lu, Z.; Wang, S.; Feng, S. Pt decorated POMOF-derived constructions for efficient electrocatalytic hydrogen evolution. *Nanoscale*. **2020**, *12*, 3902-3906.

58. Ensafi, A. A.; Heydari-Soureshjani, E.; Rezaei, B. Nanostructure Polyoxometalates Containing Co, Ni, and Cu as Powerful and Stable Catalysts for Hydrogen Evolution Reaction in Acidic and Alkaline Solutions. *Int. J. Hydrogen Energy*. **2017**, *42*, 5026-5034.
59. (a) Fernandes, D. M.; Araújo, M. P.; Haider, A.;Mougharbel, A. S.; Fernandes, A. J. S.; Kortz, U.; Freire, C. Polyoxometalate-Graphene Electrocatalysts for the Hydrogen Evolution Reaction. *ChemElectroChem.* **2018**, *5*, 273-283. (b) Zang, D.; Huang, Y.; Li, Q.; Tang, Y.; Wei, Y. Cu Dendrites Induced by the Anderson-type Polyoxometalate $NiMo_6O_{24}$ as a Promising Electrocatalyst for Enhanced Hydrogen Evolution. *Appl. Catal. B Environ.* **2019**, *249*, 163-171.
60. Liu, X.; Ni, K.; Wen, B.; Niu, C.; Meng, J.; Guo, R.; Li, Q.; Li, J.; Zhu, Y.; Wu, X.; Zhao, D.; Mai, L. Polyoxomolybdate-Derived Carbon-Encapsulated Multicomponent Electrocatalysts for Synergistically Boosting Hydrogen Evolution. *J Mater Chem A*. **2018**, *6*, 17874-17881.
61. Keita, B.; Nadjo, L. Polyoxometalate-Based Homogeneous Catalysis of Electrode Reactions: Recent Achievements. *J. Mol. Catal. A Chem*. **2007**, *262*, 190-215.
62. (a) Nohra, B.; Moll, H. E.; Albelo, L. M. R.; Marrot, J.; Mellot-Draznieks, C.; O'Keeffe, M.; Biboum, R. N.; Lemaire, J.; Keita, B.; Nadjo, L.; Dolbecq, A. Polyoxometalate-Based Metal Organic Frameworks (POMOFs): Structural Trends, Energetics, and High Electrocatalytic Efficiency for Hydrogen Evolution Reaction. *J. Am. Chem. Soc.* **2011**, *133*, 13363-13374. (b) Li, J.-S.; Tang, Y. J.; Liu, C. H.; Li, S.-L.; Li, R.-H.; Dong, L.-Z.; Dai, Z.-H.; Bao, J.-C.; Lan, Y.-Q. Polyoxometalate-Based Metal-Organic Framework-Derived Hybrid Electrocatalysts for Highly Efficient Hydrogen Evolution Reaction. *J. Mater. Chem. A.* **2016**, *4*, 1202-1207. (c) Wang, M. L.; Yin, D.; Cao, Y. D.; Gao, G.-G.; Tao, P.; Ma, L.; Liu, H. Ultralow Pt^0 Lloading on MIL-88A(Fe) Derived Polyoxometalate-Fe_3O_4@C Micro-Rods with Highly-Efficient Electrocatalytic Hydrogen Evolution. *J. Coord. Chem.* **2020**, *0*,1-15.
63. Ahmad, W.; Gao, Q.; Zhang, X. L.; Tan, W.; Zhang, L.; Gao, M.-R.; Yu, S.-H. Sandwich-Type Polyoxometalate Mediates Cobalt Diselenide for Hydrogen Evolution in Acidic Electrolyte. *ChemNanoMat.* **2020**, *6*,1164-1168.
64. Hou, Y.; Pang, H.; Zhang, L.; Li, B.; Xin, J.; Li, K.; Ma, H.; Wang, X.; Tan, L. Highly Dispersive Bimetallic Sulfides Afforded by crystalline Polyoxometalate-Based Coordination Polymer Precursors for Efficient Hydrogen Evolution Reaction. *J. Power Sources*. **2020**, *446*, 227319.
65. (a) Wang, X.-L.; Tian, Y.; Chang, Z.-H.; Lin, H. A Series of Polyoxometalate-Based Metal–Bis(pyridyl-tetrazole) Complexes with High Electrocatalytic Activity for Hydrogen Evolution Reaction in Alkaline and Acid Media. *ACS Sustainable Chem. Eng.* **2020**, *8*, 15696–15702. (b) Shen, Q.; Zhang, C.; Wang, M.; Pang, H.; Ma, H.; Wang, X.; Tan, L.; Chai, D.; Hou, Y.; Li, B.

A Novel Lindqvist Intercalation Compound: Synthesis, Crystal Structure and Hydrogen Evolution Reaction Performance. *Inorg. Chem. Commun.* **2019**, *99*, 64-69.

Chapter 2

Polyoxometalate Supported Bis(bpy)mono(aqua)Ni(II) Coordination Complex: An Efficient Electrocatalyst for Water Oxidation

OVERVIEW

Polyoxometalate (POM) supported transition metal complexes are one of the popular hybrid compounds derived from POM unit which have the properties associated with both the POM unit and the supported transition metal complexes along with some value added property due to the synergistic effect. This makes Polyoxometalte supported transition metal complexes (PMSTCs) a better candidate then its constituent units. With this in mind, we have synthesized a polyoxometalate (POM) supported nickel(II) coordination complex $[Ni^{III}(2,2'\text{-bpy})_3]_3[\{Ni^{II}(2,2'\text{-bpy})_2(H_2O)\}\{HCo^{II}W^{VI}_{12}O_{40}\}]_2\cdot 3H_2O$ (1). Since the compound 1 has been characterized with a $\{Ni^{II}(2,2'\text{-bpy})_2(H_2O)\}^{2+}$ fragment coordinated to the surface of the Keggin anion ($[H(Co^{II}W_{12}O_{40}]^{5-}$) via terminal oxo group of tungsten and the $[Ni^{II}(2,2'\text{-bpy})_3]^{2+}$ coordination complex cation sitting as the lattice component in the concerned crystals, the electronic spectroscopy of compound 1 has been described by comparing its electronic spectral features with those of $[Ni^{II}(2,2'\text{-bpy})_2(H_2O)Cl]Cl$, $[Ni^{II}(2,2'\text{-bpy})_3]Cl_2$ and $K_6[Co^{II}W_{12}O_{40}]\cdot 6H_2O$. Most importantly, compound 1 can function as heterogeneous and robust electrochemical water oxidation catalyst (WOC). To gain insights to the water oxidation protocol and to interpret the nature of active catalyst, diverse electrochemical experiments have been conducted. The mode of action of the WOC during the electrochemical process is accounted through confirming no formation/participation of metal oxide during different controlled experiments. It is found that title compound acts as true catalyst which has Ni(II), coordinated to POM surface, acting as the active catalytic center. It is also found to follow a proton coupled electron transfer (PCET) pathway (2 electrons and 1 proton) for WO catalysis with high turnover frequency of 18.49 (mol O_2)(mol Ni^{II})$^{-1}$ s^{-1}.

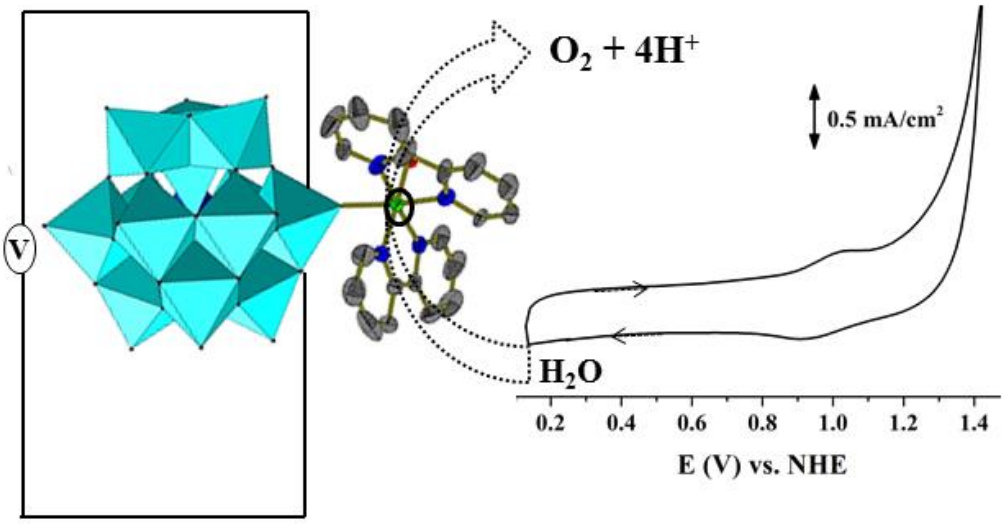

2.1. Introduction

Energy, which we derive from various sources to meet our daily needs, has non-renewable sources as the major ones. These sources' depletion rate has accelerated with the threat of an exponential decrease in our non-renewable sources of energy in the current scenario.[1] Thus, finding alternative ways to produce energy from renewable sources has been the central theme of research. One such promising alternative method could be to mimic the water-splitting process of plants that occurs during photosynthesis to convert solar energy into chemical energy.[2] A successful water splitting (WS) reaction can generate H_2 and O_2 from H_2O. Importantly, H_2 is considered one of the most promising alternative sources of conventional fossil fuels. Hydrogen chemical energy can be converted into electrical energy using fuel cells; it is also the major component of feedstock in many chemical industries (including CO_2 recycling via a chemical process, such as methanol synthesis).[3] Hence, considering the need to develop sustainable and green energy sources for the future, the discovery of an easy method for H_2 production seems to be fundamentally crucial. However, water oxidation (WO) is considered as the bottleneck process of WS as it advances in a thermodynamically uphill manner with the involvement/requirement of $4e^-$ and $4H^+$ (referring to equation 1),

$$2H_2O \rightarrow 4H^+ + O_2 + 4e^- , E^0 = -1.23 \text{ V } vs. \text{ NHE} \quad \ldots\ldots\ldots(1)$$

where E^0 is the standard Nernst potential for water oxidation, the negative potential signifies the process's thermodynamic uphill nature.

Thermodynamic potential (E) of the half-cell reaction of water oxidation depends on pH. According to the Nernst equation, the thermodynamic potential for water oxidation in pH 7 can be stated as (from equation 1): $E = E^0 + 0.059 \times pH$ ……..…(2)

Thus, at pH 7 for the process $2H_2O \rightarrow 4H^+ + O_2 + 4e^-$, E= -0.817 V *vs.* NHE (from equation 2)

Understanding the Nature's route of WO is important to design a new catalyst. Till now, researchers have been working to find out the chemistry behind the process of photosynthesis.[4] During this time stretch, scientists have contributed substantially by discovering the structure of oxygen evolving complex (OEC) and providing insights of the pathway involved during WO in photosynthesis.[5] In 2011, Shen and Kamiya and their co-workers successfully obtained and

solved the crystal structure of OEC involved in photosynthesis, verifying the cubane structure of Mn_4CaO_5 unit.[6]

These findings motivated scientists towards functional mimicking of OEC to advance artificial photosynthesis.[7] In the due course of time, not only bio-mimicking, but also the issues with structural stability of the catalyst seemed to be crucial.[8] A good WO catalyst should be robust under high anodic potential and stable towards oxidation by *in situ* generated oxygen. Over the last few decades, various homogeneous as well as heterogeneous catalysts, where polyoxometalates (POMs) and organometallic complexes have evolved as two high potential fields for homogeneous WO catalysis.[3,9] In case of heterogeneous catalysts, metal organic frameworks (MOFs), metal oxides (*e.g.*, $Co(OH)_2$) supported on solid surface, *in situ* generated CoO_x, *in situ* generated Co-phosphate, POM encapsulated in ZIF-8 cavity, etc. are few examples to name.[10]

Polyoxometalates (POMs) are one of the well-established WOCs due to their complete inorganic skeleton and the scope of fast as well as reversible electron transfer.[11,3] But there are only very few reports where POMs have been found to be stable, as they usually show high tendency towards degradation and form metal oxides (which acts as the active catalyst) under electrochemical conditions required for WO (*i.e.* under high anodic potential).[3,12] In case of coordination complexes, oxidative degradation of organic ligands and formation of metal oxides are the major drawbacks, which necessitates further advancement.[13] To overcome the stability issue, molecular level grafting of POM with coordination complex can be considered one of the most effective alternatives because the coordinate covalently attached POM can enhance the mechanical rigidity of the coordination complex increase the rate of electron transfer. These two issues are crucial regarding the lack of electrochemical stability of non-supported metal complexes during WO. In such hybrid structures, we can also exploit the advantage of both POM and metal coordination complexes.[14] This allows possible synergistic interaction between inorganic POM units and attached coordination complex(es), leading to an improved functional behavior. This enhances its potential application in WO catalysis along with other fields of sciences (such as, materials sciences, biological sciences, and pharmaceutical sciences).[15]

Inspired by the recent reports of mononuclear Co^{II}–aqua coordination complex acts as a water oxidation catalyst (WOC),[10e,16] we envisioned developing a new catalytic system have the scope to achieve WO with the aid of mononuclear Ni^{2+}–aqua coordination complex. Here, we have

successfully synthesized a Ni^{2+} based POM supported complex, in which Ni(II) is bound to a Keggin POM ($[CoW_{12}O_{40}]^{6-}$) through terminal oxygen of POM unit. Out of the remaining five coordination sites of Ni(II), one is occupied by a water molecule, and two (2,2´-bipyridine) units occupy the other four. The central Ni(II) has a distorted octahedral geometry around it.

In this scenario, it is worth mentioning that Hill and co-workers have studied intensely on various sandwiched POM containing Co^{2+} and other first-row transition metals to act as WOCs.[17] Among these, Co^{2+} containing sandwiched-POM with the formula of $[Co_4(H_2O)_2(\alpha\text{-}PW_9O_{34})_2]^{10-}$ appeared as a major breakthrough. It was proved to be an efficient and stable true molecular catalyst, unlike many other POMs.[17b] In order to synthesize cost-effective catalysts, scientists have employed 3d-transition metals, where Co, Mn, and Cu have gained more attention. Instead of the high abundance of nickel on the earth's crust and the potential biological importance of its derivatives, very few reports of Ni-based molecular WOC are available.[18,19] Especially, heterogeneous molecular catalysts containing Ni^{2+} as an active catalyst are even less explored.[9(b-d),19] To the best of our knowledge, the utilization of POM supported Ni^{2+} centered (or any other early transition metal ion as an active catalytic center) hybrid structures as electrochemical WOC are relatively less explored.[20]

Hybrid compounds, having metal complexes coordinated to POM unit, are not new to the chemical society. There are quite a few reports where metal complexes are coordinated to Keggin POMs {$K_6[CoW_{12}O_{40}]$ as well as other Keggin POMs}, but till now there is only one report where this type of hybrid structure is employed as water oxidation catalyst.[14,20] In 2003, Liu and his co-workers reported a hybrid structure containing $[SiW_{12}O_{40}]^{4-}$ as Keggin POM to which $[Co(2,2'\text{-bpy})_2(H_2O)]^{2+}$ is coordinated, but they did not report any electrochemical studies.[14c] Later, in 2009, Wang and his co-workers reported a hybrid structure using $[CoW_{12}O_{40}]^{6-}$ as Keggin anion to which $[Zn(2,2'\text{-bpy})_2(H_2O)]^{2+}$ complex is supported.[14d] In this case, Zn(II), being d^{10} system, is electrochemically inactive since it cannot oxidize further from +2 oxidation state to higher oxidation or reduce from +2 to lower oxidation state. Hence, it should not have any role as an electrocatalyst for water oxidation. In 2016, Chen and his co-workers reported two different hybrid structures, out of which one has $[CoW_{12}O_{40}]^{6-}$ as Keggin anion, forming the compound having formula '$(Hbipy)_2[Co(bipy)_2(H_2O)_4]_2(CoW_{12}O_{40})\cdot 2bipy\cdot 7H_2O$', but did not explore any electrochemical properties.[14a] So, in this context only report where such hybrid compound have been utilized as

electrocatalyst is by Wang and co-workers,[20] which lacks complete electrochemical analysis for water oxidation catalysis and did not address important issues, such as robustness of the catalyst under the operational potential for electrochemical water oxidation. Thus, in literature precedents, such a system's report lacks kinetic and mechanistic studies, which urges for significant attention. Herein, for the first time, we have provided a comprehensive analysis of a new Ni-based inorganic-organic hybrid $[Ni^{II}(2,2'\text{-bpy})_3]_3[\{Ni^{II}(2,2'\text{-bpy})_2(H_2O)\}\{HCo^{II}W^{VI}_{12}O_{40}\}]_2\cdot 3H_2O$ (**1**) as WOC, which can be truly helpful in providing the insights of such systems and developing this class of catalysts further. Compound **1** (with three lattice waters) has been studied in this work as far as its characterizations and electrochemical studies are concerned

2.2. Experimental Section

2.2.1. Material and methods

2.2.1.1. General materials and methods.

Starting materials were purchased in AR grade and were used as received. PXRD patterns were recorded on a Bruker D8-Advance diffractometer by using graphite monochromated $CuK\alpha_1$ (1.5406Å) and $K\alpha_2$ (1.55439Å) radiation. Infra-red spectra of solid samples were obtained as KBr pellets on a JASCO–5300 FT–IR spectrophotometer. Diffuse Reflectance (DRS) UV-visible electronic absorption spectra were recorded using Shimadzu-2600 spectrophotometer. Thermogravimetric (TGA) analyses were carried out on a STA 409 PC analyzer. Carl Zeiss model Ultra 55 microscope was used for Field emission scanning electron microscope (FE-SEM) imaging with energy dispersive X-ray (EDX) spectroscopy. Oxford Instruments X-Max^N SDD (50 mm^2) system and INCA analysis software were used for elemental mapping. Zahner Zanium electrochemical workstation which is operated with Thales software is used for conducting all the electrochemical activity.

2.2.1.2. Crystal Data collection

Single-crystals suitable for structural determination of the compound **1** was mounted on a three-circle Bruker SMART APEX CCD area detector system under Mo−Kα (λ = 0.71073 Å) graphite monochromated X-ray beam with a crystal-to-detector distance of 60 mm, and a collimator of 0.5 mm width (at 273 K temperature). The scans were recorded with a ω scan width of 0.3°. Data

reduction was performed by SAINT PLUS,[30] empirical absorption corrections using equivalent reflections were performed by program SADABS.[31] Structure solutions were done using SHELXS-97[32] and full-matrix least-squares refinement was carried out using SHELXL-97.[33]All the non-hydrogen atoms were refined anisotropically. Hydrogen atoms on the C atoms were introduced on calculated positions and were included in the refinement riding on their respective parent atoms. Crystal data, along with the structure refinement parameters for compound **1** is summarized in **Table 2.1.** Selected bond length and bond angle for compound **1** is summarized in the appendix **A1**. CCDC 1826902 (compound **1**) contains the supplementary crystallographic data for this compound.

2.2.1.3. Electrochemical studies

All the electrochemical experiments were carried out using a Zahner Zanium electrochemical work station operated with Thales software. Complete electrochemical experiments were accomplished using a three-electrode electrochemical cell using compound **1** modified glassy carbon as working electrode, home-made Ag/AgCl (1M) electrode as a reference, and Pt-flag as a counter electrode in acidic and neutral pH in an aqueous medium. For basic medium home-made Hg/HgO (0.1M KOH) electrode was used as a reference electrode (RE) while the other two electrodes were the same as mentioned above. For the preparation of **1** modified electrode, 4 mg of **1** and 1 mg of acetylene black carbon were taken in 1 mL of EtOH-H_2O mixture (EtOH: H_2O=3:2), and to it, 10 µL 5 wt% nafion (aq.) was added following which it sonicated for 30 min in order to obtain a homogeneous suspension. For all the electrochemical studies, 20 µL of this mixture was coated on the working electrode (glassy carbon electrode having 3 mm diameter; geometrical area = 0.0706 cm^2). This coat of sample is essentially equivalent to 40 µg (compound **1**) in every coat done on the glassy carbon electrode. The same amount on the electrode surface was maintained for all electrochemical experiments unless otherwise mentioned. In the case of FTO as working electrode, area 0.07 cm^2 was used to coat the sample or to generate the oxides/phosphates electrochemically. The coating mixture on the electrode was dried under IR-lamp (temperature ~70°C) before use. All the electrochemical experiments were performed at ambient temperature. Electrode potentials were converted to the normal hydrogen electrode (NHE) scale using the relation E (NHE) = E (Ag/AgCl) + 0.1263 V when the Ag/AgCl used as RE and E (NHE) = E (Hg/HgO) + 0.143 V for Hg/HgO as RE. Cyclic voltammetry scans

were initiated at the open circuit potential (OCP), and the anodic side was scanned first, followed by a cathodic scan. Five cycles were taken consecutively for each set of cyclic voltammetry measurements in quiescent solution. Cyclic voltammograms (CVs) were also recorded at various scan rates.

2.2.2. Synthesis

2.2.2.1. Synthesis of Compound $K_6[CoW_{12}O_{40}].6H_2O$ (POM)

$Na_2WO_4 \cdot 2H_2O$ (9.9 g, 0.03 mol.) was taken in 20 mL water, following which the pH of the solution was adjusted to 7 (between pH ranges of 6.5 to 7.5) with the subsequent addition of glacial acetic acid. The solution was then heated to boiling. An aqueous solution (6.5 mL) of cobalt acetate tetrahydrate, $Co(CH_3CO_2)_2 \cdot 4H_2O$, (1.25 g, 0.005 mol.) was then added slowly with stirring to the solution mentioned above. The mixture was then boiled again for 10 minutes. To remove the traces of any insoluble matter, it was immediately filtered under hot conditions, if any present and the filtrate was boiled again. To this solution, a hot saturated solution (15 mL) of KCl (6.5 g, 0.087 mol.) was added and was heated again to boiling. The reaction-mixture so obtained was then cooled to room temperature (25 °C) and was kept undisturbed for 24 hours. After 24 hours, a pale blue solution and the dark green residue at the bottom were formed. The solution was discarded by decantation, and 2 M sulphuric acid (20 mL) was added to the dark green precipitate formed. The reaction mixture was heated to reduce the total volume to about 5 mL. The final solution so obtained was then filtered and cooled slowly till it reached room temperature, following which it was cooled in an ice bath for about 24 hours, and POM crystals ($K_6[CoW_{12}O_{40}] \cdot 6H_2O$) were obtained.

2.2.2.2. Synthesis of Compound 1

A mixture of $Ni(OAc)_2 \cdot 4H_2O$ (71 mg, 0.28 mmol), 2,2′-bpy (114 mg, 0.73 mmol) and $K_6[CoW_{12}O_{40}] \cdot 6H_2O$ (32 mg, 0.01 mmol) in 3 ml MeOH and 2 ml water, pH=2 (using AcOH (50% w/v)) were taken in 23 mL Teflon lined reactor and was stirred for 45 min. The solution was heated to 160 ˚C for 5 days under solvothermal conditions. It was cooled down to room temperature (34˚C) in 24 h to obtain block-shaped green-colored crystals. Yield: 56% (based on W).

Anal. Calcd for $C_{130}H_{104}Co_2N_{26}Ni_5O_{85}W_{24}$: C, 19.01; H, 1.28; N, 4.43; Co, 1.43; Ni, 3.57; W, 53.72. Found: C, 20.36; H, 1.41; N, 4.65; Co, 1.40 (ICP); Ni, 3.50 (ICP), W, 53.03 (ICP).

2.3 Results and Discussion

2.3.1. Physical characterization

Compound **1** was initially characterized by single-crystal XRD analysis. Compound **1** and $K_6[CoW_{12}O_{40}]$ was later characterized by FT-IR, PXRD, UV-Vis, Raman spectroscopy, FESEM-EDX, XPS, ICP-OES analysis, and electrochemical methods whenever it was required.

2.3.1.1. Single-crystal XRD analysis

Compound **1** was characterized through X-ray crystallography at room temperature (293 K). Compound **1** crystalizes in the monoclinic unit cell with *C2/c* space group. The crystal structure shows that $[Co^{II}W_{12}O_{40}]^{6-}$ cluster unit is attached to the $[Ni^{II}(2,2'\text{-bpy})_2(H_2O)]^{2+}$ complex moiety *via* coordination of terminal oxo group of the Keggin anion to Ni(II) ion. The remaining five coordination sites of Ni(II) center in $\{Ni^{II}(2,2'\text{-bpy})_2(H_2O)\}^{2+}$ are occupied by coordinating to two 2,2′-bipyridine units and one H_2O molecule. This coordinated water molecule plays a vital role in this compound's catalytic activity (*vide infra*).

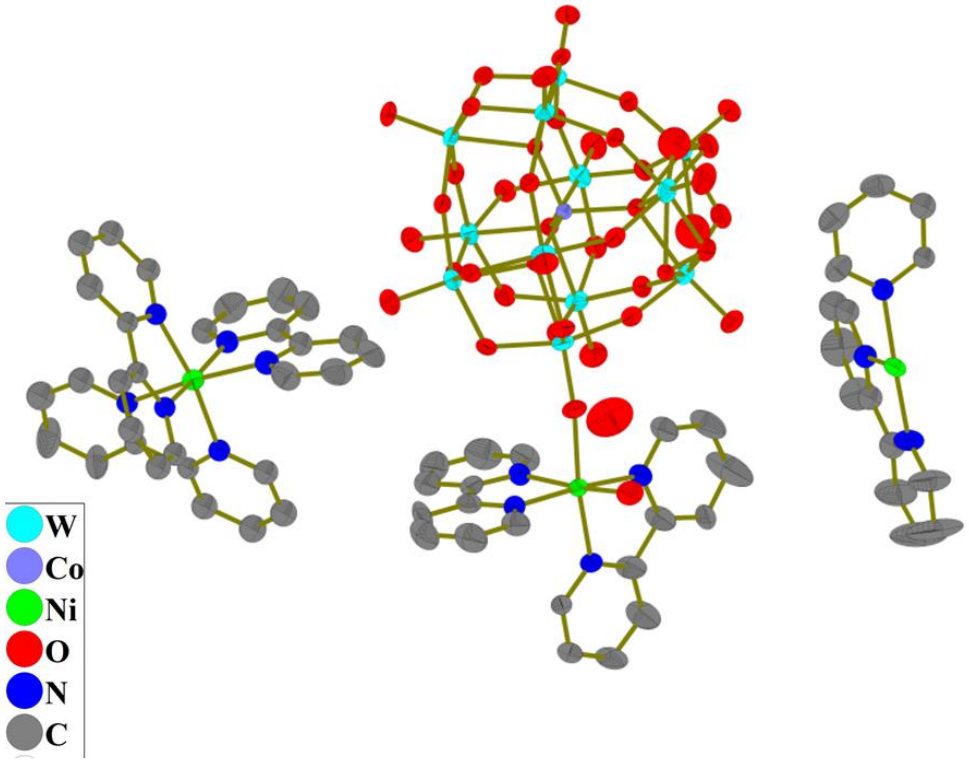

Figure 2.1. The ORTEP diagram of the asymmetric unit of compound **1** (hydrogen atoms are omitted for clarity). Thermal ellipsoids set to 50% probability level.

The concerned asymmetric unit contains one POM cluster unit coordinating bis(bpy)(aqua)Ni(II) species, $[\{Ni^{II}(2,2'\text{-bpy})_2(H_2O)\}\{HCo^{II}W^{VI}_{12}O_{40}\}]^{3-}$, 1.5 units of $[Ni^{II}(2,2'\text{-bpy})_3]^{2+}$ and 0.5 solvent water molecules, thereby bringing about the formula of compound **1** as $[Ni^{II}(2,2'\text{-bpy})_3]_3[\{Ni^{II}(2,2'\text{-bpy})_2(H_2O)\}\{HCo^{II}W^{VI}_{12}O_{40}\}]_2\cdot H_2O$ (**Figure 2.1.**).

In other words, in this system, three discrete units of $[Ni^{II}(2,2'\text{-bpy})_3]^{2+}$ complexes are shared between two adjacent unit cells. As far as the asymmetric unit is concerned, the Co(II) centered Keggin POM cluster has six negative charges (6-) and the summation of positive charges of 1.5 $[Ni^{II}(2,2'\text{-bpy})_3]^{2+}$ and one coordinated $\{Ni^{II}(2,2'\text{-bpy})_2(H_2O)\}^{2+}$ is +5. Thus, in order to fulfill the electroneutrality of the overall system (compound **1**), we have proposed the presence of a proton along with the POM cluster anion (see the formula **1**).

Table 2.1. Crystal data and structure refinement for compound 1

Empirical formula	$C_{130}H_{104}N_{26}O_{88.20}Co_2Ni_5W_{24}$
Formula weight	8265.04
Temperature/K	298K
Crystal system	monoclinic
Space group	C2/c
a/Å	46.624(4)
b/Å	14.3807(11)
c/Å	26.2047(18)
α/°	90
β/°	90.079(2)
γ/°	90
Volume/Å^3	17570(2)
Z	4
ρ_{calc}g/cm^3	3.1244

μ/mm^{-1}	16.442
F(000)	14966.1
Radiation	Mo Kα (λ = 0.71073)
2θ range for data collection/°	4.96 to 52.82
Index ranges	-58 ≤ h ≤ 58, -17 ≤ k ≤ 17, -32 ≤ l ≤ 32
Reflections collected	77175
Independent reflections	17883 [R_{int} = 0.0294, R_{sigma} = 0.0243]
Data/restraints/parameters	17883/12/1034
Goodness-of-fit on F^2	1.069
Final R indexes [I>=2σ (I)]	R_1 = 0.0364, wR_2 = 0.0807
Final R indexes [all data]	R_1 = 0.0451, wR_2 = 0.0876
Largest diff. peak/hole / e Å^{-3}	3.34/-3.04

2.3.1.2. Bond Valence Sum (BVS) analysis of compound 1

The +2 oxidation state of cobalt center of the Keggin POM anion is consistent with the bond valence sum (BVS) calculation. According to this BVS calculation, inter-atomic distances of 'Co-O' suggest the valence of Co to be 2 (**Table 2.2.**).

Table 2.2. Output File of BVS calculation for 'Co' in compound **1**

Co (27, 1.09, 1.70)	Rij	Dij	Vij
-O (8, .63, 3.15)	1.68	1.87	.60
-O (8, .63, 3.15)	1.68	1.87	.60
-O (8, .63, 3.15)	1.68	1.89	.57
-O (8, .63, 3.15)	1.68	1.88	.58

Bond valence sum calculation. Numbers in brackets after atom symbols are atomic number, r and c [1]

2.3.1.3. PXRD analysis of compound 1

To check the compound's bulk purity, the PXRD of compound **1** was obtained and compared with the simulated PXRD pattern obtained from the Single-Crystal data. **Figure 2.2.** represents the PXRD patterns comparing the simulated and experimentally obtained data, confirming the compound's bulk purity.

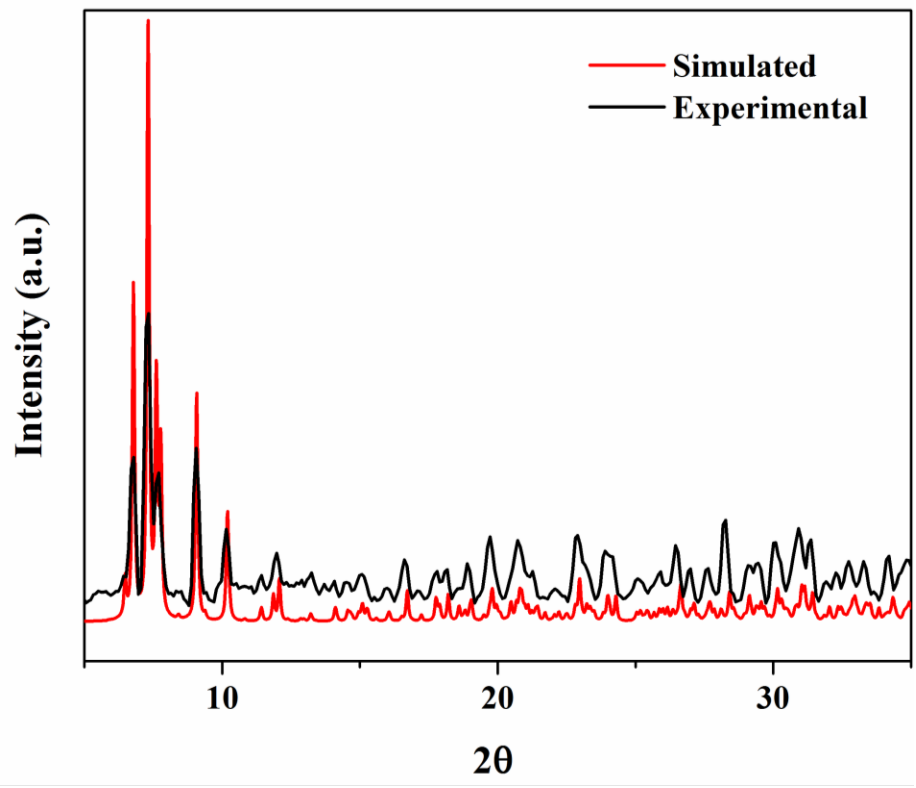

Figure 2.2. (—) Represents PXRD pattern of simulated data generated from crystal structure of **1** and (—) represents PXRD pattern experimentally obtained from bulk sample of **1**.

2.3.1.4. FTIR of POM and compound 1

FTIR spectra of compound **1**, $K_6[CoW_{12}O_{40}].6H_2O$ (**CoW_{12}**), and 2,2′-bipyridine (bpy) have been recorded and analyzed (**Figure 2.3. (a)**). Stretching frequencies arising from 'C=N' and 'C-N' bond in bpy unit in compound **1** show bands around 1600 cm^{-1} and 1460 cm^{-1} respectively. Due to POM unit, following bands are observed in compound **1**: ν(W-O)t 940 cm^{-1}, ν(W-O-W) O_h edge sharing 865 cm^{-1}, (W-O-W) corner sharing 780 cm^{-1}, ν(O-Co-O) 454 cm^{-1} (**Figure 2.3. (b)**).

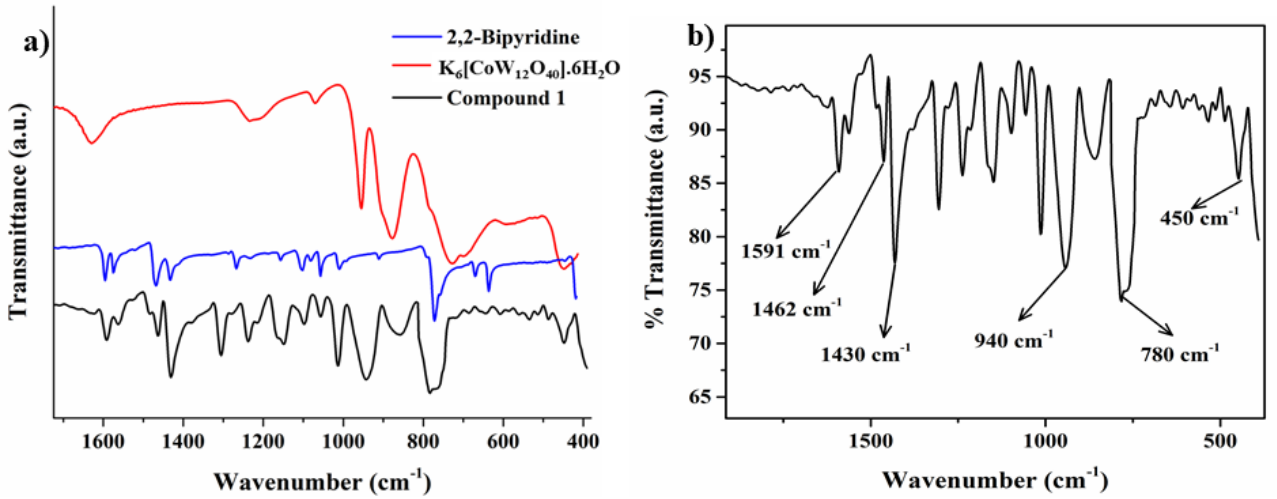

Figure 2.3. (a) FT-IR spectra of 2,2'-bipyridine (—), $K_6[CoW_{12}O_{40}]$ (—) and compound **1** (—). **(b)** Enlarged FT-IR spectrum of **1** in 1800-400 cm^{-1} range where major strechings have been labelled.

IR band around 780 cm^{-1} in compound **1** is mainly due to combine contribution from 2,2′-bipyridine and **CoW_{12}** unit. In bpy, a sharp band is seen due to out-of-plane 'C-H' bending, whereas in **CoW_{12}** cluster unit around the same region, the stretching band due to corner-sharing 'W-O-W' bond is observed as broad peak. Thus, the broad and strong IR peak which appeared at around 780 cm^{-1} in the IR spectrum of compound **1** can be assigned to the combination of 'W-O-W' fragments and bipyridine, where the broad IR band of Keggin cluster (**CoW_{12}**) masks the sharp IR peak of bipyridine.

2.3.1.5. TGA of compound 1 and POM

Thermal stability of the hybrid compound was studied by thermogravimetry analysis (TGA). Compound **1** was taken for thermal studies without prior activation in high temperature vacuum. Initially with increase in temperature (T≤400 ˚C) a steady slope for weight loss is observed (**Figure 2.4.**). This decrease in weight loss of compound can be due to lattice water present in **1**. Degradation of organic linker leads to weight loss of 28.2% (calcd 28.8%) at the temperature of 490 ˚C. POM unit in **1** starts to degrade at higher temperature (T>600 ˚C). This leads to weight loss of 35.5% (calcd 35.9%).

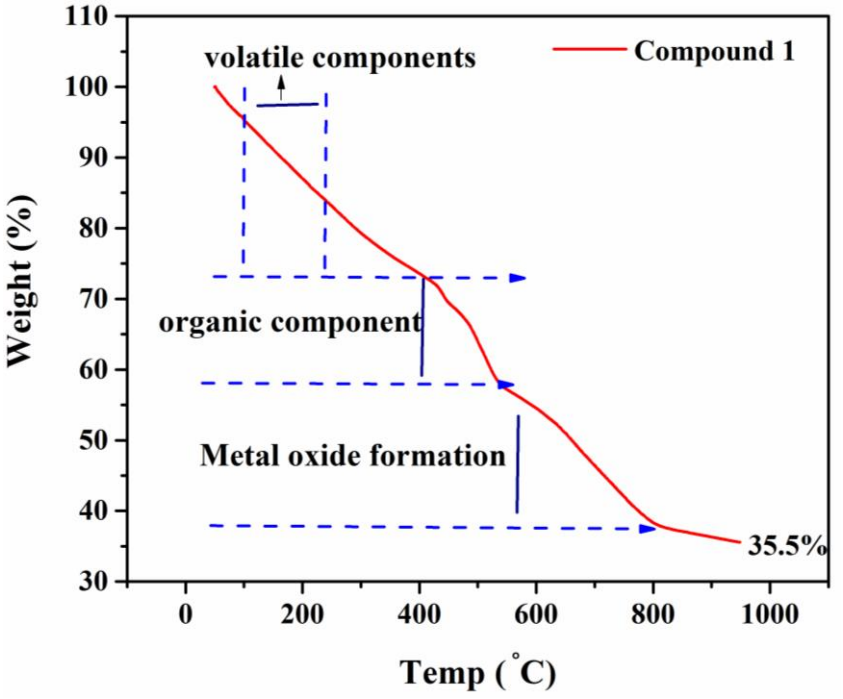

Figure 2.4. TGA plot of compound **1**.

2.3.1.6. UV-Visible spectral analysis of Compound 1 and POM

The electronic absorption spectrum of compound **1** is converted into Kubelka-Munk (K-M) derived plot. The spectrum thus obtained for **1** is compared with those of $K_6[CoW_{12}O_{40}]\cdot 6H_2O$ (**CoW_{12}**), $[Ni^{II}(2,2'\text{-bpy})_2(H_2O)Cl]Cl$ and $[Ni^{II}(2,2'\text{-bpy})_3]Cl_2$. All the spectra were recorded in solid-state diffuse reflectance spectroscopy (DRS) mode and were K-M converted for the sake of comparison. As shown in **Figure 2.5. (a)**, a direct comparison with **CoW_{12}** shows that, in the case of **1**, transitions in the near-IR range (1000-1200 nm) are due to charge transfer from $e(Co)\rightarrow t_2(W)$.[22] Again, this study shows a blue shift of 12 nm when compared to that of **CoW_{12}**, which can be attributed to the changes in the energy level of e(Co) and t_2(W). This change in electronic energy level is expected due to structural modification of the **CoW_{12}** unit in **1**. In the 700-1000 nm range (**Figure 2.5.**), a broad peak is seen in the diffuse reflectance spectra (DRS) of **1**, which is comparable to that, found in the UV-DR spectrum of $[Ni^{II}(2,2'\text{-bpy})_2(H_2O)Cl]Cl$ as shown in **Figure 2.5. (b)**.[23] This supports the presence of $\{Ni^{II}(2,2'\text{-bpy})_2(H_2O)\}^{2+}$ unit in the title compound **1**.

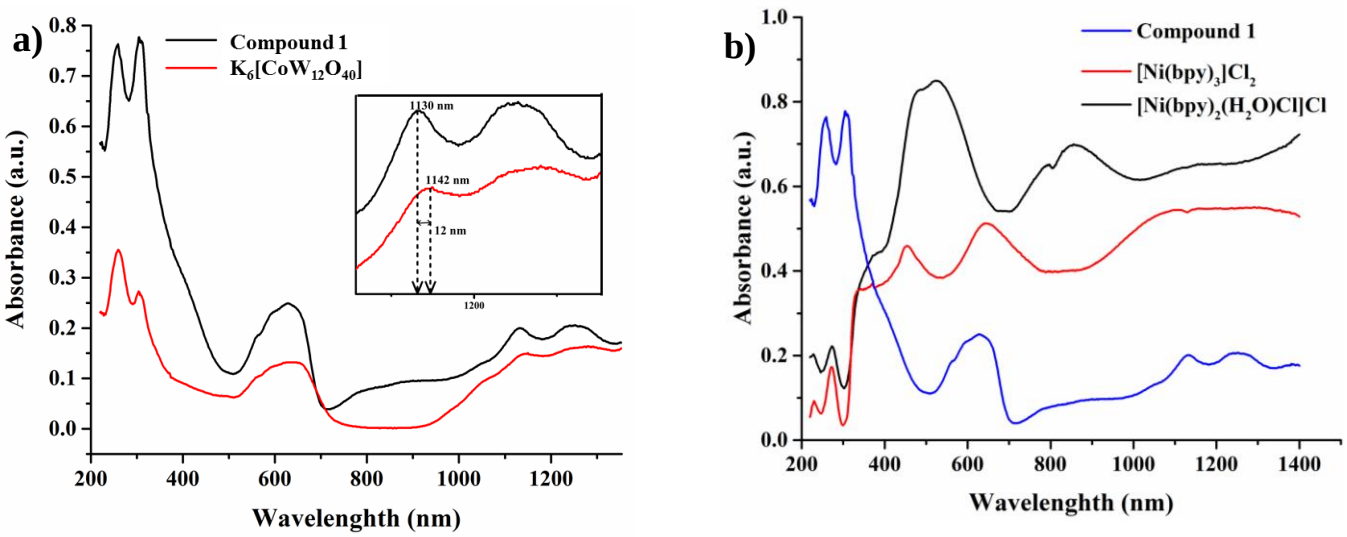

Figure 2.5. (a) K-M converted UV-vis diffuse reflectance spectra (DRS) of **1** and **$K_6[CoW_{12}O_{40}]$**·$6H_2O$. **(b)** K-M transformed UV-vis DRS spectra of **1** compared with $[Ni(2,2'\text{-bpy})_3]Cl_2$ and $[Ni(2,2'\text{-bpy})_2(H_2O)Cl]Cl$ coordination complexes.

In visible range of the spectrum of hybrid **1**, a broad peak at 630 nm and two fine shoulders at 592 nm and 560 nm are observed (**Figure 2.5. (a)**) that are characteristic transitions of tetrahedral Co^{2+}: ($^4A_2 \rightarrow {}^4T_1$), $t_2(Co_{td}) \rightarrow e(W)$ and $e(Co_{td}) \rightarrow e(W)$ respectively.[22a] In this range, a d-d transition (which is Laporte forbidden) is expected due to Ni^{2+} of $\{Ni^{II}(2,2'\text{-bpy})_2(H_2O)\}^{2+}$ (comparing the electronic spectrum of $[Ni^{II}(2,2'\text{-bpy})_2(H_2O)Cl]Cl$, **Figure 2.5. (b)**, but it is masked by d-d transition of Co^{2+} of $[CoW_{12}O_{40}]^{6-}$,which is Laporte allowed (because of tetrahedral geometry at Co^{II}).[23] At around 408 nm in the DRS spectrum of **1**, a broad shoulder is observed (**Figure 2.5.**) due to d-d transition arising from $[Ni^{II}(2,2'\text{-bpy})_3]^{2+}$ units (comparing the DRS spectrum of $[Ni^{II}(2,2'\text{-bpy})_3]Cl_2$, **Figure 2.5. (b)**.[24] In UV region of DRS spectrum of **1** (below 300 nm) peaks are mainly due to $O_{2p} \rightarrow W_{5d}$ charge transfer.[22a] Apart from this, peaks are seen in the same range (below 300 nm) which are mainly due to MLCT of $[Ni^{II}(2,2'\text{-bpy})_3]Cl_2$ unit and $\pi-\pi^*$ transition of 2,2′-bpy ligand.[24] Thus, absorption spectrum of **1** is in consistency with the structure, obtained by single crystal X-ray crystallography.

2.3.1.7. Field Emission Scanning Electron Microscopy (FESEM) and Energy-dispersive X-ray (EDX) Analysis

Compound **1** has also been characterized by elemental mapping using FESEM. Ni and Co atoms as the constituents of compound **1** were also confirmed by the EDX elemental mapping. FESEM

images and EDX-elemental mapping plots are provided in **Figure 2.6. (a-i)**. Apart from the FESEM images, EDX analysis was done over different regions of the sample to check for homogeneity in the sample's distribution. In a tabular manner we have listed the weight and atom percent of all elements which are present in compound **1** (**Table 2.3.**).

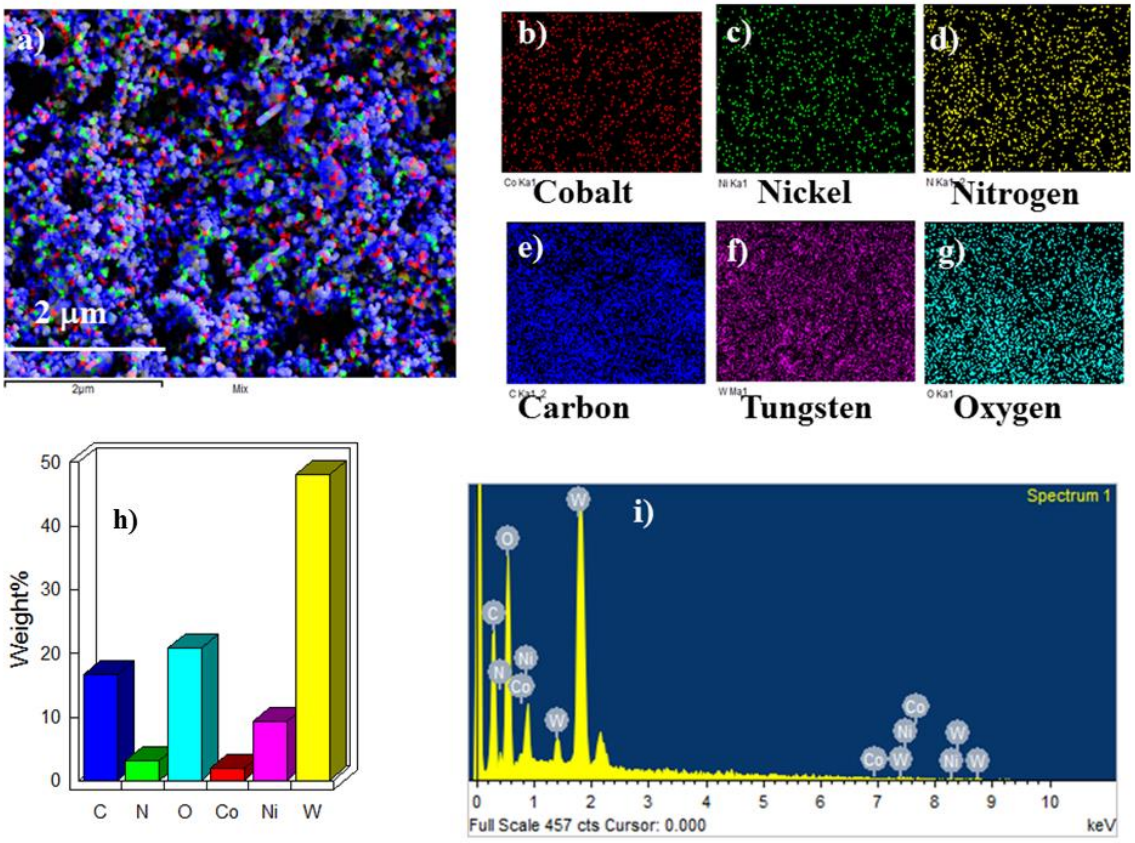

Figure 2.6. (a) EDX-elemental mapping of **1** (mixed all constituent elements). **(b-g)** EDX element mappings for Co, Ni, N, C, W and O respectively in **1**. **(h)** Quantitative results of the EDX analysis. **(i)** Energy-dispersive X-ray spectroscopy (EDX) spectrum of **1**.

Table 2.3. EDX analysis over the different region of the surface of **1**

Sample	Carbon		Nitrogen		Oxygen		Cobalt		Nickel		Tungsten	
	Wt %	Atom %	Wt %	Atom %	Wt %	Atom %	Wt %	Atom %	Wt %	Atom %	Wt %	Atom %
Area 1	41.03	60.12	11.09	13.93	20.69	22.76	0.58	0.17	2.29	0.69	24.33	2.33
Area 2	39.63	57.33	11.39	14.13	23.16	25.16	2.22	0.65	2.49	0.74	21.12	2.00
Area 3	43.44	65.77	8.81	11.43	16.96	19.27	1.46	0.45	0.84	0.26	28.50	2.82

2.3.1.8. X-ray photoelectron spectroscopy

XPS of compound **1** and **CoW_{12}** were analyzed to understand the change in POM unit's environment when present in 1 and to confirm the oxidation state of Co in **1**. Due to the very less weight percentage of Co in **1** (1.44%), the signal to noise ratio was found to be very poor (**Figure 2.7. (a)**). Co $2p_{3/2}$ and Co $2p_{1/2}$ energy levels of Co in compound **1** have the binding energies of 781.08 eV and 796.84 eV, respectively. The energy difference between these energy levels is 14.6 eV, which supports the oxidation state of Co as +2 (**Figure 2.7. (a)**, Supporting Information).[25] In case of W, a shift of 0.7 eV and 0.8 eV has been observed for W $4f_{5/2}$ and W $4f_{7/2,}$ respectively in comparison to those of **CoW_{12}**. This shift in binding energy can be attributed to the changes in W's electronic level in **1** arising due to coordination of the concerned Keggin POM to Ni through its W=O bond (**Figure 2.7.**).

The electronic redistributed in compound **1** can be confirmed by comparing the binding energy of W_{4f} levels in **CoW_{12}** and compound **1**. Shift in low energy (eV) is observed for W_{4f} levels of **1** when compared to that of **CoW_{12}** (**Figure 2.7. (b)).** The oxidation state of Ni in **1** was confirmed to be in +2 state (**Figure 2.7. (c)**).

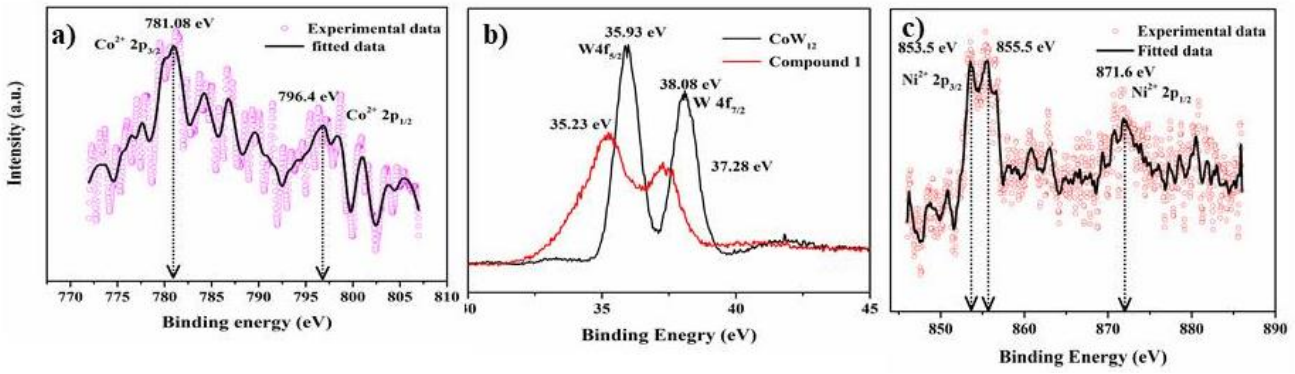

Figure 2.7. (a) Core Co_{2p} XPS spectrum of compound **1**. **(b)** Core W_{4f} XPS spectra of compound **1** and **CoW_{12}**. **(c)** Core Ni_{2p} XPS spectra of compound **1**.

2.3.1.9. Elemental analysis of Compound 1 from ICP-OES and CHN analysis

To know the elemental composition in percent mass present in compound **1**, we analyzed the sample for ICP-OES (**Figure 2.8.**) and CHN analysis (**Figure 2.9.**).

Issued to:
Prof Samar K.Das
School Of Chemistry
University of Hyderabad, Gachibowli,
Hyderabad-500046
Kind Attn.: ChandaniSingh

Report No. : LLPL/17-18/008915
Issue Date : 10/02/2018
Customer Ref.: TRF

Ref.Date : 02/02/2018

Sample Particulars : WOC-57

Qty. Received : 1no Vial

Test Parameters : Nickel as Ni,Tungsten as W,Cobalt as Co

Date of Receipt of Sample : 02/02/2018
Date of completion of analysis : 10/02/2018
Date of Starting of Analysis : 09/02/2018
SAMPLE TESTED AS RECEIVED

TEST RESULTS

S.No.	Parameters	UOM	Results
1	Nickel as Ni	% by mass	3.50
2	Tungsten as W	% by mass	53.03
3	Cobalt as Co	% by mass	1.40

Instrument Used: ICP-OES Varian 720-ES
NOTE : This report and results relate only to the sample / items tested.

Figure 2.8. ICP-AES analysis report in weight percentage of the metal constituent in compound **1.**

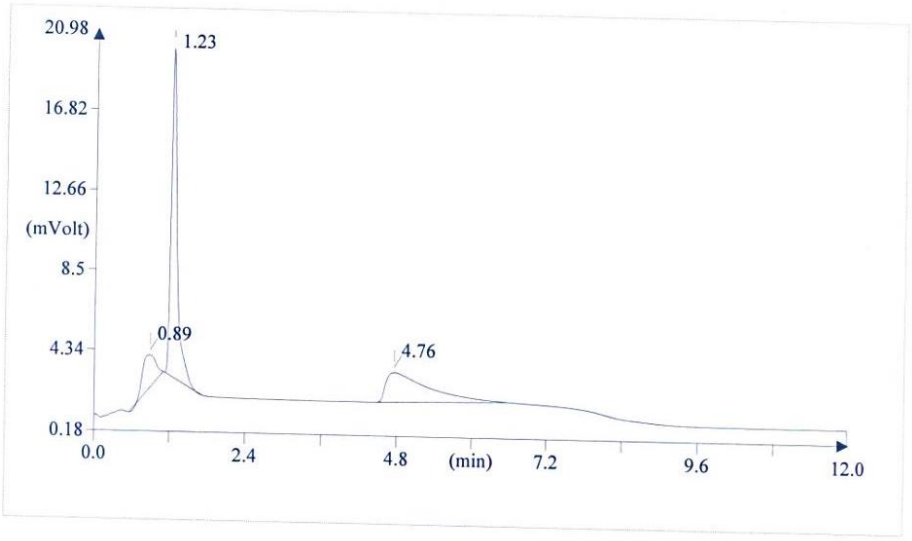

Element Name	Element %	Ret. Time
Nitrogen	4. 65	0. 89
Carbon	20. 36	1. 23
Hydrogen	1. 41	4. 76

Figure 2.9. CHN analysis report for compound **1**.

2.3.2. Electrochemical measurements and water oxidation studies of Compound 1

2.3.2.1. WO properties of Compound 1

Cyclic voltammograms (CVs) of compound **1** were recorded in a 0.1 M phosphate buffer with pH 7 (unless specified otherwise). CV of **1** shows a broad oxidation peak A1 at 1.01 V and a reduction peak C1 at 0.91 V (**Figure 2.10. (a)**). Differential pulse voltammetry (DPV) was used to understand the redox phenomenon with higher precision during the anodic scan. DPV was carried out with step width and step height of 100 ms and 5 mV, respectively, and pulse width and pulse height as 200 ms and 25 mV, respectively. From DPV measurements, two distinct peaks were found for oxidation at 0.99 V (A1′) and 1.1 V (A2′) (**Figures 2.10. (b), (c)**). This observation was correlated with the CV of $\mathbf{CoW_{12}}$, which was recorded in 0.1 M Na_2SO_4 (since $\mathbf{CoW_{12}}$ is unstable in phosphate buffer) having pH 7 by dissolving 1 mmol $\mathbf{CoW_{12}}$ in it. A quasi-reversible redox couple (A2/C2) was observed (**Figure 2.10. (d)**). Oxidation peak A2 represents the oxidation of Co(II)→Co(III) at 0.95 V, and reduction peak C2 represents the reduction of Co(III)→Co(II) at 0.83 V. Cyclic voltammetric features of $\mathbf{CoW_{12}}$ provide an approximate guideline to assign the Co^{III}/Co^{II} peak in the CV of compound **1**.

Similarities between the peak positions of the CV of $\mathbf{CoW_{12}}$ and compound **1** suggests the oxidative peak A1′ in the CV of compound **1** can be logically assumed to be the result of Co(II)→Co(III) oxidation of $\mathbf{CoW_{12}}$ unit while peak A2′ to Ni(II)→ Ni(III) oxidation. As a result of the surge of current (due to liberation of 2e- from each water molecule during catalytic WO) at higher potential, peaks for further oxidation of Ni(III) could not be observed in the CV of **1**. With the application of potential, once the reactive high valent Ni-species is formed, it catalyzes the oxidation of water molecules. This catalytic WO is accompanied by simultaneous reduction of the high valent Ni species back to Ni(III) species. Furthermore, on the reduction side, a broad peak C1 is present. This broad peak in CV in the reduction side can be a result of the close proximity of the reduction peaks of Co(III)→Co(II) and Ni(III)→Ni(II) reduction.[9c,26] The shift in the peak position of Co^{III}/Co^{II} couple in compound **1** in respect to $\mathbf{CoW_{12}}$ as such is observed. This shift in peak position can be assumed due to a change in the distribution of electron density from $\mathbf{CoW_{12}}$ unit owing to sharing of the terminal oxygen atom of $\mathbf{CoW_{12}}$ to bis(2,2´-bpy)(aqua)Ni(II) unit.

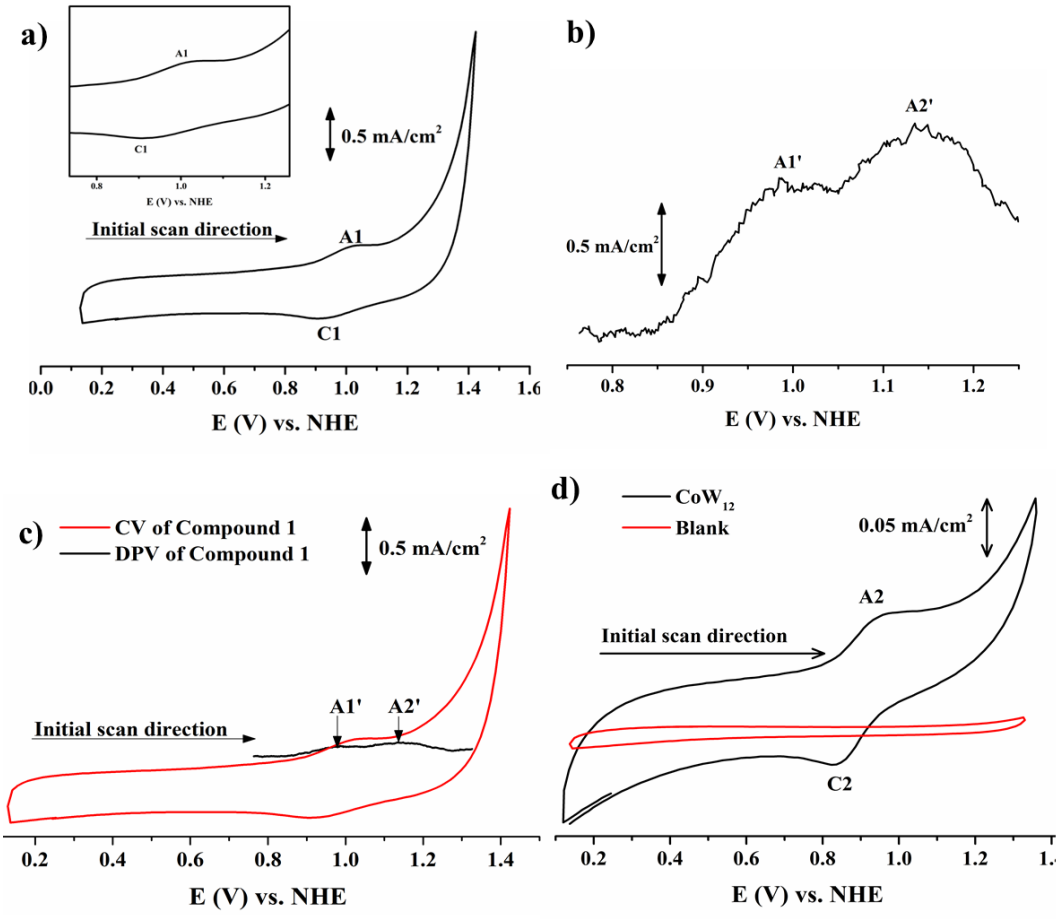

Figure 2.10. (a) Cyclic voltammogram (CV) of compound **1** in 0.1 M phosphate buffer, pH 7. **(b)** DPV of compound **1** in 0.1 M phosphate buffer, pH 7**. (c)** DPV (▬) and CV (▬) of compound **1** showing two peaks. CV and DPV of **1** were obtained using 0.1 M phosphate buffer (pH 7) as supporting electrolyte after coating sample on glassy carbon electrode (3 mm diameter). See the text for assignments. **(d)** (▬) shows CV of **CoW_{12}** recorded from 1 (mM) solution of **CoW_{12}** prepared in 0.1 M Na_2SO_4, pH 7 and (▬) shows CV of blank glassy carbon electrode in 0.1 M Na_2SO_4, pH 7.

2.3.2.2. Electrochemical stability analysis of 1

The stability of the catalyst (compound **1**) was observed by performing constant potential electrolysis (CPE) measurements at the onset potential (1.23 V) for 20 h and accelerated durability test of 1000 cycles of cyclic voltammetric scans. For CPE, the current change was negligible for 20 h (**Figure 2.11. (a)**). CV was recorded before and after CPE measurement for the coated sample of **1**. Insignificant change in water oxidation onset current (ca. 27 μA) and no

alteration in onset potential were observed in CV recorded after 20 h CPE measurement (**Figure 2.11. (b)**). The initial and final cycles of 1000 cycles of cyclic voltammetric scans were also in agreement with CPE observation as it showed imperceptible changes in catalytic current (**Figure 2.11. (c)**). This negligible loss of catalytic current, observed in both 1000th and 2nd CV cycles of **1** as well as in the CVs recorded before and after conducting 20 h CPE measurements, is a result of the loss of sample from electrode surface due to oxygen bubble evolution.

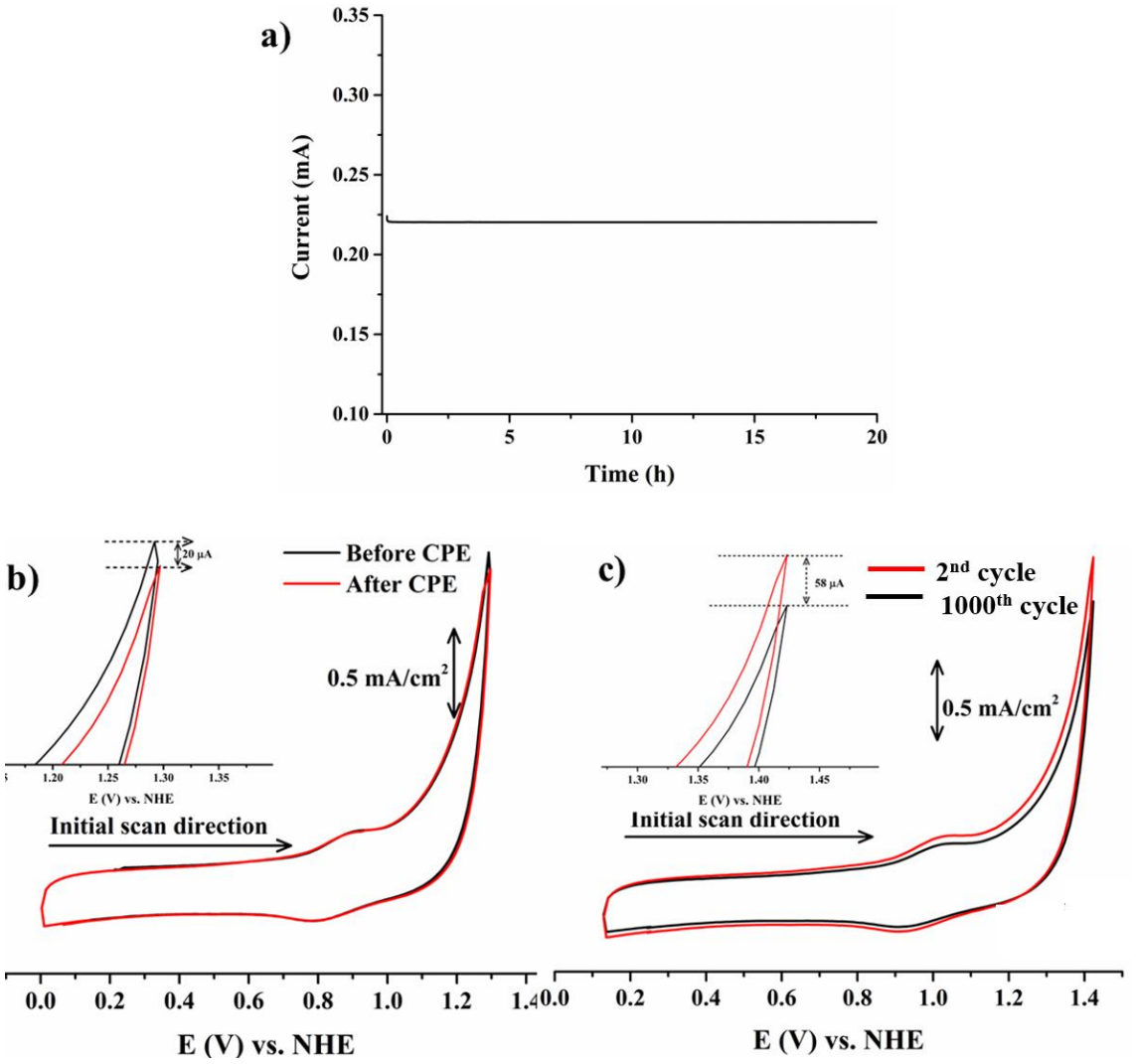

Figure 2.11. (a) CPE of **1** recorded at 1.23 V for 20 h, in 0.1 M phosphate buffer (pH 7). **(b)** Cyclic voltammograms of **1** recorded before (——) and after (——) CPE measurements in 0.1 M phosphate buffer, pH 7. Inset: enlarged region of same voltammograms showing 20 µA catalytic current differences in CV before and after performing CPE. **(c)** Stability check of **1** by 1000 cycle CV scans in 0.1 M phosphate buffer (pH 7). (——) represents the 2nd cycle CV scan and (——) represents 1000th cycle CV scan of **1**. Inset: enlarged region of the same voltammograms showing only 58 µA difference in catalytic current.

For further validation of the results obtained so far, we recorded PXRD as well as FESEM images. EDX-elemental analysis for the coated sample of **1** (sample coated on fluorine-doped tin oxide (FTO) electrode) before and after recording 1000 cycle scans of CV were also recorded (**Figure 2.12. (a-d)**). All these observations of controlled experiments provide convincing information about the robustness and stability of compound **1** as WOC.

Coated sample of compound **1** on the electrode was characterized by PXRD analysis after 1000 cycle CV scans and was compared with the simulated PXRD pattern obtained from *cif* file (crystal data) of **1** (**Figure 2.12. (g)**).

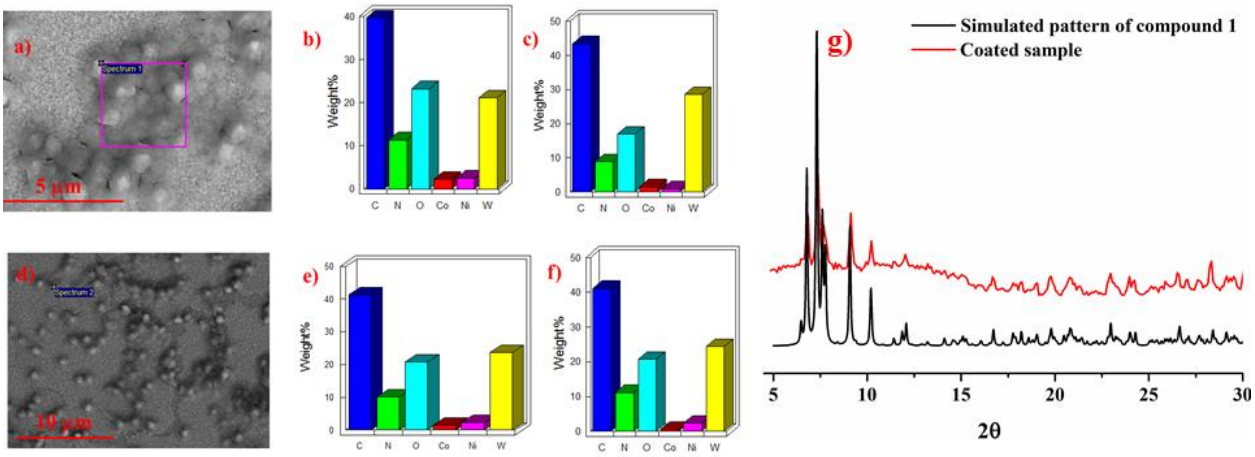

Figure 2.12. Comparison of EDX-Elemental analysis of different areas of carbon mixed coated sample on FTO before ((**a)-(c)**) and after ((**d)-(f)**) electrochemical analysis (1000 cycle scans of CV in 0.1 M phosphate buffer, pH 7). **(g)** Comparison of PXRD pattern of coated sample of **1** on FTO electrode after 1000 cycles of CV scans (red solid line) and simulated PXRD pattern generated from *cif* file of **1** (black solid line).

2.3.2.3. ICP OES report of electrolyte solution after 1000 cycles cyclic voltammetry

To check the leaching of Co^{2+}/ Ni^{2+} ions in electrolytes, ICP-OES analysis was done for the electrolyte after CPE measurement. ICP data of the electrolyte, collected after 8 h CPE measurements of **1** confirms no leaching out of Co^{2+} and $Ni^{2+,}$ making it evident that compound **1** is a true catalyst and does not degrade during WO catalysis (**Figure 2.13.**).

Issued to:
Prof Samar K.Das
School Of Chemistry
University of Hyderabad, Gachibowli,
Hyderabad-500046
Kind Attn.: Prof. Samar K Das,

Report No. :LLPL/D/17-18/001371
Issue Date : 14/09/2017
Customer Ref. TRF

Ref.Date : 30/08/2017

Sample Particulars : Neutral electrolyte of compound 1

Qty. Received : 1no Plastic Vail

Test Parameters : Nickel as Ni,Cobalt as Co

Date of Receipt of Sample : 12/09/2017 **Date of Starting of Analysis :** 13/09/2017
Date of completion of analysis : 14/09/2017 *SAMPLE TESTED AS RECEIVED*

TEST RESULTS

S.No.	Parameters	UOM	Results
1	Nickel as Ni	ppm	Not detected
2	Cobalt as Co	ppm	Not detected

Instrument Used: ICP-OES Varian 720-ES
NOTE : This report and results relate only to the sample / items tested.

Figure 2.13. Report of ICP-AES analysis of electrolyte (0.1 M phosphate buffer, pH 7) after 8 h CPE analysis of coated sample of compound **1.**

2.3.2.4. Controlled experiments

The crystal structure of compound **1** confirms the presence of three types of metal ions, which may probably catalyze electrochemical WO. These are Ni(II) from two different sources, *i.e.* $[Ni(2,2'\text{-bpy})_2H_2O]^{2+}$ and $[Ni(2,2'\text{-bpy})_3]^{2+}$ and Co(II) center from the POM unit. The mechanism of WO for the mononuclear Co^{2+} complex is well established. The requirement to form a Co(IV) intermediate in case of molecular Co-based WOC has been validated by Nocera[27a] and Berlinguette[27b], few of the pioneers in this field. Due to structural restriction for the central Co^{2+} (tetrahedral CoO_4 unit caged by 12 WO_6 units of Keggin POM) in **1**, it cannot bind to water molecule to perform catalytic WO. Involvement of central Co(II) of POM unit as a catalytic active center would probably lead to degradation of the concerned POM unit, thereby collapsing the whole structure.[12] $[Ni(2,2'\text{-bpy})_3]^{2+}$ unit, present in the crystal lattice, if participates in catalytic WO, would degrade into NiO_x due to its coordination to the rigid ligand sphere forming an octahedral geometry.

In order to negate the possibility of Keggin POM unit to function as the catalytic center in the present work, we recorded CV of $\mathbf{CoW_{12}}$ (1 mmol in an aqueous homogeneous medium) at a neutral pH using phosphate buffer (0.1 M). The formation of precipitate was observed in the cell

prior to application of any external potential. 500 cycles of CVs were carried out at 100 mV/s scan rate using the same cell without changing anything. After completing 500 cycles, the working electrode (FTO electrode) was taken out and washed with Milli-Q water slowly. A dark deposit was observed on the surface of WE after CPE measurement for 8 h. The chemical composition of this coat, obtained from the degradation of CoW_{12}, is confirmed to be composed of cobalt, phosphorous and oxygen from the EDX-elemental analysis. Henceforth, it is referred as 'CoP_xO_y generated from **CoW_{12}**'(**Figure 2.14.**). New CV and CPE for 6h were recorded with this deposited moiety using similar conditions (0.1 M phosphate buffer, pH 7) used for the CV of **1**. The nature of CV obtained from this differs in terms of peak potential, peak current, and onset potential from that obtained for compound **1** (**Figure 2.15. (a)**).

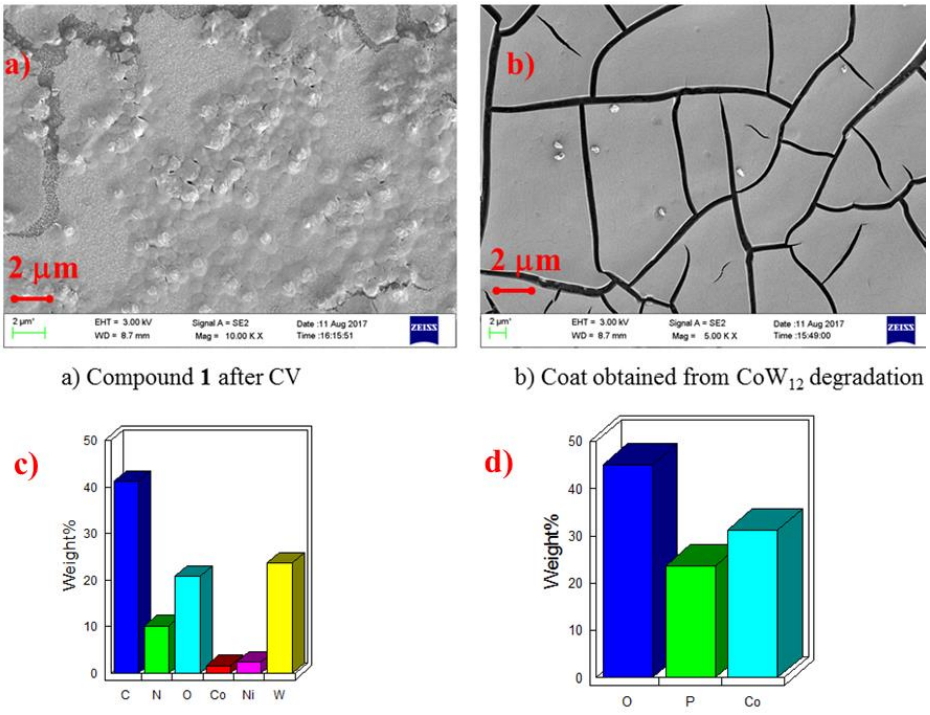

Figure 2.14. FESEM images and Quantitative representation of weight percentage of their constituent atom in sample coat on FTO electrode obtained after 8h CPE of sample, (**a**,**c**) Compound **1** (**b**,**d**) $K_6[CoW_{12}O_{40}]$; both in 0.1 M phosphate buffer, pH 7.

CPE at 1.3 V for 6 h conducted for 'CoP_xO_y generated from **CoW_{12}**' shows a steady increase in current with time (**Figure 2.15. (b)**).This nature of CPE confirms the lack of stability in 'CoP_xO_y generated from **CoW_{12}**' and the generation of more active species during this time course. It is noteworthy that the active species loses its catalytic activity after some time. These observations do not have any similarities with the electrochemical properties of compound **1**. Thus, it

confirms that there is no participation of either **CoW_{12}** as such or any degraded product formed from **CoW_{12}** while using **1** as an electrochemical WO catalyst.

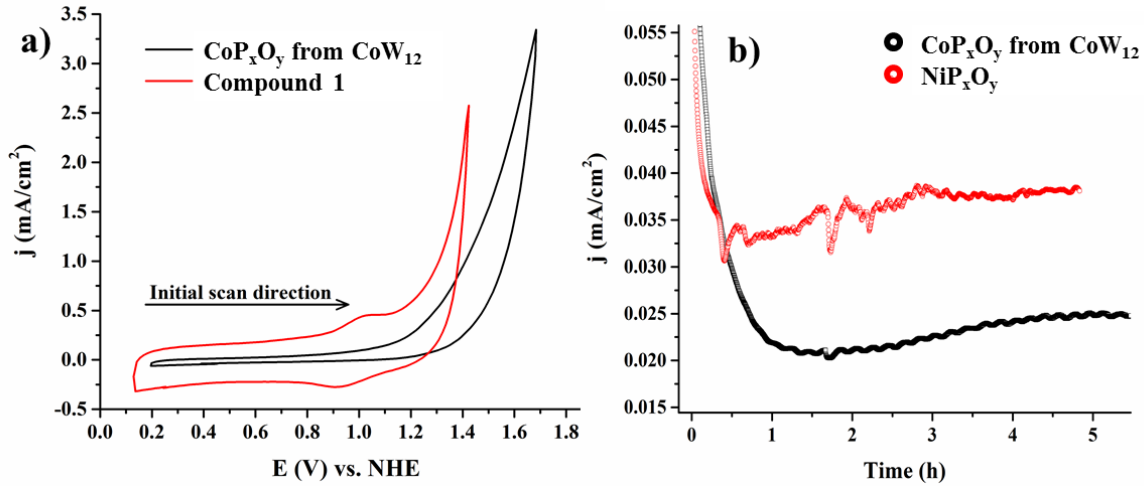

Figure 2.15. (a) Cyclic voltammograms of CoP_xO_y generated from **CoW_{12}** and compound **1** CV recorded in 0.1 M phosphate buffer, pH 7. **(b)** Constant potential electrolysis (CPE) of sample obtained after 500 cycles scan by preparing 1 (mM) **CoW_{12}** in 0.1 M phosphate buffer (pH 7) for 6 h at 1.3 V, denoted by symbol (**o**) and labeled as CoP_xO_y obtained from **CoW_{12}** and similarly for $NiCl_2$ salt, we obtained a coat on FTO electrode which was subjected to CPE at 1.3 V for 6 h,denoted by NiP_xO_y (**o**).

2.3.2.4.1. Analysis of oxides and phosphates of Ni(II) & Co(II) salts

Synthesis of NiO_x and CoO_x: 1 (mM) $NiCl_2$ solution was prepared in 0.1 M KOH and FTO electrode was used as working electrode. Constant potential electrolysis was done at high anodic potential (1.4 V vs. NHE) for 30 min to obtained a coating of NiO_x on FTO electrode. This coating was gently washed with Mili-Q water before using it further for electrochemical studies. Similar method was used for CoO_x synthesis (instead of $NiCl_2$, $CoCl_2$ was used as starting material).

Synthesis of NiP_xO_y and CoP_xO_y: 1 (mM) $NiCl_2$ solution was prepared in 0.1 M phosphate buffer having pH 11 and FTO was used as working electrode. Constant potential electrolysis was done at high anodic potential (1.4 V vs. NHE) for 30 min to obtain a coating of NiP_xO_y on FTO electrode. This coating was gently washed with Mili-Q water before using it further for electrochemical studies. Similar method was used for CoP_xO_y synthesis. Instead of $NiCl_2$, $CoCl_2$ was used as starting material.

Once these oxides are successfully generated by following above mentioned protocol, we recorded CVs in neutral pH (0.1 M Na_2SO_4, was used as electrolyte for oxides and 0.1 M

phosphate buffer, pH 7 was used as electrolyte for phosphates). For oxides (Ni & Co), 0.1 M Na_2SO_4 was used to avoid formation of phosphate layer over the oxide layer generated.

CVs recorded for every species is provided in **Figure 2.16.** and **Figure 2.17.** After recording CVs for 50 scans, FESEM images along with EDX elemental analysis of the coated samples were taken (**Figures 2.18.-2.21.**). For each sample, EDX analysis was carried over different region to check on the homogeneity of the sample.

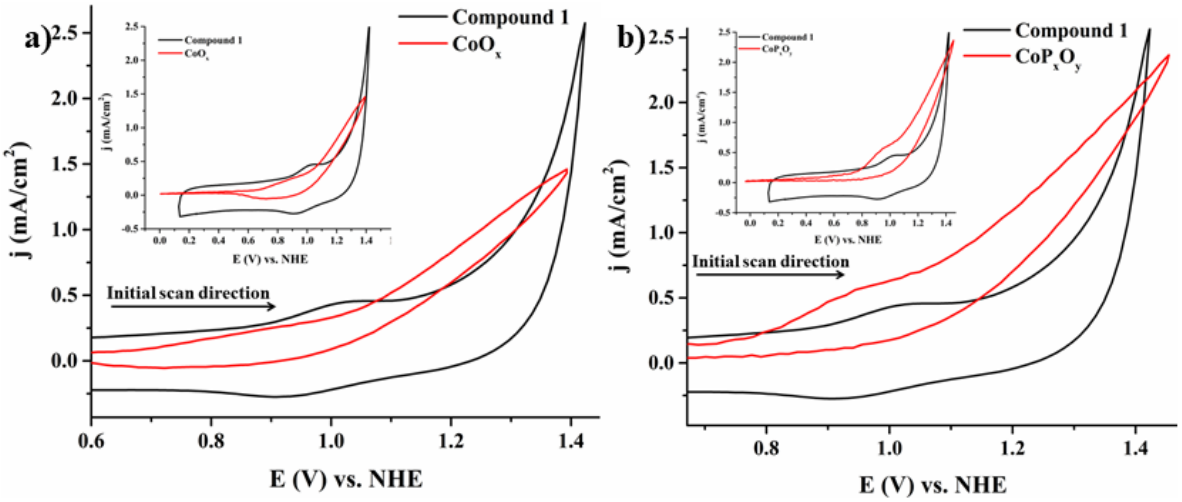

Figure 2.16. Cyclic voltammograms of **(a)** CoO_x on FTO in 0.1 M Na_2SO_4, pH 7 and compound **1** in 0.1 M phosphate buffer, pH 7 and **(b)** of CoP_xO_y generated on FTO, in 0.1 M phosphate buffer, pH 7 and compound **1** in 0.1 M phosphate buffer, pH 7.

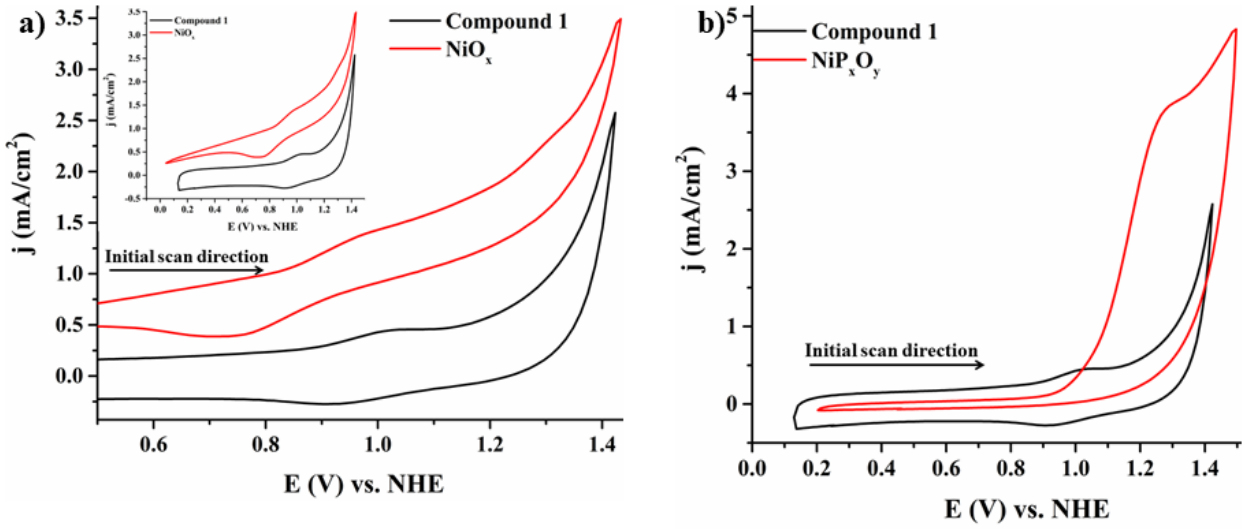

Figure 2.17. Cyclic voltammograms of **(a)** NiO_x on FTO in 0.1 M Na_2SO_4, pH 7 and compound **1** in 0.1 M phosphate buffer, pH 7 and **(b)** of NiP_xO_y generated on FTO, in 0.1 M phosphate buffer, pH 7 and compound **1** in 0.1 M phosphate buffer, pH 7.

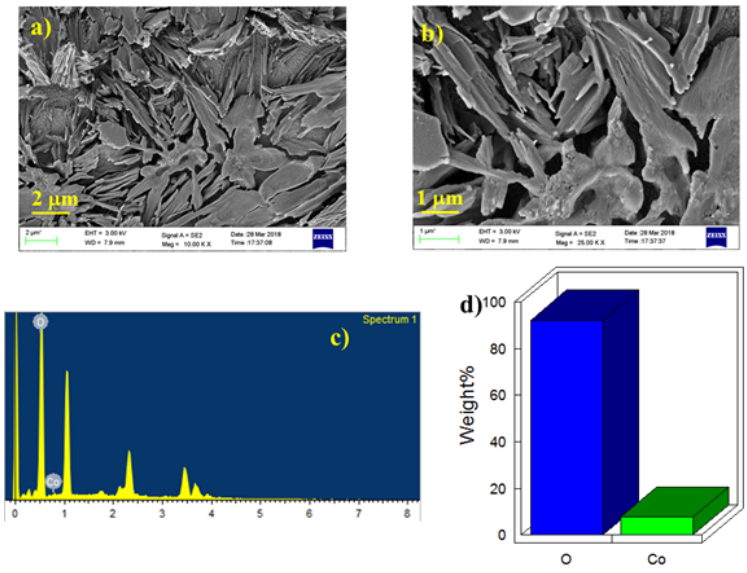

Sample	Oxygen		Cobalt	
	Wt %	Atom %	Wt %	Atom %
Area 1	92.6	97.77	7.74	2.23
Area 2	92.21	97.28	7.79	2.72
Area 3	92.83	97.93	7.17	2.07

Figure 2.18. (a)-(b) FESEM images of CoO_x deposited on FTO obtained after 100 cycle scans of CV in 0.1 M KOH containing 1 mmol $CoCl_2$. **(c)** Energy-dispersive X-ray spectroscopy (EDX) spectrum of CoO_x. **(d)** Quantitative representation of weight percentage of their constituent atom in the sample coat on FTO electrode obtained after 500 cycle scans of CV. Table represents the EDX analysis over different region of the surface of CoO_x.

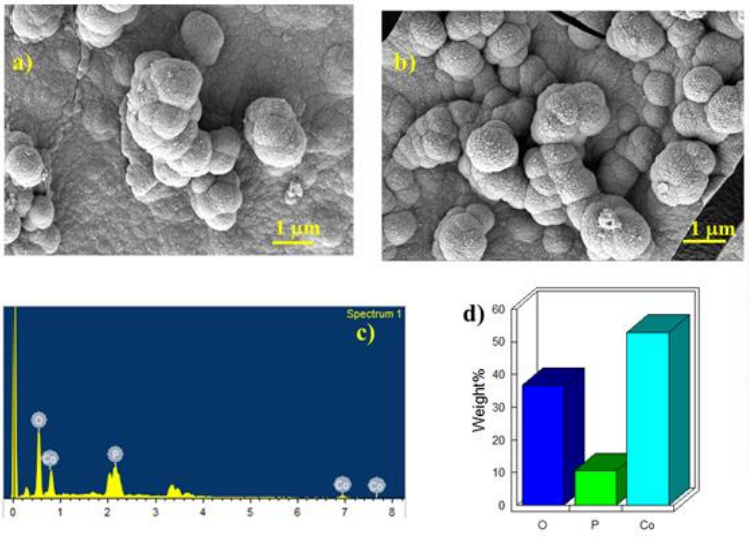

Sample	Oxygen		Cobalt		Phosphorous	
	Wt %	Atom %	Wt %	Atom %	Wt %	Atom %
Area 1	36.67	64.97	52.81	25.40	10.52	9.63
Area 2	37.20	65.45	52.54	25.21	10.26	9.33
Area 3	36.84	65.21	53.22	25.84	9.94	8.95

Figure 2.19. (a)-(b) FESEM images of CoP_xO_y deposited on FTO obtained after 100 cycle scans of CV in 0.1 M KOH containing 1 mmol $CoCl_2$. **(c)** Energy-dispersive X-ray spectroscopy (EDX) spectrum of CoP_xO_y. **(d)** Quantitative representation of weight percentage of their constituent atom in the sample coat on FTO electrode obtained after 500 cycle scans of CV. Table represents the EDX analysis over different region of the surface of CoP_xO_y.

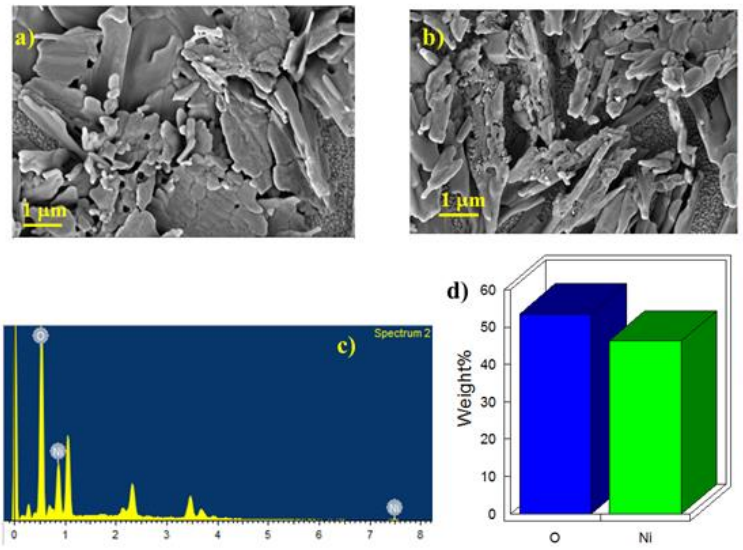

Sample	Oxygen		Nickel	
	Wt %	Atom %	Wt %	Atom %
Area 1	53.60	80.92	46.40	19.08
Area 2	52.80	79.20	47.20	20.80
Area 3	53.24	80.35	46.80	19.65

Figure 2.20. (a)-(b) FESEM images of NiO_x deposited on FTO obtained after 100 cycle scans of CV in 0.1 M KOH containing 1 mmol $NiCl_2$. **(c)** Energy-dispersive X-ray spectroscopy (EDX) spectrum of NiO_x. **(d)** Quantitative representation of weight percentage of their constituent atom in the sample coat on FTO electrode obtained after 500 cycle scans of CV. Table represents the EDX analysis over different region of the surface of NiO_x.

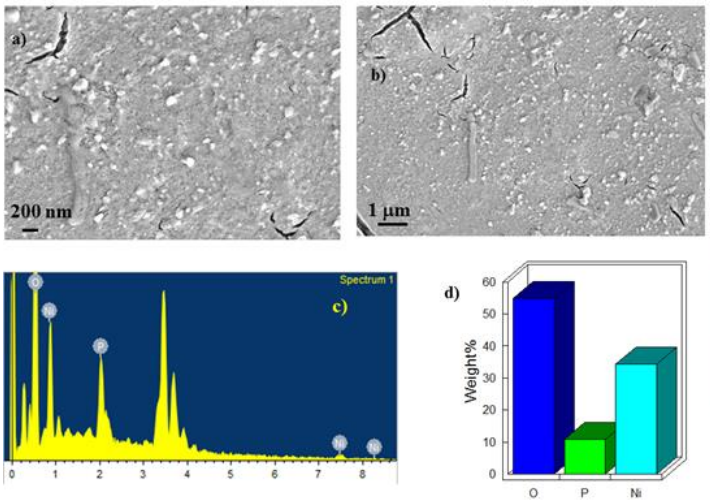

Sample	Oxygen		Nickel		Phosphorous	
	Wt %	Atom %	Wt %	Atom %	Wt %	Atom %
Area 1	54.92	78.65	34.34	13.40	10.74	7.94
Area 2	53.52	77.84	35.96	14.25	10.52	7.91
Area 3	54.77	78.30	34.85	13.83	10.31	7.86

Figure 2.21. (a)-(b) FESEM images of NiP_xO_y deposited on FTO obtained after 100 cycle scans of CV in 0.1 M KOH containing 1 mmol $NiCl_2$. **(c)** Energy-dispersive X-ray spectroscopy (EDX) spectrum of NiP_xO_y. **(d)** Quantitative representation of weight percentage of their constituent atom in the sample coat on FTO electrode obtained after 500 cycle scans of CV. Table represents the EDX analysis over different region of the surface of NiP_xO_y.

In order to understand and correlate the kinetics followed by each of these species and compound **1**, we have devised Tafel plot. iR (cell resistance) corrected Tafel plot was constructed in 0.1 M Na_2SO_4, pH 7, for oxides and 0.1 M phosphate buffer, pH 7, for phophates (**Figure 2.22.**). The

slope of Tafel plot defines the kinetics involved, which varies tremendously for each of them. In **Table 2.4.**, Tafel slopes for all these species including compound **1** is provided.

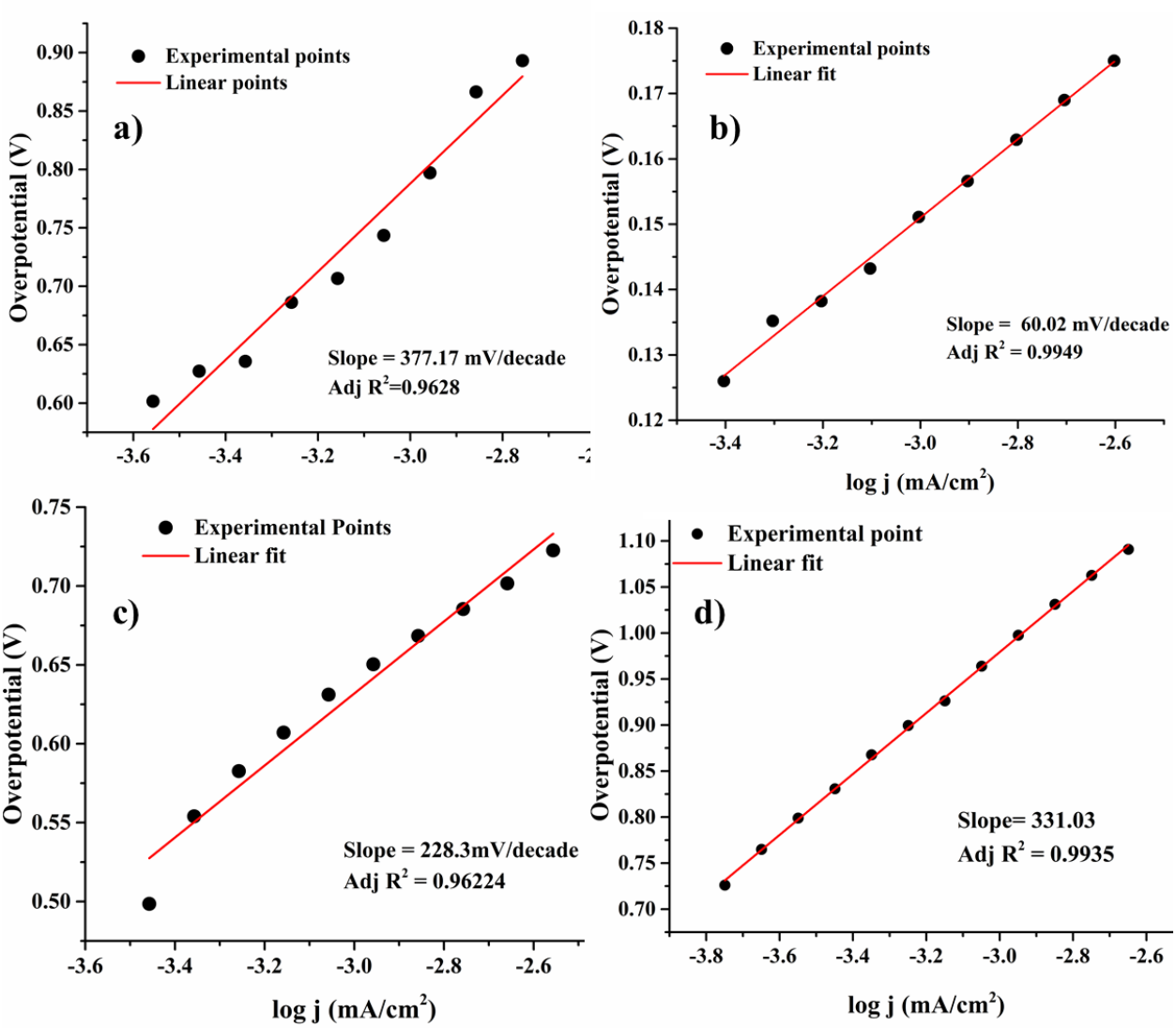

Figure 2.22. Galvanostatic iR corrected Tafel plot of **(a)** CoO_x, in 0.1 M Na_2SO_4 (pH 7), **(b)** CoP_xO_y, in 0.1 M phosphate buffer (pH 7), **(c)** NiO_x, in 0.1 M Na_2SO_4 (pH 7), **(d)** NiP_xO_y, in 0.1 M phosphate buffer (pH 7).

In order to find out whether any participation is coming from the degraded product of Ni(II) containing units ($\{Ni^{II}(2,2'\text{-bpy})_2(H_2O)\}^{2+}$ and $[Ni^{II}(2,2'\text{-bpy})_3]^{2+}$), we conducted the following controlled experiments as mentioned below:

(i) We have synthesized $[Ni^{II}(2,2'\text{-bpy})_2(H_2O)Cl]Cl$ and $[Ni^{II}(2,2'\text{-bpy})_3]Cl_2$ following reported protocols,[21] and conducted constant potential electrolysis (CPE) and cyclic voltammetry for both of them (**Figure 2.23.**).

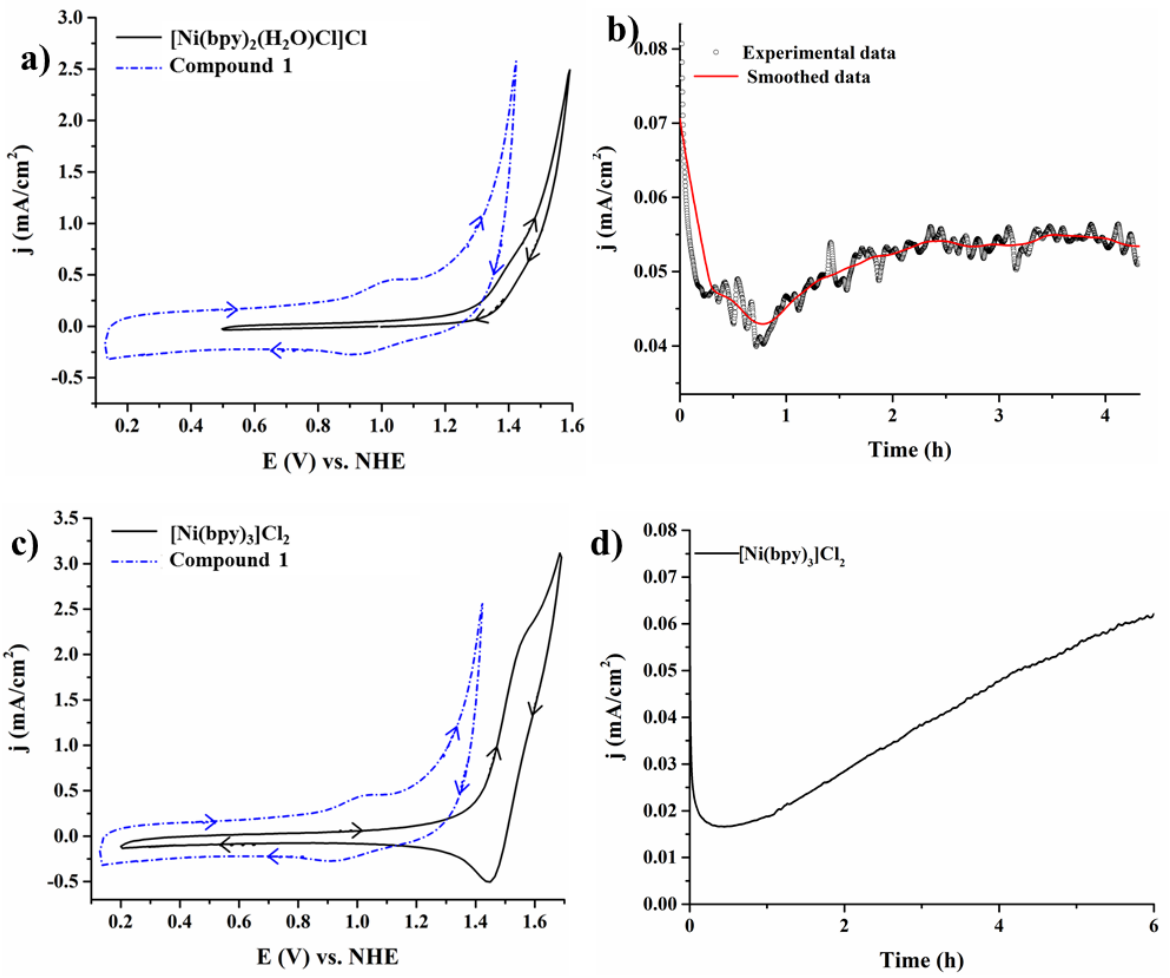

Figure 2.23. (a) Cyclic voltammograms of 1 mmol [Ni(2,2′-bpy)$_2$(H$_2$O)Cl]Cl complex and compound **1**. **(b)** CPE of [Ni(2,2′-bpy)$_2$(H$_2$O)Cl]Cl at 1.2 V for 8 h. **(c)** Cyclic voltammograms of 1 (mM) [Ni(2,2′-bpy)$_3$]Cl$_2$ and compound **1**. **(d)** CPE of [Ni(2,2′-bpy)$_3$]Cl$_2$ at 1.2 V for 8 h. All the experiments were done in 0.1 M phosphate buffer, pH 7.

(ii) 1 mmol solution of $NiCl_2$ was prepared in 0.1 M KOH, and was subjected to high anodic potential (0-1.6V) for 200 cycles of cyclic voltammetry. These CV scans were recorded with FTO as WE. Application of such high anodic potential during CV is known to form NiO_x from $NiCl_2$ salt.[9c] Formation of NiO_x was confirmed by EDX elemental mapping (**Figure 2.20.**). In similar fashion CoO_x was synthesized by using 1 mmol of $CoCl_2$ instead of $NiCl_2$ and characterized (**Figure 2.18.**). For these species, generated electrochemically on FTO, cyclic voltammetric measurements were carried out in 0.1 M Na_2SO_4 at pH 7. iR (cell resistance) corrected Tafel plot was also constructed for each of these compounds to have an idea about their water oxidation kinetics.

(iii) NiP_xO_y, was developed by preparing 1 mmol $NiCl_2$ in 0.1 M phosphate buffer having pH 10, and applying high anodic potential (0-1.6 V). A dark colored coating was formed on FTO electrode. Prior to indulging in any electrochemical study by using this coat, it was washed slowly with mili-Q water. Formation of NiP_xO_y on FTO was confirmed by EDX elemental mapping (**Figure 2.21.**). Using the same protocol CoP_xO_y was synthesized and characterized (**Figure 2.19.**). Modification in the procedure was just to replace $NiCl_2$ by $CoCl_2$. For these species generated, electrochemically on FTO, CV was recorded and iR (cell resistance) corrected Tafel plot was constructed in galvanostatic mode in 0.1 M phosphate buffer, pH 7. For NiP_xO_y CPE was conducted at 1.3 V for 6 h.

Table 2.4. Comparison of Tafel slope of electrochemically generated oxides & phosphates of Ni & Co with compound **1**.

S. No.	Name/Chemical composition	Tafel Slope (mV/decade)
1.	Compound **1**	168.41
2.	NiP_xO_y	331.03
3.	CoP_xO_y	60.02
4.	NiO_x	228.3
5.	CoO_x	377.17

FESEM images of all these electrochemically generated species (oxides and phosphates) were taken and compared with the coated sample of compound **1** obtained after 1000 cycle scans of CV on FTO electrode (**Figures 2.14.**, **2.18.**, **2.21.**).

2.3.2.5. Kinetics and Mechanism involved in catalyzing water oxidation by Compound 1

To deduce the mechanism of WO, cyclic voltammetric study was conducted in a wide pH range (acidic and neutral pH) (**Figure 2.24. (a)**). A derived plot has been constructed from these CVs of **1** obtained by varying pH, where the required potential values for a fixed current density of 0.76 mA/cm^2 is plotted against varied pH values. The reason behind the choice of large current density is to negate the interference of diffusional peak current. A linear plot is obtained over the

pH range 3-7 with the slope of -27.4 mV/pH (**Figure 2.24. (b)**). This suggests that present system **1** catalyzes WO *via* proton coupled electron transfer (PCET) pathway where 2 electrons and 1 proton are involved.[9c] The rate determining step (RDS) is confirmed by the changes observed in normalized current density ($j/\nu^{1/2}$) with variation in scan rate. CV scans were recorded by varying the scan rates (**Figure 2.25. (a)**). With increasing scan rate, normalized current density is found to decrease (**Figure 2.25. (b)**). This infers a chemical process *i.e.* formation of O-O bond as rate limiting step.[28]

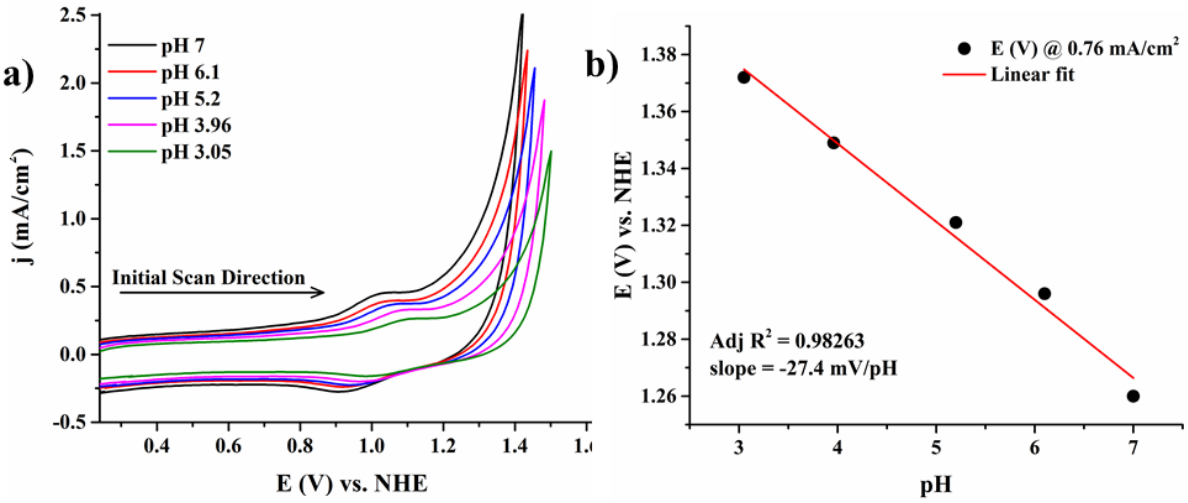

Figure 2.24. (a) Cyclic voltammograms of **1** in 0.1 M phosphate buffer by varying pH; Fresh coat of sample (compound **1**) was used before running CV in each pH. **(b)** Derived plot of potential (at j= 0.76 mA/cm^2) vs. pH for compound **1**.

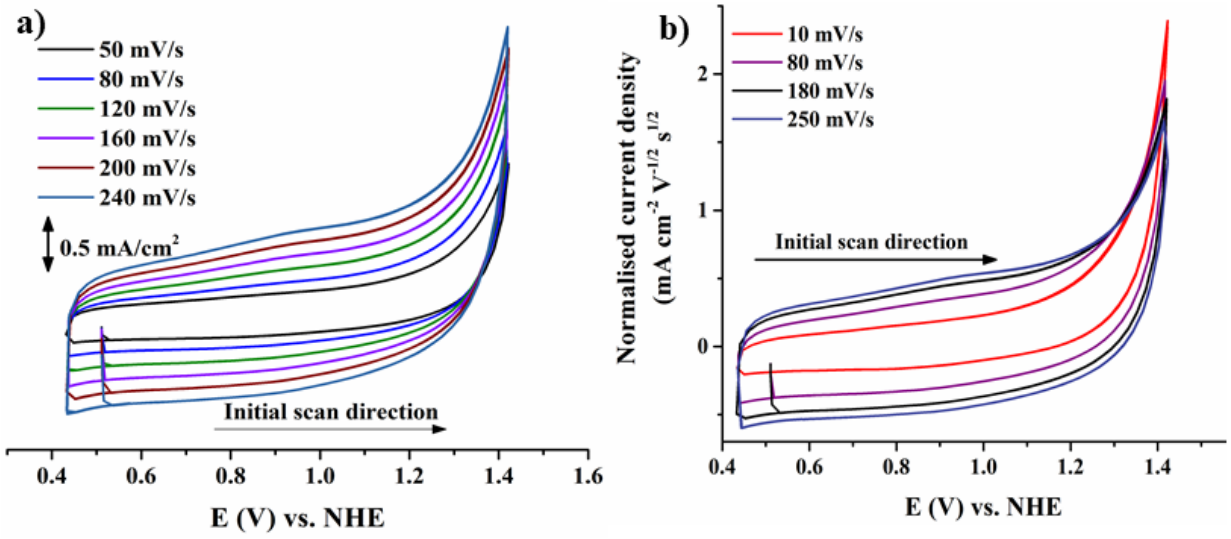

Figure 2.25. (a) Cyclic voltammograms of **1** at various scan rates in 0.1 M phosphate buffer at pH 7. **(b)** The plots of normalized current density versus potential of **1** at various scan rates in 0.1 M phosphate buffer at pH 7.

2.3.2.6. Tafel plot

The galvanostatic mode was used for calculating Tafel data. To obtain the plot, we administered a constant current for about 10 minutes, after which the steady-state potential was noted. Following a similar method for 10 different currents values in the range of 10^{-5} A to 10^{-3} A, potential values were recorded. To maintain steady-state mass flow to the electrode, the electrolyte solution was stirred at 450 rpm throughout the experiment. Before starting the measurement, the solution resistance was recorded by directly reading the instrument's iR function value. The uncompensated resistance values were manually corrected for each current value by employing this resistance value.

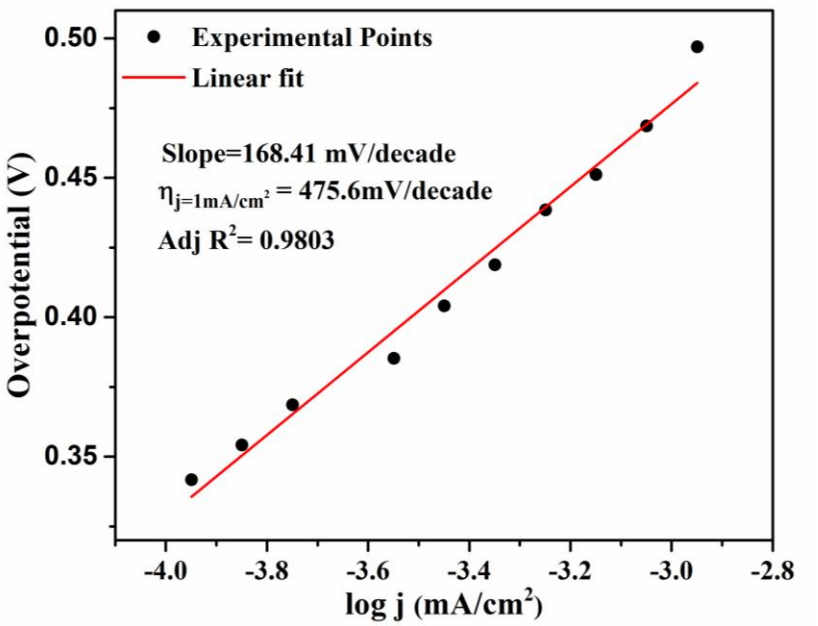

Figure 2.26. Galvanostatic *iR* corrected Tafel plot of **1** at pH 7 (0.1 M phosphate buffer).

Thus, iR (cell resistance) corrected Tafel plot was devised with 0.1 M phosphate buffer in galvanostatic mode. Overpotential (η) of 475.6 mV was observed for **1** at current density of 1mA/cm^2 (**Figure 2.26.**) and high turnover frequency (TOF) of 18.49 s^{-1} was calculated.

2.3.2.7. Faradic efficiency calculation

Calculation of Faradaic Efficiency of 1

For faradic efficiency calculation, we quantified the oxygen evolved by the system by carryin out bulk electrolysis for a constant current. This experiment was carried out using a two-electrode system where fluorinated tin oxide (FTO) with a surface area of 0.75 cm^2 was taken as working electrode while a large area platinum flag was used as the counter electrode (cathode). The loading of the catalyst was done in such a way to obtain a 1 mg/cm^{-2} of sample on FTO working electrode surface. 0.1 M phosphate buffer (pH 7) was used as the electrolyte. For this experiment, we employed a home-built set-up that can measure the volume of O_2 evolved with a precession of 0.05 mL). Bulk-electrolysis was carried out by administrating a constant current density of 1 mA/cm^2 for a period of 5 h.

During the electrolysis, oxygen bubbles evolved by the catalysis of **1,** initially gathered at the FTO electrode's surface, and later accumulating in an inverted graduated tube (previously filled with electrolyte) displacing the electrolyte (**Figure 2.27.**). The home-made set-up design is such that it separates the gas evolved at anode and cathode without hampering the measurements. A small window between the working and counter electrode maintained the electrical continuity in the system. Thus, H_2 gas generated from the counter electrode formed a ring of the bubble around the inverted graduated tube (but could not get inside the tube).

Calculation of Faradaic Efficiency of 1

Faradaic efficiency of any system describes the efficiency with which charge is utilized in an electrochemical reaction.

For oxygen evolving reaction, Faradic efficiency can be written as,

$$\frac{\text{Moles of } O_2 \text{ evolved by the system}}{\text{Moles of } O_2 \text{ that can evolve by using the applied charge}}$$

From the bulk-electrolysis, the quantitative measurement of oxygen evolved was measured under constant current condition. For this work, we found 0.15 mL/hour of O_2 evolved under 1 atm. pressure.

Thus, moles of O_2 evolved in one hour = (0.15/22400) mol = 6.21 µmol.

$$O_{2\ ideal} = \frac{\text{Q (Total Charge employed)}}{\text{n (no. of electrons required for the chemical change X 1 Farad)}}$$

Here, we employed a current density of 1 mA/cm^2 and 'n'= 4 for OER (a four-electron process).

Thus, O_2 that ideally should evolve = (75 × 3600)/(4 × 96500) mol = 6.995 µmol.

Therefore Faradaic efficiency of compound **1**,

$$= \frac{6.21}{6.995} \times 100 = 88.7\%$$

Thus, Faradic efficiency is **88.7%** for compound **1**.

Home-made set-up used for quantitative measurement of oxygen evolved

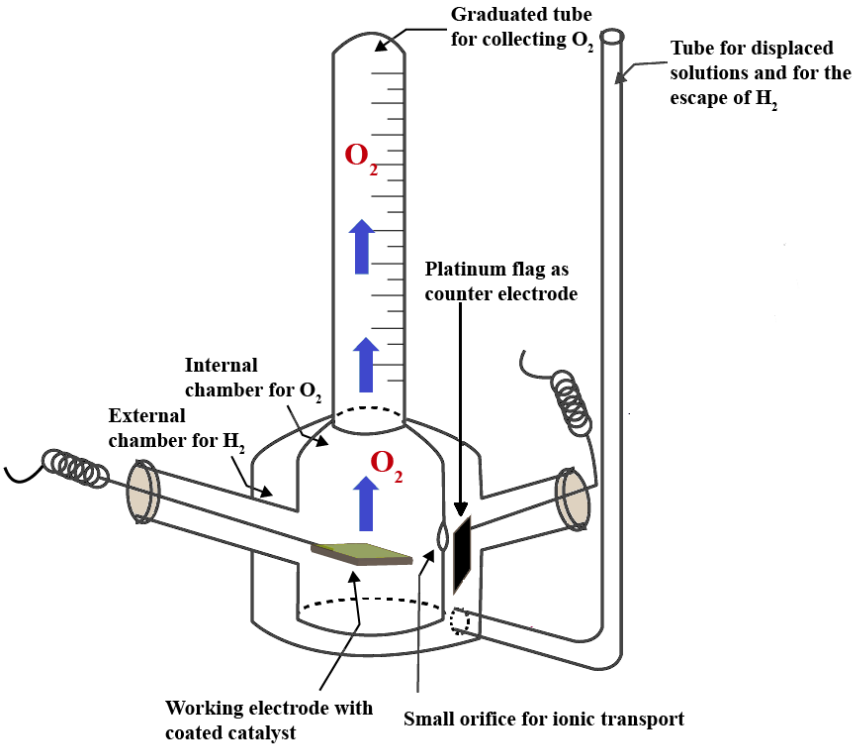

Figure 2.27. Schematic diagram of home-built set-up employed for quantitative measurement of oxygen evolution.

2.3.2.8. Turnover Frequency (TOF) Calculation

- **Calculation of Surface Coverage and number of active nickel atoms**

In order to calculated the active Ni atoms/cm^2 on the electrode surface, we measured the surface coverage (Γ_0) from the slope (9.548 E-6 F) of the i_p *vs* scan rate (**Figure 2.28.**) (obtained from **Figure 2.25. (a)**), using the equation 1 using a method recently described by Pintado *et al*.[34]

$$\text{Slope} = n^2F^2A\Gamma_0/4RT \qquad \text{..... (1)}$$

Where 'n' = No. of electrons involved, here 1. For Ni(II) – Ni(III) conversion.

'F' = 1 Farad = 96,500 C.

'A' = Geometrical surface area of electrode.

'R' = Ideal Gas Constant.

'T' = Temperature during experiment (298 K).

'Γ_0' = Surface density of active Nickel atoms.

Γ_0= (Slope)(4RT)/ n^2F^2A

By substituting all the values, we found out that surface density of active nickel atoms is 84.4×10^{12} Nickel atoms/cm^2 or 1.401×10^{-10} mol/cm^2.

- **Calculation of Turnover Frequency (TOF) for O_2 evolution from Tafel Plot:**

The TOF can be written as,

$$\text{TOF at any given over potential} = \frac{\text{Current density at given over potential}}{4 \times F \times \text{No. of active Nickel species/atoms}} \qquad \text{..... (2)}$$

OER being 4e$^-$ process, the numeric 4 can be seen in the equation 2. Hence, by dividing the current density at a particular overpotential by 4F (F = Faraday constant), we can get one catalytic turnover number, and further dividing this turnover number by the number of active Nickel atoms gives us the turnover frequency (TOF).

$$(\text{TOF})_{j=1\ \text{mA/cm}^2} = \frac{10^{-3}}{4 \times F \times 1.401E^{-10}} \qquad \text{..... (3)}$$

Thus $(TOF)_{j=1\ mA}$ = **18.49** [mol O_2 (mol Ni)$^{-1}s^{-1}$]

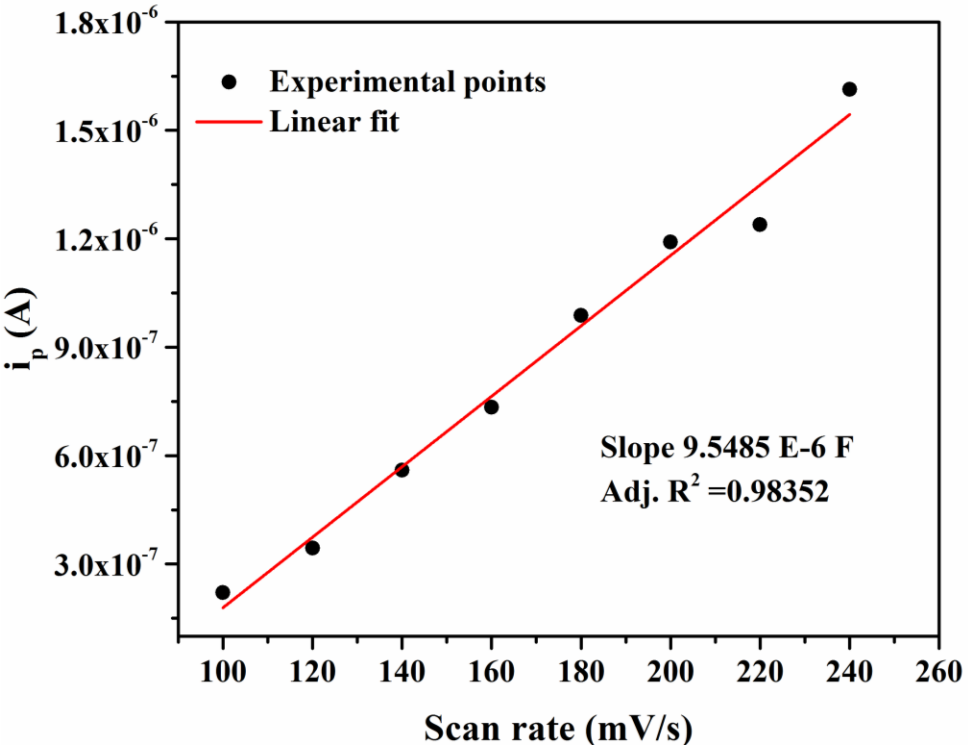

Figure 2.28. Peak current (i_p) as a function of scan rate of **1** in 0.1 M phosphate buffer (pH 7).

2.4. Conclusion

To conclude, we are able to synthesize a new hybrid compound, $[Ni^{II}(2,2'\text{-bpy})_3]_3[\{Ni^{II}(2,2'\text{-bpy})_2(H_2O)\}\{HCo^{II}W^{VI}_{12}O_{40}\}]_2\cdot 3H_2O$ (**1**), containing POM as inorganic unit and 2,2′-bipyrine as organic unit linked together with Ni(II) metal ion. This is the first report of such a class of compound where insights of water oxidation (WO) during electrochemical process are explained by **confirming no formation of metal oxide during the process**. Ni(II) from $\{Ni^{II}(2,2'\text{-bpy})_2(H_2O)\}$ unit acts as a catalytically active center. The title compound **1** is found to be highly stable, robust under the electrochemical conditions required for WO at pH 7. It shows moderate value of overpotential of 475.6 mV accompanied with a very high turnover frequency 18.49 s^{-1}. The catalytic cycle proceeds with O-O bond formation as rate-limiting step. Overall, this work has provided a glimpse that a 'wide-range' class of polyoxometalate (POM) supported

transition metal complexes with (at least) one metal-coordinated water molecule (essential for water oxidation), for example, compound $[Ni^{II}(2,2'\text{-bpy})_3]_3[\{Ni^{II}(2,2'\text{-bpy})_2(H_2O)\}\{HCo^{II}W^{VI}_{12}O_{40}\}]_2 \cdot 3H_2O$ (**1**) in the present work, have potential to act as electrocatalysts for efficient water oxidation.

2.5. References

1. (a) Davis, S. J.; Caldeira, K.; Matthews, H. D. Future CO_2 Emissions and Climate Change from Existing Energy Infrastructure. Science **2010**, *329*, 1330−1333. (b) United Nations Development Program (2003) *World Energy Assessment Report: Energy and the Challenge of Sustainability* (United Nations, New York). (c) Lewis, N. S.; Nocera, D. G. Powering the Planet: Chemical Challenges in Solar Energy Utilization. *Proc. Natl. Acad. Sci. U. S. A.* **2006**, *103*, 15729−15735. (d) Gray, H. B. Powering the Planet with Solar Fuel. *Nat. Chem.* **2009**, 1, 7−7. (e) Lewis, N. S.; Crabtree, G. Basic Research Needs for Solar Energy Utilization: Report of the Basic Energy Sciences Workshop on Solar Energy Utilization, Apr 18−21, **2005**. US Department of Energy Office of Basic Energy Sciences, **2005**.
2. (a) Kudo, A.; Miseki, Y. Heterogeneous Photocatalyst Materials for Water Splitting. *Chem. Soc. Rev.* **2009**, *38*, 253−278. (b) Kärkäs, M. D.; Verho, O.; Johnston, E. V.; Åkermark, B. Artificial Photosynthesis: Molecular Systems for Catalytic Water Oxidation. *Chem. Rev*. **2014**, *114*, 11863-12001. (c) O'Regan, B.; Grätzel, M. A Low-Cost, High-Efficiency Solar Cell Based on Dye-Sensitized Colloidal TiO_2 Films. *Nature* **1991**, *353*, 737−740. (d) Kanan, M. W.; Nocera, D. G. Future CO_2 Emissions and Climate Change from Existing Energy Infrastructure. *Science* **2008**, *321*, 1072−1075. (e) Smith, R. D. L.; Prevot, M. S.; Fagan, R. D.; Zhang, Z. P.; Sedach, P. A.; Siu, M. K. J.; Trudel, S.; Berlinguette, C. P. Photochemical Route for Accessing Amorphous Metal Oxide Materials for Water Oxidation Catalysis. *Science* **2013**, *340*, 60−63.
3. Lv, H.; Geletii, Y. V.; Zhao, C.; Vickers, J. W.; Zhu, G.; Luo, Z.; Song, J.; Lian, T.; Musaev, D. G.; Hill, C. L. Polyoxometalate Water Oxidation Catalysts and the Production of Green Fuel. *Chem. Soc. Rev.* **2012**, *41***,** 7572-7589. (b) Anantharaj, S.; Karthick, K.; Kundu, S. $NiTe_2$ Nanowire Outperforms Pt/C in High-Rate Hydrogen Evolution at Extreme pH Conditions. *Inorg. Chem.* **2018**, *57*, 3082-3096.
4. (a) Vrettos, S.; Limburg, J.; Brudvig, G. W. Mechanism of Photosynthetic Water Oxidation: Combining Biophysical Studies of Photosystem II with Inorganic Model Chemistry. *Biochim. Biophys. Acta Bioenerg.* **2001**, *1503*, 229-245. (b) Hoganson, C. W.; Babcock, G. T. A Metalloradical Mechanism for the Generation of Oxygen from Water in Photosynthesis. *Science* **1997**, *277*, 1953-1956. (c) Siegbahn, P. E. M.; Crabtree, R. H. Manganese Oxyl Radical

Intermediates and O−O Bond Formation in Photosynthetic Oxygen Evolution and a Proposed Role for the Calcium Cofactor in Photosystem II. *J. Am. Chem. Soc.* **1999**, 121, 117-127.

5. (a) Ort, D. R.; Yocum, C. F. Electron Transfer and Energy Transduction in Photosynthesis: An Overview. In Oxygenic Photosynthesis: The Light Reactions; Ort, D. R., Yocum C. F., Heichel I. F., Eds.; Advances in Photosynthesis and Respiration; Springer: Dordrecht, **1996**; Vol. 4, pp 1-9. (b) Yachandra, V. K.; DeRose, V. J.; Latimer, M. J.; Mukerji, I.; Sauer, K.; Klein, M. P. Where Plants Make Oxygen: a Structural Model for the Photosynthetic Oxygen-Evolving Manganese Cluster, *Science* **1993**, *260*, 675–679. (c) Yano, J.; Pushkar, Y.; Glatzel, P.; Lewis, A.; Sauer, K.; Messinger, J.; Bergmann, U.; Yachandra, V. High-Resolution Mn EXAFS of the Oxygen-Evolving Complex in Photosystem II: Structural Implications for the Mn_4Ca Cluster. *J. Am. Chem. Soc.* **2005**, *127*, 14974–14975. (d) Kamiya, N.; Shen, J.-R. Crystal Structure of Oxygen-Evolving Photosystem II from *Thermosynechococcus vulcanus* at 3.7-Å Resolution. *Proc. Natl Acad. Sci. USA* **2003**, *100*, 98–103. (e) Kulik, L. V.; Epel, B.; Lubitz, W.; Messinger, J. ^{55}Mn pulse ENDOR at 34 GHz of the S_0 and S_2 States of the Oxygen-Evolving Complex in Photosystem II. *J. Am. Chem. Soc.* **2005**, *127*, 2392–2393. (f) Haddy, A. EPR Spectroscopy of the Manganese Cluster of Photosystem II, *Photosynth. Res.* **2007**, *92*, 357–368.
6. Umena, Y.; Kawakami, K.; Shen, J.-R.; Kamiya, N. Crystal Structure of Oxygen Evolving Photosystem II at a Resolution of 1.9 Å. *Nat. Commun*. **2011**, *473*, 55-60.
7. (a) Das, S.; Misra, A.; Roy, S. Enhancement of Photochemical Heterogeneous Water Oxidation by a Manganese Based Soft Oxometalate K.; Karthick, K.; Mishra, S.; Kundu, S. Recent Trends and Perspectives in Electrochemical Water Splitting with an Emphasis on Sulfide, Selenide, and Phosphide Catalysts of Fe, Co, and Ni: A Review. *ACS Catal.* **2016**, *6*, 8069-8097. (b) Das, S.; Roy; S. Photochemical Water Oxidation Using $\{PMo_{12}O_{40}@Mo_{72}Fe_{30}\}_n$ Based Soft Oxometalate. *J. Mol. Eng. Mater.* **2017**, *05*, 1750001. (c) Blakemore, J. D.; Crabtree, R. H.; Brudvig, G. W. Molecular Catalysts for Water Oxidation. *Chem. Rev.* **2015**, *115*, 12974-13005. (d) Pu, Z.; Luo, Y.; Asiri, A. M.; Sun, X. Efficient Electrochemical Water Splitting catalyzed by Electrodeposited Nickel Diselenide Nanoparticles Based Film. *ACS Appl. Mater. Interfaces* **2016**, *8*, 4718–4723. (e) Anantharaj, S.; Ede, S. R.; Sakthikumar, Oxygen Evolution Reaction. *Catal. Sci. Technol.* **2017**, *7*, 5092-5104. (f) Singh, A.; Spiccia, L. Water Oxidation Catalysts Based on Abundant 1st row Transition Metals. *Coord. Chem. Rev.* **2013**, *257*, 2607-2622. (g) Lyons, M. E. G.; Doyle, R. L.; Fernandez, D.; Godwin, I. J.; Browne, M. P.; Rovetta, A. The Mechanism and Kinetics of Electrochemical Water Oxidation at Oxidized Metal and Metal Oxide Electrodes. Part 1. General Considerations: A Mini Review. *Electrochem. Commun.* **2014**, *45*, 60-62. (h) Mani, V.; Anantharaj, S.; Mishra, S.; Kalaiselvi, N.; Kundu, S. Iron Hydroxyphosphate and Sn-incorporated

Iron Hydroxyphosphate: Efficient and stable Electrocatalysts for Immobilized on a Graphene Oxide Matrix. *New J. Chem.*, **2016**, *40*, 994-1003. (i) Natarajan, S.; Anantharaj, S.; Tayade, R. J.; Bajaj, H. C.; Kundu, S. Recovered Spinel MnCo2O4 from Spent Lithium-ion Batteries for Enhanced Electrocatalytic Oxygen Evolution in Alkaline Medium. *Dalton Trans.* **2017**, *46*, 14382-14392. (j) Anantharaj, S.; Chatterjee, S.; Swaathini, K. C.; Amarnath, T. S.; Subhashini, E.; Pattanayak, D. K.; Kundu, S. Stainless Steel Scrubber: A Cost Efficient Catalytic Electrode for Full Water Splitting in Alkaline Medium. *ACS Sustainable Chem. Eng.* **2018**, *6*, 2498-2509. (k) Anantharaj, S.; Venkatesh, M.; Salunke A. S.; Simha, T. V.S.V.; Prabu, V.; Kundu, S. High-Performance Oxygen Evolution Anode from Stainless Steel via Controlled Surface Oxidation and Cr Removal. *ACS Sustainable Chem. Eng.* **2017**, *5*, 10072-10083.

8. (a) Wasylenko, D. J.; Ganesamoorthy, C.; Henderson, M. A.; Koivisto, B. D.; Osthoff, H. D.; Berlinguette, C. P. Electronic Modification of the $[Ru^{II}(tpy)(bpy)(OH_2)]^{2+}$ Scaffold: Effects on Catalytic Water Oxidation. *J. Am. Chem. Soc.* **2010**, *132*, 16094-16106. (b) Das, S.; Biswas, S.; Balaraju, T.; Barman, S.; Pochamoni, R.; Roy, S. Photochemical Reduction of Carbon Dioxide Coupled with Water Oxidation Using Various Soft-Oxometalate (SOM) Based Catalytic Systems. *J. Mater. Chem. A* **2016**, *4*, 8875-8887.
9. (a) Streb, C.; New Trends in Polyoxometalate Photoredox Chemistry: From Photosensitisation to Water oxidation Catalysis. Dalton Trans. **2012**, *41*, 1651-1659. (b) Zhu, G.; Glass, E. N.; Zhao, C.; Lv, H.; Vickers, J. W.; Geletii, Y. V.; Musaev, D. G.; Song, J.; Hill, C. L. A Nickel Containing Polyoxometalate Water Oxidation Catalyst. *Dalton Trans.* **2012**, *41*, 13043-13049. (c) Wang, L.; Duan, L.; Ambre, R. B.; Daniel, Q.; Chen, H.; Sun, J.; Das, B.; Thapper, A.; Uhlig, J.; Dinér, P.; Sun, L. A Nickel (II) PY5 Complex as an Electrocatalyst for Water Oxidation. *J. Catal.* **2016**, *335*, 72–78. (d) Han, Y.; Wu, Y.; Lai, W.; Cao, R. Electrocatalytic Water Oxidation by a Water-Soluble Nickel Porphyrin Complex at Neutral pH with Low Overpotential. *Inorg. Chem.* **2015**, *54*, 5604−5613.
10. (a) Zhang, H.; Nai, J.; Yu, L.; Lou, X. W. Metal-Organic-Framework-Based Materials as Platforms for Renewable Energy and Environmental Applications. *Joule* **2017**, *1*, 77–107. (b) Sheehan, S. W.; Thomsen, J. M.; Hintermair, U.; Crabtree, R. H.; Brudvig, G. W.; Schmuttenmaer, C. A. A Molecular Catalyst for Water Oxidation that Binds to Metal Oxide Surfaces. *Nat. Commun.* **2015**, *6*, 1-9. (c) Hunter, B. M.; Gray, H. B.; Müller, A. M. Earth-Abundant Heterogeneous Water Oxidation Catalysts. *Chem. Rev.* **2016**, *116*, 14120−14136. (d) Deng, X.; Tüysüz, H. Cobalt-Oxide-Based Materials as Water Oxidation Catalyst: Recent Progress and Challenges. *ACS Catal.* **2014**, *4*, 3701−3714. (e) Bose, S.; Debgupta, J.; Ramsundar, R. M.; Das, S. K. Electrochemical Water Oxidation Catalyzed by an in situ Generated α-$Co(OH)_2$

Film on Zeolite-Y Surface. *Chem. Eur. J.* **2017**, *23*, 8051-8057. (f) Kanan, M. W.; Nocera, D. G. In situ Formation of an Oxygen-Evolving Catalyst in Neutral Water Containing Phosphate and Co^{2+}. *Science* **2008**, *321*, 1072-1075. (g) Kanan, M. W.; Surendranath, Y.; Nocera, D. G. Cobalt–Phosphate Oxygen-Evolving Compound. *Chem. Soc. Rev*. **2009**, *38*, 109-114. (h) Mukhopadhyay, S.; Debgupta, J.; Singh, C.; Kar, A.; Das, S. K. A Keggin Polyoxometalate shows Water Oxidation Activity in Neutral pH: POM@ZIF-8 an Efficient and Robust Electrocatalyst. *Angew. Chem., Int. Ed.* **2018**, *57*, 1918-1923. (i) Aiyappa, H. B.; Thote, J.; Shinde, D. B.; Banerjee, R.; Kurungot, S. Cobalt-Modified Covalent Organic Framework as a Robust Water Oxidation Electrocatalyst. *Chem. Mater*. **2016**, *28*, 4375-4379. (j) Schöefberger, W.; Faschinger, F.; Chattopadhyay, S.; Bhakta, S.; Mondal, B.; Elemans, J.; Muellegger, S.; Tebi, S.; Koch, R.; Klappenberger, F.; Paszkiewicz, M.; Barth, J. V.; Rauls, E.; Aldahhak, Â. H.; Schmidt, W. G.; Dey, A. *A* Bifunctional Electrocatalyst for Oxygen Evolution and Oxygen Reduction Reactions in Water. *Angew. Chem., Int. Ed.* **2016**, *55*, 2350-2355. (k) Singh, A.; Roy, S.; Das, C.; Samanta, D.; Maji, T. K. Metallophthalocyanine Based Redox Active Metal-Organic Conjugated Microporous Polymers for OER Catalysis. Chem. Commun. **2018**, in press. DOI:10.1039/C8CC01291A.

11. (a) Sumliner, J. M.; Lv, H.; Fielden, J.; Geletii, Y. V.; Hill, C. L. Polyoxometalate Multi-Electron-Transfer Catalytic Systems for Water Splitting. *Eur. J. Inorg. Chem.* **2014**, *4*, 635–644. (b) Blasco-Ahicart, M.; Soriano-López, J.; Carbó, J. J.; Poblet, J. M.; Galan-Mascaros, J. R. Polyoxometalate Electrocatalysts Based on Earth Abundant Metals for Efficient Water Oxidation in Acidic Media. *Nature Chemistry* **2018**, *10*, 24-30.
12. (a) Folkman, S. J.; Finke**,** R. G. Electrochemical Water Oxidation Catalysis Beginning with Co(II) Polyoxometalates: The Case of the Precatalyst $Co_4V_2W_{18}O_{68}^{10-}$, *ACS Catal.* **2017**, *7*, 7−16. (b) Folkman, S. J.; Finke, R. G. Electrocatalytic Water Oxidation Beginning with the Cobalt Polyoxometalate $[Co_4(H_2O)_2(PW_9O_{34})_2]^{10-}$: Identification of Heterogeneous CoO_x as the Dominant Catalyst. *J. Am. Chem. Soc.* **2011**, *133*, 14872–14875.
13. Li, J.; Güttinger, R.; Moré, R.; Song, F.; Wan, W.; Patzke, G. R. Frontiers of Water Oxidation: the Quest for True Catalysts. *Chem Soc. Rev*. **2017, *46*,** 6124-6147.
14. (a) Li, X.-M.; Chen, Y.-G.; Shi, T. Hybrid Compounds of Keggin Polyoxotungstate with Transition Metal ion as the Central Atom. Synthesis, Structure and Properties. *Solid state sciences* **2016**, *52*, 112-117. (b) Li, M.-T.; Sha, J.-Q.; Zong, X.-M.; Sun, J.-W.; Yan, P.-F.; Li, L.; Yang, X.-N. Assembly of Polyoxometalate-Based Hybrids with Different Helical Channels upon Subtle Ligand Variation. *Cryst. Growth Des.* **2014**, *14*, 2794−2802. (c) Liu, C.-M.; Huang, Y.-H.; Zhang, D.-Q.; Jiang, F.-C.; Zhu, D.-B. Hydrothermal Synthesis and Crystal Structure of a New α-Keggin Unit Supported Cobalt Bipyridyl Complex: $[Co(2,2'\text{-bipy})_3]_{1.5}[SiW_{12}O_{40}Co(2,2'\text{-}$

bipy)$_2$(H_2O)].0.5H_2O. *J. Coord. Chem.* **2003**, *56*, 953-960. (d) Wang, H.; Cheng, C.; Tian, Y. A New Keggin Tungstocobaltate Decorated by Zinc (II) Complex Groups: [Zn(2,2′-bipy)$_3$]$_3${[Zn (2,2′-bipy)$_2$(H_2O)]$_2$-[$HCoW_{12}O_{40}$]$_2$}·H_2O. *Chin. J. Chem.* **2009**, *27*, 1099-1102. (e) Li, Y.-F.; Hubble, D. G.; Miller, R. G.; Zhao, H.-Y.; Pan, W.-P.; Parkin, S.; Yan, B. Synthesis and Characterization of Two Novel Organic–Inorganic Hybrid Solids From Keggin ions and Metal Coordination Complexes. *Polyhedron* **2010**, *29*, 3324–3328. (f) Yi, Z.; Zhang, X.; Yu, X.; Liu, L.; Xu, X.; Cui, X.; Xu, J. Hydrogen-Bonded Assemblies of a New Polyoxometalate-Based 3-D Supramolecular Architecture. *J. Coord. Chem.* **2013**, *66*, 1876-1888.

15. (a) Xu, Y.; Xu, J.-Q.; Zhang, K.-L.; Zhang, Y.; You, X.-Y. Keggin Unit Supported Transition Metal Complexes: Hydrothermal Synthesis and Characterization of [Ni(2,2′-bipy)$_3$]$_{1.5}$[$PW_{12}O_{40}$Ni(2,2′-bipy)$_2$(H_2O)]·0.5H_2O and [Co(1,10′-phen)$_3$]$_{1.5}$[$PMo_{12}O_{40}$Co(1,10′-phen)$_2$(H_2O)]·0.5H_2O. *Chem. Commun.*, **2000**, *0*, 153–154. (b) Wang, Y.; Zhou, B.; Xiao, L.-N.; Jin, N.; Peng, Y.; Wu, F.-Q.; Ding, H.; Wang, T.-G.; Gao, Z.-M.; Zheng, D.-F.; Cui, X.-B.; Xu, J.-Q. Two New Hybrid Compounds Assembled From Keggin-Type Polyoxometalates and Transition Metal Coordination Complexes. *J. Solid State Chem.* **2011**, *184*,557-562. (c) Cui, J.-W.; Cui, X.-B.; Yu, H.-H.; Xu, J.-Q.; Yi, Z.-H.; Duan, W.-J. Hydrothermal Syntheses and Characterizations of two Novel Heteropolytungstate Supported Coordination Compounds. *Inorg. Chim. Acta* **2008**, *361*, 2641-2647. (d) Devi, R. N.; Burkholder, E.; Zubieta, J. Hydrothermal Synthesis of Polyoxotungstate Clusters, Surface Modifiedwith M(II)-Organonitrogen Subunits. *Inorg. Chim. Acta* **2003**, *348*, 150-156. (e) Dolbecq, A.; Dumas, E.; Mayer, C. R.; Mialane, P. Hybrid Organic-Inorganic Polyoxometalate Compounds: From Structural Diversity to Applications. *Chem. Rev.* **2010,** *110*, 6009–6048. (f) Kumar, A.; Gupta, A. K.; Devi, M.; Gonsalves, K. E.; Pradeep, C. P. Engineering Multi-Functionality in Hybrid Polyoxometalates: Aromatic Sulfonium Octamolybdates as Excellent Photochromic Materials and Self-Separating Catalysts for Epoxidation. *Inorg. Chem.* **2017**, *56*, 10325-10336.

16. Manna, P.; Debgupta, J.; Bose, S.; Das, S. K. A Mononuclear CoII Coordination Complex Locked in a Confined Space and Acting as an Electrochemical Water-Oxidation Catalyst: A "Ship-in-a-Bottle" Approach. *Angew. Chem., Int. Ed.* **2016**, *55*, 2425-2430.

17. (a) Lv, H.; Song, J.; Geletii, Y. V.; Vickers, J. W.; Sumliner, J. M.; Zhu, G.; Musaev, D. G.; Gerler, P. K.; Zhuk, P. F.; Basca, J.; Zhu, G.; Hill, C. L. An Exceptionally Fast Homogeneous Carbon-Free Cobalt-Based Water Oxidation Catalyst. *J. Am. Chem. Soc.* **2014**, *136*, 9268−9271. (b) Vickers, J. W.; Lv, H.; Sumliner, J. M.; Zhu, G.; Luo, Z.; Musaev, D. G.; Geletii, Y. V.; Hill, C. L. Differentiating Homogeneous and Heterogeneous Water Oxidation Catalysis: Confirmation

that $[Co_4(H_2O)_2(\alpha\text{-}PW_9O_{34})_2]^{10-}$ Is a Molecular Water Oxidation Catalyst. *J. Am. Chem. Soc*. **2013**, *135*, 14110–14118.

18. (a) Ji, Y.; Ma, M.; Ji, X.; Xiong, X.; Sun, X. Nickel-Carbonate Nanowire Array: An Efficient and Durable Water Oxidation Electrocatalyst at Near-Neutral pH. *Front. Chem. Sci. Eng.* in press. DOI:10.1007/s11705-018-1717-8. (b) Masud, J.; loannou, P. C.; Levesanos, N.; Kyritsis, P.; Nath, M. A Molecular Ni-complex Containing Tetrahedral Nickel Selenide Core as Highly Efficient Electrocatalyst for Water Oxidation. *ChemSusChem* **2016**, *9*, 3128-3132. (c) Liu, Q.; Xie, L.; Liu, Z.; Du, G.; Asiri, A. M.; Sun, X. A Zn-Doped Ni_3S_2 Nanosheet Array as a High-Performance Electrochemical Water Oxidation Catalyst in Alkaline Solution. *Chem. Commun.* **2017**, *53*, 12446-12449. (d) Xie, F.; Wu, H.; Mou, J.; Lin, D.; Xu, C.; Wu, C.; Sun, X. Ni_3N@Ni-Ci Nanoarray as a Highly Active and Durable Non-Noble-Metal Electrocatalyst for Water Oxidation at Near-Neutral pH. *J. Catal.* **2017**, *356*, 165-172. (e) Ge, R.; Ren, X.; Qu, F.; Liu, D.; Ma, M.; Hao, S.; Du, G.; Asiri, A. M.; Chen, L.; Sun, X. Three-Dimensional Nickel–Borate NanosheetsArray for EfficientOxygen Evolution at Near-Neutral pH. *Chem. Eur. J.* **2017**, *23*, 6959-6963. (f) Jia, H.; Yao, Y.; Zhao, J.; Gao, Y.; Luob, Z.; Du, P. A Novel two-Dimensional Nickel Phthalocyanine based Metal–Organic Framework for Highly Efficient Water Oxidation Catalysis. *J. Mater. Chem. A.* **2018**, *6*, 1188-1195.
19. (a) Wang, D.; Bruner, C. O. Catalytic Water Oxidation by a Bio-inspired Nickel Complex with a Redox-Active Ligand. *Inorg. Chem.* **2017**, *56*, 13638-13641. (b) Cai, D.; Han, A.; Yang, P.-Y.; Wu, Y.-F.; Du, P.; Kurmoo, M.; Zeng, M.-H. Heptanuclear Co, Ni and Mixed Co-Ni Clusters as High-Performance Water Oxidation Electrocatalysts. *Electrochim. Acta* **2017**, *249*, 343-352. (c) Zhang, M.; Zhang, M.-T.; Hou, C.; Ke, Z.-F.; Lu, T.-B. Homogeneous Electrocatalytic Water Oxidation at Neutral pH by a Robust Macrocyclic Nickel(II) Complex. *Angew. Chem., Int. Ed.* **2014**, *53*, 13042 –13048. (d) Wang, J.-W.; Hou, C.; Huang, H.-H.; Liu, W.-J.; Ke, Z.-F.; Lu, T.-B. Further Insight into the Electrocatalytic Water Oxidation by Macrocyclic Nickel(II) Complexes: the Influence of Steric Effect on Catalytic Activity. *Catal. Sci. Technol.* **2017**, *7*, 5585-5593. (e) Luo, G.-Y.; Huang, H.-H.; Wang, J.-W.; Lu, T.-B.; Further Investigation of a Nickel-Based Homogeneous Water Oxidation Catalyst with Two cis Labile Sites. *ChemSusChem* **2016**, *9*, 485-491. (f) Lin, J.; Kang, P.; Liang, X.; Ma, B.; Ding, Y. Homogeneous Electrocatalytic Water Oxidation Catalyzed by a Mononuclear Nickel Complex. *Electrochim. Acta* **2017**, *258*, 353-359.
20. Wang, C.-J.; Yao, S.; Chen, Y.-Z.; Zhang, Z.-M.; Wang, E.-B. Assembly of Polyoxometalates and Ni-bpy Cationic Units into the Molecular Core–Shell Structures as Bifunctional Electrocatalysts. *RSC Adv.* **2016**, *6*, 99010–99015.

21. Gerasimova, T. P.; Katsyuba, S. A. Bipyridine and phenanthroline IR-spectral Bands as Indicators of Metal Spin State in Hexacoordinated Complexes of Fe(II), Ni(II) and Co(II). *Dalton Trans.* **2013**, *42*, 1787–1797.
22. (a) Glass, E. N.; Fielden, J.; Kaledin, A. L.; Musaev, D. G.; Lian, T.; Hill, C. L. Extending Metal-to-Polyoxometalate Charge Transfer Lifetimes: The Effect of Heterometal Location, *Chem. Eur. J.* **2014**, *20*, 4297-4307. (b) Maestre, J. M.; Lopez, X.; Bo, C.; Poblet, J.-M.; Casañ-Pastor, N. Electronic and Magnetic Properties of α-Keggin Anions: A DFT Study of $[XM_{12}O_{40}]^{n-}$, (M = W, Mo; X = Al^{III}, Si^{IV}, P^{V}, Fe^{III}, Co^{II}, Co^{III}) and $[SiM_{11}VO_{40}]^{m-}$ (M = Mo and W). *J. Am. Chem. Soc.* **2001**, *123*, 3749-3758.
23. Harris, C. M.; McKenzie, E. D. Nitrogenous Chelate Complexes of Transition Metals—III: Bis-Chelate Complexes of Nickel (II) with 1,10-Phenanthroline, 2,2′-Bipyridyl and Analogous Ligands. *J. inorg. nucl. Chem.* **1967**, *29*, 1047-1068.
24. (a) Sasaki, Y. Electronic Spectra of Octahedral Nickel(II) and Cobalt(II) : Complexes with 2-(2-Pyridyl)imidazole and 2-(2- Pyridyl)benzimidazole. *Bulletin of the Institute for Chemical Research, Kyoto University* **1980**, *58*, 187-192. (b) Knight, J. C.; Alvarez, S.; Amoroso, A. J.; Edwards, P. G; Singh, N. A Novel Bipyridine-based Hexadentate Tripodal Framework with a Strong Preference for Trigonal Prismatic Co-ordination Geometries. *Dalton Trans.* **2010**, *39*, 3870–3883.
25. (a) Strydom, C. A.; Strydom, H. J. X-ray Photoelectron Spectroscopy Studies of Some Cobalt(II) Nitrate Complexes. *Inorg. Chim. Acta* **1989,** *59*, 191-195. (b) Tan, B. J.; Klabunde, K. J.; Sherwood, P. M. A. XPS Studies of Solvated Metal Atom Dispersed Catalysts. Evidence for Layered Cobalt-Manganese Particles on Alumina and Silica. *J. Am. Chem. Soc.* **1991**, *113*, 855-861.
26. Nguyen, T.; Boudard, M.; Carmezim, M. J.; Montemor, M. F. Layered $Ni(OH)_2$-$Co(OH)_2$ Films Prepared by Electrodeposition as Charge Storage Electrodes for Hybrid Supercapacitors. *Scientific Reports* **2017**, *7*, 39980.
27. (a) Dogutan, D. K.; McGuire, R.; Nocera. D. G. Electocatalytic Water Oxidation by Cobalt(III) Hangman β-Octafluoro Corroles. *J. Am. Chem. Soc.* **2011**, *133*, 9178–9180. (b) Wasylenko, D. J.; Ganesamoorthy, C.; Borau-Garcia, J.; Berlinguette, C. P. Electrochemical Evidence for Catalytic Water Oxidation Mediated by a High-Valent Cobalt Complex. *Chem. Commun.* **2011**, *47*, 4249–4251.
28. Wang, D.; Groves, J. T. Efficient Water Oxidation Catalyzed by Homogeneous Cationic Cobalt Porphyrins with Critical roles for the Buffer base. *Proc. Natl. Acad. Sci.* **2013**, *110*, 15579-15584.

29. Baker, L. C. W.; Baker, V. S.; Eriks, K.; Pope, M. T.; Shibata, M.; Rollins, O. W.; Fang, J. H.; Koh, L. L. A New General Structural Category of Heteropolyelectrolytes. Unusual Magnetic and Thermal Contraction Phenomena. *J. Am. Chem. Soc.* **1966**, *88*, 2329-2331.
30. SAINT: Software for the CCD Detector System; Bruker Analytical X-ray Systems, Inc.: Madison, WI, **1998**.
31. Sheldrick, G. M. SADABS, Program for Absorption Correction; University of Gottingen: Gottingen, Germany, **1997**.
32. Sheldrick, G. M. SHELXS-97, Program for Structure Solution and Analysis*;* University of Gottingen: Gottingen, Germany, **1997**.
33. Sheldrick, G. M. SHELXL-97, Program for Crystal Structure Analysis; University of Gottingen: Gottingen, Germany, **1997**.
34. Pintado, S.; Goberna-Ferrón, S.; Escudero-Adán, E. C.; Galán-Mascarós, J. R. Fast and Persistent Electrocatalytic Water Oxidation by Co–Fe Prussian Blue Coordination Polymers. *J. Am. Chem. Soc.* **2013**, *135*, 13270-13273.

Chapter 3

Designing POM Supported Metal Complex as an Efficient Electrocatalyst for HER

OVERVIEW

Hydrogen is the solution to all the problems associated with the energy crisis. Generating hydrogen from water splitting is one of the greener approaches but it requires an efficient catalyst which is economical for the bulk production of hydrogen. In this work we have demonstrated the utilization of a POM supported Cu-complex, for the electrochemical HER activity. This is among one of the few reports available with POM supported transition metal complexes (PSTMCs) for electrochemical HER. Polyoxometalate (POM) supported transition metal complexes are one of the popular hybrid compounds derived from POM unit which have the properties associated with both the POM and the supported transition metal complexes along with some value added property due to the synergistic effect making PSTMCs a better candidate then its constituent units. In this work we have demonstrated successful synthesise of a Cu-complex coordinated to a POM molecule, forming a 2D-network with molecular formula of $[\{Cu(2,2'\text{-bpy})(H_2O)_2\}][\{CoW_{12}O_{40}\}\{(Cu(2,2'\text{-bpy})(H_2O)\}\{(Cu(2,2'\text{-bpy})\}]\cdot 2H_2O$ (1). From the electrochemical studies, we found compound 1 can function as heterogeneous and robust electrochemical catalyst for hydrogen evolution reaction (HER) in near neutral medium (pH 4.8), under buffered condition (acetate buffer). Through varied electrochemical experiments, detailed study has been conducted to gain insights to the electrocatalysis exhibited by 1. Compound 1 follows PCET pathway with one proton and one electron involvement for electrocatalyzing HER. The overpotential required to achieve a current density of 1 mA/cm^2 was found to be 520 mV with the Faradic efficiency of 81.02%.

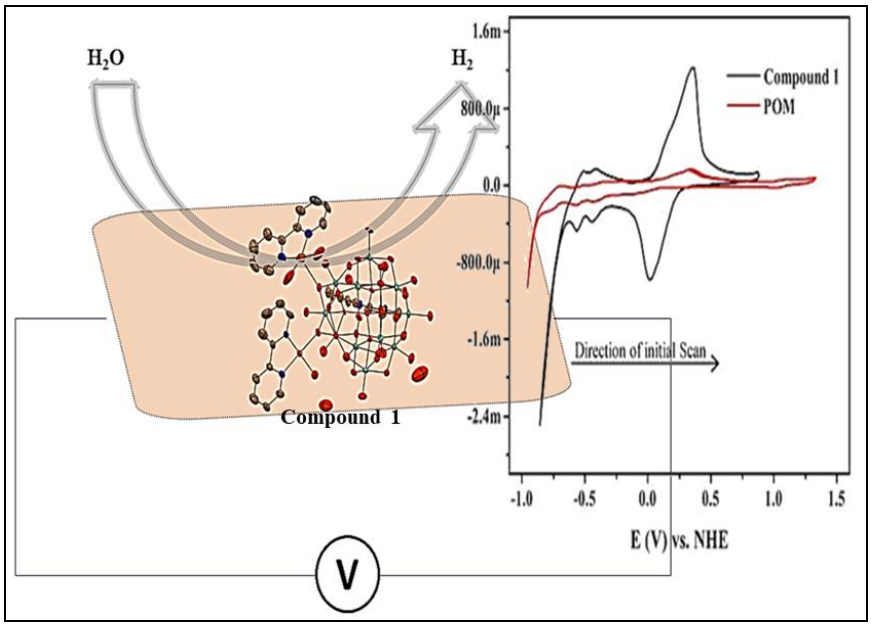

3.1. Introduction

Energy is the center of attraction, a prerequisite for development, modernization, and one of the culprits in environmental hazards due to humans' poor choice to implement energy sources. As discussed in chapter 1, how extensive use of fossil fuels has led to an increase in CO_2 emission, thereby affecting environmental health. This made us look for a sustainable energy source to replace fossil fuels for good. As mentioned in **Chapter 1**, the whole discussion boils down to water splitting (WS) for generating hydrogen gas in its purest form with no C-based waste. Thus developing a catalyst for hydrogen evolution reaction (HER) needs urgent attention, considering the less availability of low-cost catalysts. HER process's thermodynamic potential is 0 V *vs.* NHE, making it seem an easily achievable process.

But on the contrary, HER with very low overpotential is achieved to date mostly by a noble metal (*e.g.*, Pt metal).[1-4] In the last few years, research has advanced towards betterment where few noble metals based materials containing relatively less amount of Pt showed similar results.[3,4] There are reports of bimetallic compounds that contain a certain percentage of Pt along with other metals such as Ru/Rh *etc.*[5-10] Even though the results are encouraging, the catalyst's cost is still very high for practical usage.

Scientists have looked into earth-abundant transition metal-based catalysts for HER, taking HER catalyst altogether to a different level. Especially last few years have been great for HER based catalysts, which witnessed an increase in publication.[11-15] Utilizing transition metals, especially those abundant on the earth's surface, could solve the cost-related problem and be much more useful for practical purposes. Recent advancement in this direction has led to the exploration of Cu/Co/Fe/Ni-based compounds/materials for both photo/electrocatalytic HER.[16-20]

Cu is one of the metals whose presence is eminent in the biological systems. There is a high probability of it mimicking the photocatalytic WS process if designed appropriately. The catalysts prepared for HER are primarily divided into molecular and non-molecular compounds/materials. Molecular catalysts are those which many times are isolated as single crystals, could be structurally characterized; whereas non-molecular substances do not have a definite structure (mostly, infinite structure). The ease of tuning the structure in the case of molecular catalysts makes it preferable while considering designing catalysts, as it facilitates one with various opportunities to understand the chemistry. The first molecular catalyst known for HER with Cu-complex was reported in the year 2014 by Wang and his co-workers.[21] This copper

complex having a molecular formula of $[(bztpen)Cu](BF_4)_2$ (bztpen=N-benzyl-N,N′,N′-tris(pyridin-2-ylmethyl)ethylenediamine) exhibited excellent activity towards catalytic HER with a high TOF of 7000 $h^{-1}cm^{-2}$. The complex showed HER activity at low pH of 2.5 in the phosphate buffer. Late in the year 2016, the same group utilized this complex again at low pH (1.4-1.6) to obtain a deposit of Cu-Cu_xO-Pt.[22] This deposit showed exceptional results with an overpotential of 45mV at a current density of 20mA/cm^2.

Siewert and her co-workers documented two different Cu-complexes acting as precursors to form Cu(0) and Cu_2O deposition on the electrode surface.[23] These depositions act as active catalysts for HER activity.

Recently POM based materials have gained considerable attention for developing various HER catalysts. POMOF (polyoxometalate organic framework), POM@MOF, and POM supported transition metal complexes (PSTMCs) are a few to name.[24-28] These POM based composites/compounds are seldom also utilized as a as precursor to prepare an active electrocatalyst for water splitting.

POMs could be used to activate the electroactive species for HER activity. Yang, Gua, and his co-workers recently activated $CoSe_2$ for HER by clubbing it with sandwiched POM.[29] In this work, Keggin type sandwiched POM ($Na_{10}[Mn_4(H_2O)_2(VW_9O_{34})_2].26H_2O$) was immobilized on $CoSe_2$-Nanobelts(NBs). POM's synergistic effect on $CoSe_2$-NBs, coupled with its fast electron transfer property, POM solves the major obstruction in designing $CoSe_2$-based HER catalyst in an acidic medium (0.5 M H_2SO_4). This nanocomposite exhibited exceptional HER catalytic activity with an overpotential of 187 mV for the current density of 10 mA/cm^2. In the extensive available literature on POMs and POM based materials, we have observed that POMs or PSTMCs are not well explored for electrocatalytic HER activity. The majority of PSTMCs are studied for either nitrate/bromate reduction or ascorbic acid oxidation, as tabulated in **Table 1.1.** of **Chapter 1**.

The lack of literature followed by ease of metal complexes' stability by preparing PSTMCs motivated us to design new POM supported Cu-complexes. Metal complexes, especially Cu in most cases, have undergone decomposition forming elemental copper coat on the electrode in the electrocatalytic HER conditions.[23] We planned the Cu-complex synthesis on cluster surface of POM compound *via* 'W–O' bond to look into the stability. POM's employment for metal complex stability has proven to be successful by our group earlier for OER catalysis (**Chapter**

2).[30]

In this chapter, by slightly modifying the synthetic procedure from **Chapter 2**, we successfully synthesized a two-dimensional network of Cu-complex coordinated to the Keggin POM ($K_6[CoW_{12}O_{40}]\cdot 6H_2O$). The synthesized hybrid compound was characterized by single-crystal XRD and from its crystal structure, we formulated it as **[{Cu(2,2´-bpy)(H_2O)$_2$}][{$CoW_{12}O_{40}$}{(Cu(2,2´-bpy)(H_2O)}{(Cu(2,2´-bpy)}]·2H_2O** (**1**). The ease with which Cu(II) species could be reduced to Cu(I) species, we speculated this hybrid to exhibit electrocatalytic HER activity. As expected, compound **1** shows HER activity at a moderate low pH (4.8) in an acetate buffer. Details about the true catalyst nature, role of POM in this hybrid for HER catalysis including its mechanistic and kinetic details are discussed further.

3.2. Experimental Section

3.2.1. Material and methods

3.2.1.1. General materials and methods.

Starting materials were purchased in AR grade and were used as received. PXRD patterns were recorded on a Bruker D8-Advance diffractometer by using graphite monochromated CuKα1 (1.5406Å) and Kα2 (1.55439Å) radiation. Infra-red spectra of solid samples were obtained as KBr pellets on a JASCO–5300 FT–IR spectrophotometer. Diffuse Reflectance (DRS) UV-vis electronic absorption spectra were recorded using Shimadzu-2600 spectrophotometer. Thermogravimetric (TGA) analyses were carried out on a STA 409 PC analyzer. Field emission scanning electron microscope (FE-SEM) imaging with energy dispersive X-ray (EDX) spectroscopy was carried out on a Carl Zeiss model Ultra 55 microscope, EDX spectra and maps were recorded using Oxford Instruments X-Max^N SDD (50 mm^2) system and INCA analysis software. All electrochemical experiments were conducted using a Zahner Zanium electrochemical workstation operated with Thales software.

3.2.1.2. Crystal Data collection

Single-crystal suitable for structural determination of compound **1** was mounted on a three-circle Bruker SMART APEX CCD area detector system under Mo−Kα (λ = 0.71073 Å) graphite monochromated X-ray beam with the crystal-to-detector distance of 60 mm, and a collimator of 0.5 mm width (at 273 K temperature). The scans were recorded with a ω scan width of 0.3°.

SAINT PLUS performed data reduction,[31] empirical absorption corrections using equivalent reflections were performed by program SADABS.[32] Structure solutions were done using SHELXS-97[33] and full-matrix least-squares refinement was carried out using SHELXL-97.[34]All the non-hydrogen atoms were refined anisotropically. Hydrogen atoms on the C atoms were introduced on calculated positions and were included in the refinement riding on their respective parent atoms. Crystal data and structural refinement parameters for compound **1** are summarized in **Table 3.1**. Selected bond length and bond angle for compound **1** is summarized in **Appendix A2**.

3.2.1.3. Electrochemical studies

Similar protocol is followed as that discussed in **Chapter 2** under section **2.2.1.3.** All the electrochemical experiments were performed at ambient temperature. Electrode potentials were converted to the normal hydrogen electrode (NHE) scale using the relation E (NHE) = E (Ag/AgCl) + 0.2382 V when the Ag/AgCl used as RE. Cyclic voltammetry scans were initiated at the open circuit potential (OCP), and the anodic side was scanned first, followed by cathodic scan. Five cycles were taken consecutively for each set of cyclic voltammetry measurements in quiescent solution. Cyclic voltammograms (CVs) were also recorded at various scan rates.

3.2.2. Synthesis

3.2.2.1. Synthesis of Compound 1

The Keggin POM, $K_6[CoW_{12}O_{40}]\cdot 6H_2O$ (POM) was synthesized using a reported protocol which is discussed in **Chapter 2** in section **2.2.2.1**.[30] Synthesized and characterized POM was used as such for the synthesis of the hybrid compound which is formulated as **[{Cu(2,2´-bpy)(H_2O)$_2$}][{$CoW_{12}O_{40}$}{(Cu(2,2´-bpy)(H_2O)}{(Cu(2,2´-bpy)}]·2H_2O (1)**. A mixture of $CuCl_2\cdot 4H_2O$ (71 mg, 0.34 mmol) 2,2′-bpy (114 mg, 0.73 mmol) and $K_6[CoW_{12}O_{40}]\cdot 6H_2O$ (32 mg, 0.01 mmol) in 3 mL MeOH and 2 mL water, were taken in 23 mL Teflon lined reactor and was stirred for 45 min. The solution was heated to 160 ˚C for five days under solvothermal conditions. It was cooled down to room temperature (34˚C) in 24 h to obtain block-shaped green-colored crystals. Yield: 36% (based on W).

3.3. Results and Discussion

3.3.1. Physical characterization

All the compounds synthesized for this work were characterized by PXRD pattern analysis, infra-red analysis, UV-vis. diffused reflectance spectral (DRS) analysis, Raman, FESEM, TGA analysis. Compound **1** was unambiguously characterized by single-crystal X-ray diffraction. For studying the electrocatalytic activity of **1** for HER, various electrochemical techniques were employed. The details are discussed in this section later.

3.3.1.1. Single-crystal XRD analysis

Compound **1** was characterized through Single-crystal X-ray crystallography at room temperature (286 K). Compound **1** crystallizes in a monoclinic crystal system with $p2_{1/n}$ space group. The molecular formula of compound **1** is **[{Cu(2,2´-bpy)(H_2O)$_2$}][{$CoW_{12}O_{40}$}{(Cu(2,2´-bpy)(H_2O)}{(Cu(2,2´-bpy)}]·2H_2O**. In this case, Keggin POM, $K_6[CoW_{12}O_{40}]\cdot 6H_2O$, acts as a multidentate ligand coordinating *via* oxygen atom present on the bridged 'W–O–W' and terminal 'W=O' position resulting in a two-dimensional network of the polymeric system. Compound **1** consists of three different crystallographically distinct 'Cu^{2+}'; let us label them as **Cu(1)**, **Cu(2)**, and **Cu(3)** for future reference. **Cu(1)** has coordination number (C.N.) five where two nitrogens of 2,2′-bpy fulfill the two coordination sites, two from free aqua ligand (-OH_2), and one from the bridging oxygen of the 'W–O–W' bond of the POM. Thus **Cu(I)** could be formulated as [(POM-O_b-Cu^{II}(2,2′-bpy)(H_2O)$_2$)] where POM-O_b refers to the bridging oxygen of the 'W–O–W' bond of the POM.

Table 3.1. Crystal data and structure refinement for Compound 1

Empirical formula	$C_{30}H_{24}Co_1Cu_3N_6O_{45}W_{12}$
Formula weight	3644.30
Temperature	293(2) K
Wavelength	0.71073 Å
Crystal system	Monoclinic
Space group	P 21/n
Unit cell dimensions	a = 13.567(3) Å α= 90°.
	b = 19.287(6) Å β=94.427(10)°.
	c = 22.639(6) Å γ = 90°.

Volume	5906(3) $Å^3$
Z	2
Density (calculated)	4.098 Mg/m^3
Absorption coefficient	24.698 mm^{-1}
F(000)	6432
Theta range for data collection	2.297 to 27.500°.
Index ranges	-17<=h<=17, -24<=k<=24, -28<=l<=28
Reflections collected	197748
Independent reflections	12250 [R(int) = 0.0805]
Completeness to theta = 25.242°	98.7 %
Refinement method	Full-matrix least-squares on F^2
Data / restraints / parameters	12250 / 0 / 874
Goodness-of-fit on F^2	1.136
Final R indices [I>2sigma(I)]	R1 = 0.0320, wR2 = 0.0744
R indices (all data)	R1 = 0.0413, wR2 = 0.0812
Largest diff. peak and hole	2.685 and -3.013 $e.Å^{-3}$

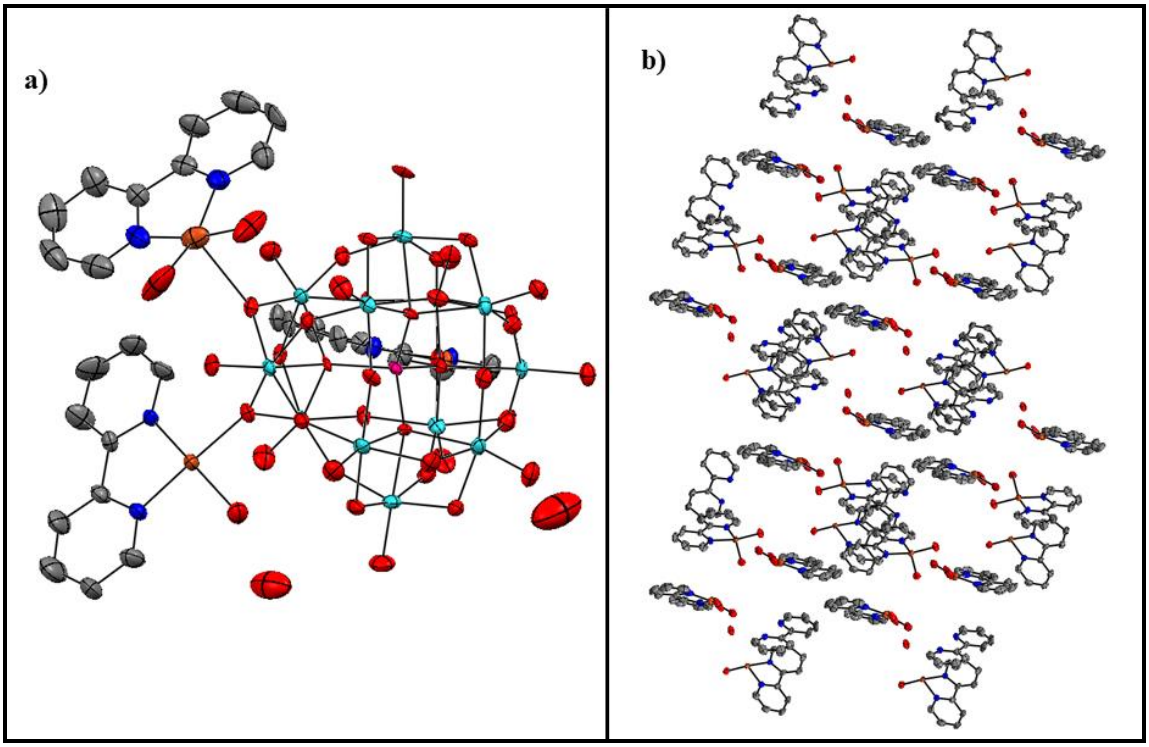

Figure 3.1. **(a)** Asymmetric unit **in** the crystal structure of compound **1** representing thermal ellipsoidal diagram with 70% probability. **(b)** Packing of the molecules in the crystal structure of **1** looking down to the crystallographic *b*-axis after omitting the POM unit for clarity. Colour code: gray-C; blue-N; cyan-W; orange-Cu; red-O; pink-Co (hydrogen is omitted for clarity purpose).

Cu(2) also has C.N. of five but differs from **Cu(1)** in terms of ligands. 2,2′-bpy occupies the two coordination sites, and one of the sites is fulfilled by aqua ligand ($–OH_2$). The remaining two sites are filled by the 'O'-atoms from two different POM units, thus resulting in the polymeric chain formation. **Cu(2)** coordinates with bridging oxygen of the 'W–O–W' bond of the POM unit and other *via* the terminal oxygen atom of the 'W=O' bond of another POM unit. Thus **Cu(2)** could be formulated as [(POM–O_b–Cu^{II} (O_t-POM(2)(2,2′-bpy)(H_2O))] where POM(2) refers to the other POM cluster through which **Cu(2)** is coordinated, forming a chained structure. **Cu(3)** has coordination number four and the ligands coordinated to it are similar to that of **Cu(2)** except for the free aqua ligand. **Cu(3)** also links through two different POM units resulting in the 2d-network formation. Thus, we can formulate the **Cu(3)** fragment as [(POM–O_b–Cu^{II} (O_t-POM(2)(2,2′-bpy)].

As already mentioned, in the crystal structure of compound **1**, both **Cu(1)** and **Cu(2)** have penta-coordination, acquiring a distorted square pyramidal geometry and **Cu(3)** has four coordination having distorted square planar arrangement around it. **Cu(2)** and **Cu(3)** centers are involved in the formation of the extended structure, while **Cu(I)** center (having two coordinated water ligands) is coordinated to the each POM cluster but not involved in the formation of the extended structure as shown in **Figure 3.2.**

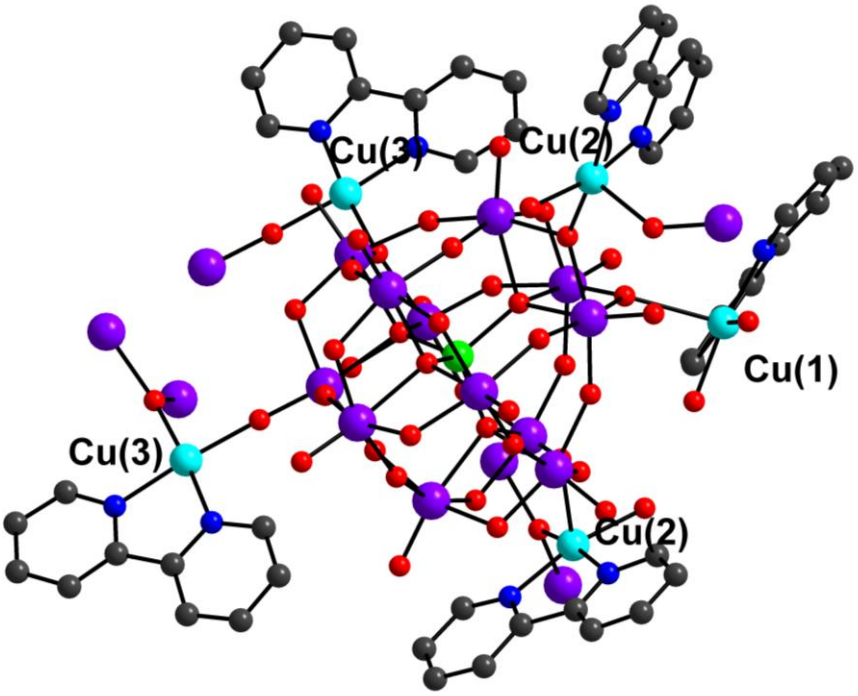

Figure 3.2. Coordination pattern around each Keggin POM unit in the crystal structure of compound **1**.

From the crystal structure, it is apparent that **Cu(1)** and **Cu(2)t** centers, having two- and one-coordinated water molecules, can act as the functional sites for HER catalysis and **Cu(3)** center cannot take part in HER because of its lack of water coordination. Moreover, among **Cu(1)** and **Cu(2)** centers, the **Cu(1)** center should be more preferred HER site than **Cu(2)** site because **Cu(2)** site is directly engaged in the formation of 2D coordination polymer involving the coordination of terminal oxo group (W=O) and bridging oxo group (W-O-W) from two different Keggin POMs (**Figure 3.2.**). Thus compound **1** consists of three distinct Cu(II)-centers, which vary from each other with respect to the co-ordination environment and geometry. From the crystal structure analysis, compound **1** is formulated as **[{Cu(2,2´-bpy)(H_2O)$_2$}$_n$][{$CoW_{12}O_{40}$}{(Cu(2,2´-bpy)(H_2O)}{(Cu(2,2´-bpy)}]$_n$·2nH_2O (1),** in which the copper(II)-bis(aqua)-bipyridine coordination complex in the first parentheses is supported on the POM cluster surface but not involved in the construction of 2D coordination polymer in contrast to the other two Cu(II) centers in the second parentheses in the formula, that are involved in the formation of extended structure.

3.3.1.2. PXRD analysis of POM and compound 1

Bulk purity of compound **1** has been confirmed by recording the powdered-XRD patterns of **1** and comparing it with the one obtained from the relevant single crystal data. Major peaks from the simulated PXRD pattern of **1** matched with that of experimentally obtained data (**Figure 3.3.**) confirming its bulk purity.

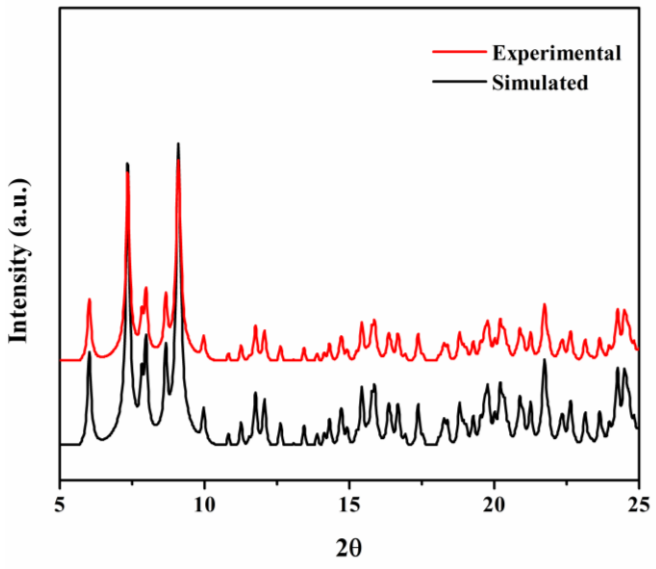

Figure 3.3. PXRD patterns of compound **1:** red plot, experimentally observed and black plot, simulated pattern from the single crystal data.

3.3.1.3. UV-vis. DRS, FTIR and Raman spectral analysis of compound 1 and the pristine POM

The solid-state diffused reflectance spectra of the title compound **1** and the pristine POM compound have been recorded and converted into absorbance by the Kubelka-Munk (K.-M.) algorithm. In the visible range of the electronic spectra of compound **1,** a broad absorbance band is seen at a wavelength of 630 nm with two humps at 748 nm and 873 nm. The absorbance at 630 nm is due to the'd-d' transition of 'Co^{2+}' from the Keggin POM; this feature is also clearly visible in the electronic spectrum of POM as shown in **Figure 3.4 (a)**. On the other hand, the absorbance observed at 748 nm and 873 nm in the electronic spectrum of compound **1** is similar to that in the electronic spectrum of $[Cu^{II}(2,2'\text{-bpy})_2(H_2O)_2]^{2+}$ complex (**Figure 3.3 (b)).** Hence, this feature at around 748 nm and 873 nm could be assigned to the absorbance of the POM supported Cu-complexes in **1**. Absorbance in the near-IR range (1000-1200 nm), found in the electronic spectra of **1** and POM itself, is mainly due to the charge transfer from *e*(Co) to t_2(W) state of the POM unit.[30]

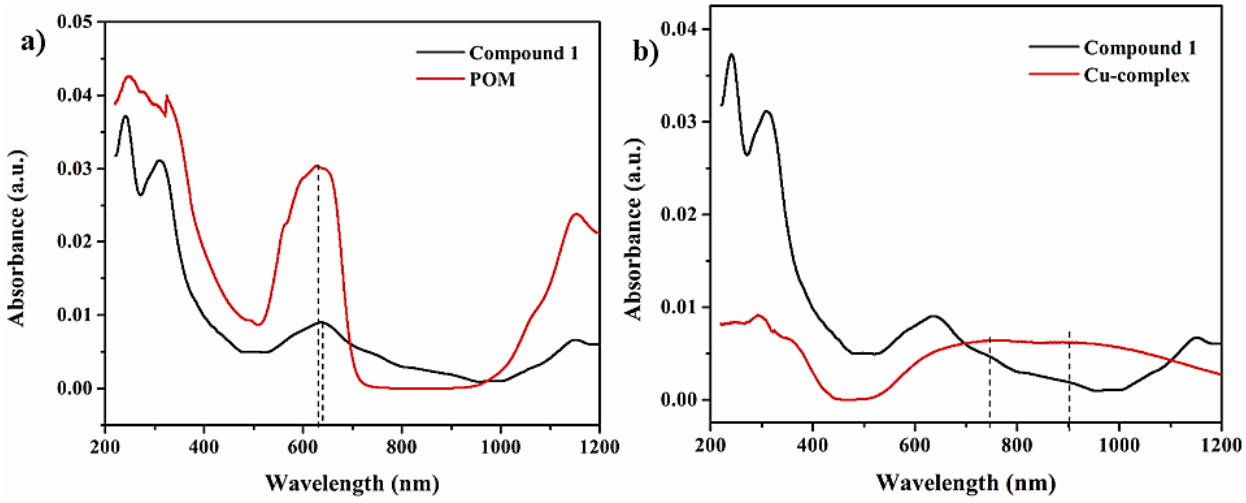

Figure 3.4. (a) Kubelka-Munk derived UV-vis. DRS spectrum of **1** and Keggin POM compound. **(b)** Kubelka-Munk derived UV-Vis. DRS spectrum of **1** and $[Cu^{II}(2,2'\text{-bpy})_2(H_2O)_2]Cl_2$ (labeled as Cu-complex in the plot).

In the UV region (below 300 nm) of the DRS spectra of **1** and POM compound, peaks are mainly due to $O_{2p} \rightarrow W_{5d}$ charge transfer of POM cluster (**Figure 3.4(a)**). Some additional features are seen in the same range (below 300 nm, **Figure 3.4(a)**) in the electronic spectrum of compound **1**, that are attributed metal to-ligand charge transfer of the Cu^{II}-complexes and the π–π^* transition due to bpy ligand by comparing the same range (Figure 3.4(b)) of as-synthesized $[Cu^{II}(2,2'\text{-bpy})_2(H_2O)_2]Cl_2$ complex . Thus, the absorption spectrum of **1** supports the presence of Co(II)-

centered Keggin anion as well as the copper-bipyridine complex, as found in the crystal structure of compound **1** (*vide supra*).

IR data of compound **1** is recorded and is provided in **Figure 3.5.** Stretching frequencies from the 'C=N' and 'C-N' bond of bpy unit in compound **1** shows bands around 1600 cm^{-1} and 1460 $cm^{-1,}$ respectively. Due to the POM unit, the following bands are observed in compound **1**: ν(W-O)t 945 cm^{-1}, ν(W-O-W) O_h edge-sharing 866 cm^{-1}, (W-O-W) corner-sharing 730 cm^{-1}, ν(O-Co-O) 456 cm^{-1}. The IR stretching of **1** is similar to that obtained for compound **1** from **Chapter 2** as expected (**Figure 2.3.**).

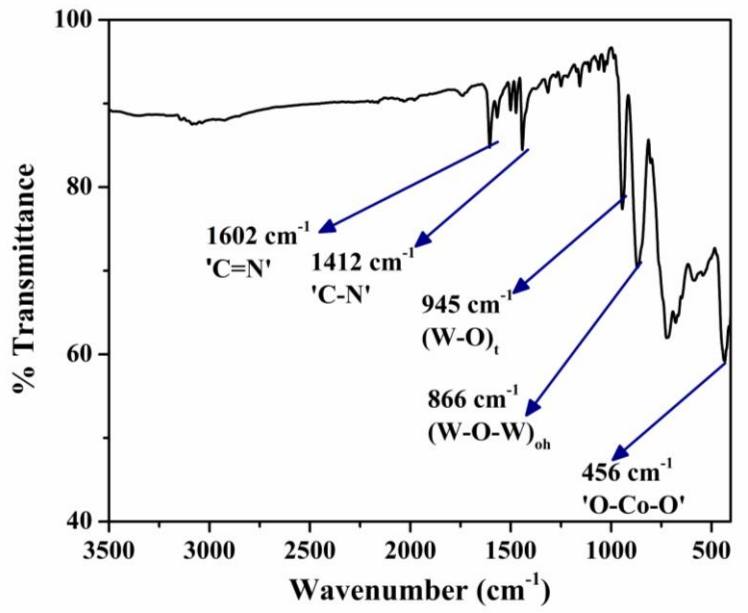

Figure 3.5. IR spectrum of compound **1**.

The concerned Keggin POM, $K_6[CoW_{12}O_{40}]\cdot 6H_2O$, is Raman active, and hence we expected **1** to show a similar Raman signature arising due to the presence of the Keggin POM. A WITec model Alpha 300 R Raman microscope was used for recording the Raman spectrum of **1** as shown in **Figure 3.6.** The excitation source used for this analysis was 633 nm laser. The Raman spectral features obtained for **1** (**Figure 3.6.**) is found to be consistent with those found in the literature report available for POM $K_6[CoW_{12}O_{40}]\cdot 6H_2O$.[35]

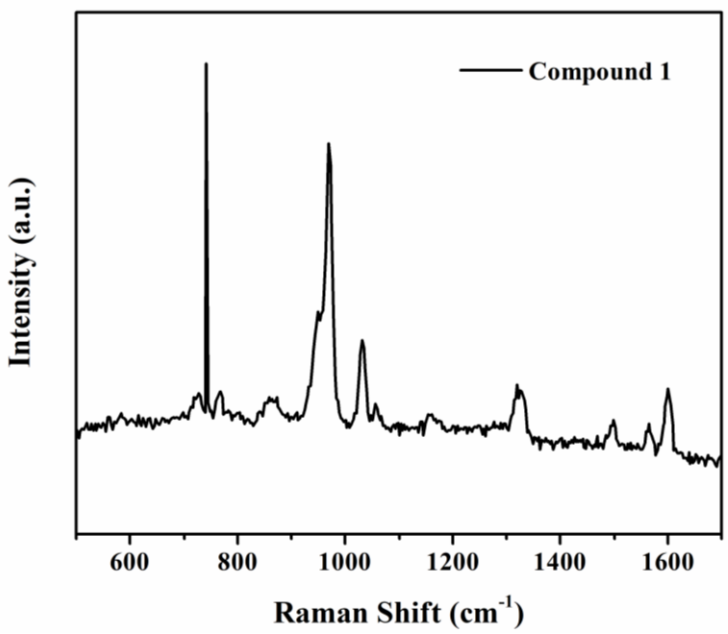

Figure 3.6. Raman spectrum of compound **1**.

3.3.1.4. TGA of compound 1

The thermal stability of compound **1** has been analyzed by recording the TGA plot. Compound **1** was taken for thermal studies without prior activation in a high-temperature vacuum. TGA curve of compound **1** shows 3 step weight loss (**Figure 3.7.**). Initially, in the temperature range of 50-250 ˚C, loss of 25% weight is observed, which is mainly due to loss of lattice water molecules from the compound. The temperature range of 250-550 ˚C shows a small hump, which could be due to the loss of coordinated water molecules followed by the organic unit's decomposition. This loss in weight is due to the decomposition of the organic component of the Cu^{II}-complexes present in compound **1**. For the temperature range of 600-800 ˚C, a steady decrease is observed. This loss is due to the complete disintegration of the POM unit, resulting in metal oxide formation after T≥800 ˚C.

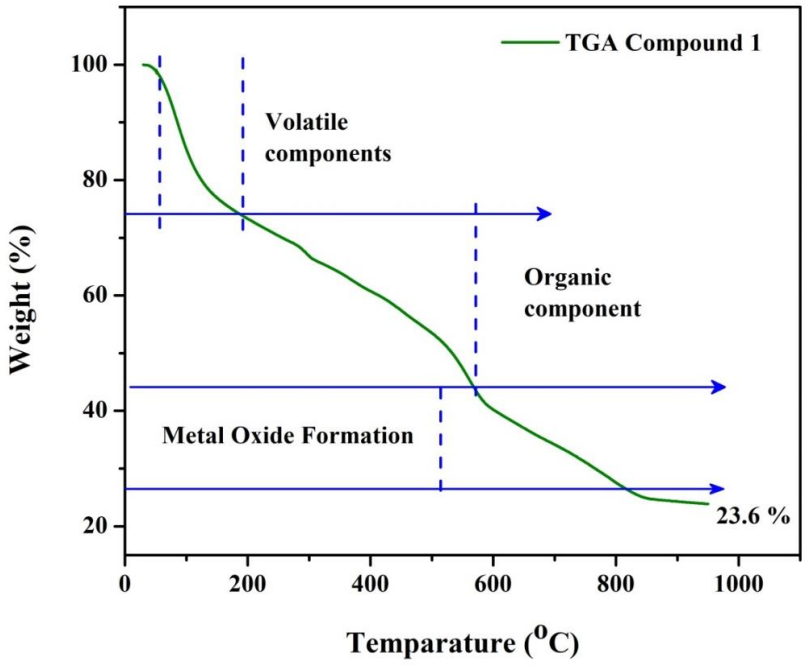

Figure 3.7. TGA plot of compound **1**.

3.3.1.5. Field Emission Scanning Electron Microscopy (FESEM) and Energy-dispersive X-ray (EDX) Analysis

The morphology and elemental mapping of compound **1** were done by FESEM and EDX analysis. Images were taken to study morphology (**Figure 3.8. (a,b)**) and EDX analysis (**Figure 3.8. (c)**) was done to confirm both Cu and Co atoms' presence. Thus, from these data, we confirmed the structure elucidated for **1** from single crystal-XRD data.

3.3.2. Electrochemical measurements and HER studies of compound 1

Cyclic voltammetric (CV) analysis of [{Cu(2,2´-bpy)(H_2O)$_2$}][{$CoW_{12}O_{40}$}{(Cu(2,2´-bpy)(H_2O)}{(Cu(2,2´-bpy)}]·2H_2O (**1**) was performed in three-electrode systems consisting of glassy carbon (GC) as working electrode, Ag/AgCl (1M) as reference and Pt-wire as the counter electrode. The sample was prepared, as mentioned in section **3.2.1.3.** and coated on the GC electrode surface. The bare GC was checked for any redox activity in the selected potential window prior to use. And bare GC was found to have no notable redox activity in the potential window of our interest.

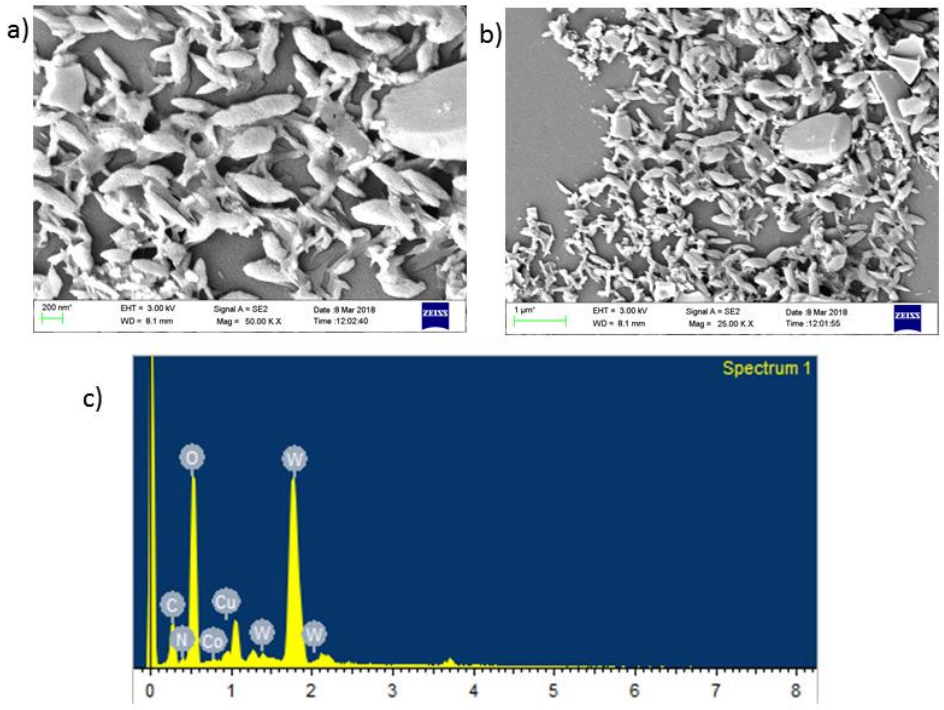

Figure 3.8. (a-b) FESEM images and **(c)** EDX of **1**.

3.3.2.1. Electrocatalytic HER catalyzed by compound 1

Compound [{Cu(2,2´-bpy)(H_2O)$_2$}][{$CoW_{12}O_{40}$}{(Cu(2,2´-bpy)(H_2O)}{(Cu(2,2´-bpy)}]·2H_2O (**1**) exhibits electrocatalytic hydrogen evolution reaction (HER) activity. All the electrochemical experiments for this study have been carried out in acetate buffer, pH 4.8 (unless mentioned otherwise). **Figure 3.9.** shows the CV of compound **1**.

The two major components of compound **1** are cobalt(II)-centered Keggin POM unit and the associated copper(II)-bipyridine moieties. Both these components are redox active: Co(II) center of this Keggin is well known to have Co^{3+}/Co^{2+} couple and Cu(II)-bipyridine complexes are generally characterized with a Cu^{2+}/Cu^{+} couple. As shown in **Figure 3.9.**, the Co^{3+}/Co^{2+} couple of the Co(II)-centered Keggin has the potential value of +1.0 V (**Figure 3.9. (b)**) which is out of the potential range selected for the present study, instead the A1C1 couple (**Figure 3.9. (a)**), assigned to Cu^{2+}/Cu^{+} couple, has appeared at +0.182 V *vs* NHE (E_{PC} = +0.013 V and E_{PA} = +0.350 V) as a major couple. This major and broad feature has been attributed to the combination of **Cu(2)** and **Cu(3)** centers, found in the crystal structure of compound **1**, having

distorted square pyramidal and distorted square planar geometry respectively (*vide supra*); the hump-like feature (A1') at 0.013 V supports the combined couples as shown in **Figure 3.9**.

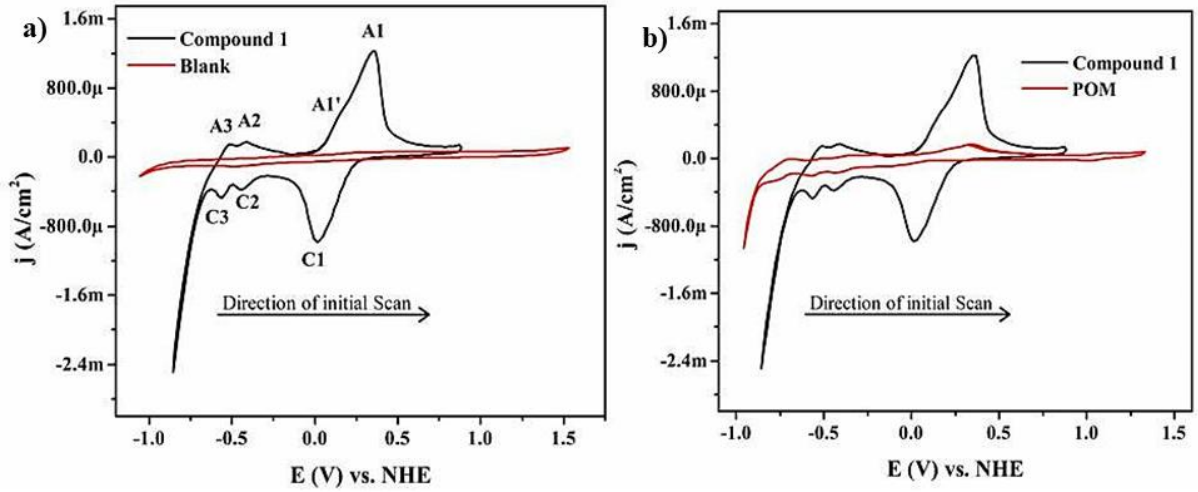

Figure 3.9. (a) CVs of **1** and Blank GC. **(b)** CVs of **1** and POM in acetate buffer, pH=4.8, scan rate 100 mV/s.

This is followed by two less-intense couples A2C2 and A3C3 at around -0.5 V and -0.6V respectively, that are assigned to reduction of tungsten centres of the Keggin POM unit by comparing the CV of compound **1** with that of POM Keggin itself. Right after the C3 (reductive) response there is a sudden surge of the current, which is not seen in the case of bare GC electrode or with POM compound *per se* indicating electrocatalytic hydrogen evolution reaction (HER), catalyzed by compound **1** coated on the working (glassy carbon) electrode. Bubbles of hydrogen evolution were visible on the working electrode during the CV scans The active site / functional site of the catalyst (compound **1**) should be **Cu(1)** center supported on the Keggin POM unit (see the crystal structure, **Figure 3.2.**, *vide supra*) having two coordinated water molecules, which is not particularly involved in the construction of the extended structure. But we could not observe the reductive response of the functional site (**Cu(3)** center) in the CV plot, instead we see the abrupt current surge at –0.67 V (onset potential). The reason of not seeing the reductive response of the **Cu(1)** center is probably due to the large HER onset current. The relevant redox reactions producing molecular hydrogen by water reduction can be described in equations 1–3.

$$2H_2O + 2e^- \rightarrow H_2 + 2OH^- \qquad \text{(eqn. 1)}$$

$$2[POM–Cu^{II}(OH_2)_2] + 2e^- \rightarrow 2[POM–Cu^{I}(OH_2)_2] \qquad \text{(eqn. 2)}$$

$$2[POM–Cu^{I}(OH_2)_2] + 2H_2O \rightarrow H_2(g) + 2OH^- + 2[POM–Cu^{II}(OH_2)_2] \qquad \text{(eqn. 3)}$$

It is expected that $Cu^{II}(1)$ center having two coordinated water molecules would be reduced to $Cu^{I}(1)$ center at a more negative potential than other two Cu^{II} centers, namely $Cu^{II}(2)$ and $Cu^{II}(3)$ centers having one coordinated water molecule and no coordinated water molecule respectively. We believe that the reductive response of the $Cu^{II}(1)$ center is just before the onset potential, which we could not see due high current surge of HER and thus $Cu^{II}(1)$ center is the active site for water reduction in the present study.

3.3.2.2. Analysis of Electrochemical stability for 1

Long term stability of compound **1** was studied by carrying out constant potential electrolysis (CPE) at the onset potential (-0.7 V). The durability of the catalysts was determined by the number of CV cycles **1** could perform without any change in its features. Compound **1** was found to be stable for 3 h when constant potential of -0.76 V was applied (**Figure 3.10.**). No notable change in the current value was observed over this period. The sample was coated on FTO electrode and images were taken with FESEM (**Figure 3.11.**).

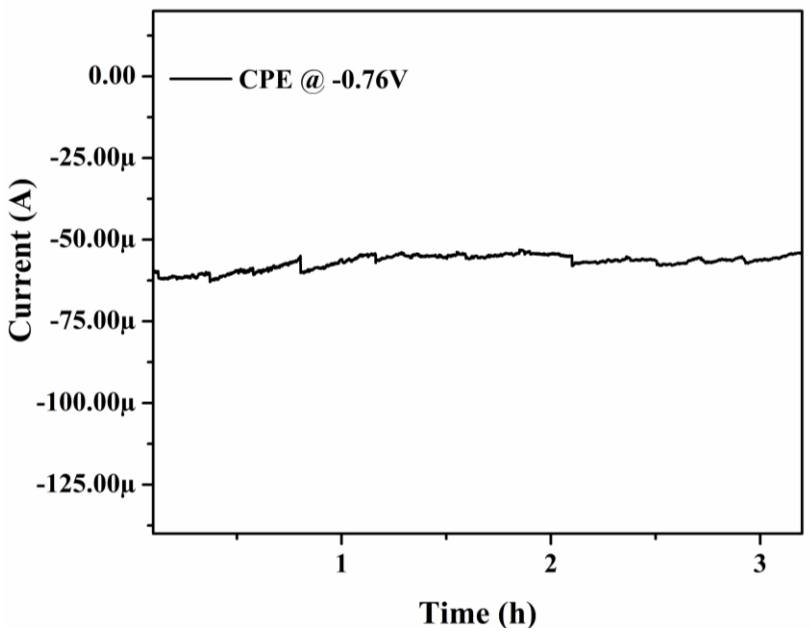

Figure 3.10. Constant Potential Electrolysis of compound **1** recorded at potential of -0.76 V.

EDX analysis was done over the surface of the electrode surface before and after the CPE experiments to monitor the elemental composition on the surface. The weight and atomic percent of all the elements present on compound **1** are tabulated in the **Table 3.2.** The ratio of the weight

percent of the Cu atoms to Co atom does not change which infers to the structural integrity of compound **1** after the said time interval (3 h) of CPE analysis. This provided us with the proof of the sustainability of the catalyst for HER activity. Apart from this, the electrolyte after 3 h CPE was collected and the absorbance spectrum was recorded for the same (**Figure 3.11.**). No absorbance was found in the spectrum recorded ruling out of leaching of metal ion in the electrolyte during HER activity (**Figure 3.12.**).

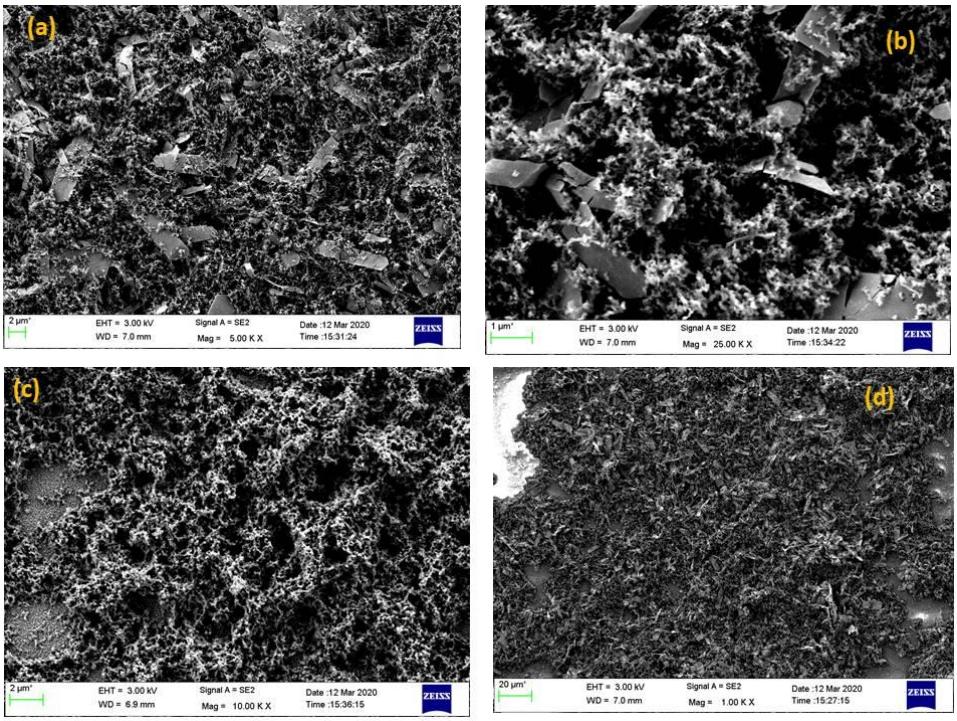

Figure 3.11. FESEM images of compound **1** coated on FTO, before (a-b) and after (c-d) CPE analysis.

Table 3.2. EDX analysis over different region of the surface of **1**.

		C	N	O	Co	Cu	W
Before	**Weight(%)**	45.89	1.55	24.04	0.92	1.46	26.14
	Atomic (%)	68.05	1.97	26.76	0.28	0.41	2.53
After	**Weight(%)**	57.06	1.16	4.13	0.68	1.85	35.12
	Atomic (%)	89.25	1.55	4.85	0.22	0.55	3.59

Compound **1** sustained 150 cycles of CV scans without any change in its feature, confirming its durability for 150 cycles in the potential window of the study (**Figure 3.12. (a)**). Initially, the CV

plot has three peaks, one in the form of a hump, which could be initially seen due to the difference in coordination geometry of all involved Cu-species. With every consecutive cycle, the hump slowly disappears, and only a single redox peak is visible. For every cycle, the peak position and the onset potential remain constant; only after 150 cycles, notable changes in terms of the area under the peak for the redox peak assigned to Cu(II)/(I) redox (C1 and A1) was observed. We compared the 10th cycle of CV scan with that recorded after continuous 150 cycles of CV scans (**Figure 3.12. (b)**). After completing long-term CV scans, the CV scans were recorded by washing gently the GC electrode containing coated sample with Mili-Q water and recording the CV with fresh electrolyte (0.1 M acetate buffer, pH=4.8).

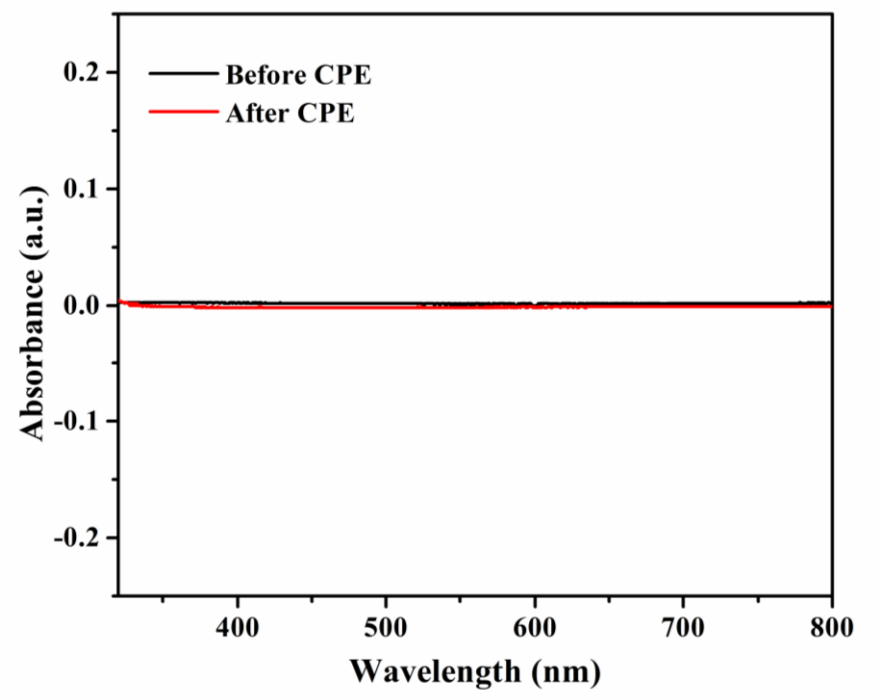

Figure 3.12. UV-visible Spectra of 0.1 M acetate buffer recorded before (black) and after (red) the CPE analysis.

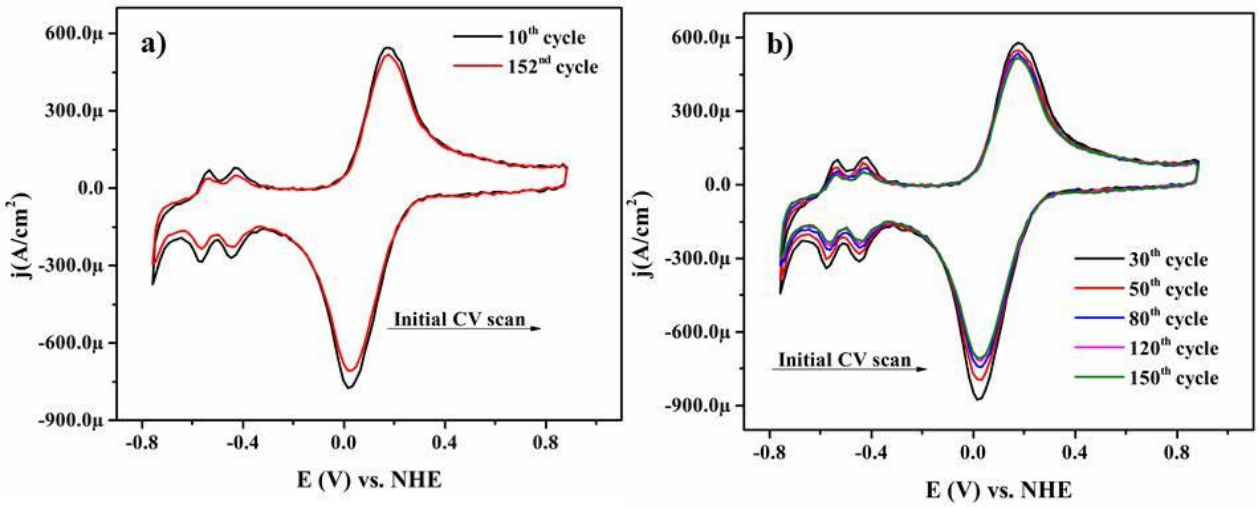

Figure 3.13. (a) CV scans of **1** for long terms durability; 10th cycle and 152nd cycle of CV scan recorded after removing the working electrode and washing gently with water after 150 cycles. **(b)** 150 CV scans of **1** in 0.1 M acetate buffer, pH 4.8, with a scan rate of 100 mV/s.

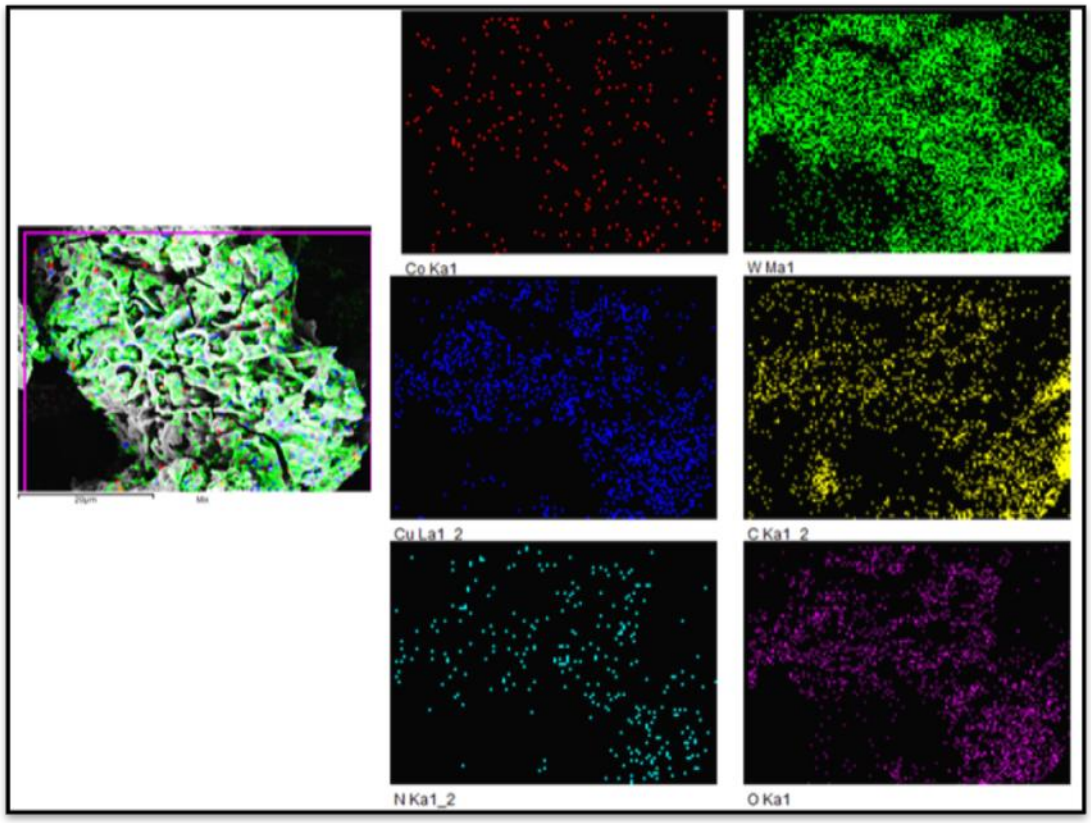

Figure 3.14. Element mapping of coated sample of **1** collected after CPE analysis.

3.3.2.3. Controlled Experiments to understand the HER catalysis by compound 1

To understand the constituent POM and metal complex's role in compound **1,** we designed varied experiments discussed below. All the experiments as discussed in this section, except compound **1**, were carried in a homogenous manner by taking 1 mmol of the concerned sample in three-electrode systems containing the same electrode mentioned in experimental section **3.2.1.3.** The electrochemical conditions were maintained the same as that of **1** unless otherwise mentioned.

[1]$K_6[CoW_{12}O_{40}]\cdot 6H_2O$ was studied for its redox activity under a potential window of (+1) V to (-1) V. No onset potential as seen in the case of **1** was observed for $K_6[CoW_{12}O_{40}]\cdot 6H_2O$ debarring the direct involvement of Keggin POM for HER activity seen in case of **1 (Figure 3.9. (b)**).

[2] $[Cu(2,2'\text{-bpy})_2(H_2O)_2]Cl_2$was prepared by following the protocol given in the literature.[36] The Cu-complex prepared was utilized for the study of its redox property by recording its CV scans. Cu(II)/(I) redox peak was seen at E=0.1125 V with cathodic peak for reduction of Cu(II) to Cu(I) at +0.046 V and the anodic peak of Cu(I) to Cu(II) at +0.179 V (**Figure 3.14**.) An onset current was observed of this Cu-complex with significantly less current at -0.82 V (**Figure 3.14**. **(b)**).

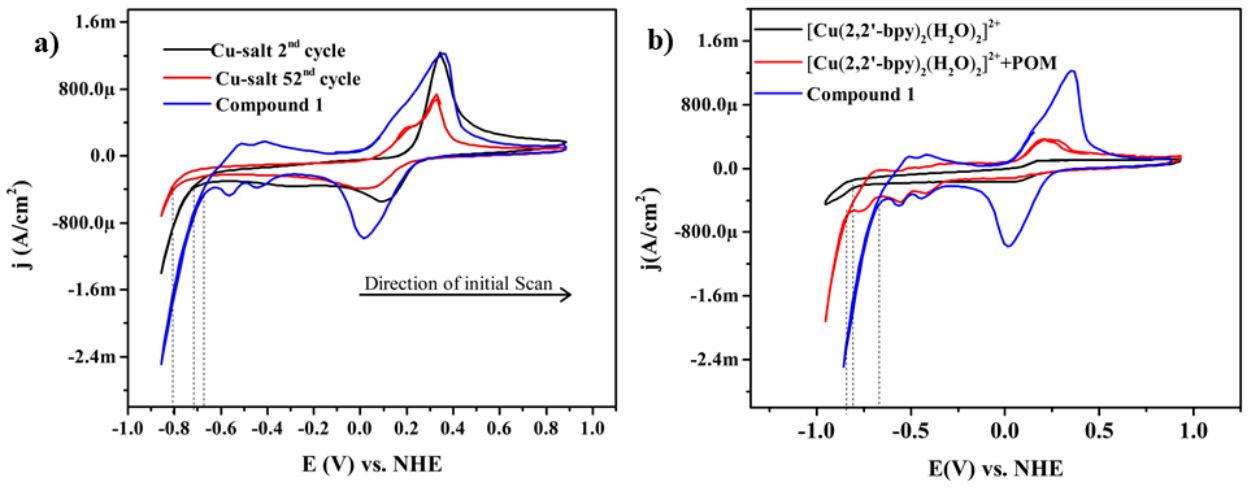

Figure 3.15. (a) CV cycles (2nd and 52nd cycles) of $Cu(CH_3COO)_2\cdot H_2O$ (labelled as Cu-salt) and compound **1**. **(b)** CVs of Cu-complex (black), physical mixture of Cu-complex and POM (red) and compound **1** (blue), recorded acetate buffer, pH=4.8, scan rate 100 mV/s.

[3] A physical mixture of $K_6[CoW_{12}O_{40}]\cdot 6H_2O$ and $[Cu(2,2'\text{-bpy})_2(H_2O)_2]Cl_2$ was prepared, and studies for their combined effect in the presence of each other were conducted. As expected, the CV of the physical mixture showed similar redox peaks as that of **1** with an onset at -0.83 V (**Figure 3.15. (b)**). The peaks for reduction of Cu(II) to Cu(I) were seen at -0.32 V, and that for its reoxidation was observed at -0.356 V. An anodic shift in the onset potential of the physical mixture was seen when compared with that of Cu-complex. The increase in onset current is due to the combined effect of Keggin POM $K_6[CoW_{12}O_{40}]\cdot 6H_2O$ and Cu-complex, and hence, the synergistic effect of POM for the catalysis seen in **1** could be easily explained.

[4] $Cu(CH_3COO)_2\cdot H_2O$ (labeled as Cu-salt henceforth) was studied for its redox property. The Cu(II)/(I) redox peak E = 0.218 V (anodic peak at 0.34 V and cathodic peak at 0.097) was observed (**Figure 3.15. (a)**). An onset of current was seen at -0.72 V, which after 51 CV cycle scans shifted to the more cathodic side, i.e., at -0.8 V. The onset current observed, in this case, is way too low compared to onset current observed for **1**.

The observations from all these studies directed us to conclude that Cu-species present in the compound **1** has direct participation for the HER catalysis facilitated by POM through a synergistic effect.

3.3.2.4. Hydrogen detection by Gas Chromatography (GC)

The gas liberated after CPE of **1** at -0.76 V for 3 h was collected and detected by GC. The gas was found to be hydrogen by comparing the retention time with that of pure hydrogen gas. The gas accumulated after the CPE experiment was collected using a home-made volumetric set-up, which is discussed later in section **3.3.2.6.**

The retention time of pure hydrogen (**Figure 3.16.**) is 2.005 minutes, which for the gas collected after the three hours of CPE analysis of **1** is 1.999 minutes (**Figure 3.17.**). The presence of hydrogen was thus confirmed by analyzing the retention time observed for the pure hydrogen gas to that of the gas collected from the electrocatalysis by **1**. A peak that appeared at the retention times of 2.550 minutes in both the chromatograms is assigned to the oxygen (from the air), which enters the chromatogram during the sample injection.

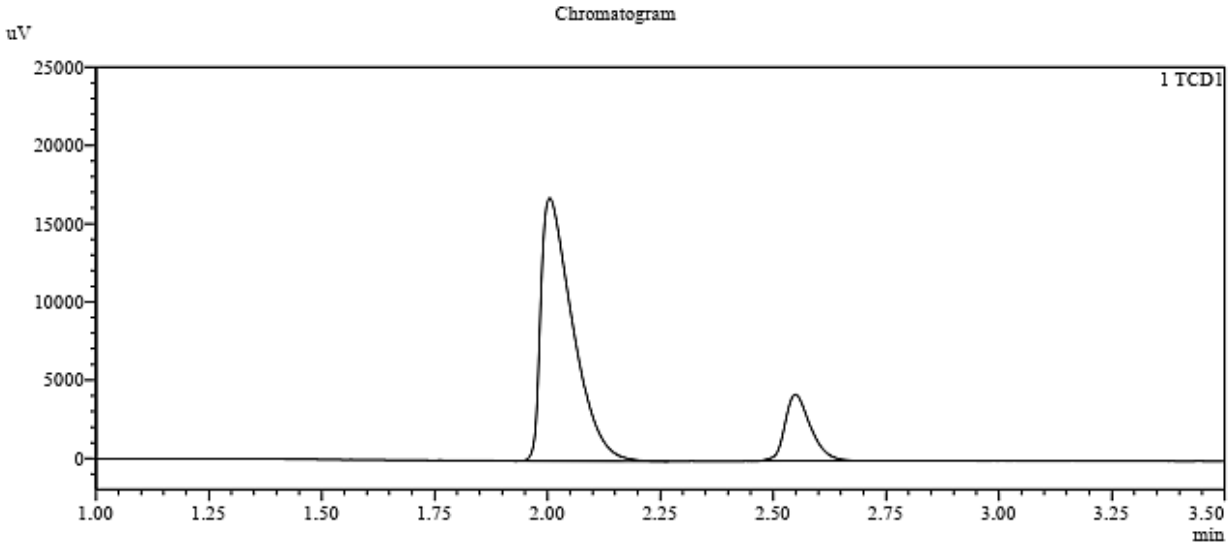

Peak Table

TCD1

Peak#	Ret. Time	Area	Height	Area%	Name
1	2.005	82223	16785	83.012	H2
2	2.550	16826	4239	16.988	O2
Total		99049	21023	100.000	

Figure 3.16. Chromatogram of pure hydrogen gas (standard sample).

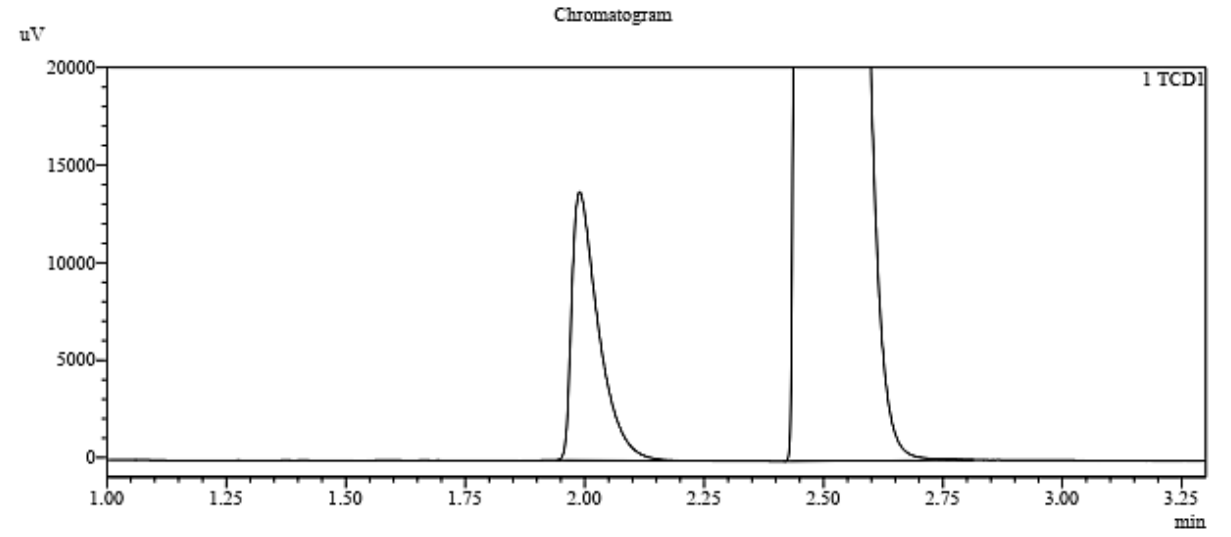

Peak Table

TCD1

Peak#	Ret. Time	Area	Height	Area%	Name
1	1.990	53505	13720	2.437	H2
2	2.466	2142374	451638	97.563	O2
Total		2195879	465358	100.000	

Figure 3.17. Chromatogram of gas collected after the CPE measurement by **1**.

3.3.2.5. Mechanistic and Kinetic analysis

3.3.2.5.1. Tafel Plot

Tafel data was calculated by following the same process as dicussed in Chapter **1** under section **2.3.2.6.** Compound **1** is found to have the overpotential of 520 mV at the current density of 1 mA/cm^2 with a slope of 181 mV/decade (**Figure 3.18.**).

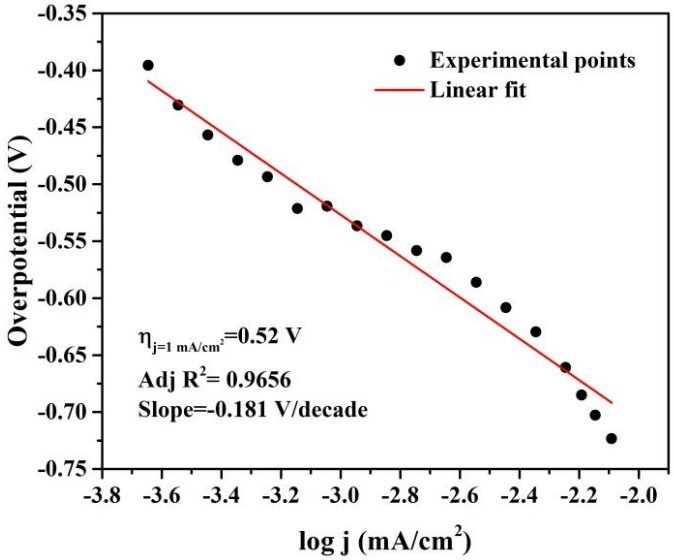

Figure 3.18. Galvanostatic iR-corrected Tafel plot of compound **1**.

3.3.2.5.2. pH dependent studies

Acetate buffer was prepared with different pH (pH 3 to pH 6), and was utilized directly for recoding CV scans of compound **1**. A plot of CVs of **1** recorded in different pH is given in **Figure 3.19. (a)**. pH values near to neutral point do not show any catalytic activity. The HER catalysis by **1** was observed from pH 5 onwards. The onset potential for HER shifts more towards the anodic side with the increase in proton concentration, suggesting the involvement of the proton-coupled electron transfer (PCET) pathway. From the CVs obtained at varied pH values, we constructed a pH *vs.* E plot by noting down the potential for every pH at the catalytic current of '-230 μA' (**Figure 3.19**. **(b)**). A linear plot is observed with the slope value of -66 mV/pH, suggesting the PCET pathway's involvement with the one electron and one proton.

3.3.2.5.3. Catalyst loading

The role of **1** in the catalytic reaction was further confirmed by recording CV scans by increasing the loading of the **1** on the working electrode. We started with a coat of 5 µL followed by 10, 15, 20 µL so on and so forth. As expected, the current catalytic increases with the catalyst loading increase (**Figure 3.20. (a)**). The plot of catalytic current (at constant potential) at different catalyst loading was found to be linear with features similar to first-order reaction (**Figure 3.20. (b)**).

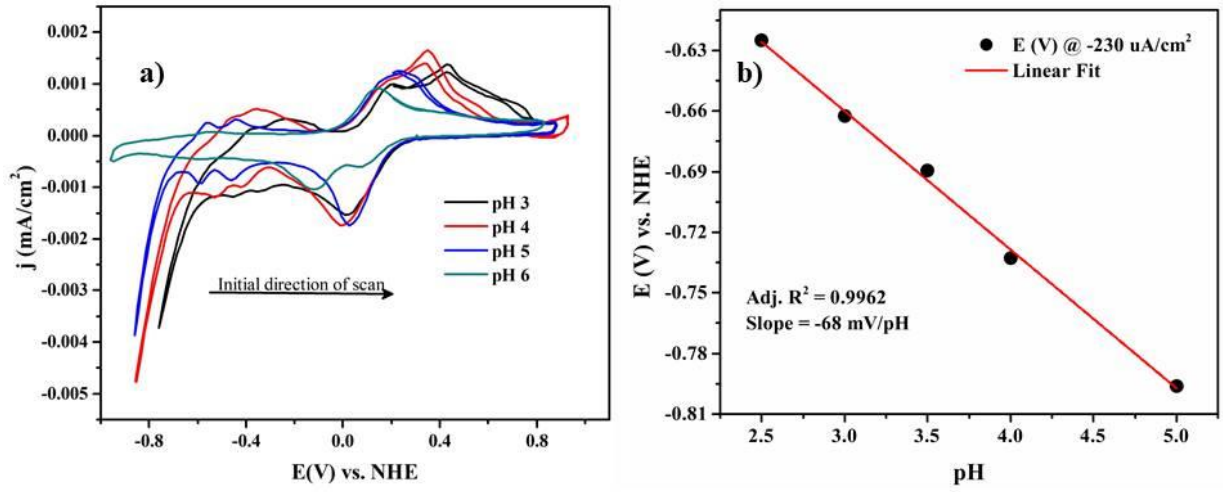

Figure 3.19. (a) CVs of **1** were recorded at different pH values. **(b)** A plot of E *vs.* pH, where for every pH at a fixed current density of '-230 µA/cm^2' E was noted.

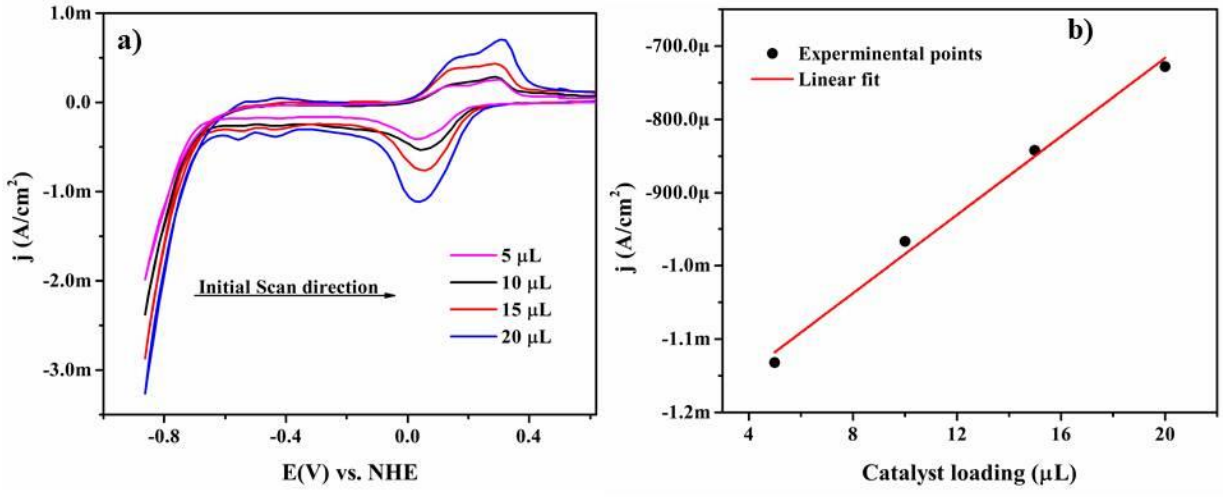

Figure 3.20. (a) CVs of **1** by varying the amount of loading of the sample on working electrode. **(b)** At the fixed potential (catalytic range -0.75 V) for every catalytic loading, current density was noted and plotted of j *vs.* catalyst load.

3.3.2.5.4. Scan rate variation

CV scans were recorded at different scan rates (0.01 V to 0.3 V), and derived plots were obtained from these CVs (**Figure 3.21.**). For the CVs recorded in different scan rate, we observed that the peak current increase with the increase in scan rate (**Figure 3.21. (a)**). A derived plot was devised as a function of cathodic peak current of Cu(II) to Cu(I) reduction to the scan rate. The linear relationship seen in the plot of i_{pc} *vs.* ν suggests the diffusion-controlled process for the redox active species.

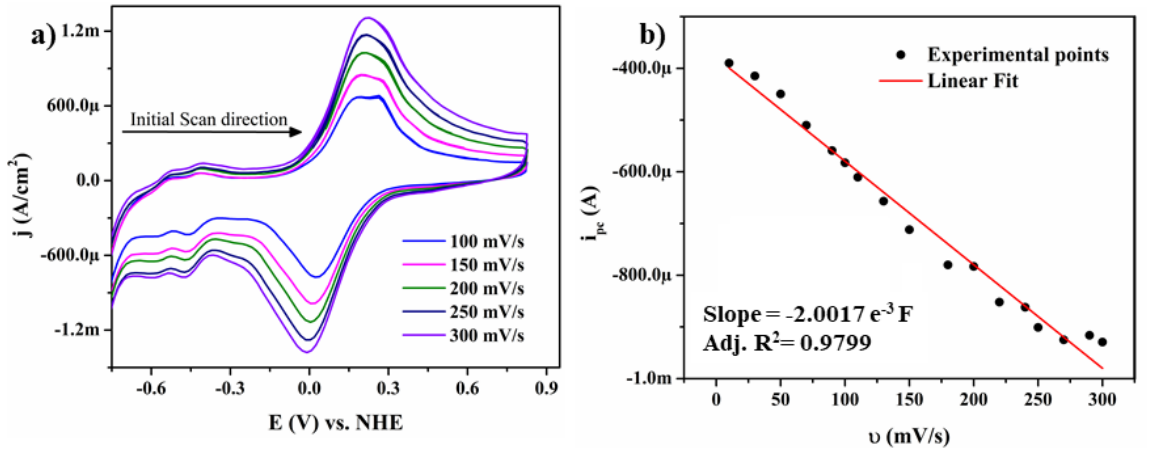

Figure 3.21. (a) CVs of compound **1** were recorded by varying the scan rate. **(b)** Plot of i_{pc} *vs.* scan rate **(c)** Plot of I_{pc} *vs.* square root of the scan rate.

3.3.2.6. Quantitative hydrogen evolution and Faradic efficiency calculation

Faradic efficiency was calculated using the similar protocol followed in **Chapter 2** as discussed under section **2.3.2.7.** It only differs in terms of reaction happening at the working electrode (HER in the present study whereas it is OER for **Chapter 2**). The home-built set-up used for this study is provided in the **Figure 3.22.**

This same home-built set-up with only a difference of open-end towards the graduated tube was used for gas detection from a gas chromatogram. The open end was sealed with septa. The gas was collected using a micro-syringe from the top of this set-up (head-space) injected directly for analysis by gas chromatogram.

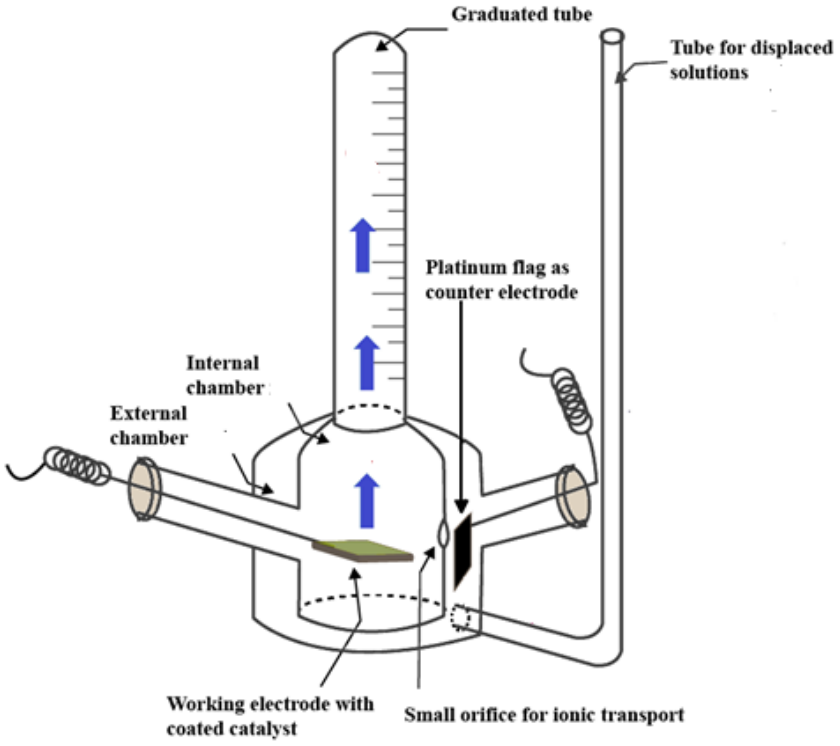

Figure 3.22. Schematic diagram of home-built set-up for quantitative measurement of hydrogen evolution.

Calculation of Faradaic Efficiency of 1

Faradaic efficiency of any system describes its efficiency with which charge is utilized in an electrochemical reaction.

For hydrogen evolving reaction, Faradic efficiency can be written as,

Moles of H_2 evolved by the system
Moles of H_2 that can evolve by using the applied charge

From the bulk-electrolysis, the quantitative measurement of hydrogen evolved was measured under constant current condition. For this work, we found 0.22 mL/hour of H_2 evolved under 1 atm. pressure.

Thus, moles of H_2 evolved in one hour = (0.22/22400) mol = **9.82 µmol**.

$H_{2\ ideal}$ =

Q (Total Charge employed)
n (no. of electrons required for the chemical change X 1 Farad)

Here, we applied a current density of 1 mA/cm^2 and 'n'= 2 for HER (a two-electron process).

Thus, H_2 that ideally should evolve with the applied current density,

= (0.00065 × 3600)/(2 × 96500) mol = 12.12 μmol.

Therefore Faradaic efficiency of compound **1**,

$= \frac{9.82}{12.12} x100 = 81.02\ \%$

Thus, Faradic efficiency is 81.02% for compound **1**.

3.3.2.7. Turnover Frequency (TOF) Calculation

- **Calculation of Surface Coverage and number of active copper atoms**

We have calculated the active Cu atoms/cm^2 on the electrode surface using similar method utilized in **Chapter 2** as discussed under section **2.3.2.8.**, by following the equation 1.

$$Slope = n^2F^2A\Gamma_0/4RT \quad \text{..... (1)}$$

Where 'n' = No. of electrons involved, here 1. For Cu(II) – Cu(I) conversion.

Here, slope refers to the slope value of i_p *vs.* scan rate plot (**Figure 3.20. (b)**), which is (2.008 E-3 F).

By substituting the values in the equation, we calculate the surface density Γ_0 for compound **1**.

Thus, for compound **1**, we obtained surface density of active copper atoms as **1.77 ×10^{16} copper atoms/cm^2** or **2.947 × 10^{-8} mol/cm^2**.

- **Calculation of Turnover Frequency (TOF) for H_2 evolution from Tafel Plot:**

$$\text{TOF at any given over potential} = \frac{\text{Current density at given over potential}}{2 \times F \times \text{No. of active copper species/atoms}} \quad \text{..... (2)}$$

Here, numeric 2 is due to the involvement of 2e$^-$ in HER process. Hence division of current density at a particular overpotential by 2F (F = Faraday constant) gives one catalytic turnover number and further division of turnover number by the number of active copper atoms results in turnover frequency (TOF).

$$\text{TOF at any given over potential} = \frac{0.01}{2 \times F \times 2.947\ E^{-8}} \quad \text{..... (2)}$$

Thus $(TOF)_{j=1\ mA} = 1.758$ [mol H_2 (mol Cu)$^{-1}$s^{-1}]

3.4. Conclusion

A new 2-dimensional Cu-complex networked with the support Keggin POM having the molecular formula of **[{Cu(2,2´-bpy)(H_2O)$_2$}][{$CoW_{12}O_{40}$}{(Cu(2,2´-bpy)(H_2O)}{(Cu(2,2´-bpy)}]·2H_2O**, is prepared *via* the hydrothermal method. Compound **1** catalyzes HER under near-neutral pH (acetate buffer, pH 4.8) with the overpotential of 520 mV and TOF of 1.758 mol of H_2 evolved for per mol of Cu atom per second at the current density of 1 mA/cm^2. The 2-dimensional network of Cu-complex plays an essential role in the stability of compound **1** towards the electrocatalytic property for HER. Compound **1** follows a PCET pathway with the involvement of one electron and one proton for the catalysis of HER. In this work, we have shown the mechanistic pathway and kinetics of the HER electrocatalysis catalyzed by compound **1**. This chapter has shown how the choice of transition metal ion chosen for the hybrid structure preparation affects the property it will exhibit under the electrochemical conditions. POM provides stability and facilitates faster electron transfer, allowing the overpotential to reduce comparing it with the parent metal complex.

3.5. References

1. Eftekhari, A. Electrocatalysts for Hydrogen Evolution Reaction. *International Journal of Hydrogen Energy*, **2017**, *42*, 11053-11077.

2. Wang, Y.; Bunshi, F.; Sakata, I.; Fujisue, C.; Kabayama, S.; Tahara, N.; Morisawa, S. Monolayered Platinum Nanoparticles as Efficient Electrocatalysts for the Mass Production of Electrolyzed Hydrogen Water. *Scientific Reports* **2020**, *10*, 10126.

3. Li, C.; Baek, J.-B. Recent Advances in Noble Metal (Pt, Ru, and Ir)-Based Electrocatalysts for Efficient Hydrogen Evolution Reaction. *ACS Omega* **2020**, *5*, 31–40.

4. Schwämmlein, J. N.; Stühmeier1, B. M.; Wagenbauer, K.; Dietz, H.; Tileli, V.; Gasteiger, H. A. El-Sayed, H. A. Origin of Superior HOR/HER Activity of Bimetallic Pt-Ru Catalysts in Alkaline Media Identified via Ru@Pt Core-Shell Nanoparticles. *J. Electrochem. Soc.* **2018**, *165*, H229.

5. Nash, J.; Zheng, J.; Wang, Y.; Xu, B.; Yan, Y. Mechanistic Study of the Hydrogen Oxidation/Evolution Reaction over Bimetallic PtRu Catalysts. *J. Electrochem. Soc.* **2018**, *165*, J3378.

6. Rezaei, B.; Mokhtarianpour, M.; Ensafi, A. A. Fabricated of Bimetallic Pd/Pt Nanostructure Deposited on Copper Nanofoam Substrate by Galvanic Replacement as an Effective Electrocatalyst for Hydrogen Evolution Reaction. *International Journal of Hydrogen Energy* **2015**, *40*, 6754-6762.

7. Li, Y.; Pei, W.; He, J.; Liu, K.; Qi, W.; Gao, X.; Zhao, S.; Xie, H.; Yin, K.; Gao, Y.; He, J.; Zhao, J.; Hu, J.; Chan, T.-S.; Li, Z.; Zhang, G.; Liu, M. Hybrids of PtRu Nanoclusters and Black Phosphorus Nanosheets for Highly Efficient Alkaline Hydrogen Evolution Reaction. *ACS Catal.* **2019**, *9*, 10870–10875.

8. Liu, X.; Jiao, Y.; Zheng, Y.; Davey, K.; Qioa, S.-Z. A Computational Study on Pt and Ru Dimers Supported on Graphene for the Hydrogen Evolution Reaction: New Insight into the Alkaline Mechanism. *J. Mater. Chem. A* **2019**, *7*, 3648-3654.

9. Li, F.; Han, G.-F.; Noh, H.-J.; Ahmad, I.; Jeon, I.-Y.; Baek, J.-B. Mechanochemically Assisted Synthesis of a Ru Catalyst for Hydrogen Evolution with Performance Superior to Pt in Both Acidic and Alkaline Media. *Adv. Mater.* **2018**, *30*, 1803676.

10. Luis-Sunga, M.; Regent, L.; Pastor, E.; García, E. Non-Precious Metal Graphene-Based Catalysts for Hydrogen Evolution Reaction. *Electrochem* **2020**, *1*, 75-86.

11. Majee, K.; Patel, J.; Das, B.; Padhi, S. K. μ-Pyridine-Bridged Copper Complex with Robust Proton-Reducing Ability. *Dalton Trans.* **2017**, *46*, 14869-14879.

12. Zhang, P.; Wang, M.; Yang, Y.; Yao, T.; Sun, L. A Molecular Copper Catalyst for Electrochemical Water Reduction with a Large Hydrogen-Generation Rate Constant in Aqueous Solution. *Angew Chemie - Int Ed.* **2014**, *53*,13803-13807.

13. Fashapoyeh, M. A.; Mirzaei, M.; Eshtiagh-Hosseini, H.; Rajagopal, A.; Lechner, M.; Liu, R.; Streb, C. Photochemical and Electrochemical Hydrogen Evolution Reactivity of Lanthanide-Functionalized Polyoxotungstates. *Chem. Commun.* **2018**, *54*, 10427-10430.

14. Wang, D.; Liu, L.; JIang, J.; Chen, L.; Zhao, J. Polyoxometalate-based Composite Materials in Electrochemistry: State-of-the-art Progress and Future Outlook. *Nanoscale* **2020**, *12*, 5705-5718.

15. Zhao, G.; Rui, K.; Dou, S. X.; Sun, W. Heterostructures for Electrochemical Hydrogen Evolution Reaction: A Review. *Adv. Funct. Mater.*, **2018**, *28* , 1803291.

16. Chen, Z.; Duan, X.; Wei, W.; Wang, S.; Ni, B.-J. Recent Advances in Transition Metal-Based Electrocatalysts for Alkaline Hydrogen Evolution. *J. Mater. Chem. A*, **2019**, *7*, 14971-15005.

17. Wang, J.; Yue, X.; Yang, Y.; Sirisomboonchai, S.; Wang, P.; Ma, X.; Abdulaa, A.; Guan, G. Earth-Abundant Transition-Metal-Based Bifunctional Catalysts for Overall Electrochemical Water Splitting: A Review. *Journal of Alloys and Compounds* **2020**, *819*, 153346.

18. Yan, Y.; Xia, B. Y.; Zhao, B.; Wang, X. A Review on Noble-Metal-Free Bifunctional Heterogeneous Catalysts for Overall Electrochemical Water Splitting. *J. Mater. Chem. A*, **2016**, *4*, 17587-17603.

19. Weng, C.-C.; Ren, J.-T.; Yuan, Z.-Y.; Transition Metal Phosphide-Based Materials for Efficient Electrochemical Hydrogen Evolution: A Critical Review. *ChemSusChem* **2020**, *13*, 3357-3375.

20. Li, D.; Shi, J.; Li, C. Transition-Metal-Based Electrocatalysts as Cocatalysts for Photoelectrochemical Water Splitting: A Mini Review. *Small*, **2018**, *14* , 1704179.

21. Zhang, P.; Wang, M.; Yang, Y.; Yao, T.; Sun, L. A Molecular Copper Catalyst for Electrochemical Water Reduction with a Large Hydrogen-Generation Rate Constant in Aqueous Solution. *Angew Chemie - Int Ed.* **2014**,*53*, 13803-13807.

22. Zhang, P.; Wang, M.; Chen, H.; Liang, Y.; Sun, J.; Sun, L. A Cu-Based Nanoparticulate Film as Super-Active and Robust Catalyst Surpasses Pt for Electrochemical H_2 Production from Neutral and Weak Acidic Aqueous Solutions. *Adv Energy Mater.* **2016**, *6*, 1-9.

23. Kügler, M.; Scholz, J.; Kronz, A.; Siewert, I. Copper Complexes as Catalyst Precursors in the Electrochemical Hydrogen Evolution Reaction. *Dalton Trans.* **2016**, *45*, 6974-6982.

24. (a) Nohra, B.; Moll, H. E.; Albelo, L. M. R.; Marrot, J.; Mellot-Draznieks, C.; O'Keeffe, M.; Biboum, R. N.; Lemaire, J.; Keita, B.; Nadjo, L.; Dolbecq, A. Polyoxometalate-Based Metal Organic Frameworks (POMOFs): Structural Trends, Energetics, and High Electrocatalytic Efficiency for Hydrogen Evolution Reaction. *J. Am. Chem. Soc.* **2011**, *133*, 13363-13374.

25. Salomon, W.; Paille, G.; Gomez-Mingot, M.; Mialane, P.; Marrot, J.; Roch-Marchal, C.; Nocton, G.; Mellot-Draznieks, C.; Fontecave, M.; Dolbecq, A. Effect of Cations on the Structure and Electrocatalytic Response of Polyoxometalate-Based Coordination Polymers. *Crystal Growth & Design* **2017**, *17*, 1600-1609.

26. Zhang, L.; Li, S.; Gómez-García, C. J.; Ma, H.; Zhang, C.; Pang, H.; Li, B. Two Novel Polyoxometalate-Encapsulated Metal–Organic Nanotube Frameworks as Stable and Highly Efficient Electrocatalysts for Hydrogen Evolution Reaction. *ACS Appl. Mater. Interfaces* **2018**, *10*, 31498–31504.

27. Jiang, M.; Zhu, D.; Cai, J.; Zhang, H.; Zhao, X. Electrocatalytic Hydrogen Evolution and Oxygen Reduction on Polyoxotungstates/Graphene Nanocomposite Multilayers. *J. Phys. Chem. C* **2014**, *118*, 14371–14378.

28. Fernandes, D. M.;. Araújo, M. P.; Haider, A,; Mougharbel, A. S.; Fernandes, A. J. S.; Kortz, U.; Freire, C. Polyoxometalate-Graphene Electrocatalysts for the Hydrogen Evolution Reaction. *ChemElectroChem* **2018**, *5*, 273-283.

29. Ahmad, W.; Gao, Q.; Zhang, X. L.; Tan, W.; Zhang, L.; Gao, M.-R.; Yu, S.-H. Sandwich-Type Polyoxometalate Mediates Cobalt Diselenide for Hydrogen Evolution in Acidic Electrolyte. *ChemNanoMat.* **2020**, *6*,1164-1168.

30. Singh, C.; Mukhopadhyay, S.; Das, S. K. Polyoxometalate-Supported Bis(2,2′-bipyridine)mono(aqua)nickel(II) Coordination Complex: An Efficient Electrocatalyst for Water Oxidation. *Inorg. Chem*. **2018**, *57*, 6479–6490.

31. SAINT: Software for the CCD Detector System; Bruker Analytical X-ray Systems, Inc.: Madison, WI, **1998**.

32. Sheldrick, G. M. SADABS, Program for Absorption Correction; University of Gottingen: Gottingen, Germany, **1997**.

33. Sheldrick, G. M. SHELXS-97, Program for Structure Solution and Analysis*;* University of Gottingen: Gottingen, Germany, **1997**.

34. Sheldrick, G. M. SHELXL-97, Program for Crystal Structure Analysis; University of Gottingen: Gottingen, Germany, **1997**

35. Mukhopadhyay, S.; Debgupta, J.; Singh, C.; Kar, A.; Das, S. K. A Keggin Polyoxometalate shows Water Oxidation Activity in Neutral pH: POM@ZIF-8 an Efficient and Robust Electrocatalyst. *Angew. Chem., Int. Ed.* **2018**, *57*, 1918-1923.

36. Garribbaa, E.; Micera, G.; Sanna, D.; Liliana Strinna-Erre, L. The Cu(II)-2,2′-bipyridine System Revisited. *Inorg. Chim. Acta* **2000**, *299*, 253– 261.

Chapter 4

Anderson Polyoxometalate Supported {Cu(H_2O)(phen)} Complex as an Electrocatalyst for Hydrogen Evolution Reaction in Neutral Medium

OVERVIEW

Two structurally analogous Anderson polyoxometalate (POM) supported copper complexes, $[Cr(OH)_6Mo_6O_{18}\{Cu(phen)(H_2O)_2\}_2][Cr(OH)_6Mo_6O_{18}\{Cu(phen)(H_2O)Cl\}_2]\cdot 5H_2O$ (1) and $[Al(OH)_6Mo_6O_{18}\{Cu(phen)(H_2O)_2\}_2][Al(OH)_6Mo_6O_{18}\{Cu(phen)(H_2O)Cl\}_2]\cdot 5H_2O$ (2), were found to be an efficient catalyst for hydrogen production from a neutral aqueous medium. These compounds, catalyzes electrochemical hydrogen evolution reaction (HER) with relatively low overpotentials of 300 mV (compound 1) and 644 mV (compound 2) at current density of 1 mA/cm^2 from water (phosphate buffer, pH 7). Compounds 1 and 2 show remarkable Faradic efficiencies of 95.7% and 89.4%, respectively. Compound 1 turns out to be a better electrocatalyst for HER from water than compound 2, in terms of overpotential and Faradic efficiency. In this report, we have evidently proved that the active site of this electrochemical HER is the water coordinated Cu(II) center, supported onto POM cluster anion; the polyoxometalate, onto which these aqua-Cu(phen)-complexes are supported, plays an important role in making the overall system heterogeneous, for designing a better electrocatalyst for direct reduction of neutral water.

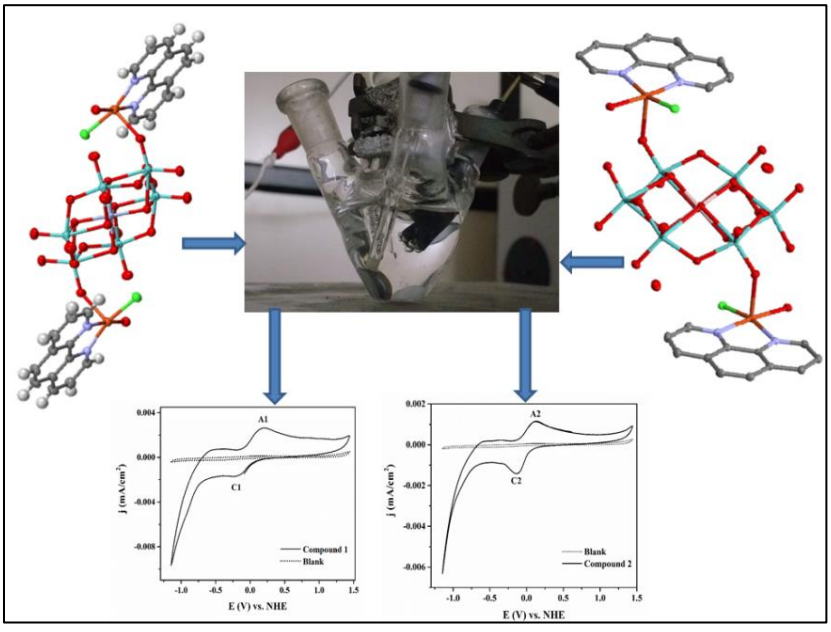

4.1. Introduction

Molecular hydrogen has gained considerable attention as an alternative source for fossil fuels to meet the energy requirement globally in a cleaner and cheaper method. Hydrogen production *via* electrochemical reduction of water can be considered as a sustainable method since this method derives hydrogen from carbon neutral process.[1] The modern world craves for renewable energy sources over fossil fuels and thus, hydrogen evolution reaction (HER) from water carries immense importance replacing these non-renewable energy sources. To achieve this, the primary focus should be catalyzing HER with a catalyst, which is cheap and can provide catalysis with a good efficiency and low overpotential. Platinum and other noble metals, known to catalyze HER efficiently with small overpotential, are expensive and less abundant on earth's crust, which limits their usage.[2-4] The most popular method to address these issues includes the usage of bimetallic system with one expensive noble metal and other cheaper transition metal.[5-6] Several nano-metal oxides and Mo-based catalysts have also acquired significant attention lately to achieve results similar to that showed by Pt-based catalyst.[7-8] However, most of the aforementioned catalysts are non-molecular, which do not offer the scope for structural tunability. In this regard, molecular catalyst would be a preferable choice, as structural and electronic properties of molecular catalysts can be tuned/modified easily, which, in turn, can supply effective catalysts. Further, the incorporation of cheaper transition metals (3d-row transition metals) to it will be an added benefit.

Designing new molecular catalysts, primarily containing earth-abundant 3d-transition metals as an active site, have attracted substantial attention in recent years. Nickel,[9] cobalt,[10] iron[11] based complexes are few popular molecular catalysts, which have been employed in electrocatalytic HER. In this regard, the noteworthy contribution has been made by Cao and his co-workers in recent years.[8g,9g,10d-10f] They have showcased various transition metal-based molecular catalysts for HER activity. In 2014, Wang and co-workers, for the first time, reported a Cu-complex that can electrochemically catalyze water reduction.[12a] This complex displayed a very high catalytic activity with 96% Faradic efficiency and 420 mV onset overpotential in pH 2.5 under buffer conditions. After this report, many Cu-based complexes were discovered, which showcased comparatively decent activity in catalyzing HER electrochemically.[12] The majority of these complexes catalyze the hydrogen evolution reaction (HER) in acidic conditions, which is one of the major drawbacks. There are very few reports of molecular catalysts, which can reduce water

in a neutral medium.[13] Herein, we report two Cu-based molecular catalysts that can reduce water electrochemically in neutral medium.

From our recent works, as discussed in **Chapters 2** and **3**, we have disclosed that polyoxometalate (POM) supported metal complexes can catalyze electrochemical oxygen evolution reaction (OER) and hydrogen evolution reaction (HER).[14] There, we have successfully proved the synergistic effect between Co(II)-centered POM and transition metal complexes (TMCs) coordinated to it, playing a significant role in electrocatalytic OER (**Chapter 2**) and HER (**Chapter 3**). Intending to introduce POM-supported Cu-aqua-coordination complex that may show catalyzing activity in water reduction in neutral medium, we have chosen two structurally analogous compounds available in the literature, $\{[Cr(OH)_6Mo_6O_{18}\{Cu(phen)(H_2O)_2\}_2][Cr(OH)_6Mo_6O_{18}\{Cu(phen)(H_2O)Cl\}_2]\cdot 5H_2O$ (**1**) and $[Al(OH)_6Mo_6O_{18}\{Cu(phen)(H_2O)_2\}_2][Al(OH)_6Mo_6O_{18}\{Cu(phen)(H_2O)Cl\}_2]\cdot 5H_2O$ (**2**), that was reported in 2005.[15] The similarity in molecular structures of compounds **1** and **2**, adds to our benefit for understanding the importance of POM and the role of synergistic effect on their catalytic behavior. These compounds, $[Cr(OH)_6Mo_6O_{18}\{Cu(phen)(H_2O)_2\}_2][Cr(OH)_6Mo_6O_{18}\{Cu(phen)(H_2O)Cl\}_2]\cdot 5H_2O$ (**1**) and $[Al(OH)_6Mo_6O_{18}\{Cu(phen)(H_2O)_2\}_2][Al(OH)_6Mo_6O_{18}\{Cu(phen)(H_2O)Cl\}_2]\cdot 5H_2O$ (**2**), are ensemble of charge complimentary copper phenanthroline complexes on Anderson type heteropolyanion. These hybrid compounds exhibit the property of both POM and the coordination complex attached to the POM cluster surface by maintaining the overall system's heterogeneity.

4.2. Experimental Section

4.2.1. Material and methods

4.2.1.1. General materials and methods

All the chemicals were received as reagent grade and used without further purification. The compounds $[Cr(OH)_6Mo_6O_{18}\{Cu(phen)(H_2O)_2\}_2][Cr(OH)_6Mo_6O_{18}\{Cu(phen)(H_2O)Cl\}_2]\cdot 5H_2O$ (**1**) and $[Al(OH)_6Mo_6O_{18}\{Cu(phen)(H_2O)_2\}_2][Al(OH)_6Mo_6O_{18}\{Cu(phen)(H_2O)Cl\}_2]\cdot 5H_2O$ (**2**) were synthesized by following protocol reported in the literature.[15] Both the compounds were characterized by analyzing and comparing their PXRD, IR, and UV-vis. spectra with those

reported in the literature. All electrochemical experiments were conducted using a Zahner Zanium electrochemical work station operated with Thales software.

Infrared spectra of solid samples were recorded on a JASCO-5300 FT-IR spectrophotometer in neat form. Powder X-ray diffraction patterns were recorded on a Bruker D8-Advance diffractometer using graphite monochromatic CuKα_1 (1.5406 Å) and Kα_2 (1.54439 Å) radiations. Diffuse Reflectance (DR) UV-vis electronic absorption spectra were recorded using Shimadzu-2600 spectrophotometer.

4.2.1.2. Electrochemical studies

Similar protocol is followed as that discussed in **Chapter 2** under section **2.2.1.3.** Electrode potentials were converted to the normal hydrogen electrode (NHE) scale using the relation E (NHE) = E (Ag/AgCl) + 0.1485 V when the Ag/AgCl used as reference electrode (RE). Cyclic voltammetry scans were initiated at the open circuit potential (OCP), and the cathodic side was scanned first, followed by an anodic scan. Five cycles were taken consecutively for each set of cyclic voltammetry measurements in quiescent solution. Cyclic voltammograms (CVs) were also recorded at various scan rates.

4.2.2. Synthesis

4.2.2.1. Synthesis of Compound 1

[Cr(OH)$_6$Mo$_6$O$_{18}${Cu(phen)(H$_2$O)$_2$}$_2$][Cr(OH)$_6$Mo$_6$O$_{18}${Cu(phen)(H$_2$O)Cl}$_2$]·5H$_2$O (1)

$CrCl_3 \cdot 6H_2O$ (1 g, 3.75 mmol) was dissolved in 50 mL of water. To this solution, 100 mL of water containing $Na_2MoO_4 \cdot 2H_2O$ (3.5 g, 14.46 mmol) followed by addition of 10 mL of glacial acetic acid. A water-methanol mixture (1:1) was prepared (100 mL), to which 1,10-phenanthroline (0.2 g, 1 mmol) and 0.7 g of $Cu(NO_3)_2 \cdot 2H_2O$ (2.9 mmol) were sequentially added. This reaction mixture was added to the former solution. Using concentrated HCl, the resulting reaction mixture's pH was adjusted to 2.6, after which it was heated till its temperature reached 90 °C. The reaction mixture was filtered immediately, and the filtrate was kept undisturbed under the closed condition at room temperature. Within one week, blue colored blocks were obtained and separated from the mother liquor by filtration. Yield: 0.65 g (16% based on Mo). IR (neat, cm^{-1}): 3328br, 1626m, 1577m, 1518m, 1492w, 1425m, 1344w, 1221w, 1145m, 1105m, 937s, 893s, 775m, 640s-br, 439w.

4.2.2.2. Synthesis of compound 2

$[Al(OH)_6Mo_6O_{18}\{Cu(phen)(H_2O)_2\}_2][Al(OH)_6Mo_6O_{18}\{Cu(phen)(H_2O)Cl\}_2]\cdot 5H_2O$ (2)

$AlCl_3\cdot 6H_2O$ (1 g, 4.14 mmol) was dissolved in 50 mL of water. To this solution, 100 mL of water containing $Na_2MoO_4\cdot 2H_2O$ (1.5 g, 6.2 mmol) and 10 mL of glacial acetic acid were added. A water methanol-mixture (1:1) was prepared (100 mL) to which 1,10-phenanthroline (0.2 g, 1 mmol) and 0.7 g of $Cu(NO_3)_2\cdot 2H_2O$ (2.9 mmol) were sequentially added. This reaction mixture was added to the former solution. Using concentrated HCl, pH of resulting reaction mixture was adjusted to 2.6, after which it was stirred for 10 min. The resulting reaction mixture was filtered immediately and kept undisturbed under the open condition at room temperature. Within one week, blue colored blocks were obtained and separated from the mother liquor by filtration. Yield: 0.80 g (47% based on Mo). IR (neat, cm^{-1}): 3325br, 1626m, 1582m, 1518m, 1493w, 1425m, 1344w, 1222w, 1145m, 1107m, 940s, 900s, 775m, 648s-br, 440w.

4.3. Results and Discussion

4.3.1. Physical characterization

All the compounds synthesized for this work were characterized by PXRD pattern analysis, FT-IR analysis, UV-vis. diffused reflectance spectral (DRS) analysis, FESEM, thermogravimetric analysis (TGA). For studying the electrocatalytic activity of both the compounds towards HER, various electrochemical techniques were employed. Some of them are cyclic voltammetry, differential pulse voltammetry (DPV), Constant potential electrolysis (CPE), *etc.;* the details are discussed later.

4.3.1.1. Description of Crystal structures

4.3.1.1.1. *$[Cr(OH)_6Mo_6O_{18}\{Cu(phen)(H_2O)_2\}_2][Cr(OH)_6Mo_6O_{18}\{Cu(phen)(H_2O)Cl\}_2]\cdot 5H_2O$ **(1)**.*
Compound **1** consists of polyoxometalate supported copper(II)-bis(aqua)-phenanthroline complex, $[Cr(OH)_6Mo_6O_{18}\{Cu(phen)(H_2O)_2\}_2]^+$ as cation and onto the same POM, copper(II)-aqua-chloro-phenanthroline complex, $[Cr(OH)_6Mo_6O_{18}\{Cu(phen)(H_2O)\text{-}Cl\}_2]^-$, as anion. The cation consists of an Anderson-type anion, $[Cr(OH)_6Mo_6O_{18}]^{3-}$, which uses its terminal oxygen atoms of nonadjacent MoO_6 octahedra to coordinate with two $[Cu(phen)(H_2O)_2]^{2+}$ complexes. Similarly, in the relevant crystal structure, the anion is formed by the coordination of $[Cr(OH)_6Mo_6O_{18}]^{3-}$ to two $[Cu(phen)(H_2O)Cl]^+$ complexes.

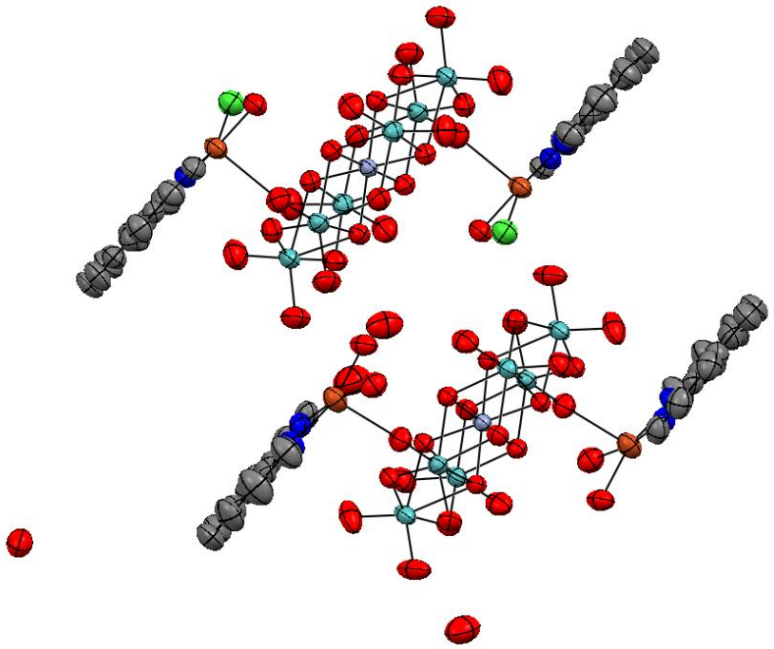

Figure 4.1. Crystal structure of compound **1**. Colour code: Gray:C; Blue:N; Red:O; Orange:Cu; Cyan:Mo; Violet:Cr; Green:Cl.

Both of these copper complexes have a coordination number of five with a distorted square pyramidal geometry. In the cation, copper has coordination from two nitrogen atoms (from phenanthroline ligand), two oxygen donors from two water molecules, and a terminal oxygen atom from the Anderson anion. Similarly, coordination around copper in the anion has two nitrogen atoms from phenanthroline ligand, one water molecule, one chloride anion, and terminal oxygen from the Anderson anion (**Figure 4.1.**).

4.3.1.1.2. *[Al(OH)$_6$Mo$_6$O$_{18}${Cu(phen)(H$_2$O)$_2$}$_2$][Al(OH)$_6$Mo$_6$O$_{18}${Cu(phen)(H$_2$O)Cl}$_2$]·5H$_2$O* ***(2).***
Compound **2** is structurally similar to compound **1**, and it only differs in terms of heteroatom of the Anderson POM onto which copper complexes are supported (**Figure 4.2.**). Compound **1** has $[Cr(OH)_6Mo_6O_{18}]^{3-}$ whereas **2** has $[Al(OH)_6Mo_6O_{18}]^{3-}$ as POM anion.

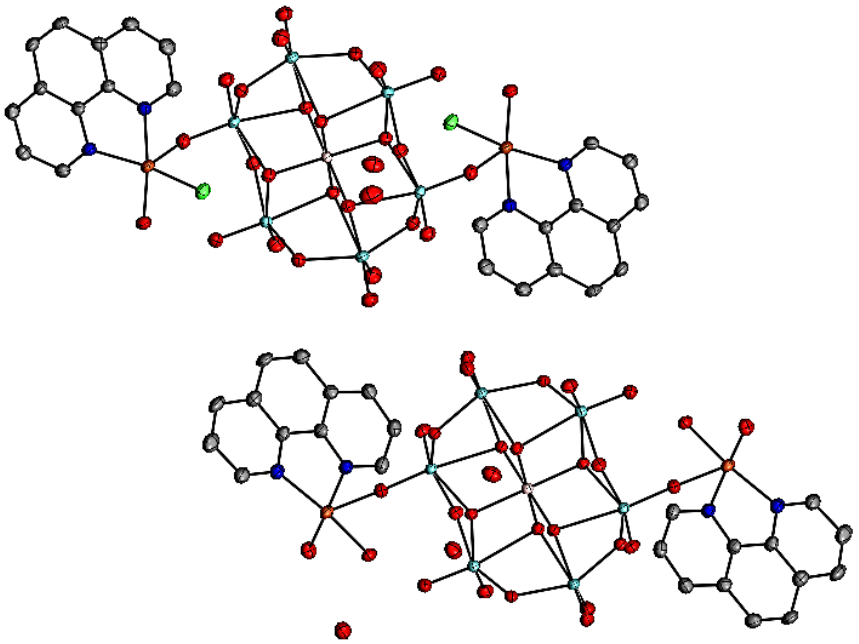

Figure 4.2. Crystal structure of compound **2**. Colour code: Gray:C; Blue:N; Red:O; Orange:Cu; Cyan:Mo; light Pink:Al; Green:Cl.

4.3.1.2. PXRD analysis

Bulk purity of both the compounds (compounds **1** and **2)** was confirmed by recording the powdered-XRD patterns and comparing them with the one obtained from the single crystal data. Major peaks from the simulated PXRD pattern of both the compounds matched with that of experimentally obtained data confirming its bulk purity (**Figure 4.3.**). PXRD analysis is one of the crucial techniques to ensure the bulk purity of the synthesized compounds.

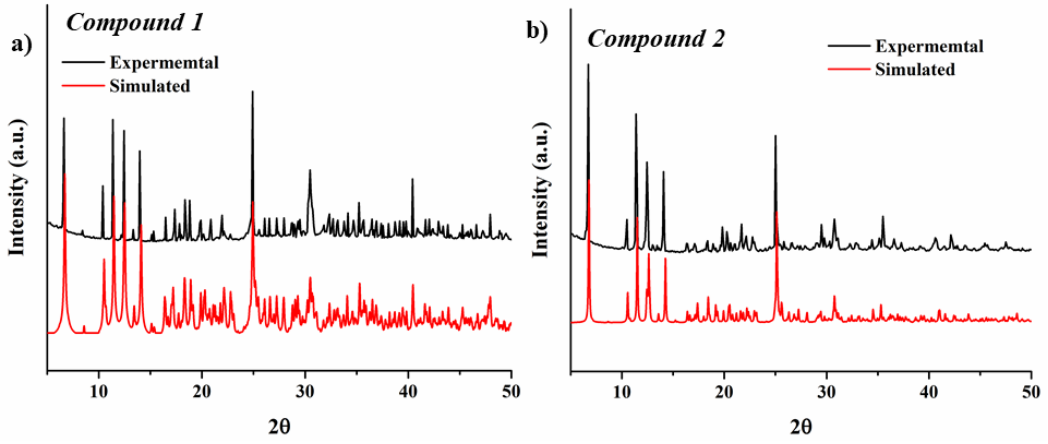

Figure 4.3. PXRD patterns of both the compounds compared with the respective simulated patterns. **(a)** compound **1** PXRD pattern. **(b)** Compound **2** PXRD pattern.

4.3.1.3. FT-IR and UV-vis. DRS spectral Analysis

The IR features of both compounds are similar (**Figure 4.4. (a)**). This similarity in FTIR spectra is due to their analogous structures. The stretching seen in the FTIR spectra is mainly attributed to the vibrations arising due to various types of (Mo–O) bonds present in the Anderson anion. The IR bands at 440, 648, 775, 900, and 940 cm^{-1} are due to the stretching arising from the following bonds of the Anderson anion: ν(Mo–O_c), ν(Mo–O_b) and ν(Mo–O_t). The bands in the range of 1100-1600 cm^{-1} are attributed to the stretching arising from the bonds of the Cu-phenanthroline complex coordinated to the Anderson anion. A broad band originating due to stretching of H-bond from the coordinated water and lattice water is seen at 3200 cm^{-1}.

The solid-state UV-vis. diffused reflectance spectral analysis was recorded to understand the electronic absorption of both the compounds. It was later converted to absorption mode by applying Kubelka-Monk (K.-M.) algorithm. Absorption at 490 and 700 nm are observed corresponding to metal to ligand charge transfer (MLCT) (absorption due to O to Mo charge transfer in Anderson POM anion) and d-d transition of Cu(II) system of $[Cu(phen)(H_2O)_2]^{2+}$ and $[Cu(phen)(H_2O)Cl]^{+}$ fragments present in both the compounds (**Figure 4.4. (b)**).

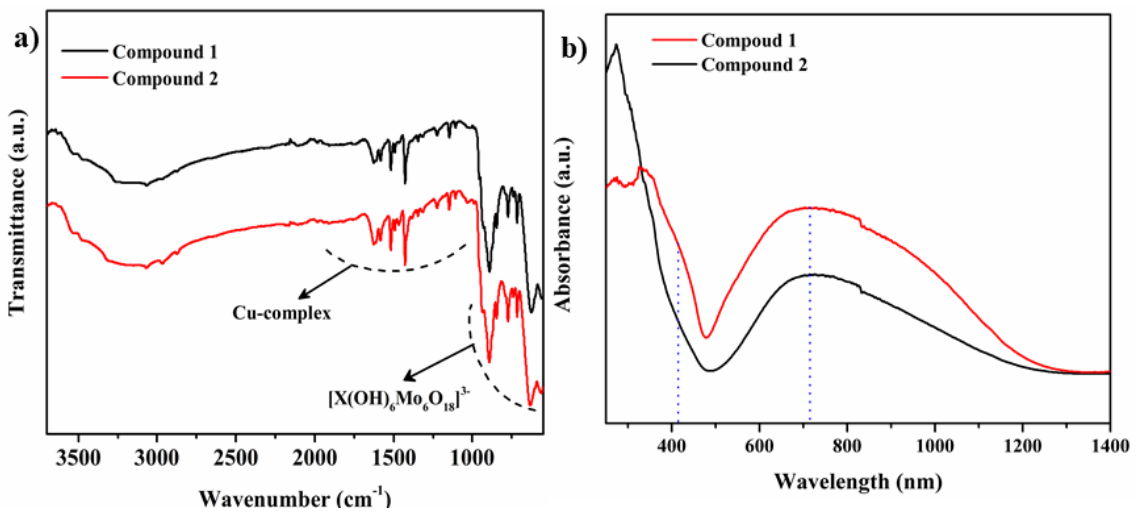

Figure 4.4. (a) FTIR analysis of Compound **1** and **2 (b)** K.M. converted UV-vis. DRS of Compound **1** and **2**.

4.3.2. Electrochemical studies

4.3.2.1. General features of cyclic voltammograms of both the compounds

Cyclic voltammograms of both the compounds, $\{[Cr(OH)_6Mo_6O_{18}\{Cu(phen)(H_2O)_2\}_2][Cr(OH)_6Mo_6O_{18}\{Cu(phen)(H_2O)Cl\}_2]\cdot 5H_2O$ (**1**) and $[Al(OH)_6Mo_6O_{18}\{Cu(phen)(H_2O)_2\}_2][Al(OH)_6Mo_6O_{18}\{Cu(phen)(H_2O)Cl\}_2]\cdot 5H_2O$ (**2**), show similar features. The similarity in CV features is a result of the structural analogy between them. Both the compounds undergoes two subsequent reductions; both the responses are due to Cu^{2+}/Cu^{+} couple, one for water-coordinated Cu(II) complex $\{Cu(phen)(H_2O)_2\}^{2+}$ and other for chloro- and water-coordinated species $\{Cu(phen)(H_2O)Cl\}^{+}$ species. [14] Initially, the chloride ion ligated Cu(II) species (anionic part of compounds **1** and **2**) is reduced to Cu(I).[14] This is mainly due to the electronegative behavior of Cl^{-}, which makes the reduction of Cu(II) to Cu(I) feasible at low potential. The second copper (copper from cationic part of compounds **1** and **2**), to which two water molecules are ligated, does not have any such electronegative group coordinated to it, thereby it reduces at relatively higher potential, which appears as a (not clearly visible) hump (**Figure 4.5. (a)**), but can be clearly seen in differential pulse voltammogram (DPV) of the compounds (**Figure 4.5. (b)**). After the reduction of second Cu(II) to Cu(I) (we mean, $\{Cu(phen)(H_2O)_2\}^{2+}$ species), water is reduced to produce hydrogen gas.

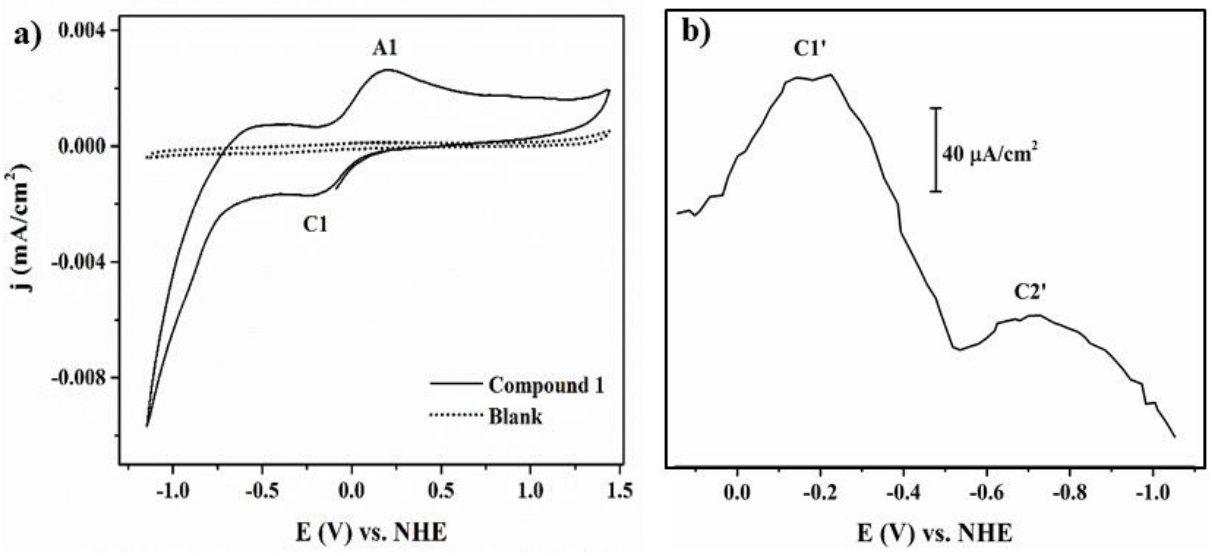

Figure 4.5. (a) Cyclic voltammograms of compound **1** (solid line) and blank glassy carbon electrode (dotted line) in 0.1 M phosphate buffer (pH 7) **(b)** Differential-pulse voltammogram of compound **1** recorded in 0.1 M phosphate buffer, pH 7 with the scan rate of 100 mV/s.

4.3.2.2. HER using compound 1 as electrocatalyst

Cyclic voltammograms of compound **1** were recorded in 0.1 M phosphate buffer, pH 7. CV of **1**, shows a peak in cathodic region C1 at −0.17 V, coupled with A1 peak at +0.18 V (**Figure 4.5. (a)**). From the relevant differential pulsed voltammogram (DPV), two consecutive redox couples are realized; in the reductive wave, two successive responses C1' at −176 mV and C2' at −735 mV are observed as shown in **Figure 4.5. (b)**.

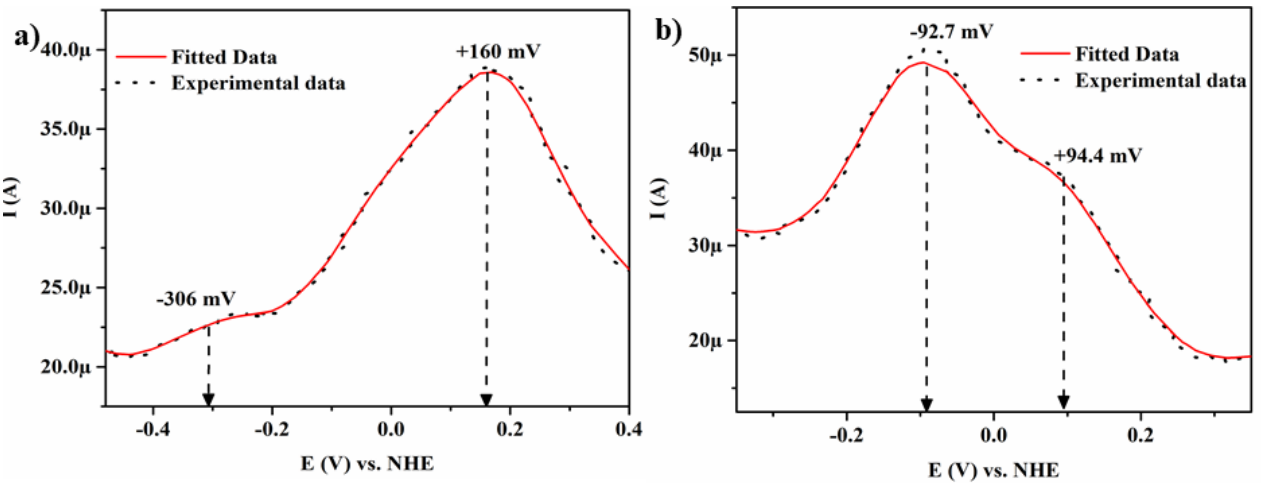

Figure 4.6. Differential pulse voltammogram of **(a)** compound **1** and **(a)** compound **2**, recorded in 0.1 M phosphate buffer, pH 7.

The second peak is masked due to catalytic current as the onset potential is seen around –0.76 V. This peak accounts for the reduction of Cu(II), which is part of the cationic fragment of compound **1** (i.e., $\{Cu(phen)(H_2O)_2\}^{2+}$ species) , to Cu(I). The two peaks, observed in DPV of **1**, are therefore mainly due to reduction of Cu(II) to Cu(I) from $\{Cu(phen)(H_2O)Cl\}^{+}$ and $\{Cu(phen)(H_2O)_2\}^{2+}$ respectively. When both the Cu(II) species in compound **1** are reduced to Cu(I), the resulting reduced system reduces the water to produce H_2 molecule accompanied by oxidation of Cu(I) to Cu(II). Towards the anodic scan of the CV of compound **1,** similar subsequent oxidation is suspected, and this is evident from the DPV recorded in that range (**Figure 4.6. (a)**).

4.3.2.3. HER using compound 2 as electrocatalyst

Cyclic voltammograms of compound **2** were recorded in similar condition, used for compound **1 (**0.1 M phosphate buffer, pH 7). CV of **2** shows a reductive response in cathodic region C2 at −0.14 V, which is coupled with oxidative response A2 at 0.12 V as shown in **Figure 4.7. (a)**.

From the relevant differential pulsed voltammogram (DPV), two peaks, expectedly, are found: C3' at −133 mV and C4' at −865 mV (**Figure 4.7. (b)**). Towards the anodic scan of the CV of compound **2,** similar subsequent oxidation is suspected, and this is evident from the DPV recorded in that range (**Figure 4.6. (b)**). This compound follows the similar two successive reductions of Cu(II) to Cu(I) from $\{Cu(phen)(H_2O)Cl\}^+$ and $\{Cu(phen)(H_2O)_2\}^{2+}$ respectively, followed by water reduction to molecular hydrogen, as observed in the case of compound **1**.[11b,11c]

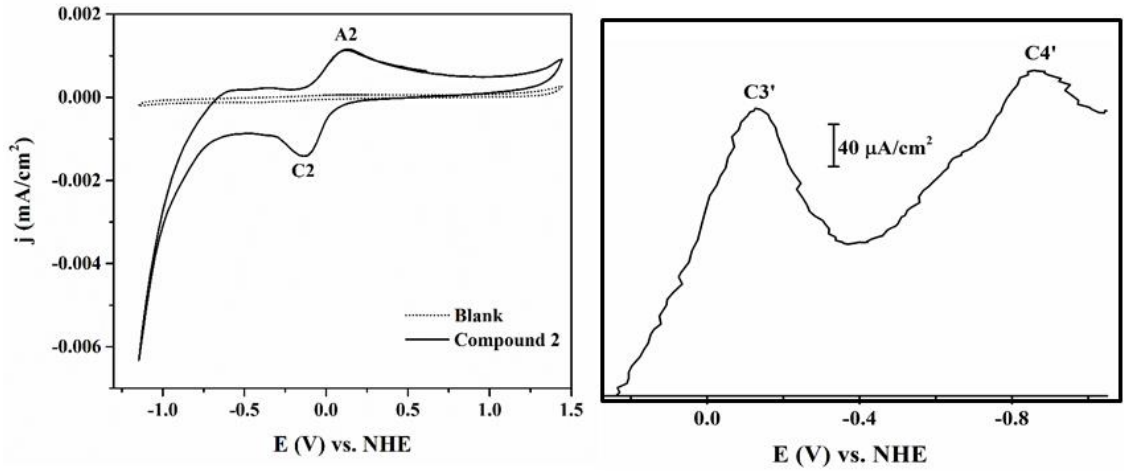

Figure 4.7. (a) Cyclic voltammogram of compound **2** (solid line) and blank glassy carbon electrode (dotted line) **(b)** Differential-pulse voltammogram of compound **2.** CVs and DPV were recorded in 0.1 M phosphate buffer, pH 7 with the scan rate of 100 mV/s.

4.3.2.4. Analysis of Electrochemical stability for both compounds (1 and 2)

The stability of both the compounds under electrochemical conditions was studied by conducting chronoamperometric studies (**Figure 4.8. (a-b)**). For this, we applied a fixed potential of –0.8 V (onset potential) for compound **1** and –0.84 V (onset potential) for compound 2, over a period for 3 h 30 min and monitored the changes in current. For both the compounds, CV is recorded before and after performing chronoamperiometric studies (**Figure 4.8. (c-d)**).

Both the compounds were found to be stable for 3 h 30 min. This was also evident from the CVs recorded before and after the chronoamperiometric studies. Negligible changes in the onset potential and peak positions were observed for both the compounds. The onset current for compound **1** had a difference of 12.6 μA (**Figure 4.8. (c)**), whereas for compound **2**, it was found to be 40 μA (**Figure 4.8. (d)**). This loss in current is minimal and is mainly due to loss of sample due to hydrogen bubbles generated on the surface of working electrode.

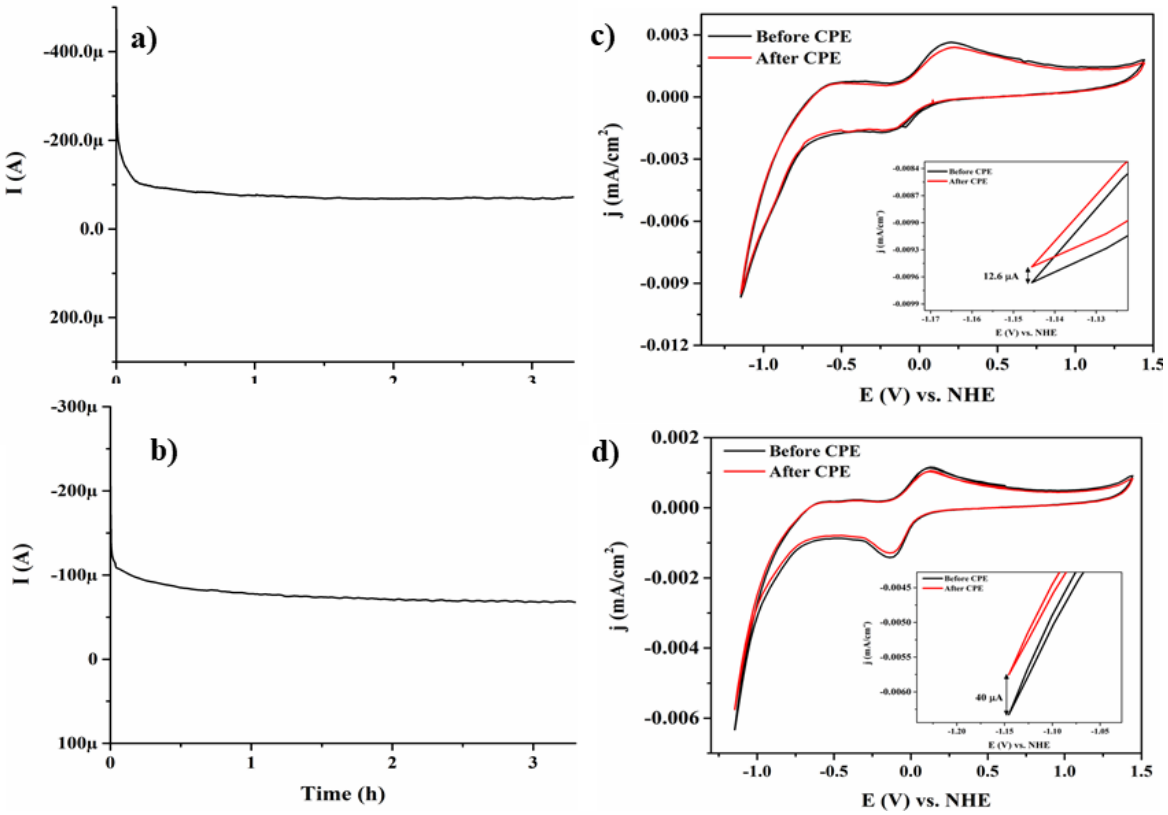

Figure 4.8. Chronoamperometric studies of **(a)** compound **1** and **(b**) compound **2**. CVs were recorded before (solid black line) and after (solid red line) chronoamperometric measurements for **(c)** compound **1** and **(d**) compound **2**, in 0.1 M phosphate buffer (pH 7). Inset in (**c-d**) shows the enlarged region of the voltammograms showing the catalytic current differences in the cyclic voltammograms before and after chronoamperometric measurements were performed.

4.3.2.5. Recognizing active site: POM unit or POM attached Cu coordination complexes

For better understanding and having a closer look for the role of POM in this HER catalysis, we synthesized the polymers of the parent POM by following the literature.[16] **$[La(H_2O)_7Cr(OH)_6Mo_6O_{18}]_n \cdot 4nH_2O)]$** and **$[La(H_2O)_7Al(OH)_6Mo_6O_{18}]_n \cdot 4nH_2O]$** are the POM polymers connected by Lanthanide ions. We prepared the sample for CV using the same protocol followed to prepare a CV sample of **1**. CVs were recorded in similar condition as that of compound **1** and **2** (Phosphate buffer, pH 7). CV of **$[La(H_2O)_7Cr(OH)_6Mo_6O_{18}]_n \cdot 4nH_2O)]$** and **$[La(H_2O)_7Al(OH)_6Mo_6O_{18}]_n \cdot 4nH_2O]$** do not show any redox features in the range recorded (+1.45 to –1.15V) (**Figure 4.9.**). This confirms that red-ox features found in CVs of **1** and **2** are solely due to copper coordination complexes.

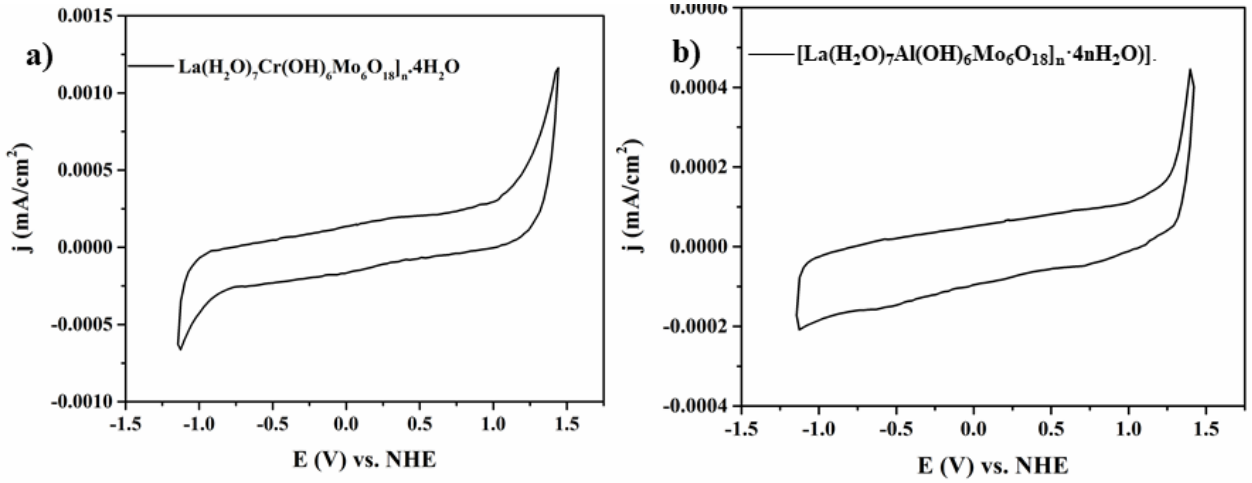

Figure 4.9. Cyclic voltammogram of **(a)** $[La(H_2O)_7Cr(OH)_6Mo_6O_{18}]_n{\cdot}4nH_2O)]$ and **(b)** $[La(H_2O)_7Al(OH)_6Mo_6O_{18}]_n{\cdot}4nH_2O)]$ recorded in 0.1 M phosphate buffer (pH 7, scan rate 100 mv/s).

We also prepared Cu-phenanthroline complex $[Cu(phen)_2(H_2O)](NO_3)_2$ to enlighten the insights of electrocatalysis of HER driven by **1** and **2**. $[Cu(phen)_2(H_2O)](NO_3)_2$ were synthesized by following the protocol available in the literature.[17] CV of $[Cu(phen)_2(H_2O)](NO_3)_2$ complex was recorded by taking 0.1 mmol of it in 0.1 M phosphate buffer, pH 7. CV of $[Cu(phen)_2(H_2O)](NO_3)_2]$ shows the anodic peak at +0.073 V and cathodic peak –0.0290 V (**Figure 4.10.**). The peak observed in the cathodic wave is mainly due to the reduction of Cu(II) to Cu(I) which gets oxidized back to Cu(II) in the anodic wave.

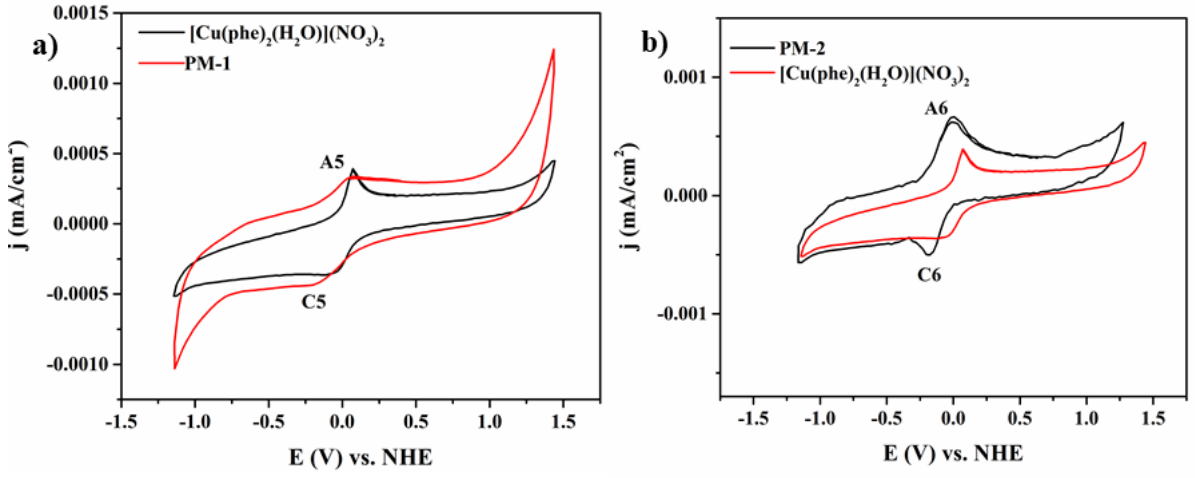

Figure 4.10. Cyclic voltammogram of **(a) $[Cu(phen)_2(H_2O)](NO_3)_2$]** complex (red line) and **PM-1** (black line) **(b) $[Cu(phen)_2(H_2O)](NO_3)_2$]** complex (red line) and **PM-2** (black line), recorded in 0.1 M phosphate buffer pH 7.

In order to check, whether the attachment (coordinate covalent bond) between POM unit and copper coordination complex, plays a role on this HER, we prepared a physical mixture of

sample by making a suspension comprising of parent POM ($[La(H_2O)_7Cr(OH)_6Mo_6O_{18}]_n \cdot 4nH_2O$ or $[La(H_2O)_7Al(OH)_6Mo_6O_{18}]_n \cdot 4nH_2O$) and $[Cu(phen)_2(H_2O)](NO_3)_2$ complex. Sample preparation for electrochemical studies from this physical mixture was done by following the similar protocol used for electrochemical studies of compounds **1** and **2**. The mixture containing $[La(H_2O)_7Cr(OH)_6Mo_6O_{18}]_n \cdot 4nH_2O$ will be denoted as physical mixture-1 (**PM-1**) and $[La(H_2O)_7Al(OH)_6Mo_6O_{18}]_n \cdot 4nH_2O$ as physical mixture-2 (**PM-2**). From the CV of **PM-1**, one reversible redox couple A5-C5 (0.053 V, –0.173 V) was found (**Figure 4.10. (a)**). The peak C5 is due to the reduction of Cu(II) to Cu(I), and A5 is for the oxidation of Cu(I) to Cu(II). Thus **PM-1** does not show any onset current for electrochemical hydrogen generation, as observed in the case of compounds **1** and **2**. For **PM-2**, CV shows similar redox behaviour with peaks A6 and C6 at –2.34 mV and –176 mV, respectively (**Figure 4.10. (a)**). The peaks C5 and C6 are consistent with the CV peak obtained for $[Cu(phen)_2(H_2O)](NO_3)_2$ complex, which denotes single electron transfer resulting in the reduction of Cu(II) to Cu(I) species (**Figure 4.10.**). For the parent compounds, $[La(H_2O)_7Cr(OH)_6Mo_6O_{18}]_n \cdot 4nH_2O$ and $[La(H_2O)_7Al(OH)_6Mo_6O_{18}]_n \cdot 4nH_2O$, neither any peak nor the onset current was seen (**Figure 4.9.**). This confirms that peaks seen in the CVs of compound **1** and **2** are solely due to Cu(II) centre of the attached Cu-aqua-phen complex. In other words, Mo(VI), Al(III), and Cr(III), the metal centers of the POM unit, do not show any redox property under these conditions (phosphate buffer, pH 7). Thus, it clearly infers that Cu(II) coordination complexes, attached to the Anderson POM, are the catalytically active site for catalyzing the HER reaction in both the compounds, where synergistic effect also plays a significant role in the catalytic property of these compounds.

4.3.2.6. Mechanistic and Kinetic analysis

To understand these compounds' kinetics, we recorded CVs for both the compounds by varying scan rates (from 60 mV/s to 300 mV/s). These CVs are depicted in **Figure 4.11. (a-b)**. A derived plot of peak current *vs.* scan rate was constructed (**Figure 4.11. (c-d)**). The linear nature of the graph confirms the diffusion-controlled nature of electron transfer for both the compounds.[14] The slope, observed from this plot of peak current vs. square root (**Figure 4.11. (c-d)**), was implemented for turnover frequency (TOF) calculation, discussed in the next section.

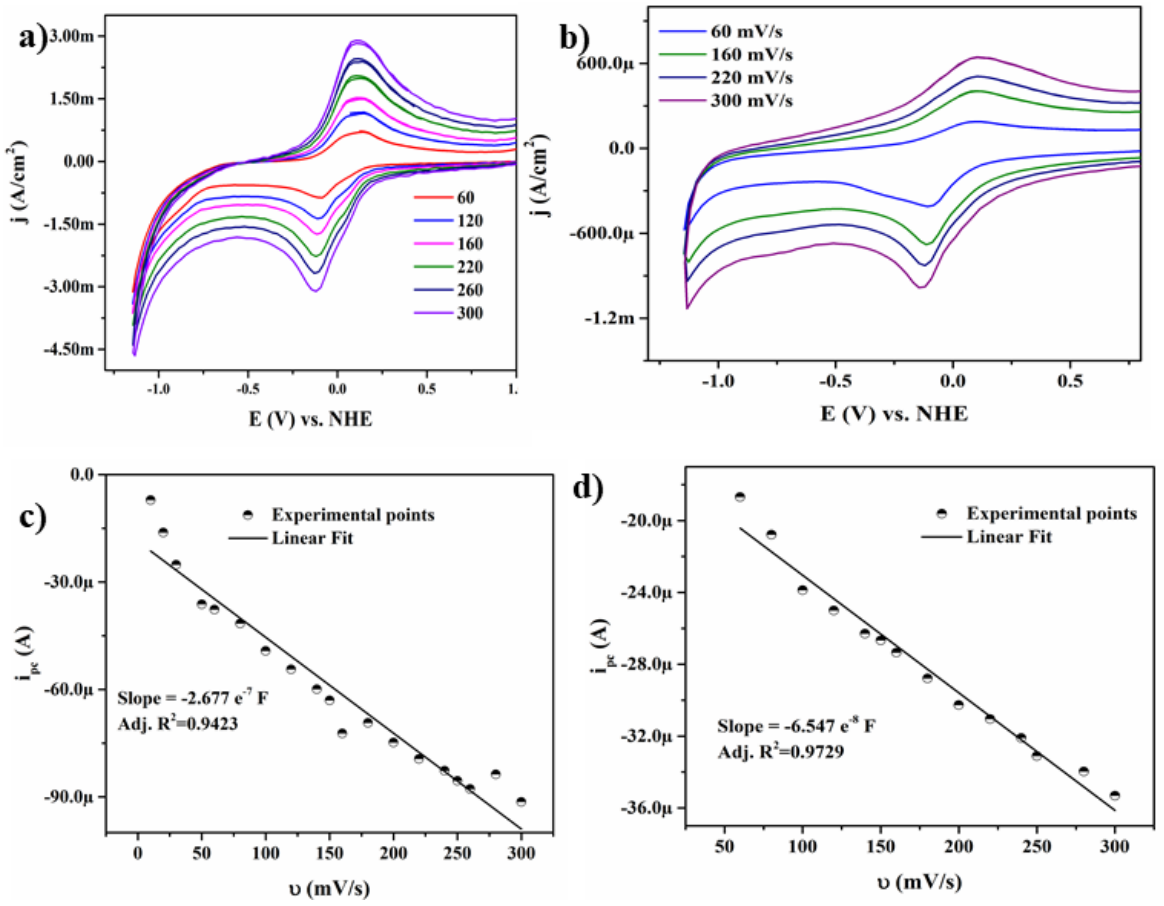

Figure 4.11. Cyclic voltammograms recorded at various scan rates for **(a)** compound **1** and **(b)** compound **2**. A plot of cathodic peak current (i_{pc}) as a function of scan rate for **(c)** compound **1** and **(d)** compound **2**.

An iR-corrected Tafel plot was devised in a galvanostatic mode for both compounds with 0.1 M phosphate buffer (pH 7). The overpotentials of 300 mV and 644 mV were observed for a current density of 1 mA/cm^2 for compounds **1** and **2**, respectively (**Figure 4.12.**). The slope, obtained from the linear fitting of Tafel plots for **1** and **2** are –668 mV/decade and –219 mV/decade. Although there is a structural similarity between both the compounds, from the Tafel slope, it is evidenced that both follow different kinetics, thereby resulting in such massive difference in their overpotential and Tafel-slope values. The overpotential obtained for compound **1** is half the value of that of compound **2**, which suggests the importance of POM onto which the complex is supported in deciding the overpotential as well as overall efficiency of the catalyst. This anomaly in the catalytic behavior, even though there is a structural resemblance, is attributed to the synergistic effect from POM to Cu-complexes. Here from our studies, we found that role of heteroatom of POM is very crucial for such POM-supported complexes. POM is not just

dormant support but plays a vital role by facilitating electron transfer for overall HER catalysis. Thus the overall efficiency of compound **1** towards electrocatalytic HER is much better than that of compound **2**.

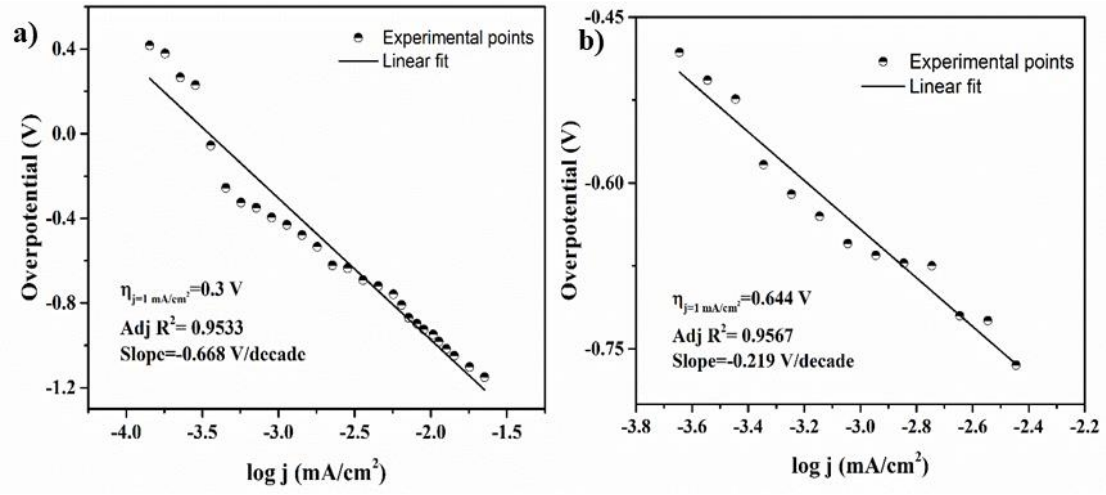

Figure 4.12. Galvanostatic *iR*-corrected Tafel plot of **(a)** compound **1 (b)** compound **2**, at pH 7 (0.1 M Phosphate buffer).

4.3.2.7. Quantitative hydrogen evolution and Faradic efficiency calculation

Following a similar method, as discussed in **Chapter 3**, section **3.3.2.6.**, we calculate the Faradic efficiency of both the compounds. For quantitative hydrogen evolution, a constant current density of 1 mA/cm^2 for a period of 3 h. During the electrolysis, hydrogen bubbles first gathered at the FTO electrode's surface and later accumulated in an inverted graduated tube (home-built set-up, **Figure 3.22.**, **Chapter 3**), which was previously filled with electrolyte, displacing the electrolyte.

Faradaic efficiency of any system describes the efficiency with which charge is utilized in an electrochemical reaction.

For HER, it can be formulated as,

Moles of H_2 evolved
Moles of H_2 that can evolve utilizing the employed charge

For **compound 1**,

From the bulk-electrolysis, the quantitative measurement of hydrogen evolved was measured under constant current condition. For this work, we found 0.30 mL/hour of H_2 evolved under 1 atm. pressure.

Thus, moles of H_2 evolved in one hour = (0.30/22400) mol = **1.3391 µmol.**

For **compound 2**:

From the bulk-electrolysis, the quantitative measurement of hydrogen evolved was measured under constant current condition. For this work, we found 0.28 mL/hour of H_2 evolved under 1 atm. pressure.

Thus, moles of H_2 evolved in one hour = (0.28/22400) mol = **1.25 µmol**.

$$H_{2\ ideal} = \frac{\text{Q (Total Charge employed)}}{\text{n (no. of electrons required for the chemical change X 1 Farad)}}$$

Here, we employed a current density of 1 mA/cm^2 and 'n'= 2 for HER (as it is a two-electron process).

Thus, H_2 that ideally should evolve = (75 × 3600)/(2 × 96500) mol = 1.398 µmol.

Faradaic efficiency of compound **1**

$$= \frac{1.3391}{1.398} \text{ x } 100 = \mathbf{95.7\%}$$

Faradaic efficiency of compound **2**

$$= \frac{1.25}{1.398} \text{ x } 100 = \mathbf{89.4\%}$$

Thus, Faradic efficiency of compound **1** and **2** was found to be **95.7%** and **89.4%** respectively.

4.3.2.8. Hydrogen detection by Gas Chromatography (GC)

To confirm hydrogen evolution by reducing water molecules due to both the compounds' electrocatalysis, constant potential electrolysis was carried out using home-made glassware. This glassware is similar to the one used for quantitative hydrogen evolution (as discussed in **Chapter 3**, section **3.3.2.6.**). It only differs in terms of the availability of an open chamber at the top of the graduated tube, which is sealed with a rubber septum after filling with electrolyte. The gas was collected from the top of this set up (head space) using a micro-syringe and analyzed by gas chromatography.

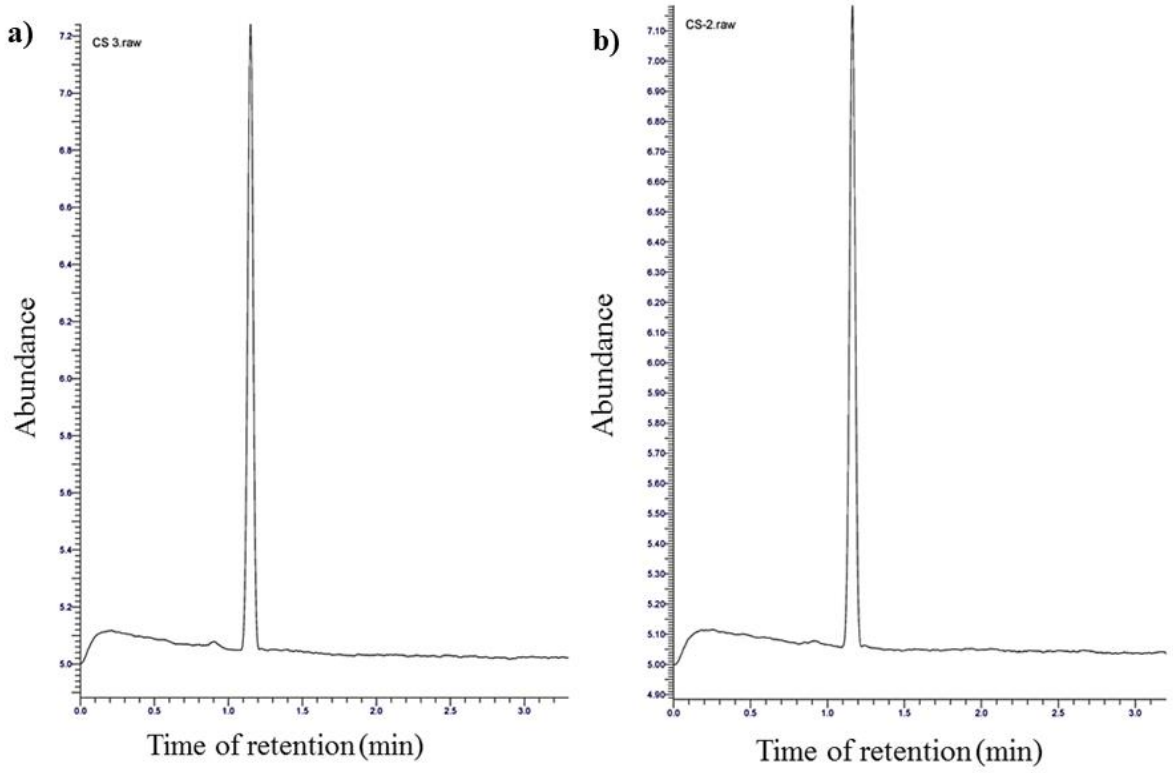

Figure 4.13. The chromatograms are showing the retention time obtained for gas collected from **(a)** compound **1** and **(b)** compound **2**.

4.3.2.9. Turnover Frequency (TOF) Calculation

- **Calculation of Surface Coverage and number of active copper atoms**

We have calculated the active Cu atoms/cm^2 on the electrode surface using a method recently described by Pintado *et al.*[18] by measuring the surface coverage (Γ_0) from the slope (2.677 E-7 F) of the i_p *vs* scan rate (**Figure 4.11. (c)**) using the equation 1.

$$\text{Slope} = n^2F^2A\Gamma_0/4RT \quad \text{..... (1)}$$

Where 'n' = No. of electrons involved, here 1. For Cu(II) – Cu(I) conversion. This equation is discussed in detail in **Chapter 2**, under section **2.3.2.8.**

Thus, for compound **1** obtained surface density of active copper atoms is **43.6×10^{12} copper atoms/cm^2** or in other words it is **7.30×10^{-11} mol/cm^2**.

We have calculated the active Cu atoms/cm^2 on the electrode surface for compound **2**, using the similar method by measuring the surface coverage (Γ_0) from the slope (6.547 E-8 F) of the i_p *vs* scan rate (**Figure 4.11. (d)**) using the equation 1.

Thus, for compound **2**, the obtained surface density of active copper atoms is **12.5×10^{12}** copper atoms/cm^{2,} or in other words, it is **2.09×10^{-11} mol/cm^2**.

- **Calculation of Turnover Frequency (TOF) for H_2 evolution from Tafel Plot:**

The activity of a catalyst can be well-expressed in terms of turn over frequency (TOF). It is defined as the number of reactant molecules converted into product molecules in unit time per active site. The TOF is measured as given in the literature.[14]

$$\text{TOF at any given over potential} = \frac{\text{Current density at given over potential}}{2 \times F \times \text{No. of active copper species/atoms}} \quad \text{..... (2)}$$

Here, 2 numeric is due to involvement of 2e$^-$ in HER process. Hence division of current density at a particular overpotential by 2F (F = Faraday constant) gives one catalytic turnover number and further division of turnover number by the number of active copper atoms results in turnover frequency (TOF).

TOF for compound **1:**

$$(TOF)_{j=1\ mA/cm^2} = \frac{10^{-3}}{2 \times F \times 7.3E^{-11}} \quad \text{..... (3)}$$

Thus $(TOF)_{j=1\ mA} = 70.90$ [mol H_2 (mol Cu)$^{-1}$s^{-1}]

$(TOF)_{j=1\ mA} =$ **2.55×10^5** [mol H_2 (mol Cu)$^{-1}$h^{-1}]

TOF for compound **2:**

$$(TOF)_{j=1\ mA/cm^2} = \frac{10^{-3}}{2 \times F \times 2.09E^{-11}} \quad \text{..... (4)}$$

Thus $(TOF)_{j=1\ mA} = 247.31\ [mol\ H_2\ (mol\ Cu)^{-1}s^{-1}]$

$(TOF)_{j=1\ mA} = \mathbf{8.90\ x\ 10^5}\ [mol\ H_2\ (mol\ Cu)^{-1}h^{-1}]$

4.4. Conclusion

To conclude, we have shown the electrocatalytic activity of compounds $\{[Cr(OH)_6Mo_6O_{18}\{Cu(phen)(H_2O)_2\}_2][Cr(OH)_6Mo_6O_{18}\{Cu(phen)(H_2O)Cl\}_2]\cdot 5\ H_2O$ (**1**) and $[Al(OH)_6Mo_6O_{18}\{Cu(phen)(H_2O)_2\}_2][Al(OH)_6Mo_6O_{18}\{Cu(phen)(H_2O)Cl\}_2]\cdot 5H_2O$ (**2**) towards HER under neutral condition (phosphate buffer, pH 7). Compound **1** showcases superior catalytic activity over compound **2**. Overpotential observed at the current density of 1 mA/cm^2 for compounds **1** and **2** is 300 mV and 644 mV, respectively. The structural analogy between these compounds has confirmed the synergistic effect between Anderson POM and the copper complex playing a critical role in qualifying **1** and **2** as an efficient electrocatalyst for water reduction. The type of POM also dictates the catalyst's overall efficiency, thereby allowing a new pavement for understanding the chemistry for POM supported complexes and designing cheap and efficient catalyst for HER activity.

4.5. References

1. (a) Jacobson, M. Z.; Colella, W. G.; Golden, D. M. Cleaning the Air and Improving Health with Hydrogen Fuel-Cell Vehicles. *Science* **2005**, 308, 1901– 1905. (b) Seh, Z. W.; Kibsgaard, j.; Dickens, C. F.; Chorkendorff, I. B.; Norskov, J. K.; Jaramillo, T. Combining Theory and Experiment in Electrocatalysis: Insights into Materials Design *Science* **2017**, *355*, 4998
2. (a) Anantharaj, S.; Karthick, K.; Kundu, S. $NiTe_2$ Nanowire Outperforms Pt/C in High-Rate Hydrogen Evolution at Extreme pH Conditions. *Inorg. Chem.* **2018**, *57*, 3082−3096. (b) Anantharaj, S.; Kathick, P. E.; Subramanian, B.; Kundu, S. Pt Nanoparticle Anchored Molecular Self-Assemblies of DNA: An Extremely Stable and Efficient HER Electrocatalyst with Ultralow Pt Content. *ACS Catal.* **2016**, *6*, 4660-4672.

3. (a) Zhang, L.; Chang, Q.; Chen, H.; Shao, M. Recent Advances in Palladium-based Electrocatalysts for Fuel cell Reactions and Hydrogen Evolution Reaction*Nano Energy* **2016**, *29*, 198-219. (b) Lv, L.; Chen, X.; Xu, D.; Hua, Y.; Zheng, H.; Sui, S. L.; Liu, B. Ultrathin PdPt Bimetallic Nanowires with Enhanced Electrocatalytic Performance for Hydrogen Evolution Reaction *Appl. Catal. B: Environ.* **2018**, *238*, 525-532.
4. (a) Smiljanić, M.; Rakočević, Z.; Maksić, A.; Štrbac, S. Hydrogen Evolution Reaction on Platinum Catalyzed by Palladium and Rhodium Nanoislands. *Electrochim Acta* **2014**, *117*, 336-343. (b) Štrbac, S.; Smiljanić, M.; Rakočević, Z. Electrocatalysis of Hydrogen Evolution on Polycrystalline Palladium by Rhodium Nanoislands in Alkaline Solution *J. Electroanal Chem* **2015**, *755*, 115-121.
5. (a) Yu, W.; Porosoff, M. D.; Chen, J. G. Review of Pt-Based Bimetallic Catalysis: From Model Surfaces to Supported Catalysts. *Chem. Rev.* **2012**, *112*, 5780-5817. (b) Duan, H.; Li, D.; Tang, Y.; He, Y.; Ji, S.; Wang, R.; Lv, H.; Lopes, P.; Paulikas, A.; Li, H.; Mao, S.; Wang, C.; Markovic, N.; Li, J.; Stamenkovic, V.; Li, Y. High-Performance Rh2P Electrocatalyst for Efficient Water Splitting. *J. Am. Chem. Soc.* **2017**, *139*, 5494-5502. (c) Zhang, H.; Liu, Y.; Wu, H.; Zhou, W.; Kou, Z.; Pennycook, S. J.; Xie, J.; Guan C.; Wang, J. Open Hollow Co–Pt Clusters Embedded in Carbon Nanoflake Arrays for Highly Efficient Alkaline Water Splitting. *J. Mater. Chem. A*, **2018**, *6*, 20214-20233. (d) Wang, S.; Yang, G.; Yang, S. Pt-Frame@Ni quasi Core–Shell Concave Octahedral PtNi3 Bimetallic Nanocrystals for Electrocatalytic Methanol Oxidation and Hydrogen Evolution. *J. Phys. Chem. C* **2016**, *120*, 802-802.
6. (a) Ensafi, A. A.; Jafari-Asl, M.; Rezaei, B. Graphene/Nano-Porous SIlicon and Graphene/Bimetallic Silicon Nanostructures (Pt–M, M: Pd, Ru, Rh), Efficient Electrocatalysts for the Hydrogen Evolution Reaction. *Phys. Chem. Chem. Phys.* **2015**, *17*, 23770-23782. (b) Cheng, M.; Zhu, M.; Du, Y.; Yangint, P. Enhanced Photocatalytic Hydrogen Evolution Based on Efficient Electron Transfer in Triphenylamine-based dye Functionalized Au@Pt Bimetallic Core/Shell Nanocomposite. *J. Hydrogen Energy* **2013**, *38*, 8631-8638. (c) Ahmed, M. E.; Chattopadhyay, S.; Brazzolotto, D.; Pramanik, D.; Aldakov, D.; Fize, J.; Morozan, A.; Gennari, M.; Duboc, C.; Dey, A.; Artero, V. Hydrogen Evolution from Aqueous Solutions Mediated by a Heterogenized [NiFe]-Hydrogenase Model: Low pH Enables Catalysis through an Enzyme-Relevant Mechanism. *Angew Chem Int. Ed.* **2018**, *57*, 16001-16004.
7. (a) Benck, J. D.; Hellstern, T. R.; Kibsgaard, J.; Chakthranont, P.; Jaramillo, T. F. Catalyzing the Hydrogen Evolution Reaction (HER) with Molybdenum Sulfide Nanomaterials. *ACS Catal.* **2014**, *4*, 3957–3971. (b) Lukowski, M.; Daniel, A. S.; Meng, F.; Forticaux, A.; Li, L.; Jin, S. Enhanced Hydrogen Evolution Catalysis from Chemically Exfoliated Metallic MoS_2 Nanosheets.

J. Am. Chem. Soc. **2013**, *135*, 10274–10277. (c) Pal, R.; Laureanti, J. A.; Groy, T. L. Jones, A. K.; Trovitch, R. J. Hydrogen Production From Water Using a Bis(imino)pyridine Molybdenum Electrocatalyst. *Chem. Commun.* **2016**, *52*, 11555—11558. (d) Chen, Z.; Leng, K.; Zhao, X.; Malkhandi, S.; Tang, W.; Tian, B.; Dong, L.; Zheng. L.; Lin, M.; Yeo, B. S.; Loh, K. P. Interface Confined Hydrogen Evolution Reaction in Zero Valent Metal Nanoparticles-Intercalated Molybdenum Disulfide. *Nat. Commun.* **2017**, *8*, 14548. (e) Wang, H.; Gao, L. Recent Developments in Electrochemical Hydrogen Evolution Reaction. *Curr. Opin. Electrochem.* **2018**, *7*, 7-14. (f) Ojha, K.; Saha, S.; Banerjee, S.; Ganguli, A. K. Efficient Electrocatalytic Hydrogen Evolution from MoS_2-Functionalized Mo_2N Nanostructures *ACS Appl. Mater. Interfaces* **2017**, *9*, 19455–19461.

8. (a) Mangrulkar, P. A.; Joshi, M. M.; Tijare, S. N.; Polshettiwar, V.; Labhsetwar, N. K.; Rayalu, S. S. Nano Cobalt Oxides for Photocatalytic Hydrogen Production *Int. J. Hydrog. Energy* **2012**, *37*, 10462-10466. (b) Kundu, S.; Polshettiwar, V. Hydrothermal Crystallization of Nano-Titanium Dioxide for Enhanced Photocatalytic Hydrogen Generation. *ChemPhotoChem* **2016**, *28*, 796–800. (c) Patra, B. K.; Khilari, S.; Pradhan, D.; Pradhan, N. Hybrid Dot–Disk Au-CuInS2 Nanostructures as Active Photocathode for Efficient Evolution of Hydrogen from Water. *Chem. Mater* **2016**, *28*, 4358-4366. (d) Das, A.; Ganguli, A. K. Design of Diverse Nanostructures by Hydrothermal and Microemulsion Routes for Electrochemical Water Splitting. *RSC Adv.* **2018**, *8*, 25065-25078. (e) Ojha, K.; Saha, S.; Dagar, P.; Ganguli, A. K. Nanocatalysts for Hydrogen Evolution Reactions. *Phys. Chem. Chem. Phys.* **2018**, *20*, 6777-6799. (f) Kumar, B.; Saha, S.; Basu, M.; Ganguli, A. K. Enhanced Hydrogen/Oxygen Evolution and Stability of Nanocrystalline (4–6 nm) Copper Particles. *J. Mater. Chem. A* **2013**, 4728-4735. (g) Wang, N.; Lei, H.; Zhang, Z.; Li, J.; Zhang, W.; Cao, R. Electrocatalytic Hydrogen Evolution with Gallium Hydride and Ligand-Centered Reduction *Chem. Sci.* **2019**, *10*, 2308-2314.

9. (a) Cao, P.; Fang, T.; Fu, L. Z.; zhou, L. L.; Zhan, S. Z. A Nickel Molecular Electro-catalyst for Generating Hydrogen from Acetic Acid or Water. *Int. J. Hydrogen Energy* **2014**, *39*, 10980-10986. (b) Zhang, P.; Wang, M.; Yong, Y.; Zheng, D.; Han, K.; Sun, L. Highly Efficient Molecular Nickel Catalysts for Eelectrochemical Hydrogen Production from Neutral Water. *Chem Commun.* **2014**, *50*, 14153-14156. (c) Aimoto, Y.; Koshiba, K.; Yamauchi, K.; Sakai, K. A Family of Molecular Nickel Hydrogen Evolution Catalysts Providing Tunable Overpotentials Using Ligand-Centered Proton-Coupled Electron Transfer Paths. *Chem. Commun.* **2018**, *54*, 12820-12823. (d) Koshiba, K.; Yamauchi, K.; Sakai, K. Consecutive Ligand-Based PCET Processes Affording a Doubly Reduced Nickel Pyrazinedithiolate Which Transforms into a Metal Hydride Required to Evolve H_2. *Dalton Trans.* **2018**, *48*, 635-640. (e) Kilgore, U. J.; Roberts, J.

A. S.; Pool, D. H.; Appel, A. M. Stewart, M. P. DuBois, M. R. Dougherty, W. S.; Kassel, R. M.; Bullock, R. M.; DuBois, D. L. $[Ni(P^{Ph}_2N^{C}_6H^{X}_4)_2]^{2+}$ Complexes as Electrocatalysts for H2 Production: Effect of Substituents, Acids, and Water on Catalytic Rates. *J. Am. Chem. Soc*. **2011**, *133*, 5861–5872. (f) Inou, S.; Mitsuhashi, M.; Ono, T.; Yan, Y,-N. Kataoka, Y.; Handa, M.; Kawamoto, T. Photo- and Electrocatalytic Hydrogen Production Using Valence Isomers of N2S2-Type Nickel Complexes. *Inorg. Chem.* **2017**, *56*, 12129−12138. (g) Han, H.; Fang, H.; Jing, H.; Sun, H.; Lei, H.; Lai, W.; Cao, R. Singly versus Doubly Reduced Nickel Porphyrins for Proton Reduction: Experimental and Theoretical Evidence for a Homolytic Hydrogen-Evolution Reaction. *Angew. Chem. Int. Ed.* **2016**, *55*, 5457 –5462.

10. (a) Liu, Y.; Fu, L.-Z.; Yang, L.-M.; Liu, X.-P.; Zhan, S.-Z.; Ni, C.-L. The Impact of Modifying the Ligands on Hydrogen Production Electro-Catalyzed by Meso-Tetra-P-X-Phenylporphin Cobalt Complexes, CoT(X)PP. *J. Mol. Catal. A: Chem* **2016**, *417*, 101-106. (b) Sun, H.; Han, Y.; Lei, H.; Chen, M.; Cao, R. Cobalt Corroles with Phosphonic Acid Pendants as Catalysts for Oxygen and Hydrogen Evolution From Neutral Aqueous Solution. *Chem. Commun.***2017**, *53*, 6195-6198. (c) Wang. J.; Li, C.; Zhou, Q.; Wang, W.; Hou, Y.; Zhang, B.; Wang, X. A Polypyridyl Co(II) Complex-Based Water Reduction Catalyst With Double H_2 Evolution Sites. *Catal. Sci. Technol.* **2016**, *6*, 8482-8489. (d) Li, X.; Lei, H.; Guo, X.; Zhao, X.; Ding, S.; Gao, X.; Zhang, W.; Cao, R. Graphene-Supported Pyrene-Modified Cobalt Corrole with Axial Triphenylphosphine for Enhanced Hydrogen Evolution in pH 0–14 Aqueous Solutions. *ChemSusChem* **2017**, *10*, 4632 – 4641. (e) Lei, H.; Han, A.; Li, F.; Zhang, M.; Han, Y.; Du, P.; Lai, W.; Cao, R. Electrochemical, Spectroscopic and Theoretical Studies of a Simple Bifunctional Cobalt Corrole Catalyst for Oxygen Evolution and Hydrogen Production. *Phys. Chem. Chem. Phys.* **2014**, *16*, 1883-1893. (f) Li, X.; Lei, H.; Liu, J.; Zhao, X.; Ding, S.; Zhang, Z.; Tao, X.; Zhang, W.; Wang, W.; Zheng, X.; Cao, R. Carbon Nanotubes with Cobalt Corroles for Hydrogen and Oxygen Evolution in pH 0–14 Solutions. *Angew. Chem. Int. Ed.* **2018**, *57*, 15070-15075.
11. (a) Mondal, B.; Dey, A. Development of Air-Stable Hydrogen Evolution Catalysts. *Chem.Commun.* **2017**, *53*, 7707-7715. (b) Du, P.; Eisenberg, R. Catalysts Made of Earth-Abundant Elements (Co, Ni, Fe) for Water Splitting: Recent Progress and Future Challenges. *Energy Environ. Sci.* **2012**, *5*, 6012–6021. (c) Rana, A.; Mondal, B.; Sen, P.; Dey, S.; Dey, A. Activating Fe(I) Porphyrins for the Hydrogen Evolution Reaction Using Second-Sphere Proton Transfer Residues. *Inorg. chem.* **2017**, *56*, 1783-1793.
12. (a) Zhang, P.; Wang, M.; Yong, Y.; Yao, T.; Sun, L. A Molecular Copper Catalyst for Electrochemical Water Reduction with a Large Hydrogen-Generation Rate Constant in Aqueous Solution *Angew. Chem Int. Ed.* **2014**, *53*, 13803-13807. (b) Fang, T.; Fu, L.-Z.; Zhou, L.-L.;

Zhan, S.-Z. A Water-Soluble Dinuclear Copper Electrocatalyst, [Cu(oxpn)Cu(OH)$_2$] for Both Water Reduction and Oxidation. *Electrochimica Acta* **2015**, *161*, 388–394. (c) Zhou, L.-L.; Fang, T.; Cao, J.-P.; Zhu, Z.-H.; Su, X.-T.; Zhan, S.-Z. A Dinuclear Copper(II) Electrocatalyst both Water Reduction and Oxidation. *J. Power Sour.* **2015**, *273*, 298-304. (d) Lei, H.; Fang, H.; Han, Y.; Lai, W.; Fu, X.; Cao, R. Reactivity and Mechanism Studies of Hydrogen Evolution Catalyzed by Copper Corroles. *ACS Catal.* **2015**, *5*, 5145−5153.

13. (a) Kleingardner, J. G.; Kandemir, B.; Bren, K. L. Hydrogen Evolution from Neutral Water under Aerobic Conditions Catalyzed by Cobalt Microperoxidase-11. *J. Am. Chem. Soc.* **2014**,*136*, 4-7. (b) Singh, W. M.; Baine, T.; Kudo, S.; Tian, S. L. Ma, X. A. N. Zhou, H. Y. DeYonker, N. J.; Pham, T. C. Bollinger, J. C.; Baker, D. L.; Yan, B.; Webster, C. E.; Zhao, H. Y. Electrocatalytic and Photocatalytic Hydrogen Production in Aqueous Solution by a Molecular Cobalt Complex. *Angew. Chem., Int. Ed.* **2012**, *51*, 5941-5944. (c) Zhang, P.; Wang, M.; Gloaguen, F.; Chen, L.; Quentel, F.; Sun, L. Electrocatalytic Hydrogen Evolution from Neutral Water by Molecular Cobalt Tripyridine–Diamine Complexes. *Chem. Commun.* **2013,** *49*, 9455-9457. (d) Lakadamyali, F.; Kato, M.; Muresan, N. M.; Reisner, E. Selective Reduction of Aqueous Protons to Hydrogen with a Synthetic Cobaloxime Catalyst in the Presence of Atmospheric Oxygen. *Angew. Chem. Int. Ed.* **2012**, *51*, 9381-9384. (e) Abdel-Hamid, R.; El-Sagher, H. M.; Abdel-Mawgoud, A. M.; Nafady, A. Electrochemistry of the bis(1,4,7-triazacyclodecane) Cobalt(III) Complex and its Role in the Catalytic Reduction of Hydrogen. *Polyhedron* **1998**, *17*, 4535-4541. (f) Sun, Y. F.; Bigi, J. P.; Piro, N. A.; Tang, M. L.; Long, J. R.; Chang, C. J. Molecular Cobalt Pentapyridine Catalysts for Generating Hydrogen from Water. *J. Am. Chem. Soc.* **2011**, *133*, 9212-9215. (g) Karunadasa, H. I.; Chang, C. J.; Long, J. R. A Molecular Molybdenum-Oxo catalyst for Generating Hydrogen from Water. *Nature* **2010**, *464*, 1329-1333.
14. Singh, C.; Mukhopadhyay, S.; Das, S. K. Polyoxometalate-Supported Bis(2,2′-bipyridine)mono(aqua)nickel(II) Coordination Complex: An Efficient Electrocatalyst for Water Oxidation. *Inorg. Chem.* **2018**, *112*, 529-586.
15. Shivaiah, V.; Das, S. K. Polyoxometalate-Supported Transition Metal Complexes and Their Charge Complementarity: Synthesis and Characterization of [M(OH)$_6$Mo$_6$O$_{18}$\{Cu(Phen)(H$_2$O)$_2$\}$_2$][M(OH)$_6$Mo$_6$O$_{18}$\{Cu(Phen)(H$_2$O)Cl\}$_2$]·5H$_2$O (M = Al^{3+}, Cr^{3+}). *Inorg. Chem.* **2005**, *44*, 8846-8854.
16. (a) Shivaiah, V.; Chatterjee, T.; Das, S. K. Coordination of Lanthanide Cation to an Anderson Type Polyoxometalate Anion Leads to Isomorphous Metal-Oxide Based One-Dimensional Inorganic Solids: Synthesis, Crystal Structure and Spectroscopy. *J. Chem. Sci*. **2014**, *126*, 1525–1533. (b) Shivaiah, V.; Reddy, P. V. N.; Cronin, L.; Das, S. K. A Novel Polyoxometalate Chain

Formed From Heteropolyanion Building Blocks and Rare Earth Metal Ion Linkers: $[La(H_2O)_7Al(OH)_6Mo_6O_{18}]n\cdot 4nH_2O$. *J. Chem. Soc. Dalton Trans.* **2002**, *0*, 3781-3782.

17. Nakai, H.; Deguchi, Y. The Crystal Structure of Monoaquobis(1,10-phenanthroline)copper(II) Nitrate, $[Cu(H_2O)(phen)_2](NO_3)_2$. *Bull. Chem. Soc. Jpn.* **1975**, *48*, 2557-2560.
18. Pintado, S.; Goberna-Ferrón, S.; Escudero-Adán, E. C.; Galán-Mascarós, J. R. Fast and Persistent Electrocatalytic Water Oxidation by Co–Fe Prussian Blue Coordination Polymers. *J. Am. Chem. Soc.* **2013**, *135*, 13270-13273.

Chapter 5

Cu(II)-bipyridine Complex and Anderson POM hybrid as a Pre-catalyst for Electrochemical Hydrogen Evolution Reaction

OVERVIEW

Energy is the necessity of today's generation to build a bright future. It is needed to meet the daily requirement as well as for the proper functioning of large scale industries. But this energy is primarily drawn from fossil fuels, a non-renewable energy source posing a threat to its existence. Thus, there is an urgent need to shift energy sources to some form of renewable energy. In this scenario, fuel cells can be a good alternative if the hydrogen required is obtained from any carbon-neutral process, such as water splitting. In this regard, the polyoxometalate (POM) supported metal complex has proved to be a suitable catalyst for water reduction/oxidation in recent studies. To catalyze hydrogen evolution reaction (HER), we have employed a POM-based inorganic-organic hybrid compound with a spiral-like structure. In this work, we have utilized this hybrid containing Anderson polyoxometalate, $[Al(OH)_6Mo_6O_{18}]^{3-}$ onto which Cu-complex, $[Cu(H_2O)_2(bpy)]^{2+}$ fragment, is supported having the resulting molecular formula of $[Cu^{II}(2,2'\text{-bpy})(H_2O)_2Cl][Cu^{II}(2,2'\text{-bpy})(H_2O)_2Al(OH)_6Mo_6O_{18}]\cdot 4H_2O$ (1). This compound acts as a pre-catalyst towards forming the active catalyst for catalyzing HER in a neutral medium. The active catalyst derived from this compound achieves a current density of 1mA/cm^2 at an overpotential of 348 mV. The turnover frequency calculated for the active catalyst is found to be 17.80 [mol H_2 (mol Cu)$^{-1}$s^{-1}] with the Faradic efficiency of 85%.

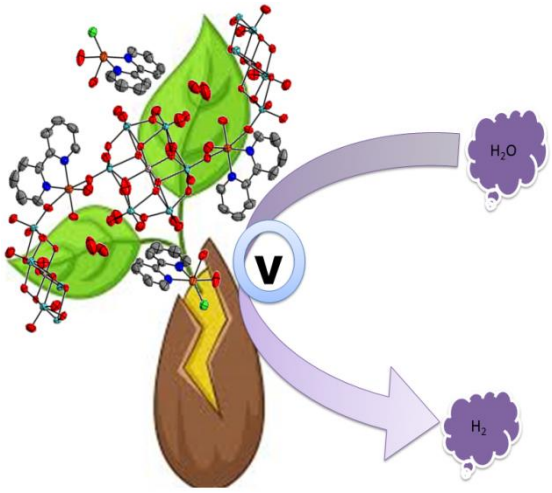

5.1. Introduction

Metal oxides are an intriguing class of inorganic compounds that have immense importance in the industrial sector due to their versatility. Polyanionic metal oxides or polyoxometalates (POMs) are closely related classes of molecular oxide that can be considered molecular analogs of traditional solid-state metal oxides. Polyoxometalates (POMs) can be classified under a special category of metal oxides that self-assemble under specific reaction conditions such as pH, temperature, metal salts concentration, *etc*., to articulate varied structures (**Figure 1.1.**).[1] As discussed in **Chapter 1** under section **1.1.**, POMs are further classified based on the structure adopted. The Anderson-type polyoxoanions are a type of heteropolyanion with the general formula of $[XM_6O_{24}]^{n-}$, where X is a heteroatom ($X=Al^{3+}/Cr^{3+}$, *etc*.) and M is an addenda atom ($M= Mo^{VI}/W^{VI}$, *etc*.). The structural arrangement of Anderson POM with the attractive planar structure and abundant oxygen coordination sites may conduce to coordinate with the transition metal ions by different coordination modes.[2] Taking the structural advantage of Anderson POM, various POM supported transition metal complexes (PSTMCs) are synthesized by different research groups.[3-5] In this work, we have employed a spirally arranged chained compound formed by connecting the Anderson anion's versatile building unit ($[Al(OH)_6Mo_6O_{18}]^{3-}$) with a Cu^{II}-bipyridine-complex.

Polyoxometalates' versatility (POMs) allows them to be used for numerous applications, such as in catalysis, material science, magnetism, *etc*. POM and POM-based hybrids have been studied extensively to understand their electrochemical properties.[6-10] More attention has been given to electrochemical water splitting catalysis by POM and POM-based hybrid in the last decades.[11-13] As the understanding of POM chemistry grew, its shortcoming towards OER and HER's electrochemical catalysis became more prominent. The major problem in dealing with POM based electrocatalyst for water splitting is its structural stability under electrochemical oxidizing/reducing conditions.[14,15] Majority of reports where POM exhibited good electrocatalytic activity towards OER/HER later were confirmed as pre-catalyst with the metal oxides/phosphates ($CoO_x/NiO_x/CoP_i/NiP_i$) as the active catalyst.[16-20]

In the last few years, POM@MOF has gained attention as POM compliments the properties of MOF, which can be further utilized for various applications such as organic catalysis, drug delivery, magnetism, *etc*.[21,22] With the increase in sustainable energy development research,

many reports of POM@MOF or POMOF for electrochemical water splitting (WS) were reported. One such work by Lan Y.-Q. and Dai Z.-H. and their co-workers for synthesizing Fe_3C/Mo_2C with N, P, Co-doped graphitic carbon (labeled as Fe_3C/Mo_2C@NPGC) by using $[PW_{12}O_{40}]^{3-}$ encapsulated in MOF-100 (PW_{12}@MOF-100), has recently been reported.[23] The Mo, N, and P sources were obtained from POM@MOF-100 (Fe) (where POM= $[PW_{12}O_{40}]^{3-}$). Fe_3C/Mo_2C@NPGC exhibited magnificent electrochemical activity towards HER with high stability (10 h) and low onset overpotential of 18 mV (vs. RHE). The electrocatalytic activity of Fe_3C/Mo_2C@NPGC is comparable to that of many Pt-based catalysts available in the literature, thus explaining the importance of POM for catalyst development.

There are various reports of utilizing POM for preparing efficient HER catalysts. In 2017, Prof. Sun-Li Li and Ya-Qian Lan and their co-workers prepared tungsten carbide material where they used POM as one of the precursor.[24] By managing the composition of Polyoxotungstate : polypyrrole : graphene, a nitrogen doped porous carbon material (NC@W_xC) was synthesized. The material so prepared catalyzed HER in acidic medium with long term durability and stability that to with low overportential of 100 mV for 10 mA/cm^2.

In a similar approach, H. Ma and H. Pang and their co-workers employed a POM-based hybrid compound for developing electroactive bimetallic sulfides, Ni_3S_2–MoS_2 and CoS_2–MoS_2, having mesoporous structure.[25] POM is used as a precursor for the formation of MoS_2, facilitating the easy formation of these bimetallic sulfides. These bimetallic sulfides exhibited an overpotential of 224 mV (Ni_3S_2–MoS_2@Carbon Cloth (CC)) and 222 mV (CoS_2–MoS_2@CC) for a current density of 10 mA cm^{-2}.

Inspired from various literature reports of POM and POM-based compounds, where they are either directly used as electrocatalysts or as a precursor for developing electrocatalysts for HER activity along with our recent observations as discussed in **Chapters 3** and **4** motivated us to pursue this work. From the electrochemical studies done in **Chapters 2** to **4**, we have concluded that PSTMCs can act as a suitable catalyst for water oxidation (WO)/ water reduction (WR).[26,27] In these kinds of POM-based hybrids, POMs do not participate directly in WO/WR but enable the overall compound's stability holding the active site. The transition metal complex, supported on to the POM, acts as an active catalyst. Intending to employ similar chemistry, we chose an Anderson POM supported Cu complex, reported previously in

2003.[28] The compound used for this study has the molecular formula of $[Cu^{II}(2,2'\text{-bpy})(H_2O)_2Cl][Cu^{II}(2,2'\text{-bpy})(H_2O)_2Al(OH)_6Mo_6O_{18}]\cdot 4H_2O$ (**1**). In this compound, Anderson anion unit, $[Al(OH)_6Mo_6O_{18}]^{3-}$, connects to a transition metal complex $[Cu^{II}(2,2'\text{-bpy})(H_2O)_2]^{2+}$ to form a spiral-shaped chain structure. From our studies, as discussed in later sections, we found out that this chained compound (**1**) acts as a pre-catalyst for electrochemical hydrogen evolution reaction (HER) in a neutral medium. The active catalyst, derived from compound **1**, under electrochemical conditions, has an overpotential of 348 mV at the current density of 1 mA/cm^2 and also shows a turnover frequency (TOF) of 17.80 [mol H_2 (mol Cu)$^{-1}s^{-1}$].

5.2. Experimental Section

5.2.1. Material and methods

5.2.1.1. General materials and methods

Starting materials were purchased in AR grade and were used as received. PXRD patterns were recorded on a Bruker D8-Advance diffractometer by using graphite monochromated $CuK\alpha_1$ (1.5406Å) and $K\alpha_2$ (1.55439Å) radiation. Infra-red spectra of solid samples were obtained directly using the sample on iD7 ATR Thermo Fisher Scientific-Nicolet iS5 instrument. Diffuse reflectance (DR) UV-visible electronic absorption spectra were recorded using Shimadzu-2600 spectrophotometer. Thermogravimetric (TGA) analyses were carried out on a STA 409 PC analyzer. Carl Zeiss model Ultra 55 microscope was used for Field emission scanning electron microscope (FE-SEM) imaging with energy dispersive X-ray (EDX) spectroscopy. Oxford Instruments X-Max^N SDD (50 mm^2) system and INCA analysis software were used for elemental mapping. Zahner Zanium electrochemical workstation which is operated with Thales software is used for conducting all the electrochemical activity.

5.2.1.2. Electrochemical studies

Similar protocol is followed as that discussed in **Chapter 2** under section **2.2.1.3.** Electrode potentials were converted to the normal hydrogen electrode (NHE) scale using the relation E (NHE) = E (Ag/AgCl) + 0.1451 V when the Ag/AgCl used as RE. Cyclic voltammetry scans were initiated at the open circuit potential (OCP), and the cathodic side was scanned first, followed by an anodic scan. Five cycles were taken consecutively for each set of cyclic

voltammetry measurements in quiescent solution. Cyclic voltammograms (CVs) were also recorded at various scan rates.

5.2.2. Synthesis

5.2.2.1. Synthesis of Compound 1

100 mL aqueous solution of $Na_2MoO_4.2H_2O$ (3.5 g, 14.46 mmol) was prepared and added to 50 mL aqueous solution of $AlCl_3.6H_2O$ (1.5 g, 6.21 mmol). To the mixture so formed, 10 mL of glacial CH_3CO_2H was added. A separate mixture was prepared containing 40 mL of 2,2′-bipyridine (0.2 g, 1.28 mmol), which was prepared by dissolving it in a mixture of 25 mL of methanol and 15 mL of water, and $Cu(NO_3)_2.2H_2O$ (0.5 g, 2.06 mmol). This mixture was added to the initially prepared reaction mixture, following which the pH was adjusted to 2.6 by the addition of concentrated HCl. The resulting mixture was then filtered, and the filtrate was kept at room temperature for crystallization. Blue blocks appeared within a week. These crystals were collected from the mother liquor, after which they were washed with water and dried at room temperature. Yield: 0.50 g (12% based on Mo).

5.3 Results and Discussion

5.3.1. Physical characterization

The synthesized compound was characterized by PXRD, FT-IR, FESEM, TGA, and UV-vis. DRS. Varied electrochemical experiments were designed to study the mechanistic and kinetic aspect of HER activity by compound **1**.

5.3.1.1. Structural Description of compound 1

$[Cu^{II}(2,2'\text{-bpy})(H_2O)_2Cl][Cu^{II}(2,2'\text{-bpy})(H_2O)_2Al(OH)_6Mo_6O_{18}]\cdot 4H_2O$ (compound **1**) consists of $[Cu^{II}(2,2'\text{-bpy})(H_2O)_2]^{2+}$ fragment which is coordinated to POM unit ($[Al(OH)_6Mo_6O_{18}]^{3-}$) from the two oxygen atoms of terminal "Mo-O" bonds of two different Anderson anions. The crystal of **1** is made up of spiral-type chains, $[Cu^{II}(2,2'\text{-bpy})(H_2O)_2Al(OH)_6Mo_6O_{18}]_n^{n-}$ as anions, chloro-copper complexes, $[Cu^{II}(2,2'\text{-bpy})(H_2O)_2Cl]_n^{n+}$ as cations, and four lattice water molecule. Thus, from the crystallographic point of view, two independent Anderson anions have a unique position, denoted by labeling their heteroatom aluminum as **Al(1)** and **Al(2)**. The figure is provided below (**Figure 5.1.**). From each Anderson anion through two non-adjacent oxygen atoms of terminal "Mo–O" bond, two $\{[Cu^{II}(2,2'\text{-bpy})(H_2O)_2]^{2+}\}$fragments are connected, forming a spiral chain type structure (**Figures 5.1.**). The chain consists alternatively of **Al(1)** and

Al(2) containing Anderson anions, which have two different orientations: alternatively, they have identical configurations along the chain. In the polymer chain, each cluster anion acts as a bidentate ligand coordinating to two $[Cu^{II}(2,2'\text{-bpy})(H_2O)_2]^{2+}$ complex fragments through the terminal oxygen atoms of two nonadjacent MoO_6 octahedra (**Figure 5.1. (a)**).

There are two crystallographically independent copper sites comprising of two different coordination environments around copper: The first one is the part of the chain, $[Cu^{II}(2,2'\text{-bpy})(H_2O)_2]^{2+}$ and the other one is the chloro complex, $[Cu^{II}(2,2'\text{-bpy})(H_2O)_2Cl]^{1+,}$ hydrogen-bonded to **Al(1)** containing Anderson anion as shown in **Figure 5.1. (b)**. The Cu-complex coordinated to the chain has distorted octahedral geometry. Its coordination geometry is fulfilled with two nitrogen atoms from bipyridine ligand, two oxygen atoms from H_2O molecule, and two oxygen from "Mo–O" of two different Anderson anions. The second copper center has square pyramidal geometry formed by two nitrogen atoms from the 2,2′-bipyridine ligand, two water molecules, and one chloride anion.

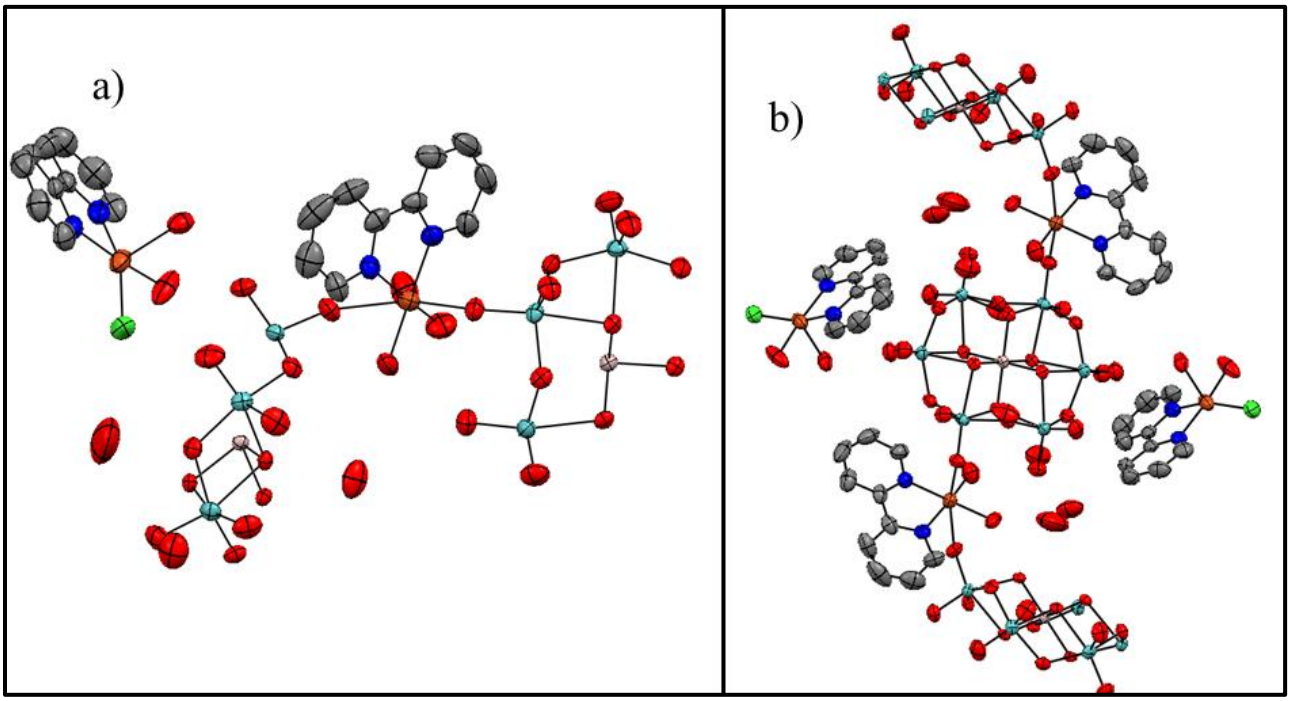

Figure 5.1. (a) Asymmetrical unit of compound **1**. (b) Representation of chain-like structure formed by compound **1**. Colour code: Red:O; blue:N; Light green:Cl; Gray:C; Violet:Al; Aqua blue:Mo; Orange:Cu.

5.3.1.2. PXRD analysis

The successful synthesis of compound **1** was confirmed from the PXRD patterns. The PXRD pattern recorded from the instrument after synthesizing the compound was compared to the simulated PXRD patterns. All the major peaks from the PXRD pattern were found to match the simulated pattern confirming the synthesized compound's bulk purity (**Figure 5.2. (a)**).

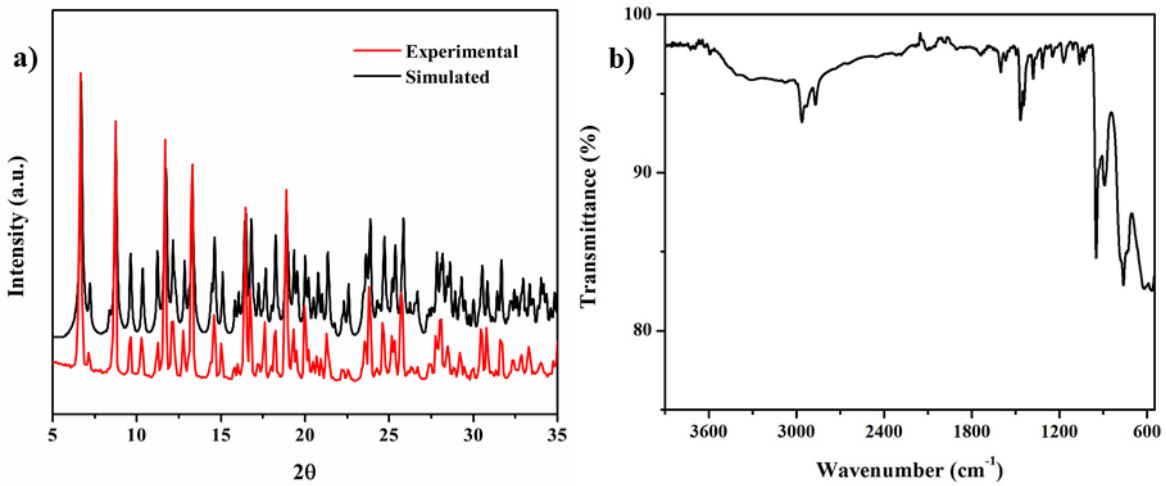

Figure 5.2. (a) PXRD pattern of compound **1** obtained experimentally compared with the simulated PXRD patterns. **(b)** FTIR of compound **1**.

5.3.1.3. FTIR and Diffused reflectance UV-vis. Spectral analysis

IR stretching observed in the region of 890-950 cm^{-1} is due to ν (Mo=O) stretching. Series of bands between 1100 and 1600 cm^{-1} are attributed to various stretching associated with the 2,2′-bipyridine ligand (**Figure 5.2. (b)**). In the lower frequency region ν (750-850 cm^{-1}), bands with medium-weak intensity are observed attributed to ν (Cu–O–Mo).

The electronic absorption spectrum of compound **1** was recorded in reflectance mode and is converted into Kubelka-Munk (K-M) derived plot (**Figure 5.3.**). The broad absorbance seen at 710 nm is due to the d-d transition from Cu^{2+} of both the Cu(II)-complexes present in compound **1**. The absorbance at 320 nm can be attributed to the ligand to metal charge transfer (LMCT) in the Anderson POM unit. This is due to the charge transfer from 'O' to 'Mo' of the POM unit. The absorbance at 250 nm is due to π to π^* transition arising from bipyridine ligand, which is present in Cu(II)-complexes in compound **1**.

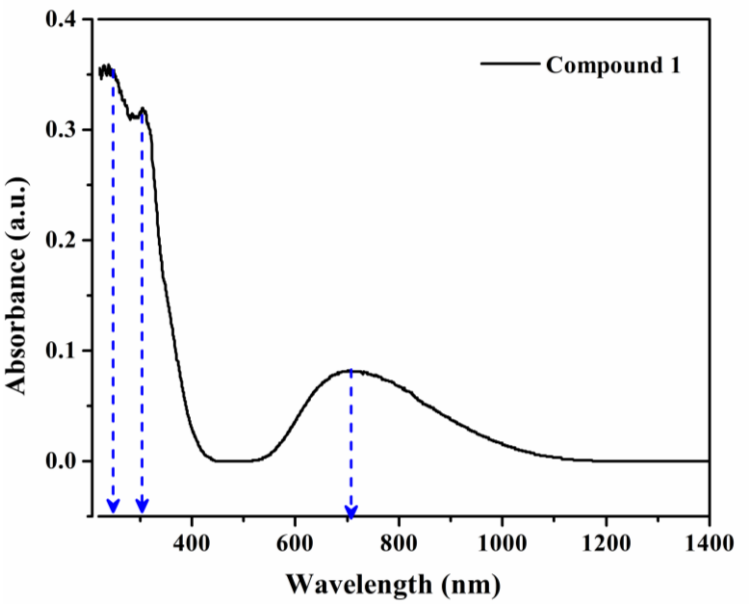

Figure 5.3. Kubelka Monk modified UV-vis. the diffused reflectance spectrum of compound **1**.

5.3.2. Electrochemical properties

All the electrochemical experiments were performed in a three-electrode system as described in the section. The cyclic voltammetric experiments were performed by following the protocols as discussed earlier in section **5.2.2.2.** The CV scans of bare glassy carbon electrodes were collected before initializing the electrochemical experiments to study the HER activity by compound **1**. Blank GC electrode showed no HER activity in the electrochemical potential window of our study.

5.3.2.1. Electrochemical property of compound 1

The Cyclic voltammograms of compound **1** has three peaks towards the cathodic sweep of the CV scan denoted as C1, C2, and C3 at the potential of +0.054 V, –0.126V, –0.845 V, respectively. Towards the anodic sweep for the CV scan of compound **1**, two peaks A1 and A2 are seen at the potential of +0.128 V and –0.089 V, respectively (**Figure 5.4.**).

As discussed in section **5.3.1.1.**, compound **1** consists two crystallographically distinct 'Cu' species; one is part of the chain (involved in coordinate covalent bond formation), and the other is present in the cationic fragment of compound **1**. These different 'Cu' species give the hump-like features we see both towards the anodic and cathodic scan of compound **1**'s CV. The

direction of the CV scan starts from the cathodic sweep with a hump-like peak C1 assigned to the reduction Cu(II)-complex, which is the part of the cationic fragment and is not coordinated to POM, from Cu(II) to Cu(I) (**Figure 5.4.)**. Immediately following C1, peak C2 for the reduction of Cu(II)-complex, which is part of the chain and is coordinated to the POM unit, from Cu(II) to Cu(I) is seen. Pre-catalytic peak C3 is slightly visible in the CV scan, following which HER activity is seen. After hydrogen generation, catalytic Cu-species revert to Cu(I) form, for which we observe two oxidation peaks (Cu(I) to Cu(II) oxidation peaks), labelled as A1 and A2.

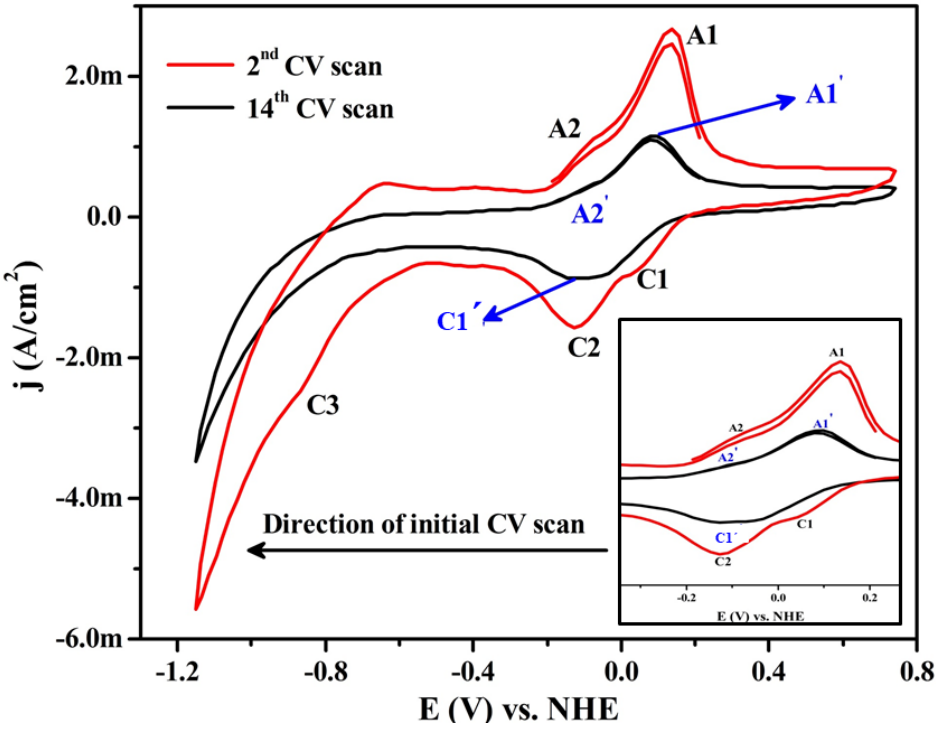

Figure 5.4. Cyclic voltammograms of compound **1** were recorded for the 2nd, and 14th CV cycles. Black coloured plot denotes the 2nd cycle of the CV scan, whereas the red one denotes the 14th cycle of the CV scan of compound **1**. Inset: zoomed CV plot showing the redox peaks region.

As we increase the number of CV scans for compound **1**, changes in its CV features are observed, which gets stabilized after running 12 CV scans and maintaining it until the next 100 cycles. We observe that area under the peak decreases significantly. The onset potential shifts towards a more cathodic value (E_{onset} = –0.74 V and E_{onset} = –0.866 V for 2nd and 14th CV scans of **1**, respectively) with a relatively less catalytic current. A broad peak is seen towards both the anodic as well as the cathodic sweep of the CV scans labelled as C1´ and A1´at the potential of

–0.097 V and –0.094 V, respectively. A very slight hump at the potential of –0.121 V is also visible towards the anodic sweep labelled as A2′ (**Figure 5.4.**).

In the 2nd CV scan, where both the Cu-complexes are structurally intact, we can speculate that both play a substantial role in HER catalysis, resulting in relatively high onset current (j~ –5.5 mA/cm^2) with low onset potential (E_{onset} = –0.74 V). As we increase the CV scans from 2nd cycle to 14th cycle of the CV scan for **1**, the onset potential also shifts to a more cathodic side (E_{onset} = –0.866 V) with relatively low catalytic current (j~ –3.5 mA/cm^2). These changes mentioned could be attributed to the structural changes happening around the Cu-species, leading to more stable species, which catalyzes HER henceforth.

5.3.2.2. Insights of the plausible structural changes

The changes in CV features could be associated with the structural modifications happening in compound **1** due to high cathodic potential. We have speculated that the Cu-complex, $\{Cu^{II}(2,2'\text{-bpy})(H_2O)_2Cl\}^{1+}$, which is part of cationic fragment of compound **1**, undergoes structural rearrangement under the electrochemical condition by substituting Cl^- ligand with aqua ligand forming $\{Cu^{II}(2,2'\text{-bpy})(H_2O)_3\}^{2+}$ resulting in weakening of its supramolecular interactions with Anderson POM. Once $\{Cu^{II}(2,2'\text{-bpy})(H_2O)_3\}^{2+}$ species is formed, it starts leaching out in solution, and the K^+ ions from K_2HPO_4 and KH_2PO_4 (phosphate buffer) of the electrolyte helps in maintaining the electroneutrality of the core structure of PSTMC. Slowly with continuous CV scans $\{Cu^{II}(2,2'\text{-bpy})(H_2O)_3\}^{2+}$ species completely leaches out in solution for which we redox couple C1′/A1′ is seen. In this situation, we expect the core structure of the PSTMC (compound **1**) changes to $K[Cu^{II}(2,2'\text{-bpy})(H_2O)_2Al(OH)_6Mo_6O_{18}]\cdot 4H_2O$ (**1′**) on the electrode surface, which catalyzes the HER generating the hydrogen. Thus, the more stable structure formed from compound **1** would be denoted as **1′** henceforth.

5.3.2.3. Stability of 1′ (active catalyst)

To understand the stability of **1′** on the electrode surface, we conducted constant potential electrolysis (CPE) experiment; we applied a constant potential (–0.9 V) and monitored the current for a fixed period (**Figure 5.5. (a)**). From this CPE experiment, we found out that the active species (**1′**) derived from compound **1** is stable for the period of 2.0 h, following which a steady increase in current is observed, indicating a further change in the active species' structure.

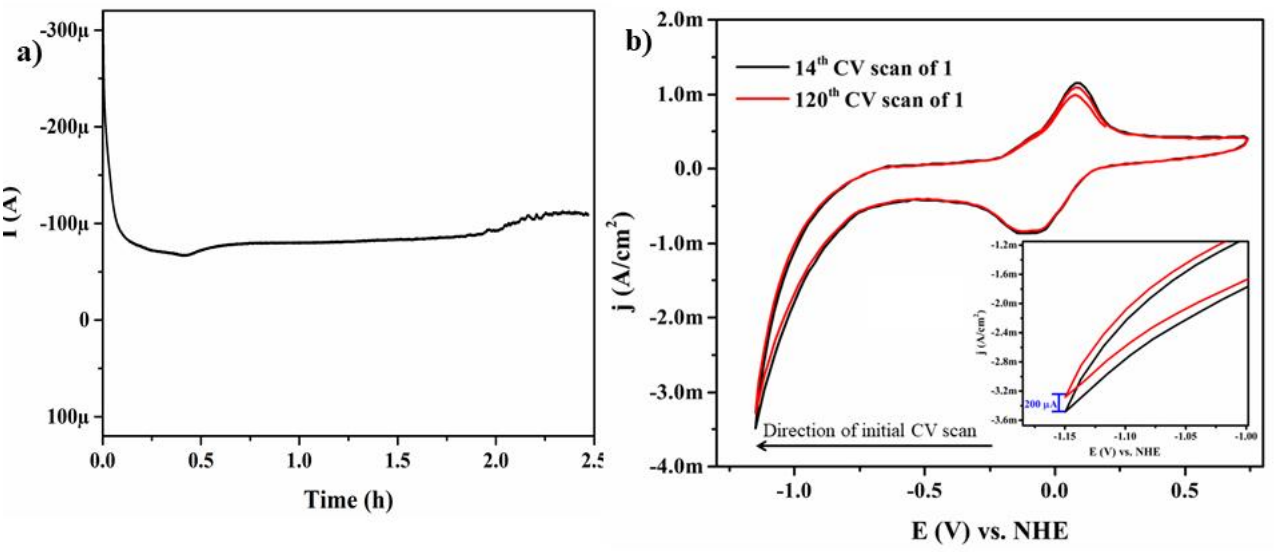

Figure 5.5. (a) Constant potential electrolysis (CPE) for compound **1´** at the potential of -0.9 V. **(b)** Comparison of the CV scans of 14th and 120th CV scans of **1**. Inset shows the difference in the catalytic current of 14th and 120th CV scans (200 µA).

Long term durability of **1´** (active catalyst) was studied by recording 100 CV scans after **1´** was formed. The CV scans were monitored for any change in the redox features and onset potential throughout, and a negligible difference was noted. The catalytic current, as shown in the inset of **Figure 5.5. (b)**), a difference of 200 µA was seen. This difference in the catalytic current could be attributed to the loss in catalytic current due to the bubbles' deposition arising from the HER activity. Thus, we confirmed that **1´** is stable for 2 hours, confirmed from CPE experiment as well as from 100 CV scans.

5.3.2.4. Controlled experiment

General methodology: For the controlled experiments, we prepared $[Cu(2,2´\text{-}bpy)_2(H_2O)_2]Cl_2$ complex and a relevant inorganic coordination polymer, $[La(H_2O)_7Al(OH)_6Mo_6O_{18}]_n\cdot 4nH_2O$, comprising of Anderson POM unit $\{(Al(OH)_6Mo_6O_{18})^{3-}\}$ by following the methodology available in the literature.[29] $[La(H_2O)_7Al(OH)_6Mo_6O_{18}]_n\cdot 4nH_2O$ was selected for these experiments due to its polymeric nature, which makes it insoluble in the water, allowing us to record its CV scans in a heterogenous manner by coating 20 µL of the sample ink on GC electrode as mentioned in section **5.2.1.2**. In the case of $[Cu(2,2´\text{-}bpy)_2(H_2O)_2]Cl_2$, CV scans were recorded in homogeneous fashion by taking 1 mmol of it in 0.1 M acetate buffer (pH 4.8). Details of the experiments carried out along with their results are discussed below:

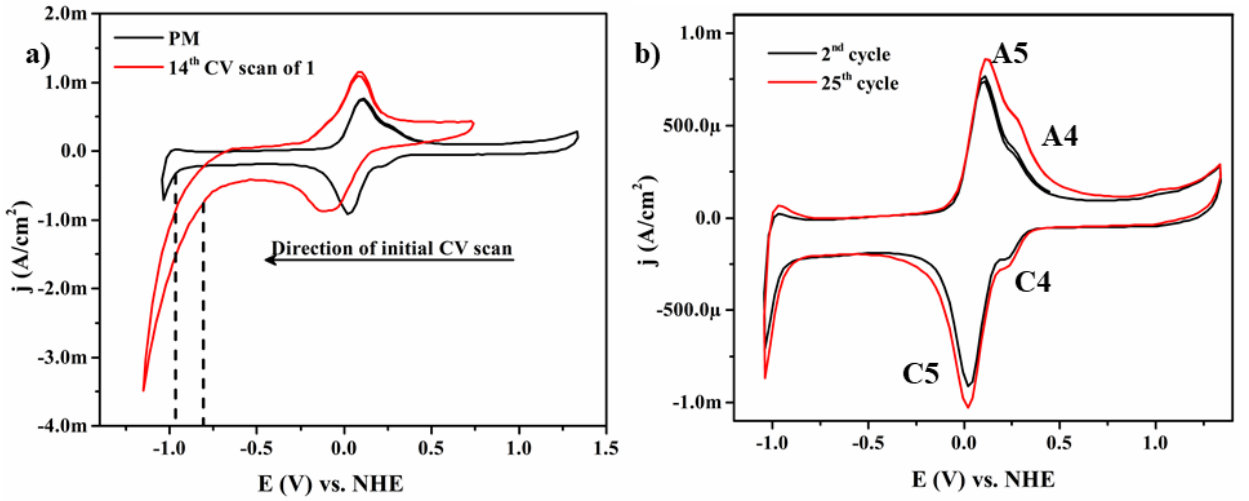

Figure 5.6. (a) Comparison of CVs of 14th CV scan of **1** (red) and physical mixture (PM) (black) prepared by coating $[La(H_2O)_7Al(OH)_6Mo_6O_{18}]_n \cdot 4nH_2O$ on GC electrode and taking 1 mmol of $[Cu(2,2'\text{-bpy})_2(H_2O)_2]Cl_2$ in the electrolyte solution. **(b)** 2nd (black) and 25th (red) CV scans of $[Cu(2,2'\text{-bpy})_2(H_2O)_2]Cl_2$.

We recorded the CVs by coating 20 µL of $[La(H_2O)_7Al(OH)_6Mo_6O_{18}]_n \cdot 4nH_2O$ sample ink on the GC electrode and taking one mmol of $[Cu(2,2'\text{-bpy})_2(H_2O)_2]Cl_2$ in the same electrolytic solution. This set up allowed us to have a mixture containing both POM and $[Cu(2,2'\text{-bpy})_2(H_2O)_2]Cl_2$ in the system (labelled as PM or physical mixture) and obtain their cyclic voltammograms (**Figure 5.6. (a)**). In the CV scan for PM, we got two features in the cathodic and anodic CV sweep labelled as C4, C5 and A4, A5. Peaks C4 and C5 were seen at +0.24 V and +0.023 V, respectively. Towards the anodic sweep of the CV scan peaks, A4 and A5 are observed at +0.28 V and +0.104 V, respectively.

On comparing the physical mixture system's CVs with that of **1´** as depicted in **Figure 5.6. (a)**, we can draw the following conclusion: (i) The CV feature varies a lot from each other. The catalytic current obtained from PM is very low relative to that of **1´** (**Figure 5.6. (a)**). **(ii)** On increasing the CV scans of the PM system, we observed that the peak current, as well as catalytic current increases, and after 25 CV cycles, a red-coloured deposit was seen on the glassy carbon electrode (**Figure 5.6. (b)**). This red colour deposition is a characteristic feature of Cu metal. No such residue was seen in the case of **1´** (title electrocatalyst). From here, we concluded that catalytic activity of **1´** is facilitated by the synergistic effect from POM, which stabilizes the overall structure by debarring reduction of Cu(II) to elemental form. From **Chapter 4**, we know that the $[La(H_2O)_7Al(OH)_6Mo_6O_{18}]_n \cdot 4nH_2O$ do not show any catalytic activity for HER in

phosphate buffer pH 7 (**Figure 4.9. (b)**, **Chapter 4**). Thus, we can conclude that Cu(II)-species coordinated to the POM unit is an active centre for HER catalysis.

5.3.2.5. Mechanistic and Kinetic study

To understand the kinetics, we recorded CVs by varying the scan rate (**Figure 5.7. (a)**). From the CVs varying from low scan rate (50 mV/s) to high scan rate (300 mV/s) and calculated the cathodic peak current of the active species which was utilized for plotting the graph of cathodic peak current (i_{pc}) *vs.* scan rate (υ) (**Figure 5.7. (b)**). The graph's linear nature confirms the involvement of diffusion-controlled process in electron transfer for the overall process.[15] The slope so obtained by linear fitting of the points is used to calculate the catalyst's turnover frequency (TOF) by finding the active Cu atoms participating in the catalysis (complete calculation for TOF is provided below in subsection of 'TOF calculation').

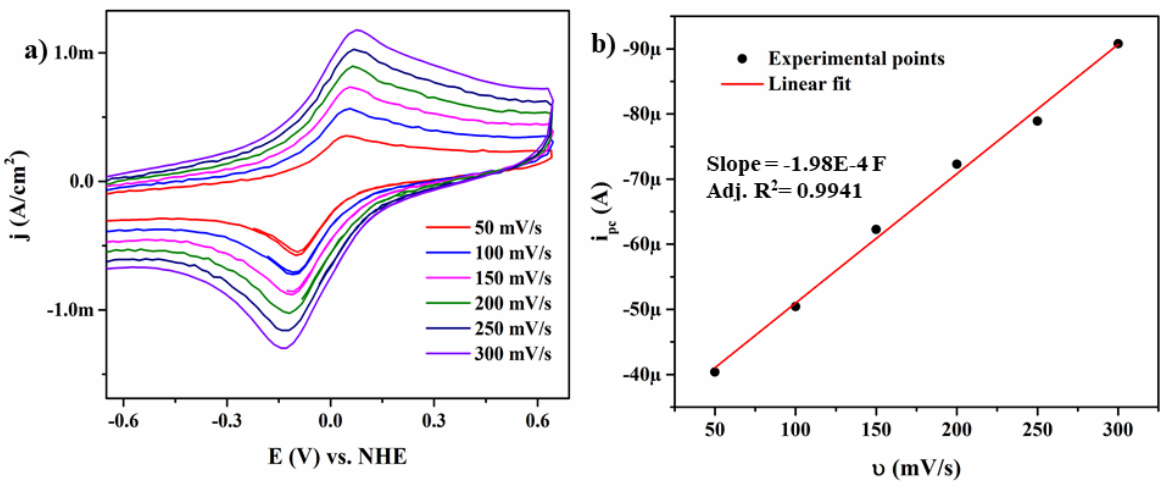

Figure 5.7. (a) Cyclic voltammograms of **1´** were recorded in 0.1 M phosphate buffer pH 7 by varying the scan rate from 50mV/s to 300 mV/s. **(b)** Cathodic peak current (i_{pc}) as a function of scan rate.

Tafel plot was constructed by following similar methodology as discussed in **Chapter 2** under section **2.3.2.6.** The overpotential required to achieve a current density of 1 mA/cm^2 by the active catalyst (**1´**) was found to be 348 mV (**Figure 5.8.**).

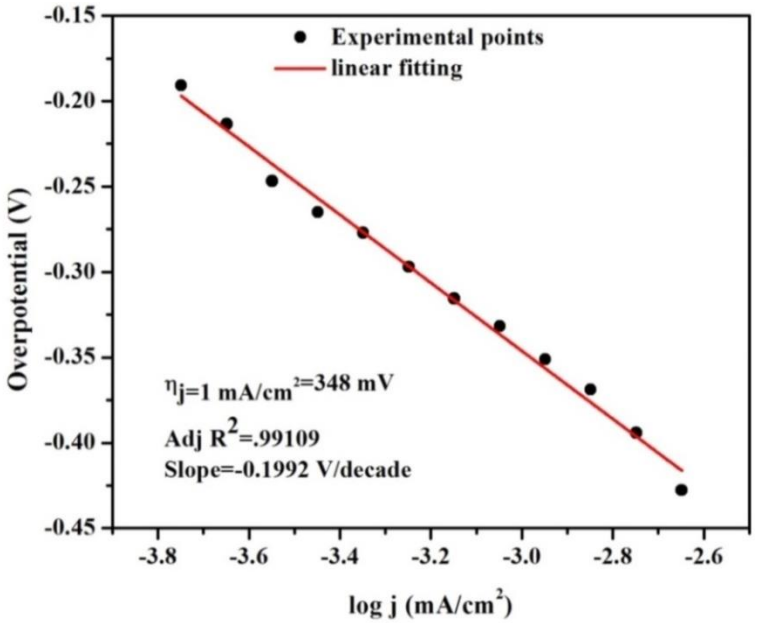

Figure 5.8. Galvanostatic *iR*-corrected Tafel plot of **1** at pH 7 (0.1 M phosphate buffer).

5.3.2.6. Quantitative hydrogen evolution and Faradic efficiency calculation

Following a similar method, as discussed in **Chapter 3**, section **3.3.2.6.**, we calculate the Faradic efficiency of both the compounds. For quantitative hydrogen evolution, a constant current density of 1 mA/cm^2 was applied for a period of 3 h. During the electrolysis, hydrogen bubbles first gathered at the FTO electrode's surface and later accumulated in an inverted graduated tube (home-built set-up, **Figure 3.22.**, **Chapter 3**), which was previously filled with electrolyte, displacing the electrolyte.

Faradaic efficiency of any system describes the efficiency with which charge is utilized in an electrochemical reaction.

For HER, it can be formulated as,

$$\frac{\text{Moles of } H_2 \text{ evolved}}{\text{Moles of } H_2 \text{ that can evolve utilizing the employed charge}}$$

Calculation of Faradic efficiency for **1´**:

From the bulk-electrolysis, the quantitative measurement of hydrogen evolved was measured under constant current condition. For this work, we found 0.27 mL/hour of H_2 evolved under 1 atm. pressure.

Thus, moles of H_2 evolved in one hour = (0.27/22400) mol = **1.205 µmol.**

$$H_{2\ ideal} = \frac{\text{Q (Total Charge employed)}}{\text{n (no. of electrons required for the chemical change X 1 Farad)}}$$

Here, we employed a current density of 1 mA/cm^2 and 'n'= 2 for HER (as it is a two-electron process).

Thus, H_2 that ideally should evolve = (76 × 3600)/(2 × 96500) mol = 1.417 µmol.

$$\text{Faradic efficiency} = \frac{1.205}{1.417} \times 100 = 85.03\%$$

Therefore, Faradaic efficiency of **1´** is **85%**.

5.3.2.7. Turnover Frequency (TOF) Calculation

- **Calculation of surface coverage and number of active copper atoms**

We have calculated the active Cu atoms/cm^2 on the electrode surface using a method recently described by Pintado *et al.*[30] by measuring the surface coverage (Γ_0) from the slope (1.985 E-4 F) of the i_p *vs* scan rate (**Figure 5.7.**, derived from **Figure 5.7. (a)**) using the equation 1.

$$\text{Slope} = n^2F^2A\Gamma_0/4RT \qquad \text{..... (1)}$$

Where 'n' = No. of electrons involved, here 1. For Cu(II) – Cu(I) conversion.

Slope of i_{pc} vs. scan rate plot, which is 1.98 E-7 A/mV = 1.98 E-4 A/mV

$$\Gamma_0 = (\text{Slope})(4RT)/\ n^2F^2A \qquad \text{..... (2)}$$

By substituting all the values in equation 2, we obtain Γ_0 as **2.91×10^{-9} mol/cm^2**

Thus, for compound **1** obtained surface density of active copper atoms is **1.75 ×10^{15} copper atoms/cm^2** or in other words, it is **2.91 × 10^{-9} mol/cm^2**.

- **Calculation of Turnover Frequency (TOF) for H_2 evolution from Tafel Plot:**

TOF can be written as,

$$\text{TOF at any given over potential} = \frac{\text{Current density at given over potential}}{2 \times F \times \text{No. of active copper species/atoms}} \quad \ldots\ldots (2)$$

HER process being a two-electron process, numeric 2 is included in the equation. Thus, division of current density at a particular overpotential by 2F (F = Faraday constant) gives one catalytic turnover number and it's further division by the number of active copper atoms gives us turnover frequency (TOF).

TOF for compound **1:**

$$(TOF)_{j=1\ mA/cm^2} = \frac{10^{-3}}{2 \times F \times 2.91\ E^{-9}} \quad \ldots\ldots (3)$$

Thus $(TOF)_{j=1mA/cm^2}$ = 17.80 [mol H_2 (mol Cu)$^{-1}$s^{-1}]

5.4. Conclusion

$[Cu^{II}(2,2'\text{-bpy})(H_2O)_2Cl][Cu^{II}(2,2'\text{-bpy})(H_2O)_2Al(OH)_6Mo_6O_{18}]\cdot 4H_2O$, Anderson POM supported Cu-bipyridine metal complex, having a spiral-type chained structure, acts as the precursor to produce an active catalyst under the electrochemical condition for hydrogen evolution reaction. The high cathodic potential application led to the structural rearrangement, which is stable for 2 h and 100 CV cycle scans. This work shows that even though compound **1** is not the active catalyst, POM still plays an intrinsic role in the HER activity, which is not possible otherwise. This emphasizes the importance of POM supported transition metal complexes for designing catalysts for HER activity. **1´** shows electrocatalytic activity for HER, where a current density of 1 mA/cm^2 is achieved at the expense of **348** mV (overpotential). Turnover frequency calculated for the active catalyst is **17.80** [mol H_2 (mol Cu)$^{-1}$s^{-1}].

5.5. References

1. (a) Pope, M. T.; Muller, A. Polyoxometalate Chemistry: An Old Field with New Dimensions in Several Disciplines. *Angew. Chem. Int. Ed.* **1991**, *30*, 34-48. (b) Omwoma, S.; Gore, C. T.; Ji, Y.; Hu, C.; Song, Y.-F. Environmentally benign polyoxometalate materials. Coord. Chem. Rev. 2015, 286, 17-29.
2. (a) Anderson, J. S. Constitution of the Poly-acids. Nature, 1937, 140, 850. (b) Song, Y.-F.; Long, D.-L.; Kelly, S. E.; Cronin, L. Sorting the Assemblies of Unsymmetrically Covalently Functionalized Mn-Anderson Polyoxometalate Clusters with Mass Spectrometry. *Inorg. Chem.*, **2008**, *47*, 9137–9139.
3. Joshi, A.; Vaidya, S.; Singh, M. Synthesis and Structure of Anderson Cluster based Organic–Inorganic Hybrid Solid, $[\{Cu(2\text{-}pzc)(H_2O)_2\}_2\{H_7AlMo_6O_{24}\}]\cdot 17H_2O$ and its Dye Adsorption Properties. *J. Chem. Sci.* **2019**, *131*, 7.
4. Blazevic, A.; Al-Sayed, E.; Roller , A.; Giester, G.; Rompel, A. Tris-Functionalized Hybrid Anderson Polyoxometalates: Synthesis, Characterization, Hydrolytic Stability and Inversion of Protein Surface Charge. *Chem. Eur. J.* **2015**, *21*, 4762-4771.
5. Xu, J.; Zhu, Z.; Su, T.; Liao, W.; Deng, C.; Hao, D.; Zhao, Y.; Ren, W.; Lü, H. Green Aerobic Oxidative Desulfurization of Diesel by Constructing an Fe-Anderson type Polyoxometalate and Benzene Sulfonic Acid-Based Deep Eutectic Solvent Biomimetic Cycle. *Chinese Journal of Catalysis* **2020**, *41*, 868-876.
6. (a) Dolbecq, A.; Dumas, E.; Mayer, C. R.; Mialane, P. Hybrid Organic– Inorganic Polyoxometalate Compounds: From Structural Diversity to Applications *Chem. Rev.* **2010,** *110,* 6009–6048. (b) Yan-Ling Xiong, Ming-Yue Yu, Ting-Ting Guo, Jin Yang, Jian-Fang Ma. A Nanosized Propeller-like Polyoxometalate-linked Copper(I)-Resorcin[4]arene for Efficient Catalysis. *Inorg. Chem.* **2020**, *59*, 15402-15409.
7. Sadakane, M.; Steckhan,E. Electrochemical Properties of Polyoxometalates as Electrocatalysts. *Chem. Rev.* **1998**, *98*, 219–238.
8. Buvailo, H. I.; Makhankova, V. G.; Kokozay, V. N.; Omelchenko, I. V.; Shishkina, S. V.; Jezierska, J.; Pavliuk, M. V.; Shylin, S. I. Copper-Containing Hybrid Compounds Based on Extremely Rare $[V_2Mo_6O_{26}]^{6-}$ POM as water oxidation catalysts. *Inorg. Chem. Frontiers* **2019**, *6*, 1813-1823.
9. Karunadasa, H. I.; Chang, C. J.; Long, J. R. A Molecular Molybdenum-oxo Catalyst for Generating Hydrogen from Water. *Nature* **2010**, *464*, 1329-1333.

10. Zhu, G.; Glass, E. N.; Zhao, C.; Lv, H.; Vickers, J. W.; Geletii, Y. V.; Musaev, D. G.; Song, J.; Hill, C. L. A Nickel Containing Polyoxometalate Water Oxidation Catalyst. *Dalton Trans.* **2012**, *41*, 13043−13049.
11. Lv, H.; Geletii, Y. V.; Zhao, C.; Vickers, J. W.; Zhu, G.; Luo, Z.; Song, J.; Lian, T.; Musaev, D. G.; Hill, C. L. Polyoxometalate Water Oxidation Catalysts and the Production of Green Fuel. *Chem. Soc. Rev.* **2012**, *41*, 7572−7589.
12. Song, Y.-F.; Tsunashima, R. Recent Advances on Polyoxometalate-Based Molecular and Composite Materials. *Chem. Soc. Rev.* **2012**, *41*, 7384-7402.
13. (a) Nohra, B.; Moll, H. E.; Marleny, L.; Albelo, R.; Mialane, P.; Marrot, J.; Mellot-Draznieks, C.; O'Keeffe, M.; Biboum, R. N.; Lemaire, J.; Keita, B.; Nadjo, L.; Dolbecq. A. Polyoxometalate-Based Metal Organic Frameworks (POMOFs): Structural Trends, Energetics, and High Electrocatalytic Efficiency for Hydrogen Evolution Reaction. *J. Am. Chem. Soc*. **2011**, *133*, 13363-13374. (b) Zhang, L.-N.; Li, S.-H.; Tan, H.-Q.; Khan, S. L.; Ma, Y.-Y.; Zang, H.-Y.; Wang, Y.-H.; Li, Y.-G. MoP/Mo_2C@C: A New Combination of Electrocatalysts for Highly Efficient Hydrogen Evolution over the Entire pH Range. *ACS Appl. Mater. & Interfaces* **2017**, *9*, 16270-16279. (c) Luo, X.-M.; Cui, C.-H.; Cao, J.-P.; Lin, Q.-F.; Xu. Y. Two new POM-Based Compounds Modified by Lanthanide–Schiff Base Complexes with Interesting NLO Properties. *Acta Crystallographica Section C Structural Chemistry* **2018**, *74*, 1370-1377.
14. Kanan, M. W.; Nocera, D. G. In-Situ Formation of an Oxygen-Evolving Catalyst in Neutral Water Containing Phosphate and Co^{2+}. *Science* **2008**, *321*, 1072−1075.
15. Kanan, M. W.; Surendranath, Y.; Nocera, D. G. Cobalt–Phosphate Oxygen-Evolving Compound. *Chem. Soc. Rev*. **2009**, *38*, 109−114.
16. Folkman, S. J.; Finke, R. G. Electrochemical Water Oxidation Catalysis Beginning with Co(II) Polyoxometalates: The Case of the Precatalyst $Co_4V_2W_{18}O_{68}^{10-}$. *ACS Catal.* **2017**, *7*, 7−16.
17. Stracke, J. J.; Finke, R. G. Electrocatalytic Water Oxidation Beginning with the Cobalt Polyoxometalate $[Co_4(H_2O)_2(PW_9O_{34})_2]^{10-}$: Identification of Heterogeneous CoO_x as the Dominant Catalyst. *J. Am. Chem. Soc.* **2011**, *133*, 14872−14875.
18. Stracke, J. J.; Finke, R. G. Distinguishing Homogeneous From Heterogeneous Water Oxidation Catalysis when Beginning with Polyoxometalates. *ACS Catal.* **2014**, 4, 909–933.
19. Tang, Y.-J.; Zhang, A.-M.; Zhu, H.-J.; Dong, L.-Z.; Wang, X.-L.; Li, S.-L.; Han, M.; Xu, X.-X.; Lan, Y.-Q. Polyoxometalate Precursors for Precisely Controlled Synthesis of Bimetallic Sulfide Heterostructure Through Nucleation-Doping Competition. *Nanoscale*, **2018**, *10*, 8404-8412.
20. Wang, Z.-H.; Wang, X.-F.; Tan, Z.; Song, X.-Z. POM/MOF Hybrids and Their Derivatives for Hydrogen and Oxygen Evolution Electrocatalysis. Materials Today Energy, 2020, 100618.

21. (a) Wang, S.-S.; Yang, G.-Y. Recent Advances in Polyoxometalate-Catalyzed Reactions. *Chem. Rev.* **2015,** *115*, 11, 4893–4962. (b) Koutsouroubi, E. D.; Papadas, I. T.; Armatas, G. S. Ordered Mesoporous Polyoxometalate-Organosilica Frameworks as Efficient Photocatalysts of the Hydrogen Evolution Reaction. *ChemPlusChem* **2016**, *81*, 947-954. (c) Patel, A.; Sadasivan, R. Modified Mn Substituted POMs: Synthetic Strategies, Structural Diversity to Applications. *Progress in Materials Science* **2020**, 100759.
22. (a) Katsoulis, D. E. A Survey of Applications of Polyoxometalates. *Chem. Rev.* **1998**, *98*, 1, 359–388. (b) Coronado, E.; Gómez-García, C.-J. Polyoxometalate-Based Molecular Materials. *Chem. Rev.* **1998**, *98*, 1, 273–296.
23. Polyoxometalate-based Metal–Organic Framework-Derived Hybrid Electrocatalysts for Highly Efficient Hydrogen Evolution Reaction. Li, J.-S.; Tang, Y.-J.; Liu, C.-H.; Li, S.-L.; Li, R.-H.; Dong, L.-Z.; Dai, Z.-H.; Baoa, J.-C.; Lan, Y.-Q. *J. Mater. Chem. A*, **2016**, *4*, 1202-1207.
24. Wang, X.-L.; Tang, Y.-J.; Huang, W.; Liu, C.-H.; Dong, L.-Z.; Li, S.-L.; Lan, Y.-Q. Efficient Electrocatalyst for the Hydrogen Evolution Reaction Derived from Polyoxotungstate/Polypyrrole/Graphene. *ChemSusChem* **2017**, *10*, 2402-2407.
25. Hou, Y.; Pang, H.; Zhang, L.; Li, B.; Xin, J.; Li, K.; Ma, H.; Wang, X.; Tan, L. Highly Dispersive Bimetallic Sulfides Afforded by crystalline Polyoxometalate-Based Coordination Polymer Precursors for Efficient Hydrogen Evolution Reaction. *J. Power Sources*. **2020**, *446*, 227319.
26. Singh, C.; Mukhopadhyay, S.; Das, S. K. Polyoxometalate-Supported Bis (2, 2′-bipyridine) mono (aqua) nickel (II) Coordination Complex: an Efficient Electrocatalyst for Water Oxidation. *Inorg. Chem.* **2018**, *112*, 529-586.
27. Singh, C.; Das, S. K. Anderson Polyoxometalate Supported $Cu(H_2O)$(Phen) Complex As An Electrocatalyst for Hydrogen Evolution Reaction in Neutral Medium. *Polyhedron*, **2019**, *172*, 80-86.
28. Shivaiah, V.; Nagaraju, M.; Das, S. K. Formation of a Spiral-Shaped Inorganic−Organic Hybrid Chain, $[Cu^{II}(2,2´\text{-bipy})(H_2O)_2Al(OH)_6Mo_6O_{18}]_n^{n-}$: Influence of Intra- and Interchain Supramolecular Interactions. *Inorg. Chem.*, **2003**, *42*, 6604-6606.
29. Shivaiah, V.; Reddy, P. V. N.; Cronin, L.; Das, S. K. A Novel Polyoxometalate Chain Formed From Heteropolyanion Building Blocks and Rare Earth Metal Ion Linkers: $[La(H_2O)_7Al(OH)_6Mo_6O_{18}]_n \cdot 4nH_2O$. *J. Chem. Soc. Dalton Trans.* **2002**, *0*, 3781-3782.
30. Pintado, S.; Goberna-Ferrón, S.; Escudero-Adán, E. C.; Galán-Mascarós, J. R. Fast and Persistent Electrocatalytic Water Oxidation by Co–Fe Prussian Blue Coordination Polymers. *J. Am. Chem. Soc.* **2013**, *135*, 13270-13273.

Concluding Remarks and Future Scope

Concluding Remarks

This thesis, entitled "Designing Polyoxometalate Based Hybrid Compounds as Electrocatalysts for Water Splitting" describes designing and utilizing different POM supported transition metal complexes (PSTMCs) for electrocatalytic activity towards both OER and HER. In this thesis work, we have shown, how to tune the structure of PSTMCs by considering different factors such as reaction conditions, precursors employed, *etc*., while designing the synthetic methodology of PSTMCs. Strategically incorporating synthetic protocol allowed us to obtain the different structures of PSTMCs, thereby resulting in different catalytic activity.

In **Chapters 2** and **3**, we have utilized a Keggin type of POM, $K_6[CoW_{12}O_{40}]\cdot 6H_2O$, as the POM support to obtain two different PSTMCs. We have shown, how the catalytic activity could be changed from OER to HER by substituting Ni(II)-complex (which shows OER activity in **Chapter 2**) with that of Cu(II)-complex (when it shows HER activity in **Chapter 3**). This also explains the transition metal (TM) of the transition metal complex supported on the POM unit acts as the active center for the OER/HER catalysis. The POM unit does not participate directly in this catalytic process.

In **Chapter 2**, more specifically, we synthesized a robust and efficient electrocatalyst for water oxidation, which has the molecular formula of $[Ni^{II}(2,2'\text{-bpy})_3]_3[\{Ni^{II}(2,2'\text{-bpy})_2(H_2O)\}\{HCo^{II}W^{VI}_{12}O_{40}\}]_2\cdot 3H_2O$. The catalyst was found to be stable for 20 h and durable for 1000 cycles under the catalytic conditions. We confirmed our compound's structural stability during the electrocatalytic process from various controlled experiments, and the active catalyst was found to be the 'Ni' center of the transition metal complex. The overpotential to achieve a current density of 1 mA/cm^2 was found to be 475.6 mV and a turnover frequency (TOF) of 18.49 (mol O_2)(mol Ni^{II})$^{-1}$ s^{-1}.

On the other hand, in **Chapter 3**, we successfully synthesized a 2-dimensional coordination polymer containing compound comprising three crystallographically distinct Cu(II)-complexes supported on a Keggin POM, $K_6[CoW_{12}O_{40}]\cdot 6H_2O$, achieved by slightly modifying the synthetic protocol from **Chapter 2**. This compound, $[\{Cu^{II}(2,2'\text{-bpy})(H_2O)_2\}][\{Co^{II}W^{VI}_{12}O_{40}\}\{(Cu^{II}(2,2'\text{-bpy})(H_2O)\}\{(Cu^{II}(2,2'\text{-bpy})\}]\cdot 2H_2O$, exhibited electrochemical HER activity in the acetate buffer at pH 4.8. The overpotential required to achieve a current density of 1 mA/cm^2 was 520

mV with the Faradic efficiency of 81.02%. This study intrigued us to dig down into other POM's role in the PSTMC catalyzed OER/HER and led to **Chapters 4** and **5** as described below.

In **Chapters 4** and **5**, we have utilized an Anderson type POM supporting Cu-complexes. In **Chapter 4**, for our study, we used two PSTMCs, $[Cr(OH)_6Mo_6O_{18}\{Cu(phen)(H_2O)_2\}_2][Cr(OH)_6Mo_6O_{18}\{Cu(phen)(H_2O)Cl\}_2]\cdot 5H_2O$ (**1**) and $[Al(OH)_6Mo_6O_{18}\{Cu(phen)(H_2O)_2\}_2][Al(OH)_6Mo_6O_{18}\{Cu(phen)(H_2O)Cl\}_2]\cdot 5H_2O$ (**2**) having the analogous structure. The structural similarity between these two compounds enabled us to understand the POM unit's role in overall catalytic activity (HER). Both these compounds catalyze HER under the neutral condition of phosphate buffer. From the observation we obtained from our studies, we conclude that 'Cr'-centered Anderson POM based Cu(II)-complex hybrid compound **1** is a better catalyst than that containing the 'Al'-centered Anderson POM, compound **2**. This conclusion was drawn based on low overpotential and high faradic efficiency (FE) obtained for compound **1** ($\eta_{j=1\ mA/cm^2}$ = 300 mV, and FE is 95.7%) relative to compound **2** ($\eta_{j=1\ mA/cm^2}$ = 644 mV and FE is 89.4 %).

In **Chapter 5**, for our study, we once again incorporated Anderson POM supported transition metal complex. The Cu(II)-bipyridine complex is coordinated to the Anderson POM, forming a chain-like structure with the molecular formula of $[Cu^{II}(2,2'\text{-bpy})(H_2O)_2Cl][Cu^{II}(2,2'\text{-bpy})(H_2O)_2Al(OH)_6Mo_6O_{18}]\cdot 4H_2O$. From the electrochemical studies (phosphate buffer, pH 7), we found that this compound act as a pre-catalyst as it undergoes structural rearrangement forming the active catalyst. The POM unit stabilizes the active catalyst; this was confirmed from the various controlled experiment. The active catalyst derived from this compound achieves a current density of $1mA/cm^2$ at an overpotential of 348 mV. The turnover frequency calculated for the active catalyst was found to be 17.80 [mol H_2 (mol Cu)$^{-1}s^{-1}$] with the Faradic efficiency of 85%.

To conclude, from the studies carried out for this thesis work, we found out that POM supported transition metal complexes (PSTMCs) can be employed as an electrocatalyst for OER and HER, depending upon the transition metal complex coordinated to it. It can be easily tuned by changing the ligand or transition-metal employed or by administering different POM units. By structural tuning, one can achieve better catalytic results with a good understanding of the catalytic mechanism. From our observations, we confirmed that in the electrochemical activity of

PSTMCs, POM does not participate directly in the catalytic activity but has a synergistic effect and plays an essential role in stabilizing the overall structure. The active center is always the transition metal of the transition metal complex containing the labile ligand, coordinated to the POM unit. Thus, by incorporating different transition metal complexes, one can easily change / tune the electrocatalytic activity of PSTMCs.

Future Scope

For future work, we want to synthesize Ni-supported PSTMC where Anderson POM, preferably $[Cr(OH)_6Mo_6O_{18}]^{3-}$ anion as support. This will allow us to compare and analyze the results and observations discussed in Chapter 2, providing us with a better outlook.

We believe ligand present in the transition metal complex supported on the POM unit also plays a decisive role in its catalytic activity. Literature is filled with a large pool of ligands from which we can choose our ligands and plan a synthetic methodology. So, our approach is to synthesize a series of PSTMCs containing the same POM unit (preferably Keggin POM) and transition metal but differing only in terms of ligands utilize. Since in this thesis work we have only dealt with 2,2´-bipyridine (bpy) and 1,10-phenanthroline (phen) as ligands, for future work, we want to use other N-donor ligands such 4,4′-dimethyl-2,2′-dipyridyl, 1,2-bis(4-pyridyl)ethane (bpa); 1,3-bis(1H-imidazol-l-yl)methyl)-benzene (m-bimb); 1,3-bis(4-pyridyl)-propane (bpp); 1,3-bis(1H-imidazol-1-yl)benzene (bib), 4,4′-di(1H-imidazol-1-yl)-1,1′-biphenyl (bibm), *etc*. (**Figure 1**), which will allow us to study and understand the role of ligands in the catalytic activity of PSTMCs.

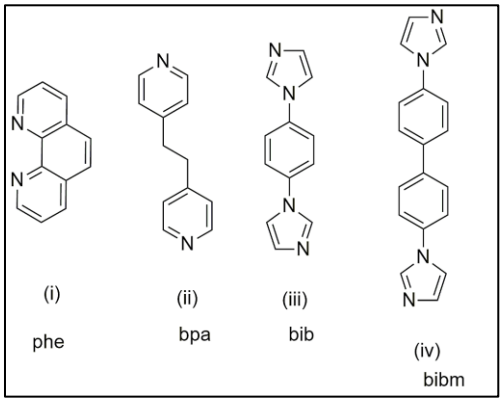

Figure 1. N-donor ligands that can be used for the PSTMCs' syntheses.

PSTMCs have rich literature, which allows us to choose relevant compounds for the study as per our convenience. One such PSTMC containing B-centred-Keggin POM with Ni-complex coordinated to it is provided in **Figure 2**. Similarly, we can select different PSTMCs from the literature to study the electrochemical properties to understand better the catalytic activity (for OER and HER) they pose.

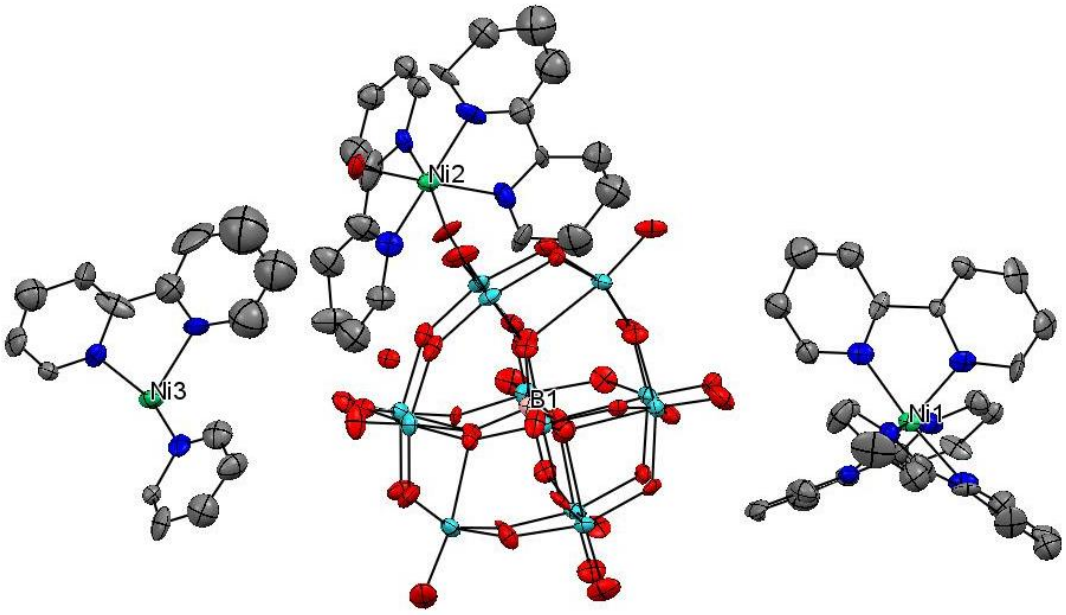

Figure 2. ORTEP diagram of a PSTMC of $[Ni(2,2'\text{-bipy})_3]_{1.5}[\{Ni(2,2'\text{- bipy})_2(H_2O)\}(BW_{12}O_{40})]$, adapted from *AKU J. Sci. Eng.* **2020**, *20*, 576-581.

==========

Appendix

Single-Crystal Data

A1. Chapter 2. Polyoxometalate Supported Bis(bpy)mono(aqua)Ni(II) Coordination Complex: An Efficient Electrocatalyst for Water Oxidation

Table A1.1. Bond lengths [Å] and angles [deg] for compound $[Ni^{II}(2,2'\text{-bpy})_3]_3[\{Ni^{II}(2,2'\text{-bpy})_2(H_2O)\}\{HCo^{II}W^{VI}_{12}O_{40}\}]_2\cdot 3H_2O$.

Bond Lengths		Bond angles	
O(2)-W(5)	1.881(10)	W(5)-O(2)-W(3)	152.5(6)
O(2)-W(3)	1.938(10)	W(12)-O(3)-W(11)	114.4(5)
O(3)-W(12)	1.934(10)	Co(1)-O(4)-W(12)	120.4(5)
O(3)-W(11)	1.970(10)	Co(1)-O(4)-W(5)	118.8(4)
O(4)-Co(1)	1.891(9)	W(12)-O(4)-W(5)	100.8(4)
O(4)-W(12)	2.149(9)	Co(1)-O(4)-W(11)	117.0(5)
O(4)-W(5)	2.174(10)	W(12)-O(4)-W(11)	98.4(4)
O(4)-W(11)	2.185(9)	W(5)-O(4)-W(11)	97.0(4)
O(5)-W(1)	1.875(10)	W(1)-O(5)-W(5)	152.5(5)
O(5)-W(5)	1.961(10)	Co(1)-O(6)-W(4)	118.9(5)
O(6)-Co(1)	1.877(9)	Co(1)-O(6)-W(7)	118.8(4)
O(6)-W(4)	2.162(10)	W(4)-O(6)-W(7)	98.2(4)
O(6)-W(7)	2.165(9)	Co(1)-O(6)-W(1)	120.5(5)
O(6)-W(1)	2.187(10)	W(4)-O(6)-W(1)	98.4(4)
O(7)-W(1)	1.928(10)	W(7)-O(6)-W(1)	97.3(4)
O(7)-W(7)	1.986(10)	W(1)-O(7)-W(7)	113.2(5)
O(8)-W(4)	1.948(11)	W(4)-O(8)-W(1)	113.7(5)
O(8)-W(1)	1.984(10)	W(4)-O(9)-W(9)	149.0(6)
O(9)-W(4)	1.927(11)	W(2)-O(10)-W(9)	153.9(5)
O(9)-W(9)	1.938(10)	Co(1)-O(11)-W(9)	118.7(5)
O(10)-W(2)	1.908(10)	Co(1)-O(11)-W(10)	120.3(4)
O(10)-W(9)	1.929(10)	W(9)-O(11)-W(10)	97.5(4)
O(11)-Co(1)	1.872(9)	Co(1)-O(11)-W(8)	121.2(5)
O(11)-W(9)	2.148(9)	W(9)-O(11)-W(8)	96.9(3)
O(11)-W(10)	2.169(10)	W(10)-O(11)-W(8)	96.9(4)
O(11)-W(8)	2.198(9)	W(2)-O(12)-W(6)	114.5(5)
O(12)-W(2)	1.921(10)	W(12)-O(13)-W(8)	150.4(6)
O(12)-W(6)	1.951(10)	W(12)-O(14)-W(6)	151.1(6)
O(13)-W(12)	1.876(11)	W(6)-O(18)-W(3)	115.0(5)

O(13)-W(8)	1.947(11)	Co(1)-O(19)-W(6)	120.1(4)
O(14)-W(12)	1.914(10)	Co(1)-O(19)-W(3)	119.1(4)
O(14)-W(6)	1.918(10)	W(6)-O(19)-W(3)	97.8(4)
O(15)-W(5)	1.714(11)	Co(1)-O(19)-W(2)	120.7(5)
O(16)-W(6)	1.715(10)	W(6)-O(19)-W(2)	96.8(3)
O(17)-W(2)	1.697(10)	W(3)-O(19)-W(2)	97.1(4)
O(18)-W(6)	1.896(10)	W(3)-O(20)-W(2)	114.7(5)
O(18)-W(3)	1.991(10)	W(11)-O(22)-W(5)	114.3(5)
O(19)-Co(1)	1.870(9)	W(10)-O(23)-W(11)	154.0(5)
O(19)-W(6)	2.171(9)	W(11)-O(24)-W(7)	152.6(6)
O(19)-W(3)	2.181(9)	W(7)-O(25)-Ni(1)	162.3(7)
O(19)-W(2)	2.185(9)	W(4)-O(26)-W(2)	153.0(5)
O(20)-W(3)	1.932(9)	W(10)-O(28)-W(8)	120.9(12)
O(20)-W(2)	1.953(10)	W(9)-O(29)-W(8)	120.0(11)
O(21)-W(12)	1.716(11)	W(8)-O(30)-W(6)	152.9(6)
O(22)-W(11)	1.943(11)	W(5)-O(31)-W(12)	114.0(5)
O(22)-W(5)	1.943(10)	W(7)-O(34)-W(4)	112.7(5)
O(23)-W(10)	1.877(11)	W(10)-O(35)-W(9)	112.9(5)
O(23)-W(11)	1.945(11)	W(7)-O(37)-W(10)	154.2(6)
O(24)-W(11)	1.887(10)	C(65)-N(13)-C(61)	118.5(14)
O(24)-W(7)	1.944(11)	C(65)-N(13)-Ni(3)	126.2(11)
O(25)-W(7)	1.706(11)	C(61)-N(13)-Ni(3)	115.3(10)
O(25)-Ni(1)	2.101(10)	C(41)-N(9)-C(45)	120.0(15)
O(26)-W(4)	1.857(9)	C(41)-N(9)-Ni(2)	125.7(12)
O(26)-W(2)	1.975(9)	C(45)-N(9)-Ni(2)	114.2(11)
O(27)-W(1)	1.712(10)	C(36)-N(8)-C(40)	116.9(13)
O(28)-W(10)	1.775(19)	C(36)-N(8)-Ni(2)	114.8(10)
O(28)-W(8)	1.980(16)	C(40)-N(8)-Ni(2)	127.8(10)
O(29)-W(9)	1.84(2)	C(50)-N(10)-C(46)	119.8(14)
O(29)-W(8)	1.913(17)	C(50)-N(10)-Ni(2)	126.1(12)
O(30)-W(8)	1.895(10)	C(46)-N(10)-Ni(2)	112.9(10)
O(30)-W(6)	1.946(10)	C(31)-N(7)-C(35)	117.3(14)
O(31)-W(5)	1.957(10)	C(31)-N(7)-Ni(2)	125.2(11)
O(31)-W(12)	2.015(10)	C(35)-N(7)-Ni(2)	115.7(10)
O(32)-W(3)	1.712(10)	C(51)-N(11)-C(55)	117.4(18)

O(33)-W(4)	1.717(11)	C(51)-N(11)-Ni(3)	127.5(14)
O(34)-W(7)	1.919(11)	C(55)-N(11)-Ni(3)	115.0(13)
O(34)-W(4)	2.008(10)	C(56)-N(12)-C(60)	117.1(16)
O(35)-W(10)	1.940(11)	C(56)-N(12)-Ni(3)	116.0(11)
O(35)-W(9)	1.955(10)	C(60)-N(12)-Ni(3)	126.0(12)
O(36)-W(11)	1.707(11)	C(21)-N(5)-C(25)	117.9(16)
O(37)-W(7)	1.862(10)	C(21)-N(5)-Ni(2)	126.2(12)
O(37)-W(10)	2.004(10)	C(25)-N(5)-Ni(2)	114.5(11)
O(38)-W(9)	1.708(12)	C(26)-N(6)-C(30)	118.7(15)
O(39)-W(10)	1.739(11)	C(26)-N(6)-Ni(2)	116.0(11)
O(40)-W(8)	1.695(11)	C(30)-N(6)-Ni(2)	125.3(12)
N(13)-C(65)	1.31(2)	C(6)-N(2)-C(10)	117.1(15)
N(13)-C(61)	1.36(2)	C(6)-N(2)-Ni(1)	116.1(11)
N(13)-Ni(3)	2.079(12)	C(10)-N(2)-Ni(1)	126.6(13)
N(9)-C(41)	1.32(2)	C(15)-N(3)-C(11)	116.1(14)
N(9)-C(45)	1.32(2)	C(15)-N(3)-Ni(1)	115.8(11)
N(9)-Ni(2)	2.100(13)	C(11)-N(3)-Ni(1)	127.9(11)
N(8)-C(36)	1.32(2)	C(1)-N(1)-C(5)	121.8(17)
N(8)-C(40)	1.32(2)	C(1)-N(1)-Ni(1)	125.5(14)
N(8)-Ni(2)	2.092(12)	C(5)-N(1)-Ni(1)	112.5(12)
N(10)-C(50)	1.31(2)	N(7)-C(35)-C(34)	123.2(15)
N(10)-C(46)	1.36(2)	N(7)-C(35)-C(36)	112.6(13)
N(10)-Ni(2)	2.108(13)	C(34)-C(35)-C(36)	124.2(15)
N(7)-C(31)	1.33(2)	N(8)-C(36)-C(37)	124.2(14)
N(7)-C(35)	1.35(2)	N(8)-C(36)-C(35)	115.3(13)
N(7)-Ni(2)	2.062(12)	C(37)-C(36)-C(35)	120.5(15)
N(11)-C(51)	1.28(3)	C(33)-C(32)-C(31)	118.7(18)
N(11)-C(55)	1.34(3)	C(39)-C(38)-C(37)	121.7(17)
N(11)-Ni(3)	2.123(14)	C(35)-C(34)-C(33)	118.8(16)
N(12)-C(56)	1.29(2)	C(38)-C(39)-C(40)	117.3(16)
N(12)-C(60)	1.36(2)	C(36)-C(37)-C(38)	116.2(16)
N(12)-Ni(3)	2.125(14)	C(32)-C(33)-C(34)	120.2(18)
N(5)-C(21)	1.35(2)	N(8)-C(40)-C(39)	123.8(15)
N(5)-C(25)	1.36(2)	N(7)-C(31)-C(32)	121.3(17)
N(5)-Ni(2)	2.097(14)	C(49)-C(48)-C(47)	114.8(17)

N(6)-C(26)	1.34(2)	N(9)-C(45)-C(44)	121.9(17)
N(6)-C(30)	1.40(2)	N(9)-C(45)-C(46)	117.1(14)
N(6)-Ni(2)	2.084(13)	C(44)-C(45)-C(46)	121.0(16)
N(2)-C(6)	1.35(2)	N(10)-C(50)-C(49)	122.7(16)
N(2)-C(10)	1.39(2)	N(6)-C(26)-C(27)	122.0(19)
N(2)-Ni(1)	2.062(13)	N(6)-C(26)-C(25)	115.3(15)
N(3)-C(15)	1.34(2)	C(27)-C(26)-C(25)	122.8(19)
N(3)-C(11)	1.37(2)	N(5)-C(25)-C(24)	121.0(19)
N(3)-Ni(1)	2.052(13)	N(5)-C(25)-C(26)	115.1(16)
N(1)-C(1)	1.33(3)	C(24)-C(25)-C(26)	124.0(18)
N(1)-C(5)	1.37(2)	C(30)-C(29)-C(28)	122(2)
N(1)-Ni(1)	2.042(14)	C(48)-C(49)-C(50)	121.6(17)
C(35)-C(34)	1.36(2)	N(9)-C(41)-C(42)	121.6(17)
C(35)-C(36)	1.54(2)	C(43)-C(42)-C(41)	117.7(19)
C(36)-C(37)	1.39(2)	C(29)-C(30)-N(6)	120.1(19)
C(32)-C(33)	1.34(3)	C(46)-C(47)-C(48)	120.9(19)
C(32)-C(31)	1.42(3)	N(13)-C(61)-C(62)	120.8(16)
C(38)-C(39)	1.32(3)	N(13)-C(61)-C(61)#1	114.5(8)
C(38)-C(37)	1.39(3)	C(62)-C(61)-C(61)#1	124.6(11)
C(34)-C(33)	1.36(3)	C(63)-C(62)-C(61)	120.0(19)
C(39)-C(40)	1.40(2)	N(13)-C(65)-C(64)	123.2(17)
C(48)-C(49)	1.34(3)	C(59)-C(60)-N(12)	126(2)
C(48)-C(47)	1.48(3)	C(63)-C(64)-C(65)	115.4(19)
C(45)-C(44)	1.40(3)	C(62)-C(63)-C(64)	121.8(19)
C(45)-C(46)	1.49(2)	C(29)-C(28)-C(27)	118.1(17)
C(50)-C(49)	1.39(3)	C(24)-C(23)-C(22)	120(2)
C(26)-C(27)	1.42(3)	N(11)-C(55)-C(54)	121.2(19)
C(26)-C(25)	1.48(3)	N(11)-C(55)-C(56)	115.1(18)
C(25)-C(24)	1.38(3)	C(54)-C(55)-C(56)	124(2)
C(29)-C(30)	1.36(3)	C(21)-C(22)-C(23)	119(2)
C(29)-C(28)	1.38(3)	C(22)-C(21)-N(5)	121.8(19)
C(41)-C(42)	1.40(3)	N(12)-C(56)-C(57)	120.6(18)
C(42)-C(43)	1.36(3)	N(12)-C(56)-C(55)	116.3(16)
C(47)-C(46)	1.37(3)	C(57)-C(56)-C(55)	123.1(19)
C(61)-C(62)	1.37(2)	N(10)-C(46)-C(47)	119.7(16)

C(61)-C(61)#1	1.54(3)	N(10)-C(46)-C(45)	115.0(13)
C(62)-C(63)	1.32(3)	C(47)-C(46)-C(45)	125.3(16)
C(65)-C(64)	1.42(3)	C(42)-C(43)-C(44)	121(2)
C(60)-C(59)	1.34(3)	C(20)-N(4)-C(16)	116.1(15)
C(64)-C(63)	1.37(3)	C(20)-N(4)-Ni(1)	128.3(11)
C(28)-C(27)	1.40(3)	C(16)-N(4)-Ni(1)	115.5(11)
C(23)-C(24)	1.30(4)	N(2)-C(6)-C(7)	122.7(19)
C(23)-C(22)	1.40(4)	N(2)-C(6)-C(5)	112.6(14)
C(55)-C(54)	1.36(3)	C(7)-C(6)-C(5)	124.5(19)
C(55)-C(56)	1.51(3)	N(4)-C(20)-C(19)	126.1(17)
C(22)-C(21)	1.35(3)	N(1)-C(5)-C(4)	120(2)
C(56)-C(57)	1.39(3)	N(1)-C(5)-C(6)	118.9(15)
C(43)-C(44)	1.37(3)	C(4)-C(5)-C(6)	121(2)
O(41)-Ni(1)	2.122(11)	C(11)-C(12)-C(13)	118.1(17)
N(4)-C(20)	1.33(2)	C(8)-C(7)-C(6)	116(2)
N(4)-C(16)	1.34(2)	C(12)-C(11)-N(3)	124.3(17)
N(4)-Ni(1)	2.036(13)	N(3)-C(15)-C(14)	122.1(17)
C(6)-C(7)	1.41(3)	N(3)-C(15)-C(16)	113.8(14)
C(6)-C(5)	1.45(3)	C(14)-C(15)-C(16)	123.1(18)
C(20)-C(19)	1.37(3)	C(10)-C(9)-C(8)	121(3)
C(5)-C(4)	1.44(3)	C(9)-C(10)-N(2)	123(3)
C(12)-C(11)	1.36(2)	N(4)-C(16)-C(17)	123.4(18)
C(12)-C(13)	1.37(3)	N(4)-C(16)-C(15)	115.3(15)
C(7)-C(8)	1.39(4)	C(17)-C(16)-C(15)	121.3(18)
C(15)-C(14)	1.41(3)	C(23)-C(24)-C(25)	121(2)
C(15)-C(16)	1.50(3)	C(3)-C(4)-C(5)	117(3)
C(9)-C(10)	1.29(3)	C(28)-C(27)-C(26)	119(2)
C(9)-C(8)	1.37(4)	C(2)-C(3)-C(4)	119(3)
C(16)-C(17)	1.38(4)	C(13)-C(14)-C(15)	118.5(19)
C(4)-C(3)	1.42(4)	C(14)-C(13)-C(12)	120.4(17)
C(3)-C(2)	1.38(4)	N(1)-C(1)-C(2)	121(2)
C(14)-C(13)	1.36(3)	C(9)-C(8)-C(7)	121(2)
C(1)-C(2)	1.40(3)	C(3)-C(2)-C(1)	120(3)
C(19)-C(18)	1.37(3)	C(43)-C(44)-C(45)	117(2)
C(58)-C(59)	1.37(3)	C(18)-C(19)-C(20)	117(2)

C(58)-C(57)	1.39(3)	C(59)-C(58)-C(57)	117(2)
C(54)-C(53)	1.32(4)	C(53)-C(54)-C(55)	119(2)
C(52)-C(51)	1.32(4)	C(51)-C(52)-C(53)	118(3)
C(52)-C(53)	1.36(4)	C(60)-C(59)-C(58)	117(2)
C(18)-C(17)	1.45(4)	N(11)-C(51)-C(52)	125(2)
O(1)-W(3)	1.890(9)	C(56)-C(57)-C(58)	121(2)
O(1)-W(1)	1.956(9)	C(54)-C(53)-C(52)	119(2)
		C(19)-C(18)-C(17)	117(3)
		C(16)-C(17)-C(18)	117(2)
		W(3)-O(1)-W(1)	152.4(5)
		O(19)-Co(1)-O(11)	109.0(4)
		O(19)-Co(1)-O(6)	109.1(4)
		O(11)-Co(1)-O(6)	111.0(4)
		O(19)-Co(1)-O(4)	108.0(4)
		O(11)-Co(1)-O(4)	108.5(4)
		O(6)-Co(1)-O(4)	111.1(4)
		N(4)-Ni(1)-N(1)	98.6(6)
		N(4)-Ni(1)-N(3)	79.4(5)
		N(1)-Ni(1)-N(3)	93.3(6)
		N(4)-Ni(1)-N(2)	174.7(5)
		N(1)-Ni(1)-N(2)	79.8(6)
		N(3)-Ni(1)-N(2)	95.6(5)
		N(4)-Ni(1)-O(25)	92.5(5)
		N(1)-Ni(1)-O(25)	87.9(5)
		N(3)-Ni(1)-O(25)	172.0(5)
		N(2)-Ni(1)-O(25)	92.4(5)
		N(4)-Ni(1)-O(41)	90.0(6)
		N(1)-Ni(1)-O(41)	168.8(6)
		N(3)-Ni(1)-O(41)	95.4(5)
		N(2)-Ni(1)-O(41)	92.3(6)
		O(25)-Ni(1)-O(41)	84.5(5)
		N(7)-Ni(2)-N(6)	95.3(5)
		N(7)-Ni(2)-N(8)	79.2(5)
		N(6)-Ni(2)-N(8)	169.9(5)
		N(7)-Ni(2)-N(5)	96.9(6)

N(6)-Ni(2)-N(5)	77.8(6)
N(8)-Ni(2)-N(5)	94.4(5)
N(7)-Ni(2)-N(9)	92.2(6)
N(6)-Ni(2)-N(9)	94.7(5)
N(8)-Ni(2)-N(9)	93.9(5)
N(5)-Ni(2)-N(9)	168.7(5)
N(7)-Ni(2)-N(10)	170.9(5)
N(6)-Ni(2)-N(10)	86.5(5)
N(8)-Ni(2)-N(10)	100.3(5)
N(5)-Ni(2)-N(10)	92.2(5)
N(9)-Ni(2)-N(10)	78.8(5)
N(13)-Ni(3)-N(13)#1	79.9(7)
N(13)-Ni(3)-N(11)#1	168.4(5)
N(13)#1-Ni(3)-N(11)#1	95.8(6)
N(13)-Ni(3)-N(11)	95.8(6)
N(13)#1-Ni(3)-N(11)	168.4(5)
N(11)#1-Ni(3)-N(11)	90.5(9)
N(13)-Ni(3)-N(12)	94.4(5)
N(13)#1-Ni(3)-N(12)	92.2(5)
N(11)#1-Ni(3)-N(12)	96.6(5)
N(11)-Ni(3)-N(12)	77.3(5)
N(13)-Ni(3)-N(12)#1	92.2(5)
N(13)#1-Ni(3)-N(12)#1	94.4(5)
N(11)#1-Ni(3)-N(12)#1	77.3(5)
N(11)-Ni(3)-N(12)#1	96.6(5)
N(12)-Ni(3)-N(12)#1	171.4(7)
O(27)-W(1)-O(5)	100.3(5)
O(27)-W(1)-O(7)	97.7(5)
O(5)-W(1)-O(7)	92.2(4)
O(27)-W(1)-O(1)	101.5(5)
O(5)-W(1)-O(1)	84.3(4)
O(7)-W(1)-O(1)	160.8(4)
O(27)-W(1)-O(8)	98.2(5)
O(5)-W(1)-O(8)	161.0(4)
O(7)-W(1)-O(8)	89.8(4)

O(1)-W(1)-O(8)	87.6(4)
O(27)-W(1)-O(6)	168.5(5)
O(5)-W(1)-O(6)	89.0(4)
O(7)-W(1)-O(6)	75.0(4)
O(1)-W(1)-O(6)	86.1(4)
O(8)-W(1)-O(6)	73.2(4)
O(17)-W(2)-O(10)	102.1(5)
O(17)-W(2)-O(12)	99.0(5)
O(10)-W(2)-O(12)	89.9(4)
O(17)-W(2)-O(20)	98.6(5)
O(10)-W(2)-O(20)	158.9(4)
O(12)-W(2)-O(20)	91.2(4)
O(17)-W(2)-O(26)	101.0(5)
O(10)-W(2)-O(26)	83.9(4)
O(12)-W(2)-O(26)	159.8(4)
O(20)-W(2)-O(26)	87.9(4)
O(17)-W(2)-O(19)	169.6(5)
O(10)-W(2)-O(19)	86.2(4)
O(12)-W(2)-O(19)	74.5(4)
O(20)-W(2)-O(19)	73.8(4)
O(26)-W(2)-O(19)	86.0(4)
O(32)-W(3)-O(1)	101.5(5)
O(32)-W(3)-O(20)	96.8(5)
O(1)-W(3)-O(20)	92.4(4)
O(32)-W(3)-O(2)	101.9(5)
O(1)-W(3)-O(2)	85.1(4)
O(20)-W(3)-O(2)	161.3(4)
O(32)-W(3)-O(18)	97.3(5)
O(1)-W(3)-O(18)	161.0(4)
O(20)-W(3)-O(18)	88.3(4)
O(2)-W(3)-O(18)	88.2(4)
O(32)-W(3)-O(19)	166.3(4)
O(1)-W(3)-O(19)	89.4(4)
O(20)-W(3)-O(19)	74.3(4)
O(2)-W(3)-O(19)	87.1(4)

O(18)-W(3)-O(19)	72.5(4)
O(33)-W(4)-O(26)	104.1(5)
O(33)-W(4)-O(9)	101.1(5)
O(26)-W(4)-O(9)	87.8(4)
O(33)-W(4)-O(8)	97.7(5)
O(26)-W(4)-O(8)	92.6(4)
O(9)-W(4)-O(8)	160.6(4)
O(33)-W(4)-O(34)	93.5(5)
O(26)-W(4)-O(34)	162.2(4)
O(9)-W(4)-O(34)	86.2(4)
O(8)-W(4)-O(34)	87.7(4)
O(33)-W(4)-O(6)	164.9(4)
O(26)-W(4)-O(6)	89.3(4)
O(9)-W(4)-O(6)	86.1(4)
O(8)-W(4)-O(6)	74.5(4)
O(34)-W(4)-O(6)	73.6(4)
O(15)-W(5)-O(2)	100.9(5)
O(15)-W(5)-O(22)	98.0(5)
O(2)-W(5)-O(22)	160.9(4)
O(15)-W(5)-O(31)	95.5(5)
O(2)-W(5)-O(31)	90.8(4)
O(22)-W(5)-O(31)	89.9(4)
O(15)-W(5)-O(5)	102.5(5)
O(2)-W(5)-O(5)	85.0(4)
O(22)-W(5)-O(5)	88.5(4)
O(31)-W(5)-O(5)	162.0(4)
O(15)-W(5)-O(4)	165.7(4)
O(2)-W(5)-O(4)	87.7(4)
O(22)-W(5)-O(4)	74.3(4)
O(31)-W(5)-O(4)	72.8(4)
O(5)-W(5)-O(4)	89.5(4)
O(16)-W(6)-O(18)	98.9(5)
O(16)-W(6)-O(14)	103.0(5)
O(18)-W(6)-O(14)	92.0(4)
O(16)-W(6)-O(30)	99.7(5)

O(18)-W(6)-O(30)	161.4(4)
O(14)-W(6)-O(30)	84.8(5)
O(16)-W(6)-O(12)	94.4(5)
O(18)-W(6)-O(12)	90.5(4)
O(14)-W(6)-O(12)	161.8(4)
O(30)-W(6)-O(12)	87.1(4)
O(16)-W(6)-O(19)	166.6(5)
O(18)-W(6)-O(19)	74.5(4)
O(14)-W(6)-O(19)	89.1(4)
O(30)-W(6)-O(19)	87.0(4)
O(12)-W(6)-O(19)	74.2(4)
O(25)-W(7)-O(37)	101.2(5)
O(25)-W(7)-O(34)	98.6(5)
O(37)-W(7)-O(34)	93.3(5)
O(25)-W(7)-O(24)	100.6(5)
O(37)-W(7)-O(24)	84.7(4)
O(34)-W(7)-O(24)	160.7(4)
O(25)-W(7)-O(7)	96.4(5)
O(37)-W(7)-O(7)	161.6(4)
O(34)-W(7)-O(7)	89.2(5)
O(24)-W(7)-O(7)	86.9(4)
O(25)-W(7)-O(6)	168.8(4)
O(37)-W(7)-O(6)	88.7(4)
O(34)-W(7)-O(6)	75.2(4)
O(24)-W(7)-O(6)	85.5(4)
O(7)-W(7)-O(6)	74.4(4)
O(40)-W(8)-O(30)	102.3(5)
O(40)-W(8)-O(29)	103.2(8)
O(30)-W(8)-O(29)	88.0(7)
O(40)-W(8)-O(13)	99.9(5)
O(30)-W(8)-O(13)	85.6(5)
O(29)-W(8)-O(13)	156.8(7)
O(40)-W(8)-O(28)	102.6(7)
O(30)-W(8)-O(28)	154.5(7)
O(29)-W(8)-O(28)	91.6(7)

O(13)-W(8)-O(28)	84.8(6)
O(40)-W(8)-O(11)	168.7(5)
O(30)-W(8)-O(11)	87.0(4)
O(29)-W(8)-O(11)	70.3(7)
O(13)-W(8)-O(11)	87.1(4)
O(28)-W(8)-O(11)	69.0(7)
O(38)-W(9)-O(29)	99.4(8)
O(38)-W(9)-O(10)	101.9(6)
O(29)-W(9)-O(10)	86.1(7)
O(38)-W(9)-O(9)	100.5(6)
O(29)-W(9)-O(9)	159.8(7)
O(10)-W(9)-O(9)	86.5(4)
O(38)-W(9)-O(35)	96.0(6)
O(29)-W(9)-O(35)	92.1(6)
O(10)-W(9)-O(35)	162.1(4)
O(9)-W(9)-O(35)	89.3(4)
O(38)-W(9)-O(11)	167.5(5)
O(29)-W(9)-O(11)	72.8(6)
O(10)-W(9)-O(11)	87.5(4)
O(9)-W(9)-O(11)	88.2(4)
O(35)-W(9)-O(11)	74.9(4)
O(39)-W(10)-O(28)	101.6(8)
O(39)-W(10)-O(23)	102.3(5)
O(28)-W(10)-O(23)	89.8(7)
O(39)-W(10)-O(35)	96.6(5)
O(28)-W(10)-O(35)	92.6(6)
O(23)-W(10)-O(35)	160.1(4)
O(39)-W(10)-O(37)	100.3(5)
O(28)-W(10)-O(37)	158.0(7)
O(23)-W(10)-O(37)	83.1(4)
O(35)-W(10)-O(37)	87.5(4)
O(39)-W(10)-O(11)	169.4(5)
O(28)-W(10)-O(11)	73.2(7)
O(23)-W(10)-O(11)	87.1(4)
O(35)-W(10)-O(11)	74.7(4)

O(37)-W(10)-O(11)	85.7(4)
O(36)-W(11)-O(24)	101.6(5)
O(36)-W(11)-O(22)	98.9(5)
O(24)-W(11)-O(22)	90.1(4)
O(36)-W(11)-O(23)	100.4(6)
O(24)-W(11)-O(23)	85.8(4)
O(22)-W(11)-O(23)	160.7(4)
O(36)-W(11)-O(3)	98.0(5)
O(24)-W(11)-O(3)	160.2(4)
O(22)-W(11)-O(3)	89.8(5)
O(23)-W(11)-O(3)	87.7(5)
O(36)-W(11)-O(4)	168.1(5)
O(24)-W(11)-O(4)	88.2(4)
O(22)-W(11)-O(4)	74.1(4)
O(23)-W(11)-O(4)	86.9(4)
O(3)-W(11)-O(4)	72.7(4)
O(21)-W(12)-O(13)	101.8(5)
O(21)-W(12)-O(14)	101.6(5)
O(13)-W(12)-O(14)	87.0(5)
O(21)-W(12)-O(3)	97.1(5)
O(13)-W(12)-O(3)	92.5(5)
O(14)-W(12)-O(3)	161.0(4)
O(21)-W(12)-O(31)	95.3(5)
O(13)-W(12)-O(31)	162.7(4)
O(14)-W(12)-O(31)	86.6(4)
O(3)-W(12)-O(31)	88.4(4)
O(21)-W(12)-O(4)	164.7(5)
O(13)-W(12)-O(4)	91.3(4)
O(14)-W(12)-O(4)	86.8(4)
O(3)-W(12)-O(4)	74.2(4)
O(31)-W(12)-O(4)	72.3(4)

Symmetry transformations used to generate equivalent atoms: #1 –x,y,-z+3/2

A2. Chapter 3. Designing POM Supported Metal Complex as an Efficient Electrocatalyst for HER

Table A2.1. Bond lengths [Å] and angles [deg] for compound [{Cu(2,2´-bpy)(H_2O)$_2$}][{$CoW_{12}O_{40}$}{(Cu(2,2´-bpy)(H_2O)}{(Cu(2,2´-bpy)}]·2H_2O

Bond Lengths		Bond angles	
W(4)-O(019)	1.749(4)	O(019)-W(4)-O(5)	101.9(2)
W(4)-O(5)	1.884(4)	O(019)-W(4)-O(8)	100.47(19)
W(4)-O(8)	1.908(4)	O(5)-W(4)-O(8)	90.04(18)
W(4)-O(11)	1.937(5)	O(019)-W(4)-O(11)	98.8(2)
W(4)-O(10)	1.951(4)	O(5)-W(4)-O(11)	159.19(18)
W(4)-O(1)	2.182(4)	O(8)-W(4)-O(11)	84.17(18)
W(12)-O(01C)	1.711(5)	O(019)-W(4)-O(10)	97.85(19)
W(12)-O(20)	1.900(4)	O(5)-W(4)-O(10)	92.29(18)
W(12)-O(010)	1.937(4)	O(8)-W(4)-O(10)	160.62(19)
W(12)-O(00Z)	1.938(4)	O(11)-W(4)-O(10)	86.88(19)
W(12)-O(6)	1.993(4)	O(019)-W(4)-O(1)	170.92(17)
W(12)-O(4)	2.190(4)	O(5)-W(4)-O(1)	74.64(17)
W(2)-O(80)	1.705(5)	O(8)-W(4)-O(1)	88.01(16)
W(2)-O(00X)	1.924(4)	O(11)-W(4)-O(1)	85.17(17)
W(2)-O(17)	1.928(4)	O(10)-W(4)-O(1)	74.12(16)
W(2)-O(013)	1.939(4)	O(01C)-W(12)-O(20)	98.1(2)
W(2)-O(19)	1.968(4)	O(01C)-W(12)-O(010)	97.5(2)
W(2)-O(3)	2.198(4)	O(20)-W(12)-O(010)	93.82(18)
W(11)-O(01F)	1.705(5)	O(01C)-W(12)-O(00Z)	101.9(2)
W(11)-O(7)	1.875(4)	O(20)-W(12)-O(00Z)	92.06(18)
W(11)-O(16)	1.909(4)	O(010)-W(12)-O(00Z)	158.67(17)
W(11)-O(010)	1.943(4)	O(01C)-W(12)-O(6)	101.0(2)
W(11)-O(00Y)	2.038(4)	O(20)-W(12)-O(6)	160.72(17)
W(11)-O(4)	2.164(4)	O(010)-W(12)-O(6)	86.31(17)
W(10)-O(01A)	1.712(5)	O(00Z)-W(12)-O(6)	81.48(17)
W(10)-O(18)	1.844(4)	O(01C)-W(12)-O(4)	168.5(2)
W(10)-O(19)	1.889(4)	O(20)-W(12)-O(4)	75.73(16)
W(10)-O(00Y)	1.991(4)	O(010)-W(12)-O(4)	73.57(16)
W(10)-O(20)	2.063(4)	O(00Z)-W(12)-O(4)	88.10(17)
W(10)-O(4)	2.131(4)	O(6)-W(12)-O(4)	85.87(16)

W(5)-O(01K)	1.720(5)	O(80)-W(2)-O(00X)	98.7(2)
W(5)-O(6)	1.861(4)	O(80)-W(2)-O(17)	101.1(2)
W(5)-O(00R)	1.873(4)	O(00X)-W(2)-O(17)	91.09(18)
W(5)-O(0AA)	2.026(4)	O(80)-W(2)-O(013)	98.8(2)
W(5)-O(5)	2.038(4)	O(00X)-W(2)-O(013)	91.48(18)
W(5)-O(1)	2.130(4)	O(17)-W(2)-O(013)	159.27(17)
W(1)-O(81)	1.727(4)	O(80)-W(2)-O(19)	100.8(2)
W(1)-O(00Z)	1.901(4)	O(00X)-W(2)-O(19)	160.45(17)
W(1)-O(013)	1.935(4)	O(17)-W(2)-O(19)	83.29(18)
W(1)-O(015)	1.948(4)	O(013)-W(2)-O(19)	87.48(18)
W(1)-O(00R)	1.949(4)	O(80)-W(2)-O(3)	169.5(2)
W(1)-O(3)	2.160(4)	O(00X)-W(2)-O(3)	74.40(16)
W(1)-W(3)	3.2384(9)	O(17)-W(2)-O(3)	87.09(16)
W(6)-O(01G)	1.714(5)	O(013)-W(2)-O(3)	73.84(16)
W(6)-O(12)	1.858(5)	O(19)-W(2)-O(3)	86.58(16)
W(6)-O(10)	1.920(4)	O(01F)-W(11)-O(7)	105.0(2)
W(6)-O(7)	1.959(4)	O(01F)-W(11)-O(16)	100.9(2)
W(6)-O(0AA)	2.010(4)	O(7)-W(11)-O(16)	87.19(19)
W(6)-O(1)	2.167(4)	O(01F)-W(11)-O(010)	98.2(2)
W(8)-O(01D)	1.718(5)	O(7)-W(11)-O(010)	92.03(19)
W(8)-O(17)	1.899(4)	O(16)-W(11)-O(010)	160.46(18)
W(8)-O(14)	1.910(4)	O(01F)-W(11)-O(00Y)	91.8(2)
W(8)-O(15)	1.970(4)	O(7)-W(11)-O(00Y)	163.01(18)
W(8)-O(18)	1.979(4)	O(16)-W(11)-O(00Y)	87.42(18)
W(8)-O(2)	2.182(4)	O(010)-W(11)-O(00Y)	87.72(18)
W(9)-O(01J)	1.713(5)	O(01F)-W(11)-O(4)	161.86(19)
W(9)-O(9)	1.903(4)	O(7)-W(11)-O(4)	91.79(17)
W(9)-O(11)	1.911(5)	O(16)-W(11)-O(4)	86.44(17)
W(9)-O(14)	1.946(5)	O(010)-W(11)-O(4)	74.06(16)
W(9)-O(13)	1.990(4)	O(00Y)-W(11)-O(4)	71.81(16)
W(9)-O(2)	2.160(4)	O(01A)-W(10)-O(18)	103.4(2)
W(3)-O(01E)	1.711(4)	O(01A)-W(10)-O(19)	101.4(2)
W(3)-O(015)	1.917(4)	O(18)-W(10)-O(19)	90.24(18)
W(3)-O(9)	1.935(4)	O(01A)-W(10)-O(00Y)	96.6(2)
W(3)-O(8)	1.937(4)	O(18)-W(10)-O(00Y)	90.79(18)

W(3)-O(00X)	1.944(4)	O(19)-W(10)-O(00Y)	161.21(18)
W(3)-O(3)	2.160(4)	O(01A)-W(10)-O(20)	92.4(2)
W(7)-O(01I)	1.720(5)	O(18)-W(10)-O(20)	164.23(18)
W(7)-O(13)	1.895(5)	O(19)-W(10)-O(20)	86.40(18)
W(7)-O(16)	1.932(4)	O(00Y)-W(10)-O(20)	87.54(17)
W(7)-O(15)	1.941(4)	O(01A)-W(10)-O(4)	163.1(2)
W(7)-O(12)	1.969(5)	O(18)-W(10)-O(4)	90.60(17)
W(7)-O(2)	2.179(4)	O(19)-W(10)-O(4)	87.81(17)
Co(0E)-O(2)	1.879(4)	O(00Y)-W(10)-O(4)	73.42(16)
Co(0E)-O(3)	1.884(4)	O(20)-W(10)-O(4)	73.89(16)
Co(0E)-O(4)	1.896(4)	O(01K)-W(5)-O(6)	104.2(2)
Co(0E)-O(1)	1.904(4)	O(01K)-W(5)-O(00R)	103.6(2)
O(00Y)-Cu(0A)	1.983(4)	O(6)-W(5)-O(00R)	88.14(18)
O(019)-Cu(1)#1	1.959(4)	O(01K)-W(5)-O(0AA)	92.4(2)
O(81)-Cu(0A)#2	2.330(4)	O(6)-W(5)-O(0AA)	91.58(17)
N(4)-C(6)	1.325(9)	O(00R)-W(5)-O(0AA)	163.54(18)
N(4)-C(8)	1.349(8)	O(01K)-W(5)-O(5)	93.6(2)
N(4)-Cu(0A)	1.997(5)	O(6)-W(5)-O(5)	162.14(18)
N(2)-C(11)	1.350(9)	O(00R)-W(5)-O(5)	88.16(17)
N(2)-C(15)	1.356(8)	O(0AA)-W(5)-O(5)	87.09(17)
N(2)-Cu(1)	1.992(5)	O(01K)-W(5)-O(1)	160.22(19)
N(1)-C(20)	1.322(8)	O(6)-W(5)-O(1)	89.71(17)
N(1)-C(16)	1.359(8)	O(00R)-W(5)-O(1)	90.58(17)
N(1)-Cu(1)	1.986(5)	O(0AA)-W(5)-O(1)	72.96(16)
N(6)-C(7)	1.336(10)	O(5)-W(5)-O(1)	72.87(17)
N(6)-C(2)	1.348(10)	O(81)-W(1)-O(00Z)	102.3(2)
N(6)-Cu(1A)	1.965(6)	O(81)-W(1)-O(013)	98.06(19)
C(18)-C(17)	1.381(10)	O(00Z)-W(1)-O(013)	89.59(18)
C(18)-C(19)	1.394(9)	O(81)-W(1)-O(015)	95.6(2)
N(3)-C(33)	1.336(9)	O(00Z)-W(1)-O(015)	161.90(18)
N(3)-C(9)	1.349(8)	O(013)-W(1)-O(015)	90.76(18)
N(3)-Cu(0A)	1.976(5)	O(81)-W(1)-O(00R)	100.9(2)
C(8)-C(29)	1.385(9)	O(00Z)-W(1)-O(00R)	85.45(18)
C(8)-C(9)	1.488(9)	O(013)-W(1)-O(00R)	161.02(17)
C(15)-C(14)	1.385(9)	O(015)-W(1)-O(00R)	88.39(18)

C(15)-C(16)	1.454(9)	O(81)-W(1)-O(3)	167.21(18)
C(19)-C(20)	1.397(9)	O(00Z)-W(1)-O(3)	88.44(17)
N(5)-C(28)	1.327(11)	O(013)-W(1)-O(3)	74.81(16)
N(5)-C(3)	1.346(10)	O(015)-W(1)-O(3)	74.21(17)
N(5)-Cu(1A)	1.972(7)	O(00R)-W(1)-O(3)	86.74(16)
C(3)-C(24)	1.393(11)	O(81)-W(1)-W(3)	128.16(15)
C(3)-C(2)	1.466(10)	O(00Z)-W(1)-W(3)	129.54(13)
C(14)-C(13)	1.388(10)	O(013)-W(1)-W(3)	82.98(13)
C(9)-C(30)	1.365(10)	O(015)-W(1)-W(3)	32.80(13)
C(11)-C(12)	1.379(10)	O(00R)-W(1)-W(3)	86.09(12)
C(12)-C(13)	1.375(11)	O(3)-W(1)-W(3)	41.44(11)
C(6)-C(5)	1.385(11)	O(01G)-W(6)-O(12)	104.1(2)
C(2)-C(23)	1.390(10)	O(01G)-W(6)-O(10)	97.9(2)
C(5)-C(27)	1.358(12)	O(12)-W(6)-O(10)	93.3(2)
C(17)-C(16)	1.361(9)	O(01G)-W(6)-O(7)	101.3(2)
C(7)-C(21)	1.384(12)	O(12)-W(6)-O(7)	85.59(19)
C(23)-C(22)	1.375(12)	O(10)-W(6)-O(7)	160.45(17)
C(32)-C(31)	1.391(12)	O(01G)-W(6)-O(0AA)	93.2(2)
C(32)-C(33)	1.393(11)	O(12)-W(6)-O(0AA)	161.70(17)
C(28)-C(26)	1.385(14)	O(10)-W(6)-O(0AA)	90.30(18)
C(24)-C(25)	1.381(13)	O(7)-W(6)-O(0AA)	85.07(18)
C(30)-C(31)	1.356(12)	O(01G)-W(6)-O(1)	163.7(2)
C(22)-C(21)	1.371(14)	O(12)-W(6)-O(1)	91.12(18)
C(27)-C(29)	1.383(12)	O(10)-W(6)-O(1)	75.07(16)
C(25)-C(26)	1.340(14)	O(7)-W(6)-O(1)	85.43(16)
O(0AA)-Cu(1)	1.942(4)	O(0AA)-W(6)-O(1)	72.47(16)
Cu(0A)-O(1AA)	1.999(5)	O(01D)-W(8)-O(17)	102.1(2)
Cu(1A)-O(2AA)	1.965(7)	O(01D)-W(8)-O(14)	98.7(2)
Cu(1A)-O(3AA)	1.975(6)	O(17)-W(8)-O(14)	91.64(19)
		O(01D)-W(8)-O(15)	97.3(2)
		O(17)-W(8)-O(15)	159.65(18)
		O(14)-W(8)-O(15)	91.45(19)
		O(01D)-W(8)-O(18)	100.0(2)
		O(17)-W(8)-O(18)	84.39(18)
		O(14)-W(8)-O(18)	161.29(18)

O(15)-W(8)-O(18)	86.26(18)
O(01D)-W(8)-O(2)	168.92(19)
O(17)-W(8)-O(2)	86.99(16)
O(14)-W(8)-O(2)	74.49(17)
O(15)-W(8)-O(2)	74.48(17)
O(18)-W(8)-O(2)	87.02(16)
O(01J)-W(9)-O(9)	102.1(2)
O(01J)-W(9)-O(11)	101.2(2)
O(9)-W(9)-O(11)	85.95(19)
O(01J)-W(9)-O(14)	97.1(2)
O(9)-W(9)-O(14)	91.07(19)
O(11)-W(9)-O(14)	161.65(18)
O(01J)-W(9)-O(13)	95.5(2)
O(9)-W(9)-O(13)	162.20(18)
O(11)-W(9)-O(13)	88.48(19)
O(14)-W(9)-O(13)	88.91(19)
O(01J)-W(9)-O(2)	165.7(2)
O(9)-W(9)-O(2)	89.64(17)
O(11)-W(9)-O(2)	87.56(17)
O(14)-W(9)-O(2)	74.30(17)
O(13)-W(9)-O(2)	73.22(16)
O(01E)-W(3)-O(015)	97.7(2)
O(01E)-W(3)-O(9)	100.5(2)
O(015)-W(3)-O(9)	161.70(18)
O(01E)-W(3)-O(8)	101.5(2)
O(015)-W(3)-O(8)	90.87(18)
O(9)-W(3)-O(8)	83.70(18)
O(01E)-W(3)-O(00X)	97.0(2)
O(015)-W(3)-O(00X)	90.91(18)
O(9)-W(3)-O(00X)	88.77(18)
O(8)-W(3)-O(00X)	161.06(18)
O(01E)-W(3)-O(3)	168.67(18)
O(015)-W(3)-O(3)	74.81(17)
O(9)-W(3)-O(3)	87.46(17)
O(8)-W(3)-O(3)	87.35(16)

O(00X)-W(3)-O(3)	74.93(16)
O(01E)-W(3)-W(1)	130.80(15)
O(015)-W(3)-W(1)	33.38(13)
O(9)-W(3)-W(1)	128.64(13)
O(8)-W(3)-W(1)	88.11(12)
O(00X)-W(3)-W(1)	83.05(13)
O(3)-W(3)-W(1)	41.45(11)
O(01I)-W(7)-O(13)	100.3(2)
O(01I)-W(7)-O(16)	100.8(2)
O(13)-W(7)-O(16)	158.45(18)
O(01I)-W(7)-O(15)	96.3(2)
O(13)-W(7)-O(15)	92.8(2)
O(16)-W(7)-O(15)	89.02(19)
O(01I)-W(7)-O(12)	100.8(2)
O(13)-W(7)-O(12)	88.23(19)
O(16)-W(7)-O(12)	83.74(19)
O(15)-W(7)-O(12)	162.38(18)
O(01I)-W(7)-O(2)	169.5(2)
O(13)-W(7)-O(2)	74.59(17)
O(16)-W(7)-O(2)	85.17(17)
O(15)-W(7)-O(2)	75.11(17)
O(12)-W(7)-O(2)	88.27(17)
O(2)-Co(0E)-O(3)	109.10(18)
O(2)-Co(0E)-O(4)	107.99(18)
O(3)-Co(0E)-O(4)	109.13(17)
O(2)-Co(0E)-O(1)	109.65(18)
O(3)-Co(0E)-O(1)	109.22(18)
O(4)-Co(0E)-O(1)	111.70(18)
Co(0E)-O(4)-W(10)	119.6(2)
Co(0E)-O(4)-W(11)	116.07(19)
W(10)-O(4)-W(11)	102.20(17)
Co(0E)-O(4)-W(12)	119.0(2)
W(10)-O(4)-W(12)	98.71(16)
W(11)-O(4)-W(12)	97.37(16)
Co(0E)-O(1)-W(5)	116.34(19)

Co(0E)-O(1)-W(6)	119.2(2)
W(5)-O(1)-W(6)	102.34(17)
Co(0E)-O(1)-W(4)	119.6(2)
W(5)-O(1)-W(4)	98.88(17)
W(6)-O(1)-W(4)	96.59(15)
Co(0E)-O(2)-W(9)	118.4(2)
Co(0E)-O(2)-W(7)	120.6(2)
W(9)-O(2)-W(7)	97.70(15)
Co(0E)-O(2)-W(8)	121.14(19)
W(9)-O(2)-W(8)	96.58(16)
W(7)-O(2)-W(8)	97.07(17)
Co(0E)-O(3)-W(3)	121.06(19)
Co(0E)-O(3)-W(1)	120.1(2)
W(3)-O(3)-W(1)	97.11(16)
Co(0E)-O(3)-W(2)	119.8(2)
W(3)-O(3)-W(2)	96.39(16)
W(1)-O(3)-W(2)	96.78(15)
W(11)-O(16)-W(7)	152.6(3)
W(4)-O(8)-W(3)	154.5(3)
W(11)-O(7)-W(6)	150.5(3)
W(8)-O(17)-W(2)	156.8(2)
W(9)-O(9)-W(3)	151.9(2)
W(5)-O(6)-W(12)	153.0(2)
W(5)-O(00R)-W(1)	148.9(2)
W(10)-O(18)-W(8)	148.8(2)
W(4)-O(5)-W(5)	113.3(2)
W(9)-O(11)-W(4)	152.7(3)
W(10)-O(19)-W(2)	149.8(2)
W(2)-O(00X)-W(3)	114.3(2)
Cu(0A)-O(00Y)-W(10)	131.7(2)
Cu(0A)-O(00Y)-W(11)	114.7(2)
W(10)-O(00Y)-W(11)	112.1(2)
W(1)-O(00Z)-W(12)	155.2(2)
W(12)-O(010)-W(11)	114.8(2)
W(7)-O(13)-W(9)	114.5(2)

W(12)-O(20)-W(10)	111.57(19)
W(1)-O(013)-W(2)	114.6(2)
W(8)-O(14)-W(9)	114.4(2)
W(3)-O(015)-W(1)	113.8(2)
W(7)-O(15)-W(8)	113.3(2)
W(6)-O(12)-W(7)	153.1(3)
W(6)-O(10)-W(4)	114.1(2)
W(4)-O(019)-Cu(1)#1	170.6(3)
W(1)-O(81)-Cu(0A)#2	137.4(2)
C(6)-N(4)-C(8)	120.7(6)
C(6)-N(4)-Cu(0A)	126.1(5)
C(8)-N(4)-Cu(0A)	113.0(4)
C(11)-N(2)-C(15)	119.5(6)
C(11)-N(2)-Cu(1)	126.7(4)
C(15)-N(2)-Cu(1)	113.6(4)
C(20)-N(1)-C(16)	118.7(6)
C(20)-N(1)-Cu(1)	126.0(4)
C(16)-N(1)-Cu(1)	115.0(4)
C(7)-N(6)-C(2)	118.4(7)
C(7)-N(6)-Cu(1A)	128.1(6)
C(2)-N(6)-Cu(1A)	113.5(5)
C(17)-C(18)-C(19)	118.1(6)
C(33)-N(3)-C(9)	117.3(6)
C(33)-N(3)-Cu(0A)	126.6(5)
C(9)-N(3)-Cu(0A)	115.7(4)
N(4)-C(8)-C(29)	120.2(6)
N(4)-C(8)-C(9)	116.3(5)
C(29)-C(8)-C(9)	123.4(6)
N(2)-C(15)-C(14)	120.3(6)
N(2)-C(15)-C(16)	115.7(5)
C(14)-C(15)-C(16)	124.0(6)
C(18)-C(19)-C(20)	118.2(6)
C(28)-N(5)-C(3)	119.0(7)
C(28)-N(5)-Cu(1A)	127.3(6)
C(3)-N(5)-Cu(1A)	112.6(5)

N(5)-C(3)-C(24)	121.1(7)
N(5)-C(3)-C(2)	115.2(6)
C(24)-C(3)-C(2)	123.7(7)
C(15)-C(14)-C(13)	120.2(6)
N(3)-C(9)-C(30)	123.1(7)
N(3)-C(9)-C(8)	112.6(6)
C(30)-C(9)-C(8)	124.3(6)
N(1)-C(20)-C(19)	122.7(6)
N(2)-C(11)-C(12)	121.6(6)
C(13)-C(12)-C(11)	119.7(7)
N(4)-C(6)-C(5)	120.6(7)
N(6)-C(2)-C(23)	121.8(7)
N(6)-C(2)-C(3)	114.6(6)
C(23)-C(2)-C(3)	123.6(7)
C(12)-C(13)-C(14)	118.6(6)
C(27)-C(5)-C(6)	120.1(7)
C(16)-C(17)-C(18)	120.5(6)
N(6)-C(7)-C(21)	122.4(8)
N(1)-C(16)-C(17)	121.6(6)
N(1)-C(16)-C(15)	113.6(6)
C(17)-C(16)-C(15)	124.8(6)
C(22)-C(23)-C(2)	119.0(8)
C(31)-C(32)-C(33)	119.2(8)
N(5)-C(28)-C(26)	122.3(9)
C(25)-C(24)-C(3)	118.2(8)
N(3)-C(33)-C(32)	122.2(7)
C(31)-C(30)-C(9)	120.2(8)
C(21)-C(22)-C(23)	119.2(8)
C(22)-C(21)-C(7)	119.1(8)
C(5)-C(27)-C(29)	118.9(7)
C(27)-C(29)-C(8)	119.4(7)
C(26)-C(25)-C(24)	120.5(9)
C(30)-C(31)-C(32)	118.0(8)
C(25)-C(26)-C(28)	118.8(9)
Cu(1)-O(0AA)-W(6)	117.6(2)

Cu(1)-O(0AA)-W(5)	129.9(2)
W(6)-O(0AA)-W(5)	112.08(19)
O(0AA)-Cu(1)-O(019)#1	90.61(18)
O(0AA)-Cu(1)-N(1)	94.2(2)
O(019)#1-Cu(1)-N(1)	175.2(2)
O(0AA)-Cu(1)-N(2)	175.1(2)
O(019)#1-Cu(1)-N(2)	93.8(2)
N(1)-Cu(1)-N(2)	81.4(2)
N(3)-Cu(0A)-O(00Y)	170.5(2)
N(3)-Cu(0A)-N(4)	82.1(2)
O(00Y)-Cu(0A)-N(4)	93.6(2)
N(3)-Cu(0A)-O(1AA)	95.3(2)
O(00Y)-Cu(0A)-O(1AA)	87.1(2)
N(4)-Cu(0A)-O(1AA)	167.6(2)
N(3)-Cu(0A)-O(81)#3	85.85(19)
O(00Y)-Cu(0A)-O(81)#3	103.52(17)
N(4)-Cu(0A)-O(81)#3	107.49(19)
O(1AA)-Cu(0A)-O(81)#3	84.35(19)
N(6)-Cu(1A)-O(2AA)	164.6(3)
N(6)-Cu(1A)-N(5)	82.9(3)
O(2AA)-Cu(1A)-N(5)	90.8(3)
N(6)-Cu(1A)-O(3AA)	91.8(3)
O(2AA)-Cu(1A)-O(3AA)	92.2(3)
N(5)-Cu(1A)-O(3AA)	170.1(2)

Symmetry transformations used to generate equivalent atoms: #1 -x+1, -y+1, -z+1 #2 -x+1/2, y-1/2, -z+1/2 #3 -x+1/2, y+1/2, -z+1/2

==========

LIST OF PUBLICATIONS

1. **Polyoxometalate-Supported Bis(2,2′-bipyridine)mono(aqua)nickel(II) Coordination Complex: An Efficient Electrocatalyst for Water Oxidation.**

   C. Singh, *S. Mukhopadhyay, S. K. Das. Inorg. Chem.* ***2018,*** *57,* 6479-6490.

2. **Anderson polyoxometalate supported $\{Cu^{II}(H_2O)(phen)\}$ complex as an electrocatalyst for hydrogen evolution reaction in neutral medium.**

   C. Singh *and S. K. Das. Polyhedron,* **2019,** *172,*80-86.

3. **A Keggin Polyoxometalate Shows Water Oxidation Activity at Neutral pH: POM@ ZIF-8, an Efficient and Robust Electrocatalyst.**

   S. Mukhopadhyay, J. Debgupta, ***C. Singh****, A. Kar and S. K. Das. Angew. Chemie,* **2018**, *130,* 1936-194.

4. **Designing UiO-66-Based Superprotonic Conductor with the Highest Metal-Organic Framework Based Proton Conductivity.**

   S. Mukhopadhyay, J. Debgupta, ***C. Singh****, R. Sarkar, O. Basu, and S. K. Das. ACS applied materials & interfaces* **2019**, *11*, 13423-13432.

5. **Proton Conductivity in $\{Mo_{72}Fe_{30}\}$-Type Keplerate.**

   K. Tandekar, ***C. Singh*** *and S. Supriya. Eur. J. Inorg. Chem.* (just accepted). doi.org/10.1002/ejic.202000889 (online available).

6. **Keggin POM Supported Cu(II) Coordination Complexes for Electrocatalytic Hydrogen Evolution Reaction (HER).**

   C. Singh*, A. Haldar and S. K. Das,* Manuscript under preparation.

7. **Anderson Polyoxometalate Supported $[Cu(H_2O)_2(bipy)]^{2+}$ Complex: A Pre-catalyst for Electrochemical Hydrogen Evolution Reaction.**

   C. Singh *and S. K. Das,* Manuscript under preparation.

POSTERS AND PRESENTATIONS

1. Subhabrata Mukhopadhyay, **Chandani Singh**, Samar K. Das
   A Keggin Polyoxometalate shows Water oxidationActivity at neutral pH: POM@ZIF-8, an efficient and robust electrocatalyst.
   Poster presentation in "CHEMFEST-2016" held at University of Hyderabad, during 3-4 March 2016.

2. Subhabrata Mukhopadhyay, **Chandani Singh**, Samar K. Das
   Assembly of organic-inorganic hybrid solid from Keggin type Polyoxometalate and their function as Electrocatalyst.
   Poster presentation in "20th NSC CRSI" held at IISER Pune, during 2-5 February 2017.

3. **Chandani Singh**, Samar K. Das
   Polyoxometalate Supported Bis(bipyridine)(aqua) Ni(II) Coordinated complexes: Electrocatalytic Water Oxidation.
   Poster presentation in "i2CAM-Energy School" held at JNCASR, Banglore during November 27- December 4, 2017.

4. **Chandani Singh**, Samar K. Das
   Polyoxometalate Supported Bis(bipyridine)(aqua) Ni(II) Coordinated complexes: Electrocatalytic Water Oxidation.
   Poster presentation in "MTIC-XVII" held at CSIR NCL, Pune, during 11-14 December 2017.

5. **Chandani Singh**, Samar K. Das
   Polyoxometalate Supported Bis(bipyridine)(aqua)Ni(II) Coordinated complexes: Electrocatalytic Water Oxidation.
   Poster presentation in "CHEMFEST-2018" held at University of Hyderabad, during 9-10 March 2018.

6. **Chandani Singh**, Samar K. Das

   One-pot Hydrothermal Synthesis of two new Keggin based Hybrid Compounds and their Potential as an Electrocatalytic Water Reduction.

   Poster presentation in "MTIC-XVIII" held at IIT-Guwahati, during 11-14 December 2019.

7. **Chandani Singh**, Samar K. Das

   Polyoxometalate Supported Bis(bipyridine)(aqua)Ni(II) Coordinated complexes: Electrocatalytic Water Oxidation.

   Oral and Poster presentation in "CHEMFEST-2020" held at University of Hyderabad, during 27-28 February 2020.

   Received Oral presentation award.

8. **Chandani Singh**, Samar K. Das

   Keggin POM Supported Cu(II) Coordinated complexes for Electrocatalytic Hydrogen Evolution Reaction (HER).

   Oral presentation in "CPECE-2020" virtual conference organized by NIT Jamshedpur, during 9-10 October 2020.

   Received Oral presentation award.

Designing Polyoxometalate Based Hybrid Compounds as Electrocatalysts for Water Splitting

by Chandani Singh

Submission date: 29-Dec-2020 04:02PM (UTC+0530)
Submission ID: 1481857086
File name: Thesis_CS.pdf (14.05M)
Word count: 32693
Character count: 160160

Designing Polyoxometalate Based Hybrid Compounds as Electrocatalysts for Water Splitting

ORIGINALITY REPORT

40%	9%	34%	10%
SIMILARITY INDEX	INTERNET SOURCES	PUBLICATIONS	STUDENT PAPERS

PRIMARY SOURCES

1	Chandani Singh, Subhabrata Mukhopadhyay, Samar K. Das. "Polyoxometalate-Supported Bis(2,2′-bipyridine)mono(aqua)nickel(II) Coordination Complex: an Efficient Electrocatalyst for Water Oxidation", Inorganic Chemistry, 2018 Publication	17%
2	Chandani Singh, Samar K. Das. "Anderson polyoxometalate supported Cu(H2O)(phen) complex as an electrocatalyst for hydrogen evolution reaction in neutral medium", Polyhedron, 2019 Publication	10%
3	Submitted to University of Hyderabad, Hyderabad Student Paper	5%
4	Vaddypally Shivaiah, M. Nagaraju, Samar K. Das. " Formation of a Spiral-Shaped Inorganic−Organic Hybrid Chain, [Cu (2,2'-bipy) (H O) Al(OH) Mo O] : Influence of Intra- and	1%

S.K.Das 30/12/2020
Prof. Samar K. Das
School of Chemistry
University of Hyderabad
Hyderabad-500 046., INDIA.

S.K.Das 30/12/2020
Prof. Samar K. Das
School of Chemistry
University of Hyderabad
Hyderabad-500 046., INDIA.

S.K.Das 30/12/2020
Prof. Samar K. Das
School of Chemistry
University of Hyderabad
Hyderabad-500 046., INDIA.

S.K.Das 30/12/2020
Prof. Samar K. Das
School of Chemistry
University of Hyderabad
Hyderabad-500 046., INDIA.

Interchain Supramolecular Interactions ", Inorganic Chemistry, 2003
Publication

5	www.journaltocs.ac.uk Internet Source	1%
6	Submitted to University of Sheffield Student Paper	1%
7	pubs.acs.org Internet Source	<1%
8	Vaddypally Shivaiah, Samar K. Das. " Polyoxometalate-Supported Transition Metal Complexes and Their Charge Complementarity: Synthesis and Characterization of [M(OH) Mo O {Cu(Phen)(H O) }][M(OH) Mo O {Cu(Phen)(H O) Cl}]·5H O (M = Al , Cr) ", Inorganic Chemistry, 2005 Publication	<1%
9	www.mdpi.com Internet Source	<1%
10	pubs.rsc.org Internet Source	<1%
11	Xiu-Li Wang, Yuan Tian, Zhi-Han Chang, Hongyan Lin. "A Series of Polyoxometalate-Based Metal–Bis(pyridyl-tetrazole) Complexes with High Electrocatalytic Activity for Hydrogen Evolution Reaction in Alkaline and Acid Media",	<1%

ACS Sustainable Chemistry & Engineering, 2020
Publication

12	w210.ub.uni-tuebingen.de Internet Source	<1%
13	www.tdx.cat Internet Source	<1%
14	Bharat Kumar Tripuramallu, Sandip Mukherjee, Samar K. Das. "Mechanistic Aspects for the Formation of Copper Dimer Bridged by Phosphonic Acid and Extending Its Dimensionality by Organic and Inorganic Linkers: Synthesis, Structural Characterization, Magnetic Properties, and Theoretical Studies", Crystal Growth & Design, 2012 Publication	<1%
15	Cao, R.. "An organic-inorganic hybrid compound constructed by Strandberg-type polyoxoanions and transition metal coordination complexes", Journal of Molecular Structure, 20081015 Publication	<1%
16	etheses.whiterose.ac.uk Internet Source	<1%
17	Ma, P.-T.. "Sandwich-type polyoxotungstate hybrids decorated by nickel-aromatic amine complexes", Journal of Solid State Chemistry,	<1%

	201001 Publication	
18	thesis.library.caltech.edu Internet Source	<1%
19	N. Tanmaya Kumar, Umashis Bhoi, Pragya Naulakha, Samar K. Das. "A polyoxometalate supported copper dimeric complex: Synthesis, structure and electrocatalysis", Inorganica Chimica Acta, 2020 Publication	<1%
20	baadalsg.inflibnet.ac.in Internet Source	<1%
21	www.frontiersin.org Internet Source	<1%
22	researchportal.bath.ac.uk Internet Source	<1%
23	Hongjin Lv, Weiwei Guo, Kaifeng Wu, Zheyuan Chen et al. "A Noble-Metal-Free, Tetra-nickel Polyoxotungstate Catalyst for Efficient Photocatalytic Hydrogen Evolution", Journal of the American Chemical Society, 2014 Publication	<1%
24	Submitted to University of South Florida Student Paper	<1%
25	www.sigmaaldrich.com Internet Source	<1%

26	Baran, E.J.. "Spectroscopic, magnetic, and electrochemical behavior of the copper(II) complex of carnosine", Journal of Inorganic Biochemistry, 199506 Publication	<1%
27	Scott J. Folkman, Joaquin Soriano-Lopez, José Ramón Galán-Mascarós, Richard G. Finke. " Electrochemically Driven Water-Oxidation Catalysis Beginning with Six Exemplary Cobalt Polyoxometalates: Is It Molecular, Homogeneous Catalysis or Electrode-Bound, Heterogeneous CoO Catalysis? ", Journal of the American Chemical Society, 2018 Publication	<1%
28	file.scirp.org Internet Source	<1%
29	Khorasani-Motlagh, M.. "Iron(III) octaethylporphyrin chloride supported on glassy carbon as an electrocatalyst for oxygen reduction", Journal of Electroanalytical Chemistry, 20040401 Publication	<1%
30	Vedichi Madhu, Ramababu Bolligarla, Indravath K. Naik, Raju Mekala, Samar K. Das. " A {Cu I } Cluster Supported on a Metal-Dithiolato Complex Anion Causes its Conformational Change Leading to a Doubly-Bridged Curved	<1%

Coordination Polymer and its Reactivity with a Diamine Resulting in the Emergence of a [M(diamine)(dithiolate)] System ", European Journal of Inorganic Chemistry, 2016
Publication

31	link.springer.com Internet Source	<1%
32	Submitted to Universidade do Porto Student Paper	<1%
33	Markus D. Kärkäs, Oscar Verho, Eric V. Johnston, Björn Åkermark. "Artificial Photosynthesis: Molecular Systems for Catalytic Water Oxidation", Chemical Reviews, 2014 Publication	<1%
34	Harikleia Sartzi, Haralampos N. Miras, Laia Vilà-Nadal, De-Liang Long, Leroy Cronin. "Trapping the δ Isomer of the Polyoxometalate-Based Keggin Cluster with a Tripodal Ligand", Angewandte Chemie International Edition, 2015 Publication	<1%
35	Liu, Yuping, SiXuan Guo, Liang Ding, C. André Ohlin, Alan M Bond, and Jie Zhang. "Lindqvist Polyoxoniobate Ion Assisted Electrodeposition of Cobalt and Nickel Water Oxidation Catalysts", ACS Applied Materials & Interfaces Publication	<1%

onlinelibrary.wiley.com

36	Internet Source	<1%
37	www.yumpu.com Internet Source	<1%
38	De-Chuan Zhao, Yang-Yang Hu, Hong Ding, Hai-Yang Guo, Xiao-Bing Cui, Xiao Zhang, Qi-Sheng Huo, Ji-Qing Xu. "Polyoxometalate-based organic–inorganic hybrid compounds containing transition metal mixed-organic-ligand complexes of N-containing and pyridinecarboxylate ligands", Dalton Transactions, 2015 Publication	<1%
39	chemistry-europe.onlinelibrary.wiley.com Internet Source	<1%
40	Jorge Pasán, Joaquín Sanchiz, Catalina Ruiz-Pérez, Francesc Lloret, Miguel Julve. "Phenylmalonate-Containing Copper(II) Complexes: Synthesis, Crystal Structure and Magnetic Properties", European Journal of Inorganic Chemistry, 2004 Publication	<1%
41	real.mtak.hu Internet Source	<1%
42	repository.kaust.edu.sa Internet Source	<1%

43	Haijuan Wang, Wansheng You, Bifang Meng, Xianfeng Sun, Hongwei Cheng, Wenjuan Shan. "A New 2D Layered Co(II) Complex Based on Monosubstituted Keggin Anions and its Electrocatalytic O2 Evolution", Journal of Cluster Science, 2010 Publication	<1%
44	Hussain, F.. "Tungstoarsenate(III) polyoxoanions as inorganic ligands for polynuclear copper complexes", Polyhedron, 20090622 Publication	<1%
45	T. Arumuganathan, Samar K. Das. " Discrete Polyoxovanadate Cluster into an Organic Free Metal-Oxide-Based Material: Syntheses, Crystal Structures, and Magnetic Properties of a New Series of Lanthanide Linked-POV Compounds [{Ln(H O) } As V O (SO)]·8H O (Ln = La , Sm , and Ce) ", Inorganic Chemistry, 2009 Publication	<1%
46	Jordan J. Stracke, Richard G. Finke. " Water Oxidation Catalysis Beginning with 2.5 μM [Co (H O) (PW O)] : Investigation of the True Electrochemically Driven Catalyst at ≥600 mV Overpotential at a Glassy Carbon Electrode ", ACS Catalysis, 2013 Publication	<1%

47	Xiaobin Xu, Farhat Nosheen, Xun Wang. "Ni-Decorated Molybdenum Carbide Hollow Structure Derived from Carbon-Coated Metal–Organic Framework for Electrocatalytic Hydrogen Evolution Reaction", Chemistry of Materials, 2016 Publication	<1%
48	Submitted to Indian Institute of Technology Student Paper	<1%
49	Submitted to Pusan National University Library Student Paper	<1%
50	dspace-unipr.cineca.it Internet Source	<1%
51	Jialei Du, Jianying Wang, Lvlv Ji, Xiaoxiang Xu, Zuofeng Chen. "A Highly Active and Robust Copper-Based Electrocatalyst toward Hydrogen Evolution Reaction with Low Overpotential in Neutral Solution", ACS Applied Materials & Interfaces, 2016 Publication	<1%
52	chalk.coas.unf.edu Internet Source	<1%
53	Walter, Michael G., Emily L. Warren, James R. McKone, Shannon W. Boettcher, Qixi Mi, Elizabeth A. Santori, and Nathan S. Lewis. "Solar Water Splitting Cells", Chemical Reviews,	<1%

2010.
Publication

54	chemistry.uohyd.ac.in Internet Source	<1%
55	Sengeni Anantharaj, Pula Nagesh Reddy, Subrata Kundu. "Core-Oxidized Amorphous Cobalt Phosphide Nanostructures: An Advanced and Highly Efficient Oxygen Evolution Catalyst", Inorganic Chemistry, 2017 Publication	<1%
56	Sa-Sa Wang, Guo-Yu Yang. "Recent Advances in Polyoxometalate-Catalyzed Reactions", Chemical Reviews, 2015 Publication	<1%
57	Xiu-Li Wang, Dan-Na Liu, Hong-Yan Lin, Guo-Cheng Liu, Xing Rong. "Different Anderson-Type Polyoxometalate-Directed Metal–Organic Complexes Based on 2-Pyrazine Carboxylic Acid: Assembly, Structures and Properties", Journal of Cluster Science, 2015 Publication	<1%
58	Kazuhiko Ozutsumi, Takuji Kawashima. "Structure of copper(II)-bpy and -phen complexes: EXAFS and spectrophotometric studies on the structure of copper(II) complexes with 2,2′-bipyridine and 1,10-phenanthroline in aqueous solution", Inorganica Chimica Acta,	<1%

1991
Publication

59	studylib.es Internet Source	<1%
60	Blazevic, Amir, and Annette Rompel. "The Anderson–Evans polyoxometalate: From inorganic building blocks via hybrid organic–inorganic structures to tomorrows “Bio-POM”", Coordination Chemistry Reviews, 2016. Publication	<1%
61	Samar K. Das. "Supramolecular Structures and Polyoxometalates", Macromolecules Containing Metal and Metal-Like Elements, 10/12/2009 Publication	<1%

Exclude quotes	On	Exclude matches	< 14 words
Exclude bibliography	On		